Institutionen för Vattenbyggnad
Chalmers Tekniska Högskola

Department of Hydraulics
Chalmers University of Technology

WAVE FORCES ON A VERTICAL SLENDER CYLINDER

by

Göran Moberg

Submitted to the School of Civil Engineering, Chalmers University of Technology in partial fulfillment of the requirements for the degree of Doctor of Philosophy.

Opponent: Prof. J. R. Chaplin, City University, London.

Report
Series A:16
ISSN 0348 - 1050

Göteborg 1988

Address: Department of Hydraulics
Chalmers University of Technology
S-412 96 Göteborg, Sweden

Telephone: +46 31 721000

To my friends

SUMMARY

This thesis deals with wave forces on a slender surface-piercing vertical cylinder. Measurements of the total wave force, the pressure distribution, the local water level and the particle kinematics under the wave were made. The Reynolds numbers attained ranges between $0.3 \cdot 10^5$ and $2.3 \cdot 10^5$, the orbital shape parameter between 0.03 and 0.86 and the Keulegan-Carpenter number between 1 och 11.

The basic phenomena for a time dependent separated flow are reviewed and applied for a wavy flow around a surface-piercing vertical cylinder.

The mayor areas of findings concern:

- The importance of using relevant wave kinematics for the calculation of wave forces.

- The influence of a free water surface on the pressure distribution and resulting wave force.

- An alternative r.m.s. technique for the calculation of maximum forces along the cylinder.

Further work is needed with regard to the effect of the free surface on a time dependent separated wave flow i.e. wave forces, near the actual water surface, caused by both non-breaking and breaking waves.

PREFACE

At the Department of Hydraulics, Chalmers University of Technology, studies concerning wave energy utilization, interaction between wave forces and offshore structures and mooring system have been in progress since the mid 1970's. Together with the industry and the Stockholm University of Technology a cooperation project, "Offshore Structures-Wave Forces and Motions", was carried out between 1980 and 1985. The project was sponsored by the National Swedish Board of Technical Development (STU).

This thesis is the result of a part of the project and is submitted to the School of Civil Engineering, Chalmers University of Technology in partial fulfillment of the requirements for the degree of Doctor of Philosophy. Opponent: Prof. John R. Chaplin, City University, London.

I wish to express my thanks to all my colleagues and friends who have contributed to the accomplishment of this study. Especially, I would like to thank my tutor Dr. Lars Bergdahl who has helped and supported me throughout all phases of the study. I would also like to mention Bengt Carlsson, technician who manufactured most of the experimental equipment, always giving a helping hand during the experimental stage of the program. Furthermore, I would thank Ann-Marie Holmdahl who typed the manuscript and Alicja Janiszewska who prepared the figures, both always willing and helpful.

Finally, I want to thank my parents Kerstin and Hans Moberg. Without their support and encouragement my work would not have been possible.

Göteborg, February 1988

Göran Moberg

LIST OF CONTENTS

1. INTRODUCTION

1.1 Wave induced load

Over the past few decades considerable efforts have been devoted to studying the interaction of waves and offshore structures. There have been numerous studies made of wave forces on vertical circular cylinders, which have meant considerable improvements in our understanding of the physics of underlying time dependent flow.

The choice of method for the calculation of wave forces depends on the influence of flow separation, i.e. on the size and shape of the structure being studied. For larger structures, the presence of the structure disturbs the incident wave. Scattering effects become significant, and so viscous effects and the consequent effect of flow separation may be considered secondary. This hydrodynamic loading situation is well understood and is described accurately using diffraction theory. For slender structures, however, the problem of separated flow still remains theoretically unresolved, necessitating further experiments.

This is a study of the hydrodynamic loads for a separated flow, more precisely of wave forces on a vertical slender surface-piercing circular cylinder in shallow water.

Wave flow around a vertical cylinder is a complex phenomenon. In addition to the effect of the free surface, the orbital motion of the fluid particles gives rise to a three-dimensional time dependent flow. A further complication is the exponential decay of the particle velocity. The key to the explanation of this time dependent separated flow is the understanding of the formation, growth and motion of vortices.

In determining the forces on a structure in waves, two distinct stages can be distinguished. Firstly, it is necessary to gather information on the particle kinemat-

ics under the wave. This can be done either by making measurements or using a suitable wave theory. Secondly, a method of calculation must be used, relating the force on the structure to the wave in question.

Morison's well-known equation is often used to calculate forces on slender structures. This equation expresses the total force as the sum of a drag component and an inertia component, each governed by an empirical force coefficient. Since its introduction in 1950, numerous attempts have been made to calibrate or to improve Morison's equation. However, the results have varied, and there are still aspects of the flow which are not fully understood. Nevertheless under certain circumstances, Morison's equation works quite well. The scatter of measured force coefficients reported depends on the experimental technique, the wave theory used, and other effects.

The procedure of wave force calculation needed for structural loading generally involves the following steps.

(i) establishment of the wave climate on the basis of recorded waves or meteorological and geographical data

(ii) determination of design wave

(iii) selection of wave theory

(iv) selection of wave force formula - force coefficients

(v) calculation of hydrodynamic forces

(vi) calculation of structural response

(vii) calculation of structural loading

In the present report steps (iii), (iv) and (v) are considered.

1.2 Aim of the study

The aim of this study was to:

- investigate wave forces and pressure distribution on a slender surface-piercing vertical cylinder in shallow water

- investigate the mass and drag coefficients in Morison's equation

- discuss the validity of various wave theories used in wave force calculations

- improve wave force calculations.

Chapter 2 describes some of the most important findings of other investigators who have considered hydrodynamic loading in time dependent separated flow. Morison's equation, its validity and proposed improvements to it, are also discussed.

Chapter 3 covers the experimental setup. It describes the equipment and the pressure synchronization with its wave train averaging technique. The chapter is concluded with a description of a system for measuring water velocity which was partly developed at our hydraulics laboratory.

Chapter 4 examines the validity of some wave theories used for the calculation of wave forces. The theories investigated include linear, 2nd, 3rd and 5th order theories and the cnoidal theory. Chapter 4 points out that the type of kinematics used is one of the most important factors influencing the value of the calculated force coefficients. Consequently, it is important to use the same types of velocity and acceleration in the design step as in the experiments from which the coefficients were calculated. The chapter is concluded with recommendations to be used in wave force calculations.

Chapter 5 accounts for time dependent separated flow around a vertical surface-piercing circular cylinder. Planar steady flow and planar oscillating flow around a circular cylinder are accounted for. These two flow situations may be used to describe the basic phenomena for a wavy flow. Chapter 5 is concluded with a discussion of the influence of and the mechanisms behind the effects of a free water surface.

Chapter 6 describes the measurement of the force and the calculation of the integrated pressure around the cylinder. The chapter is concluded with a discussion of measured transverse forces.

Chapter 7 treats force coefficients used in Morison's equation. Different evaluation procedures are analysed and their results are presented. The values given in literature are usually time invariant but are averaged over whole periods.

In reality, both the drag and the inertia coefficients show large variations during a given cycle, and this variation is therefore studied. Our conclusion, especially for waves on shallow water, is that wave force calculations may be substantially improved by considering wave crests and troughs as two different types of event characterized by velocity decreasing with depth and the use of a local Keulegan-Carpenter number.

This chapter also discusses and applies results from the present study for the calculation of wave force. The total force along the cylinder given by Morison's equation is evaluated. It is shown that a good wave force calculation requires force coefficients insuring correct maximum forces. Otherwise, the order of magnitude as well as the phase of the force may be in poor agreement with measurements.

Chapter 8 describes the use of a root mean square force coefficient. Good agreement between measured maximum to-

tal forces and maximum total forces calculated by the use of the root mean square force coefficient was obtained for waves included in the experimental program.

In the final chapter, Chapter 9, observations and conclusions made during the present report are listed, with reference to the chapter that discusses them.

In order to discuss and account for measured variables, observations, results, etc. three typical waves from the experiments are followed as examples throughout the report. In the present report wave A represents deep water, wave B transitional water and wave C shallow water conditions.

2. WAVE FORCES ON SMALL BODIES

In determining the forces on a structure in waves, two distinct stages can be distinguished. Firstly, it is necessary to gather information on the particle kinematics under the wave. This can be done either by making measurements or using a suitable wave theory. Secondly, a method of calculation must be used, relating the force on the structure to the wave in question.

There are various wave theories, each of which is applicable over certain ranges of water depth, wave length and wave height. Their classification according to closeness to measured wave profile, horizontal velocity and acceleration is given in Chapter 4.

Wave forces on structures have been studied for a long time. Numerous studies have been made of wave forces on vertical circular cylinders. However, no calculation procedure for which there is universal agreement has been developed.

This chapter gives a literature survey of some of the most important work on the hydrodynamic loading in time dependent separated flow. Morison's equation, its validity and proposed improvements is also discussed.

The papers reported on are grouped on the basis of the experimental approach used. Lift forces, surface roughness and the effect of current are reported separately.

2.1 Literature survey

2.1.1 The assumption of Morison et al.

In 1950 Morison, O'Brien, Johnson and Schaaf proposed an approximate expression for loading on offshore structures due to waves. In their expression, now known as Morison's

equation, the total force on a vertical cylinder was formulated as

$$F = \tfrac{1}{2}\,\rho\, C_D\, A\, u|u| + C_M\,\rho\, V\,\frac{\partial u}{\partial t} \qquad \ldots\ (2.1)$$

where

F = force
ρ = density of water
C_D = drag coefficient
A = characteristic area
u = water particle velocity
C_M = mass or inertia coefficient
V = immersed volume
$\partial u/\partial t$ = water particle acceleration*)

The first term is the drag force proportional to the square of the velocity. This drag force term, with a form similar to that in a steady flow situation, contains the drag coefficient (C_D), which was expected to have substantially the same value as for steady flow. The second term depends on the pressure gradient associated with the horizontal acceleration of the ambient flow. This latter term is proportional to the acceleration of the mass of water displaced by the cylinder. A coefficient of mass (C_M), later referred to as the inertia coefficient, is used to account for the added mass effects of the flow around the cylinder.

It is recognized that the force coefficients (C_D, C_M) are not constant throughout the wave cycle. Variables (factors) which may influence the values of C_D and C_M include

---

*) The acceleration is assumed to be given exclusively by the local component, $\frac{\partial u}{\partial t}$. However, the total acceleration is given by the sum of local and convective components i.e. $\frac{du}{dt} = \frac{\partial u}{\partial t} + u\,\frac{\partial u}{\partial x} + v\,\frac{\partial u}{\partial y}$. For further information, see Appendix 2.

$$C_{D,M} = f(KC, Re, \Omega, F.S.E., \frac{k_s}{D}, \frac{t}{T}) \qquad \ldots (2.2)$$

where

KC = Keulegan-Carpenter number (= u_m T/D)
Re = Reynolds number (= u D/ν)
Ω = Orbital shape parameter (= u_v/u_h)
F.S.E. = free surface effects
k_s/D = relative roughness
t/T = time instant during the wave cycle
u_m = maximum horizontal particle velocity
T = period of the wave cycle
D = diameter of cylinder
ν = kinematic viscosity
u_v = vertical particle velocity
u_h = horizontal particle velocity

which are discussed throughout this report.

It should be noted that in 1851 Stokes showed that the force on a sphere oscillating in an unseparated viscous fluid can be described by two terms, one involving the acceleration and the other the velocity of the sphere. However, Stokes' drag force had a linear dependence on the velocity. For very low Reynolds numbers (Re), the drag force is attributable to skin friction rather than to pressure, as is the case in separated flow. Obviously, Morison's equation is an extension of Stokes' solution applied to a time-dependent separated flow. Its quadratic velocity term and empirical coefficients compensate for the effects introduced by separation. Consequently, its validity and its limits have to be determined experimentally.

Morison et al. conducted a series of experiments in a wave tank. In these experiments the force was obtained by measuring the total moment acting on a vertical circular cylinder. The measured moments at the instant of zero

velocity and acceleration, determined from the measured wave profile and linear wave theory, were used to evaluate C_D and C_M, respectively. In spite of the assumption that either force component is equal to zero at the instant of zero velocity or acceleration, the authors found that the graph of the computed moment agreed well with the measured values over the entire wave cycle. However, they found no trend for any function in the C_D and C_M values over the range examined ($0.22 \cdot 10^4 < Re < 1.11 \cdot 10^4$).

Morison's equation was proposed as an approximate solution to a complex problem. In fact the proposors' intention was to present: "Essentially a preliminary report submitted at the time because of the current importance of wave forces in the design of offshore structures". However, Morison's equation has been and remains the main technique used in estimating the wave force on small or slender structures, in relation to the wave length. When the size of the structure becomes a substantial fraction of the wave length, scattering effects become significant and a diffraction technique such as that of MacCamy and Fuchs (1954) must be used. However, since only forces on a small diameter cylinder have been studied in this report, the diffraction forces are not further considered here.

In the absence of any adequate theoretical description of fluid-structure interaction, numerous attempts have been made either to calibrate or to improve Morison's equation. A few of the important papers are discussed below.

2.1.2 Different experimental approaches

There are basically three possible types of experiment for establishing drag and inertia coefficients.

One type is experiments where the complex kinematics of

the fluid under a wave is replaced by a simple harmonic oscillation of water past the body. This was done by Sarpkaya (1976a,b) by oscillating water in a U-tube past a fixed cylinder and by Garrison et al. (1977) by oscillating a cylinder through still water. One advantage in such experiments is that the water velocities and accelerations are easily determined, and these determinations are therefore very accurate. Very high Reynolds numbers (Re) can also be realized. One disadvantage is that the undisturbed water paths are straight lines rather than ellipses. Nor are the exponential decay of the kinematics considered.

Another type of experiment is one in which a wave tank is used, as example the experiments of Chakrabarti (1980a). The advantage is that the undisturbed water paths and free surface effects are correctly modelled, while the disadvantages are that it is difficult to obtain realistic Re, and that the water velocity and acceleration must be measured separately or evaluated from a suitable wave theory.

The third type of experiment is measurements made on test structures in the ocean environment, such as those carried out by Bishop (1982). Such experiments have shown that it is possible to obtain force coefficients useful for designing structures. However, it has not been possible to distinguish the influence of various major parameters on the force coefficients, because of a large scatter attributed to surface roughness of object, free stream turbulence, current, structural oscillations etc., and to the use of different wave theories when evaluating the kinematics of the flow.

2.1.3 Planar oscillating flow

Keulegan and Carpenter

Among the most important laboratory experiments to date

are those conducted by Keulegan and Carpenter (1958). Keulegan and Carpenter carried out the first systematic evaluation of the Fourier averaged drag and inertia coefficients and investigated the dependence of the averaged coefficients in Morison's equation on a periodic parameter. This parameter, referred to as the Keulegan-Carpenter number (KC), expresses the ratio between the diameter of the water particle path and the structure diameter, see Chapter 2.2.1.

The authors' measurements were carried out on submerged horizontal cylinders placed in the node of a standing wave. Since the fluid motion was assumed to be uni-directional and velocities and accelerations were derived from linear theory, this study can be considered in the same category as the U-tube experiments.

Keulegan and Carpenter were able to relate the C_D and C_M coefficients to KC. However, they found no correlation between the coefficients and the Reynolds numbers over the range examined ($0.7 \cdot 10^4 < Re < 3.0 \cdot 10^4$), see Fig. 2.1 a,b. The results for the coefficients also indicate the existence of a critical KC (15) at which C_M reached a minimum while C_D was at its maximum. A physical explanation of this was given in terms of separation effects.

The Keulegan-Carpenter number is an important parameter in determining the relative magnitudes of the drag and inertia forces. For constant drag and inertia coefficients and when using linear theory, the ratio of drag forces to inertia forces are directly proportional to KC. Thus low values of KC indicate inertia-dominated regions while higher KC values indicate predominant drag. Keulegan and Carpenter were also concerned with improving Morison's equation by evaluation of a residual force function to account for the differences between measured and calculated forces.

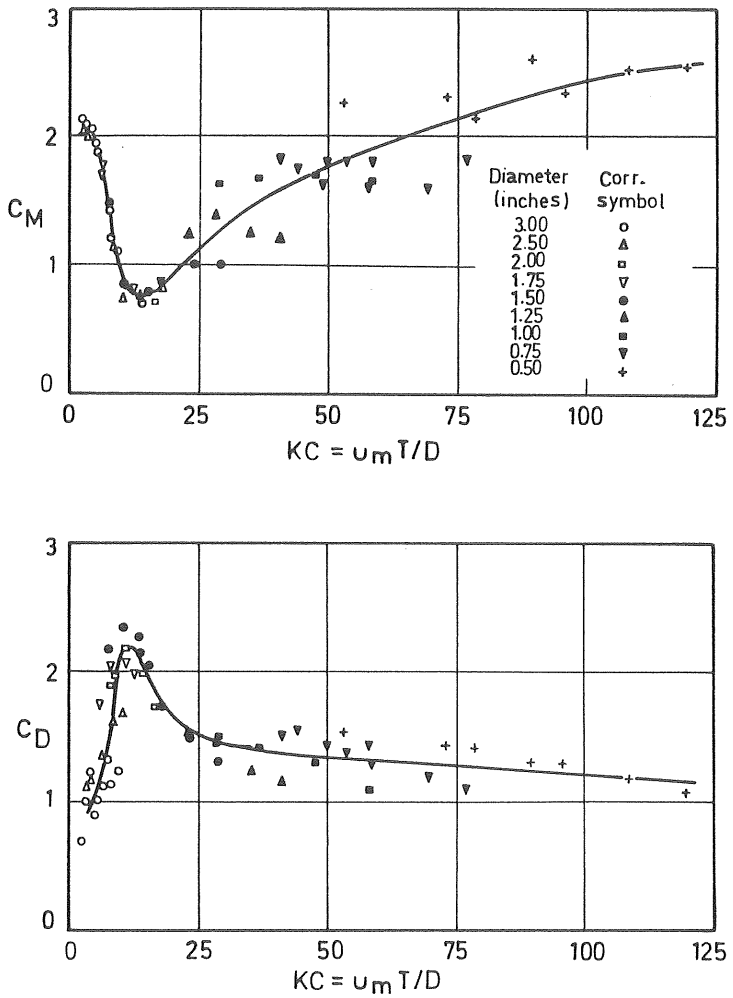

Figure 2.1 a,b Variation of inertia and drag coefficients of cylinders as function of KC. (Keulegan and Carpenter, 1958).

Sarpkaya

In 1976 Sarpkaya reported the results of a series of experiments with a sinusoidally oscillating flow around cylinders in a U-tube. Using his own tests and from re-analysing the results of Keulegan and Carpenter, Sarpkaya

demonstrated that there are clearly defined relations between the coefficients and the Reynolds number as well as the Keulegan-Carpenter number. This was demonstrated by introducing a frequency parameter (β), which is the ratio between Re and KC.

The use of a frequency parameter as an intermediate step in determining the Reynolds number dependence was very convenient for carrying out experiments in U-tubes, because for any given U-tube arrangement the frequency parameter varies solely with the cylinder diameter.

The variation of the drag and inertia coefficients with both KC and Re is shown in Figs. 2.2 a-d. As Re increases, the drag coefficient is reduced to a minimum, after which it begins to increase slowly with further increase of Re, reaching a value of about 0.62 at Re = $7 \cdot 10^5$. The inertia coefficient was found to increase with increasing Re, reach a maximum, and then gradually level off at a value of about 1.75. The drag and inertia coefficients were found not to vary appreciably for Re below 20,000, which may explain the conclusions reached by Keulegan and Carpenter.

Garrison et al.

The dependence of C_D and C_M on Re was observed by Garrison, Field and May (1977) at about the same time as Sarpkaya. In order to study the Reynolds number dependence they made a horizontal cylinder oscillate sinusoidally through stagnant water. The only hydrodynamic difference in this case was the absence of a bouancy-like force caused by the pressure gradient due to fluid acceleration. The buoyancy-like force or Froude-Krylow force is expressed as the product of the displaced mass and the fluid acceleration. Thus, the recorded added mass coefficient (C_m) in the experiments was equivalent to C_M-1.

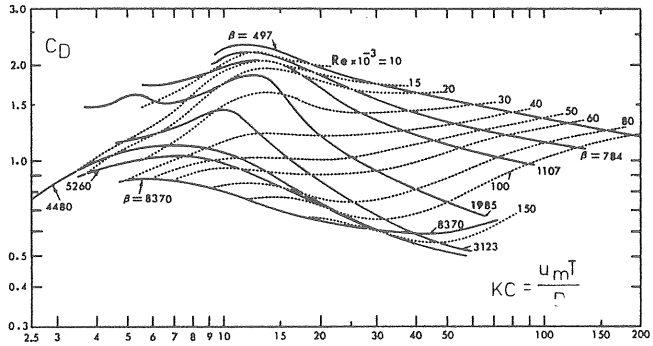

Figure 2.2 a C_D versus KC for various Re and β (Sarpkaya, 1976a).

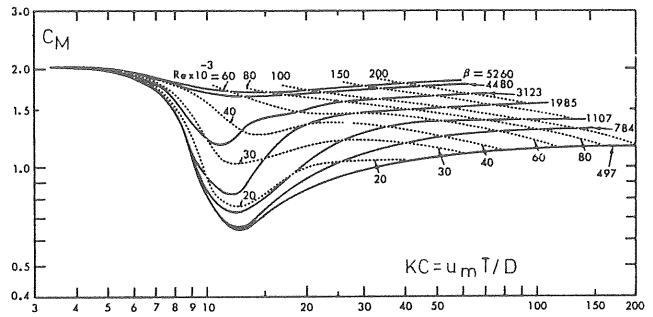

Figure 2.2 b C_M versus KC for various Re and β (Sarpkaya, 1976a).

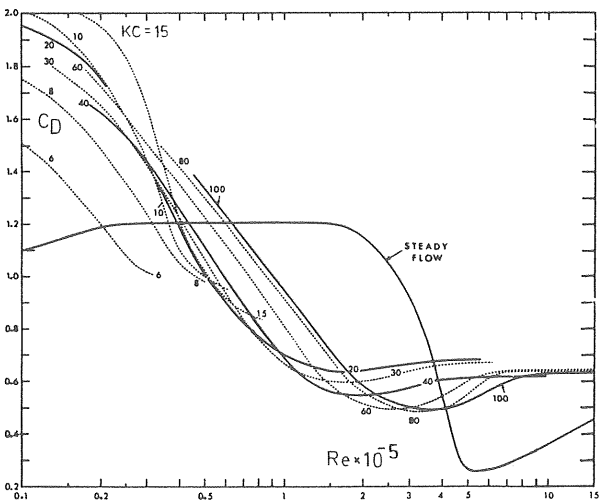

Figure 2.2 c C_D versus Re for various KC (Sarpkaya, 1976a).

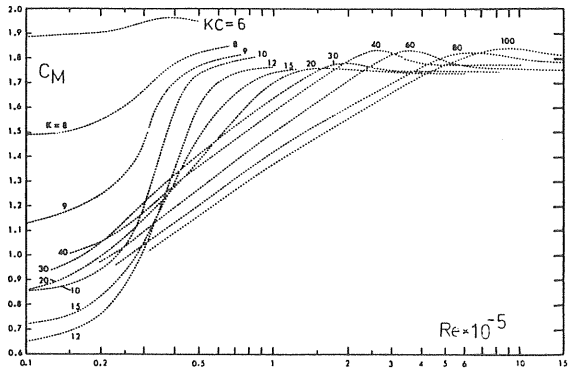

Figure 2.2 d C_M versus Re for various KC (Sarpkaya, 1976a).

The advantage of the experimental technique used by Garrison et al. was that the frequency of the oscillation could be varied, while the amplitude of the motion could be held constant, making it possible to examine the variation of the Reynolds number for constant KC. The study gave substantially the same values as those by Sarpkaya for KC larger than about 10. However, C_D was found to decrease to very low values as KC decreased below the value of 10. This was explained in terms of the fluid not moving far enough in one direction for separation to occur.

Maull and Milliner

Maull and Milliner (1978) suggested the use of a total force coefficient expressing the non-dimensionalized root-mean-square (r.m.s.) force on the cylinder. They proposed that the force could be considered as a sum of an inertia force with its ideal C_M value of two and another term which is a function of the movement of the vortices produced. Their measurement results demonstrated that constant C_D and C_M are quite adequate to predict the total force. However, their experiments were conducted in a small U-tube with sinusoidal flow at Reynolds numbers less than 4000. The use of a single r.m.s. force coefficient obscures the time-dependence of the force and hence the physics of the problem.

Bearman and Graham

Bearman and Graham (1979) measured forces on several cylindrical bodies in planar oscillating flow in a U-tube. They noted a considerable cycle to cycle variation in the drag and inertia components, although the root-mean-square of the force is shown to remain fairly constant at fixed Keulegan-Carpenter numbers.

Bearman and Graham concluded that different modes of vortex shedding occur over different ranges of KC but also that a random variation of drag and inertia coefficients is caused by small changes in the phase of the vortex shedding. However, as the r.m.s. force was more stable it was suggested that this representation may be more useful than the usual division into drag and inertia components.

Rodenbusch and Källström

In 1986, Rodenbusch and Källström reported an experiment where a circular cylinder of 1 m diameter in a large basin was subjected to various types of forced oscillations. Reynolds numbers up to about $2 \cdot 10^6$ and amplitudes of oscillation up to 15 m were studied. The data presented showed large scatter. The large scatter in C_D obscured any possible trends for low KC values, but the drag coefficient approached 0.7 for a KC above 40. The inertia coefficient showed a trend of decreasing values from 2.0 to 1.6 as KC increased from 0 to 90. In conclusion the authors stated that Morison's equation still appears to be a good tool for predicting hydrodynamic forces.

Sarpkaya (1985) discussed a paper by Rodenbusch and Gutierrez (1983) based on the experiment mentioned above. Sarpkaya compared his results from 1976 with those of Rodenbusch and Gutierrez and found good agreement between the two studies.

Experiments and flow visualisation of vortex shedding for low KC have lately been conducted as reported by Honji (1981), Bearman et al. (1981), Bearman, Downie et al. (1985), Williamson (1985), Bearman (1985) and by Sarpkaya (1985, 1986).

At low β values the flow around a cylinder is attached. Experiments carried out by Bearman, Downie et al. (1985) and Sarpkaya (1985, 1986) show that the drag coefficient falls, roughly proportional to KC^{-1} as KC is increased from values less than one, see Fig. 2.3. Depending upon the magnitude of β, a minimum is reached for C_D somewhere in the KC region of 2. It was postulated that the minimum drag coefficient just precedes the first appearance of separation, after which C_D increases and behaves as reported by Sarpkaya (1976a). The inertia coefficient was reported to be almost constant, and slightly higher than 2 for the low KC values.

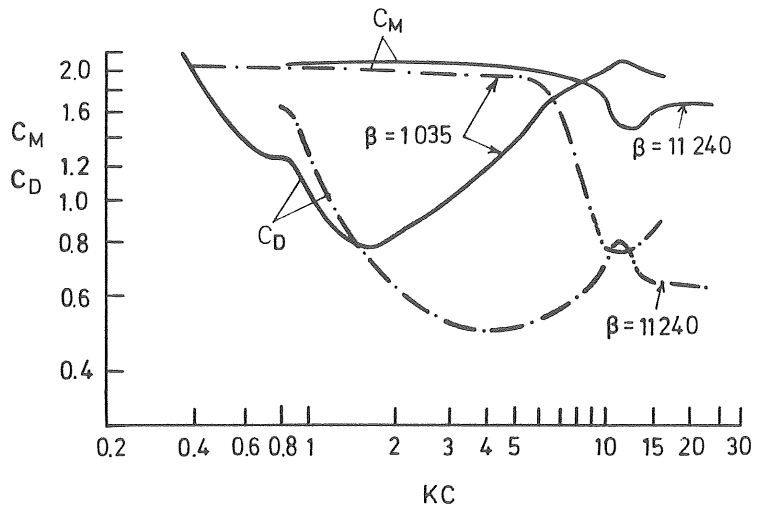

Figure 2.3 Drag and inertia coefficients versus KC (Sarpkaya, 1986).

2.1.4 Wave tank experiments

Most of the early investigators failed to obtain a consistent set of drag and added mass coefficients. Some of these investigations also showed large scatter (see, for instance, Goda (1964)).

Chakrabarti, Wolbert and Tam

In 1976 Chakrabarti, Wolbert and Tam conducted a series of experiments where some consistent trends in the drag and inertia coefficients were found.

The total load on a vertical circular cylinder and the load on two short sections below the still water level were recorded. From the measured wave profile the wave kinematics at the depth of the test sections was evaluated, using linear theory. Attempts were made to measure the water particle kinematics. However, the velocity data were found to be unreliable and could not be used. In a later study Chakrabarti (1980a) reanalysed the data from 1976 and conducted further tests. In this later study the kinematics were calculated using the stream function theory, see Fig. 2.4 a.

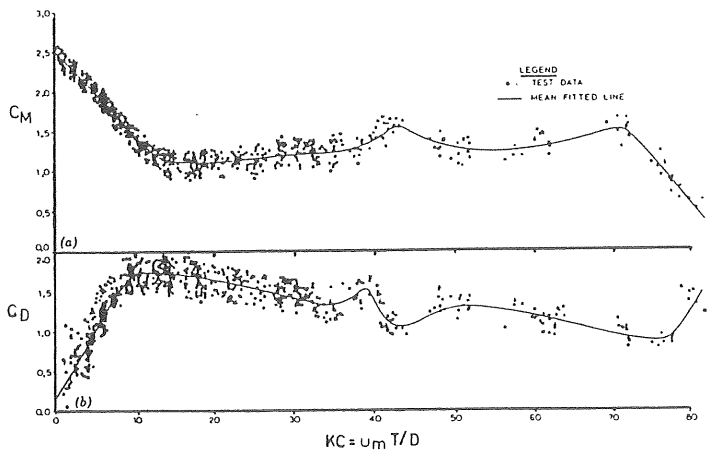

Figure 2.4 a C_M and C_D versus KC for Reynolds number range of $2 \cdot 10^4$ to $3 \cdot 10^4$ (Chakrabarti, 1980a).

For KC values smaller than 40 in the Reynolds number range covered, $(2 \cdot 10^4 - 3 \cdot 10^4)$, Chakrabarti found reasonably good agreement between his C_D and C_M values and those obtained by Sarpkaya (1976a), see Fig. 2.4 b. However, the results from the wave tank tests yielded somewhat larger C_M values in the range of KC values from about 8 to 15. For KC between 40 and 80, C_D values were lower while C_M were higher than their corresponding values in Sarpkaya's two-dimensional tests.

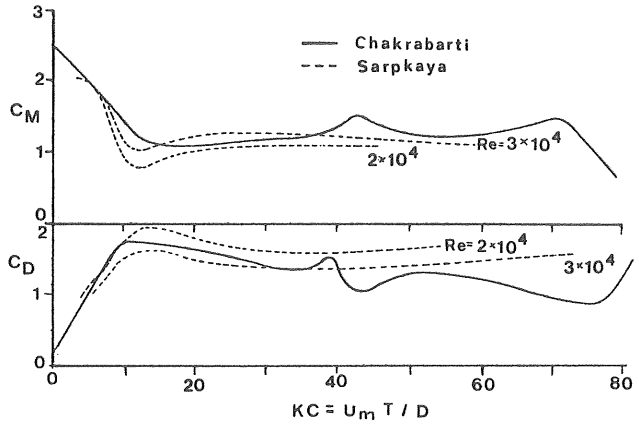

Figure 2.4 b Comparison of Sarpkaya's two-dimensional flow test with Chakrabarti's test (Chakrabarti, 1980a).

In both studies the authors concluded that the limited range of Reynolds number and the large scatter in the results, particularly at higher KC values, make it difficult to establish the dependence of C_D and C_M on the Reynolds number.

Ramberg and Niedzwecki

The use of drag and inertia coefficients obtained from planar oscillating flow for the calculation of forces under wave conditions have stimulated a great deal of research activity. In planar oscillating flow the particle motion is unidirectional instead of orbital and varying with depth.

Ramberg and Niedzwecki (1979) criticized the assumption of constant C_D and C_M coefficients along the length of the cylinder. Experiments were performed in a small wave tank in which the drag and inertia coefficients were determined from wave loading on a vertical cylinder with the use of linear theory. The coefficients obtained were then compared with those from Sarpkaya's (1976a) U-tube results. The comparison showed that the assumption of uniform coefficients from planar flow can lead to significant errors, with an overprediction mainly of the drag force. This was attributed to the "steepness" of the velocity gradient along the cylinder and to eccentricity of the water particle orbits.

Stansby, Bullock and Short

Stansby, Bullock and Short (1983) carried out an investigation of the hydrodynamic coefficients in relation to the force on a vertical circular cylinder in waves and their dependence on the water particle orbital motion. They introduced an orbital shape parameter Ω, defined as the ratio between the vertical and horizontal water particle velocity. Thus, if the value of Ω is near unity the coefficient represents deep water, whereas a value of zero represents a planar flow in a U-tube. Stansby et al. performed experiments in a wave tank in which the local forces on a short section of a vertical cylinder and the water particle velocities without the cylinder were measured. They then compared their findings with the corresponding results of Sarpkaya (1976a). Their results showed that the effect of the orbital motion is to decrease C_D and to increase C_M relative to the values found in planar oscillatory flow. The authors conclude that C_D and C_M values from planar oscillating flows give an accurate or possibly conservative prediction of the force. Only when orbital shapes approach circular ($\Omega > 0.7$) will the force be significantly overestimated.

This may explain the conflicting conclusions drawn by Chakrabarti (1980a) and Ramberg and Niedzwecki (1979), as the latter measured the forces in deep water while the former had more shallow water contribution.

To reduce the scatter in the coefficients Stansby et al. also compared the r.m.s. force coefficient C_F with those found by Sarpkaya (1976a). The wave test values and U-tube values for $\Omega \leq 0.7$ were in very good agreement.

Sarpkaya

Sarpkaya (1984, 1985) confirms the findings of Stansby et al. by moving a cylinder in a U-tube in such a way that it experiences the effect of orbital motion about a vertical cylinder in waves (small Re). The results show that the effect of the orbital motion is generally to decrease C_D and to increase C_M in the drag and inertia dominated region. It also appears that the effect of the orbital motion is negligible for KC larger than 35. Sarpkaya concludes that the effect of the orbital motion is very important and must be taken into consideration in the design, in the analysis of ocean data, and in the comparison of the planar oscillatory flow data with data obtained in waves.

Chakrabarti

Chakrabarti (1985) reanalysed his data as presented in 1980, now considering the orbital motion of the fluid particles. When analysing the data he found that the experiments covered both intermediate and deep waters (Ω = 0.3 - 0.9). However, Chakrabarti found that the coefficients C_D and C_M as well as the r.m.s. force coefficient C_F were insensitive to the value of Ω in the actual range. In conclusion he stated that the dependence of C_M and C_D on Ω is, at best, weak.

Dawson

Dawson (1985) measured the total force on a vertical cylinder in deep water and compared it with predictions from Morison's equation. The author found that Morison's equation with Stokes' second order theory and constant drag and inertia coefficients of 1.2 and 1.8, respectively, provide good agreement with the measured maximum wave forces.

The force variation over the entire wave cycle was well represented. The inertia coefficient was determined in that region where the inertia component dominated the maximum force. Holding this value fixed, the best value of the drag coefficient was found by trial calculation using the data associated with the larger waves.

Dawson also showed that variable coefficients determined from planar oscillatory flows generally overpredict the measured force by about 30 percent in the studied KC range of about 3 to 40. Re was of the order 10^4.

Törum

Törum (1985) and Dean, Törum and Kjeldsen (1985) presented some data on an experimental investigation performed in a large wave basin, where the wave force along a cylinder in the surface zone from the wave crest to below the wave trough was studied.

A 6 cm diameter cylinder was instrumented with 26 force transducers, mainly spaced 5 cm apart. Both time invariant and time varying coefficients throughout the wave cycle were calculated from averaged wave force records, and kinematics from Stokes' second order theory. KC and Re in the experiments reached up to about 50 and 10^5, respectively.

The authors preliminarily concluded that the wave force on a cylinder is zero at the maximum run up on the cylinder and that this run up is approximately equal to the particle velocity head at the wave crest. The wave force also increases and becomes, at largest, 1 to 2 times the velocity head below the wave crest.

Törum also concludes that the C_M values tend to stay uniform up to the S.W.L. and increase from there and upward (for steeper waves). However, the C_D values tended to stay uniform all along the cylinder up to the water surface. These conclusions were explained in terms of surface effects i.e. water run up and draw down at the cylinder

Bearman, Chaplin et al.

Bearman, Chaplin, Graham, Kostense, Hall and Klopman (1985) presented measurements of the loads on a small element of a vertical and horizontal cylinder at very high Re. The maximum Re was about $5.0 \cdot 10^5$ for KC up to 20. Morison's equation was found to give a good fit for the vertical cylinder to the measured force, with drag and inertia coefficients calculated from velocity measurements. However, no obvious dependence of C_D and C_M on the Re was found. In both orientations, the cylinder loads also showed little influence of the water particle orbital shape. The orbital shape parameter, defined as the ratio of r.m.s. vertical velocity to r.m.s. horizontal velocity, varied over the range of 0.11 to 0.65.

The C_M values presented varied substantially, as did those for large values of the frequency parameter β presented by Sarpkaya (1976a), see Fig. 2.5. For KC above 10 the values of C_D are close to the ones generally accepted in postcritical flow. However, C_D drops to a very low value at a KC around 5. This observation for C_D at low KC agrees

well with the observation by Garrison et al. (1977), that C_D tends to decrease as KC decreases because the fluid does not move far enough in one direction for separation to occur.

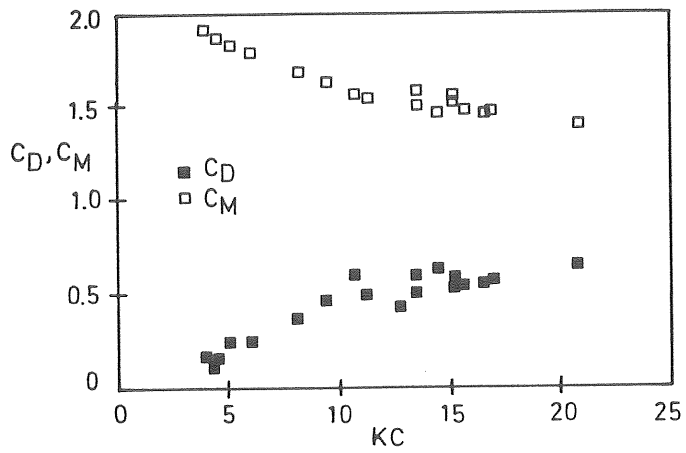

Figure 2.5 Drag and inertia coefficients versus KC (Bearman, Chaplin et al., 1985).

In order to avoid a decomposition of the force into drag and inertia components, the r.m.s. force coefficient was evaluated for both the regular and random waves measured. The agreement between the two sets of data was excellent, confirming that regular wave data can be used to predict forces in random waves.

2.1.5 Ocean experiments

A number of large scale experiments have been undertaken in the ocean environment. Among them are those by Wiegel et al. (1957), Evans (1969), Kim and Hibbard (1975), Heideman et al. (1979), Borgman and Yfantis (1979), Bishop (1979), Ohmart and Gratz (1979), Pearcey and Bishop (1979), Dean et al. (1981) and Bishop (1982).

These experiments have shown that it is possible to obtain

force coefficients useful for designing structures. However, it has not been possible to isolate and interpret the significance of various parameters. A characteristic feature of the experiments is that their results show large scatter that can be attributed to free stream turbulence, surface roughness, currents, structural oscillations etc., and to the use of different wave theories when evaluating the kinematics of the flow. Nor did the results of the experiments reduce the difficulties associated with the applicability of Morison's equation. While laboratory experiments are made for the purpose of understanding underlying mechanisms, the value of ocean experiments lies in their reflecting the effects of all influences, when Morison's equation is used for actual sea states.

2.1.6 Lift forces

In addition to the in-line or longitudinal force there are lift or transverse forces acting perpendicular to the direction of the wave motion. These forces are caused by asymmetrical shedding of vortices from the surface of the body. In analogy with the drag force in the longitudinal direction, the lift force is taken to be proportional to the square of the velocity and is written $F_L = \pm\frac{1}{2}\rho C_L A u^2$. Like the drag force the lift force is correlated with a lift coefficient C_L.

The lift forces are important not only because of their magnitude (which may be considerably greater than the in-line force), but also because of their frequencies which may cause resonance motions of the structure.

Bidde

Bidde (1971) carried out a study on lift forces on a vertical circular cylinder. Both in-line and lift forces were recorded in a wave tank. The lift force was also

associated with eddy shedding regimes given by flow observations. A vortex pattern was established at small KC and it was judged that the separation took place from Keulegan-Carpenter values of about 3. This was also confirmed by studying the maximum ratio of lift to in-line force. Above a KC of 3 to 5 the lift forces increased steadily with increasing KC. The results indicated that the lift forces may reach a peak at a KC of about 15.

In conclusion Bidde stated that lift force behaviour is primarily dependent on KC rather than on Re.

Isaacson and Maull

In 1976, Isaacson and Maull presented an extension of Bidde's investigation on lift forces. They found the r.m.s. lift coefficient to be zero for a KC less than 5. The peak value of the lift coefficient was found at a KC of about 12 and, depending on the water depth, varied between 0.5 and 1.2. At higher values of KC the lift coefficient approached a steady value of about 0.3.

To establish the frequencies of the lift force, they also used a circular cylinder oscillating in still water. The authors suggested that when N vortices are shed in each half cycle, the ratio of the lift frequency to the oscillating frequency is N+1.

Sarpkaya

Sarpkaya (1976a) measured the lift force in planar oscillating flow. He found that after the lift coefficient reached its maximum value at a KC of about 12 it decreased rapidly with increasing KC, see Fig. 2.6 a,b. Furthermore the C_L coefficient decreases for all values of KC with increasing frequency parameter β. The minimum value of KC at which asymmetrical flow/lift forces develop is extremely

sensitive to the experimental conditions. Sarpkaya found that there was a 90 percent chance that the asymmetry would appear at a KC of 5. At a KC of 4 there was only a 5 percent chance that the asymmetry would appear, and then only for very short periods of time. By using the parameter β Sarpkaya established the dependence of C_L on KC and Re. For Re smaller than about $2 \cdot 10^4$ the C_L coefficient depends primarily on the KC. In the Reynolds number range from about $2 \cdot 10^4$ to $1 \cdot 10^5$ the C_L coefficient depends to varying extents on both the Re and the KC. For a Re greater than $1 \cdot 10^5$ the dependence on Re and KC was found to be negligible.

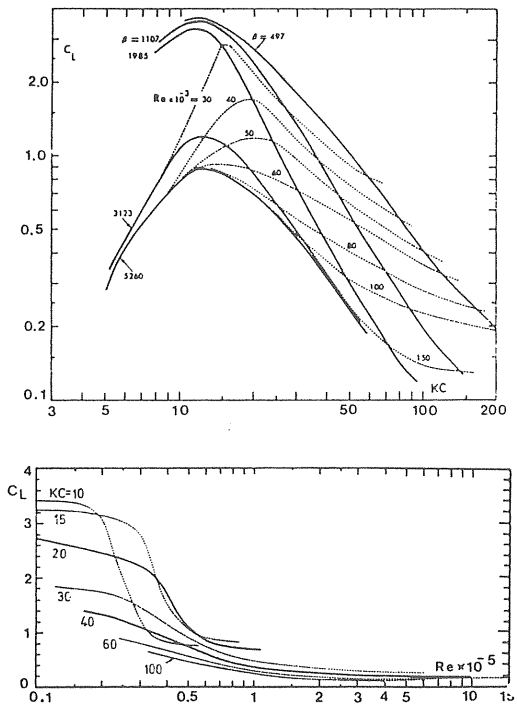

Figure 2.6 a,b Lift coefficient versus KC (above) and Re(below) (Sarpkaya, 1976a).

Several investigators have pointed out the irregular feature of the transverse force. Aside from the frequency variation with KC, Re and time in a given cycle, there is also a large cycle to cycle variation. Bearman and Graham

(1979) still found a considerable scatter in their results after averaging their data over 100 cycles. Sawaragi et al. (1976), Chakrabarti et al. (1976), Isaacson and Maull (1976), Sarpkaya (1976a), Maull and Milliner (1978), Bearman and Graham (1979) obtained the first multiple of the oscillatory frequency, using spectral analysis. Some of these experiments show progressive occurrence of higher order components in the frequency domain with increasing KC. Maull and Milliner (1978) showed that the r.m.s. lift force reaches its first maximum at a KC of about 13 where the dominant frequency is twice the flow frequency. The next maximum occurs at a KC of about 18 and is associated with a dominant frequency of three times the flow frequency. Further increases in KC result in decreases in the r.m.s. lift coefficient, and the frequency component becomes an increasingly higher multiple of the flow frequency.

Sarpkaya (1976a) gave the frequency ratio (f_r) of the dominant lift frequency (f_s) to the flow frequency (f) for values for KC up to 200 and Re up to $5 \cdot 10^5$, see Fig. 2.7. Each line in Fig. 2.7 represents the maximum KC for a given Re and f_r. However, Sarpkaya points out that each line does not represent an absolute dividing line between

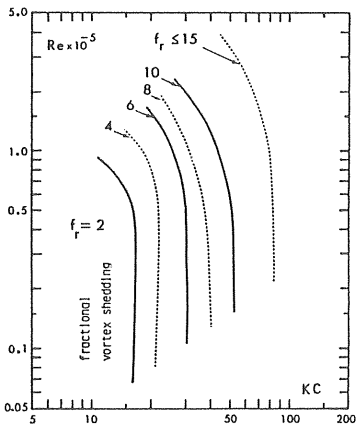

Figure 2.7 Relative frequency of vortex shedding as a function of KC and Re (Sarpkaya, 1976a).

the frequencies N-1 and N+1, and also that the frequency of vortex shedding is not a pure multiple of the flow oscillation frequency.

Stansby et al. (1983) suggest that in the same way as velocity variation and orbital eccentricity may influence the force along a vertical cylinder, vortex shedding near the surface probably triggers vortex shedding and lift at depths in which the KC is less than 5.

Bearman, Chaplin et al. (1985) measured the transverse forces at high Re ($5 \cdot 10^5$) in a wave tank. Their values for the lift coefficient were essentially equal to those presented by Sarpkaya (1976) for large β-values. The lift coefficient rose rapidly between KC 5 and 10, which indicates strong vortex shedding. In KC range 10 to 15 they observed occasions when the maximum force component during a cycle was in the transverse rather than the in-line direction. Measurements of the lift force at elements spaced only 2 diameters apart can be 180° out of phase, i.e. the correlation length may be less than 2 diameters.

Evidently the random nature of vortex shedding and associated lift forces in oscillatory flow is a complex problem. From the point of view of dynamic analysis of structures Verley (1982) and Bearman et al. (1984) proposed expressions for the transverse force incorporating the effect of vortex shedding and wake return.

2.1.7 Surface roughness

Marine growth is important because it increases the effective diameter-mass and changes the roughness of the surface, and because it is thickest in the uppermost region of the structure where the wave motions are largest.

Sarpkaya

Sarpkaya (1976b) carried out a series of experiments with sand roughened cylinders in a harmonically oscillating flow. These experiments show that the effect of surface roughness on the drag and inertia coefficients is quite marked.

For low Re the drag coefficient did not significantly differ from that of a smooth cylinder. However, the drag coefficient at the critical Re increased with increasing relative roughness. The critical Re also decreased with increasing relative roughness. At larger values of Re the drag coefficient increased sharply to a nearly steady value, considerably higher than that for the smooth cylinder.

The inertia coefficient for a given relative roughness rises rapidly to a maximum at a Re which corresponds to that at which C_D drops to a minimum. At higher Re the inertia coefficient decreases to an almost constant value which is lower than for the smooth cylinder.

Concerning the lift coefficient for the roughened cylinder Sarpkaya found that the smooth cylinder data at relatively low values of β more or less form the upper limit of the rough cylinder data.

Sarpkaya and Isaacson (1981) suggest that the influence of roughness on the drag coefficient, as compared to a smooth cylinder, is to increase the strength of the vortices, to increase the correlation length, and also to decrease the separation angles. They also state that the noted counter variation of C_D and C_M is a consequence of the use of Morison's equation with time-invariant coefficients and not a fluid mechanical phenomenon.

Gaston and Ohmart

In order to study the effects of roughness Gaston and Ohmart (1979) carried out experiments on a vertical cylinder subjected to waves with calculated kinematics. They reported that the drag coefficient was significantly affected by surface roughness, being approximately double the value for rough cylinders as for smooth cylinders. They also reported that a further increase in roughness had less effect than the initial change from smooth to rough cylinder.

The inertia coefficient was computed using a 60 degree region (60 to 120 degrees) before the crest where the inertia forces were at a maximum. This inertia coefficient was less sensitive to surface roughness, being just a little higher than for smooth cylinders.

2.1.8 Effect of current

The conventional way of including the effect of current into the wave force calculations is to add the current profile vectorially onto the wave motion obtained under no-current conditions.

Sarpkaya and Storm

Sarpkaya and Storm (1985) examined the hydrodynamic forces for cylinders moving at a constant velocity in a sinusoidally oscillating flow. They found that Morison's equation, with force coefficients obtained under no-current conditions, is not applicable to the prediction of wave and current induced loads on circular cylinders. Particularly in KC range of about 8 to 25, the inertia coefficient increased and the drag coefficient decreased with increased relative current due to the effect of the current on the wake. This was the case for both smooth and rough cylinders. They also found that for KC larger than about 30, the effect of current on the force coefficients and on the calculated in-line force is negligible.

2.1.9 Summary of data

Table 2.1 gives a summary of the majority of reported investigations together with the range of Re and KC for which they apply. Due to the variation in experimental arrangement, geometries, wave theories, method of data analysis, experimental errors, etc., the scatter in the reported force coefficient is large. Consequently it is difficult to recommend or specify single values of force coefficients to be used.

Most of the reported investigations, particularly those performed in wave tanks, are made at low Reynolds number ($Re < 10^5$). For such Re there is a large variation of C_D, C_M and C_L for both Re and KC. However, for Re greater than about $2 \cdot 10^5$ the dependence of C_D, C_M and C_L on Re and KC is weaker. Sarpkaya (1976) reports that C_D, C_M, C_L gradually approaches 0.6, 1.75 and 0.2 respectively for $Re > 10^5$-10^6.

Table 2.2 summarizes the influence of various parameters on the force coefficients.

To get an idea of the order of Re and KC to be considered in the design of slender offshore structures two wave situations are studied, see Table 2.3.

Table 2.3 indicate that very high Re can be expected, and also that $Re < 2 \cdot 10^5$ are not common in design situations. The table also shows that a large variation of KC may be expected ($0.1 < KC < 1200$), depending on the diameter of the structure.

As discussed below, Morison's equation works quite satisfactorily outside $8 < KC < 30$, where one of the force components is the dominant one.

Table 2.1 Summary of Data from most of the reported investigations.

Reference	Test Structure	Location, Particulars (Length, width, depth)	Wave theory Meth. of evaluation	$Re \cdot 10^4$	KC	C_D	C_M	C_L
PLANAR OSCILLATING FLOW								
Keulegan and Carpenter (1958)	Horiz. cyl. smooth D=1.3-7.6 cm	Wave basin (L, 0.52, 0.70 m)	Linear Fourier	0.7-3	2.7-119.9	0.70-2.36	0.70-2.60	-
Sarpkaya (1976a,b)	Horiz. cyl. D = 5.1-16.5 cm	U-tube cross section 0.91 by 0.91 m	Fourier					
		Smooth		0.5-50	2.5-200	0.5-2.40	0.65-2.05	0.2-3.4
		Rough			(9-60)			
		k_s/D=1/800-1/50				0.6-1.9	1.0-1.98	0.3-3.4
Garrison et al. (1977)	Sinusoidal osc. horiz. cyl. smooth D = 5.1-11.4 cm	Water channel (4.88, 0.58, 1.22 m) Still water	Least squares	1-30	6-35	0.4-1.9	0.6-1.95	-
Maull, Milliner (1978)	Horiz. cyl. smooth D = 2.5-3.8 cm	U-tube cross section 0.45 by 0.45 m	r.m.s.tech.	(0.4	6-28	1.45	2.0	
Bearman, Graham (1979)	Horiz. cyl. smooth D = 3.97 cm	U-tube cross section 0.61 by 0.61 m	Fourier	(4	3-70	1.4-2.05	0.8-1.7	
Rodenbusch, Källström (1986)	Osc. vert. cyl. D = 1.0 m	Basin (88, 39, 3.5 m)	Least squares					
		Smooth		(200	0-90	0.3-0.9	1.4-2.2	
		Rough				0.55-1.95	0.7-2.3	
Bearman, Downie et al. (1985)	Horiz. cyl. smooth D = 2.56-7.48 cm	U-tube cross section 0.61 by 0.61 m	Fourier	0.03-1.7	0.1-10	0.7-4.0	0.95-2.15	
Sarpkaya (1986)	Horiz. cyl. smooth D = 2.5-7.7 cm	U-tube cross section 0.92 by 1.45 m	Fourier	0.04-24	0.4-22	0.5-2.1	0.7-2.1	
WAVY FLOW								
Morison et al. (1950)	Vert. cyl. smooth D = 2.5 cm	Wave tank (L, W, 0.6 m) Force meas. - Moment at one end	Linear zero vel. and acc.	0.22-1.11	-	1.626±0.414	1.508±0.197	-
Bidde (1971)	Vert. cyl. smooth D = 4.1-15.2 cm	Wave tank (30.5, 0.3, 0.9 m) Force meas. - Total force at one end	Linear	0.08-3.7	0.9-20.4	1.0-2.4	-	0.2-1.5
Isaacson, Maull (1976)	Vert. cyl. smooth	Wave tank (17.8, 0.6, 0.8 m) Force meas. - Total force at one end + pressure meas.	Linear Fourier r.m.s.tech.	0.1-1.0	5-20	-	-	0.1-1.7

continued

Reference	Test Structure	Location, Particulars (Length, width, depth)	Wave theory Meth. of evaluation	$Re \cdot 10^4$	KC	C_D	C_M	C_L
Chakrabarti et al. (1976)	Vert. cyl. smooth D = 7.6 cm	Wave tank (76, 10, 3 m) Force meas. - Total force at one end + at two sect. (0.3 m long)	Linear Least squares	(2.8	0-16	-2.0-2.0	1.5-3.8	
Chakrabarti (1980a)	Vert. cyl. Smooth D = 3.8-7.6 cm	- " -	Stream function Least squares	2-3	0-82	0-2.0	0.5-2.6	
Gaston, Ohmart (1979)	Vert. cyl. D = 0.3 m	Wave tank (104, 3.6, 3.5 m) Force meas. - Total force at one end.	Stream function Least squares - 60° regions					
		Smooth		20-30	-	0.77	1.81 (average)	
		Rough k_s/D = 1/96-1/24				1.34-1.42	1.87-2.01(-"-)	
Ramberg, Niedzwecki (1979)	Vert. (Horiz) cyl. Smooth D=2.5 cm	Wave tank (30.5, 1.2, 1.1 m) Force meas. - Force gages at each end	Linear Least squares	0.4-0.56	6-18	0.11-0.63	0.58-0.76	0.06-0.35 (r.m.s)
Stansby, Bullock Short (1983)	Vert.cyl. Smooth	Wave tank Force meas. - On a small section	Measured- Laser Doppler Anemometer Least squares	0.4-0.75	5-24	0.7-2.2	0.7-2.0	
Dawson (1985)	Vert.cyl. Smooth D = 5 cm	Wave tank (116, 7.9, 4.9 m) Force meas. - Force gauges at one end.	Stokes' 2nd Short segm.	≅1	3-40	1.2	1.8	
Törum (1985)	Vert. cyl. Smooth D = 6 cm	Wave basin (80, 50, 3 m) Force meas. - 26 force transducers c/c≧5 cm	Stokes' 2nd Least Squares	1.5-6	10-55	0.8-1.3	1.4-1.6	
Bearman, Chaplin et al. (1985)	Vert. cyl. Smooth D = 0.5 m	Wave tank (230, 5, 5) Force meas. - at two sect. (0.25 m long) + pressure meas.	Measured Colebrook Electro-magnetic flowmeters Fourier	14.6-50.5	4-21	0.1-0.65	1.4-1.9	
Present test	Vert.cyl. Smooth D=0.3 m	Wave tank (80, 2, 0.8) Force meas.- Force gauges at one end + pressure dist. at 6 levels	Measured Micro propeller Stokes' 5th Cnoidal Least squares r.m.s. tech. max.vel. and acc. zero and max.force short segments	3-23	1-11	0.7-1.4	0.7-2.2	
OCEAN EXPERIMENTS								
Bishop (1982)	Vert. columns D = 0.48, 2.8 m	Depth 9 m Force meas.at 5 levels (3 presented)	Measured Perforated ball r.m.s. tech.	20-200	2-40	0.5-1	1.4-2	

Table 2.2 Effect of various parameters on force coefficients.

In-line and transverse forces	C_D, C_M, C_L = f(KC,Re) for Re $<$ 10^5-10^6, see Fig. 2.2, 2.6
	$C_D, C_M, C_L \cong$ 0.6, 1.75, 0.2 resp. for Re $>$ 10^5-10^6, see Figs. 2.2, 2.6
Surface roughness	increased C_D, decreased C_M } about critical Re
Current	decreased C_D, increased C_M } for 8 $<$ KC $<$ 25
Orbital motion	decreased C_D, increased C_M } rel. to those in planar oscillatory flow

Table 2.3 Range of Re and KC for slender structures for the average apparent wave (D=0.1-6.8 m) and 100 year wave (D=0.1-75 m) in the North sea. (Fifth order theory).

Average apparent wave (H_s=2.95 m, T_z=4.5 s)	S.W.L.	15 m below S.W.L.
Re	$2 \cdot 10^5$-$1 \cdot 10^7$	$1 \cdot 10^4$-$8 \cdot 10^5$
KC	1.8-120	0.1-7
100 year wave (H=30 m, T=15 s)		
Re	$6 \cdot 10^5$-$5 \cdot 10^8$	$4 \cdot 10^5$-$3 \cdot 10^8$
KC	1.6-1200	1-720

The findings of Bearman, Chaplin et al. (1985) (wavy flow) and those by Rodenbusch and Källström (1986) confirm that the findings of Sarpkaya (1976a) at high Re should be representative in design, see Table 2.4. This table also gives the values of C_D and C_M recommended by Det norske Veritas (DnV). The recommended values give a conservative estimate of wave forces.

Table 2.4 Comparison of results at high Re which may be used in design. DnV recommended values are also given.

	C_D	C_M	C_L
Sarpkaya (1976a) $Re > 10^5 - 10^6$	0.6	1.75	0.2
Bearman, Chaplin et al. (1985) $1.46 \cdot 10^5 < Re < 5.05 \cdot 10^5$, $KC > 15$	$\cong 0.6$	$\cong 1.5$	
Rodenbusch, Källström (1986) $Re < 2 \cdot 10^6$	0.7 $(KC > 40)$	decrease from 2.0 to 1.6 as KC increase from 0 to 90	
DnV (March 1981) (5th order theory)	0.5-1.2 > 0.7 at high Re	2 ($D/l \leqq 0.1$)	

In conclusion, Sarpkaya's results established from planar sinusoidally oscillating flow are highly consistent. However, further experiments in waves at high Re, such as those performed by Bearman, Chaplin et al. (1985) are needed for the calculation of wave forces with sufficient accuray in design situations. Reported experiments performed at low Re are also valuable for the understanding of the mechanism behind time dependent separated flow around a vertical cylinder.

2.2 Morison's equation

The force exerted by surface waves on a vertical cylinder may, as suggested by Morison et al. (1950), be divided into two force components. One of these, the drag force, is in phase with the fluid velocity while the other, the inertia force, is in phase with the fluid acceleration. It is assumed that these forces are independent and that their effect can be added to obtain the total force on the body. It is also assumed that the cylinder diameter

is small relative to the wave length, and that scattering effects are negligible. Therefore the body has a negligible effect on the waves, so that the applicable velocities and accelerations are those calculated as if the body were absent.

The drag force on a cylinder is mainly due to the pressure difference across the cylinder. This pressure difference is caused by separation of the flow from some point on the cylinder surface which creates a low pressure region behind it. The position at which separation occurs, the way in which it occurs, and the resultant wake width all influence the pressure difference and thus the drag force.

Analogous to steady flow, the drag force is taken to be proportional to the square of the instantaneous fluid velocity (u). One of the major differences between wave motion and steady flow is that the fluid is swept back past the cylinder each time the flow reverses. These effects are accounted for in the emperical drag coefficient used, C_D.

The drag force per unit length may be written as

$$F_D = \frac{1}{2} \rho C_D A u|u| \qquad \ldots \quad (2.3)$$

where

F_D = drag component of force
C_D = drag coefficient
ρ = density of water
A = characteristic area
u = water particle velocity

The inertia force is due to acceleration of the ambient flow. The acceleration is caused by a pressure gradient in the fluid which acts on the volume (V) displaced by the cylinder. The resulting force on the cylinder may be considered to be made up of two parts. The Froude-Krylov part of the inertia force is due to the undisturbed press-

ure field which would exist on the body boundary in the absence of the body. This force has a similar form to the buoyancy force acting on a submerged body, and is given by the mass of fluid displaced by the element times the acceleration, $\rho V \cdot \frac{\partial u}{\partial t}$. However, the fluid in the wave must encircle the cylinder, and thus additional accelerations are involved. This imposes a force on the cylinder given by $m_a \frac{\partial u}{\partial t}$, where m_a is termed the added mass. The total inertia force on the cylinder becomes

$$F_M = (\rho V + m_a) \frac{\partial u}{\partial t} \qquad \ldots (2.4)$$

where

F_M = inertia component of force
V = immersed volume
m_a = added mass
$\partial u/\partial t$ = water particle acceleration

Introducing an empirical inertia or mass coefficient C_M defined as

$$C_M = 1 + \frac{m_a}{\rho V} = 1 + C_m \qquad \ldots (2.5)$$

where

C_m = added mass coefficient

Eq. (2.4) may be written as

$$F_M = C_M \rho V \frac{\partial u}{\partial t} \qquad \ldots (2.6)$$

The added mass part of the inertia force is dependent on the form of the wake in the separated flow. However, in ideal flow m_a is equal to ρV for a circular cylinder and thus the inertia coefficient in Morison's equation will take the value of 2.

The total force according to Morison et al. is obtained by adding drag and inertia forces. Thus Morison's equation becomes

$$F = F_D + F_M = \frac{1}{2} \rho C_D A u|u| + C_M \rho V \frac{\partial u}{\partial t} \quad \ldots (2.7)$$

In the simplest application of Morison's equation the wave kinematics may be described using linear theory. The wave profile, η, horizontal particle velocity, u, and acceleration $\partial u/\partial t$ are given by

$$\eta = a \sin (kx - \omega t) \quad \ldots (2.8)$$

$$u = \frac{agk}{\omega} \frac{\cosh k(y+d)}{\cosh kd} \sin(kx-\omega t) \quad \ldots (2.9)$$

and

$$\frac{\partial u}{\partial t} = -agk \frac{\cosh k(y+d)}{\cosh kd} \cos(kx-\omega t) \quad \ldots (2.10)$$

respectively, where a is the wave amplitude, d is the still water depth, $k=2\pi/L$ is the wave number and $\omega=2\pi/T$ is the angular frequency with L for wave length and T for wave period.

The total force on a vertical cylinder piercing the water surface is obtained by integration of the elemental forces between the bottom and the water surface. However, the assumptions of small amplitude waves in linear theory make the Eqs. (2.9 - 2.10) valid up to the still water level only. Nevertheless, the error introduced by calculating the force from linear theory above the still water level is less than that obtained by completely omitting the same force.

The total horizontal force on a vertical cylinder becomes

$$F=F_D+F_M=\frac{1}{2} \rho C_D D \int_{-d}^{\eta} u|u| dY + \rho \frac{\pi D^2}{4} C_M \int_{-d}^{\eta} \frac{\partial u}{\partial t} dY \quad \ldots (2.11)$$

where

Y is a vertical coordinate along the axis of the cylinder.

and η the instantaneous level of the water surface.

In the expression given above, the drag and inertia coefficients are assumed to be constant over the length of the cylinder. This assumption is necessary if their vertical variation is unknown.

The total wave force is finally obtained by substituting Eqs. (2.9 - 2.10) into Eq.(2.11) and calculating the integrals:

$$F_D = \frac{1}{4} \rho C_D D a^2 g \frac{\sinh 2k(\eta+d)+2k(\eta+d)}{\sinh 2kd} \sin\omega t|\sin\omega t| \quad \text{and} \quad \ldots (2.12)$$

$$F_M = \rho\frac{\pi D^2}{4} C_M ag \frac{\sinh k(\eta+d)}{\cosh kd} \cos\omega t \quad \ldots (2.13)$$

respectively.

The wave force for three different wave situations according to Morison's equation with the use of linear theory (Eqs. (2.8), (2.12) and (2.13)) is compared with the total measured force as described in Chapter 6, see Figs. 2.8 a-c. Wave A applies to deep water, wave B to transitional water depth and finally wave C to shallow water. It can be seen that Morison's equation succeeds fairly well in predicting the wave force and its time variation, except for shallow water.

2.2.1 Relative importance of drag and inertia force components

The ratio of drag to inertia force may be expressed by the Keulegan-Carpenter number (KC), defined as

$$KC = \frac{u_m \cdot T}{D} \quad \ldots (2.14)$$

where

u_m = maximum horizontal particle velocity in a wave cycle

T = period of the wave cycle

D = diameter of cylinder

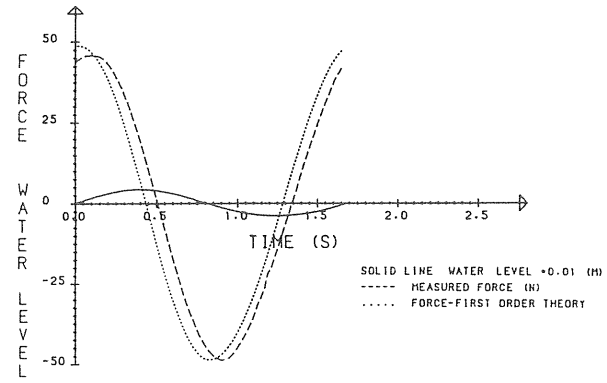

Figure 2.8 a WAVE FORCE. Wave A. "Deep water". Wave characteristics are given in Table 4.1. C_D=1.0. C_M=2.0, KC=1.0.

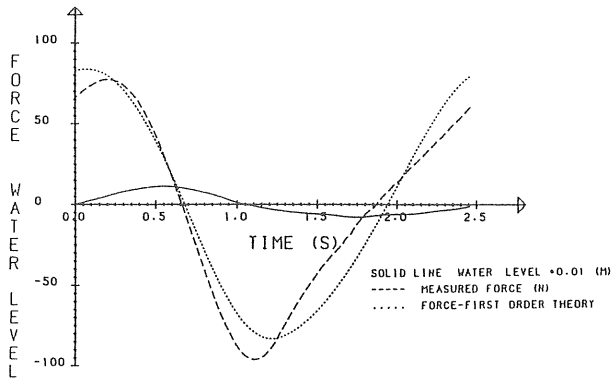

Figure 2.8 b WAVE FORCE. Wave B. "Transitional water". Wave characteristics are given in Table 4.1. C_D=1.0, C_M=2.0, KC=4.2.

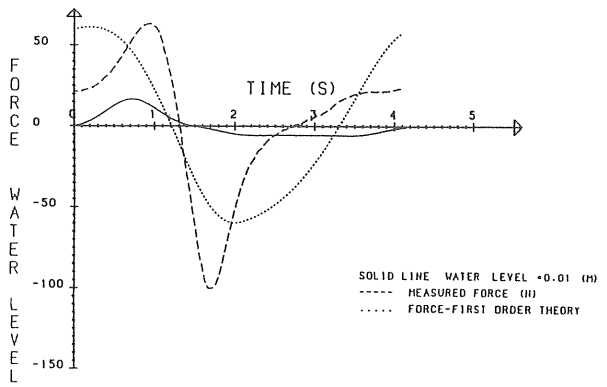

Figure 2.8 c WAVE FORCE. Wave C. "Shallow water". Wave characteristics are given in Table 4.2. C_D=1.0, C_M=2.0, KC=9.0.

This parameter may be seen as the ratio of the length of the water particle path to the cylinder diameter. KC may also be seen as representing the time for development of the wake compared with the time available, representing the number of vortices shed in half a cycle.

By using the maximum velocity according to linear theory (Eq. (2.9)), KC along the vertical cylinder is given by

$$KC = \frac{agkT}{\omega D} \frac{\cosh k(y+d)}{\cosh kd} =$$

$$= \frac{2\pi a}{D} \frac{\cosh k(y+d)}{\sinh kd} \qquad \ldots (2.15)$$

The ratio of maximum drag force to maximum inertia force along the vertical cylinder, given by Morison's equation is

$$\frac{F_D \text{ max}}{F_M \text{ max}} = \frac{C_D \, 2a}{C_M \pi D} \frac{\cosh k(y+d)}{\sinh kd} \qquad \ldots (2.16)$$

Finally the ratio of maximum drag force to maximum inertia force in harmonic flow is obtained by substituting Eq. (2.15) into Eq. (2.16). We get

$$\frac{F_D \text{ max}}{F_M \text{ max}} = \frac{KC}{\pi^2} \frac{C_D}{C_M} \qquad \ldots (2.17)$$

From Eq. (2.17) with $C_D = 1.0$ and $C_M = 2.0$ it is seen that for KC greater than $2\pi^2 \cong 20$ the drag force is the predominant force and for KC less than 20 the inertia force is the predominant force. For KC less than about 8 the inertia force dominates and for KC greater than about 30 the drag force dominates.

Outside $8 < KC < 30$ the assumption of Morison et al., in obtaining the force from a linear-quadratic sum, is not so critical because one of the force components dominates over the other. Also, since Morison's equation yields no information about transverse forces, its applicability

should be better in regions where the vortex activity is less dominant. As reported by Bearman (1985) no or just few slightly asymmetrical vortices may be found in half a cycle for KC less than about 7. For higher KC, say KC > 30, many vortices are developed per half cycle and the flow should fairly well resemble that behind a cylinder in a steady unidirectional stream. Sarpkaya (1981, 1985) states that Morison's equation does not apply uniformly well to all KC with constant averaged force coefficients. The equation seems to be best adapted to the range of KC smaller than about 8 and larger than about 25, where the complex problem associated with the motion of a few vortices is not pronounced.

2.2.2 Improvements of Morison's equation

Attempts have been made to improve the wave force calculation by devising new equations (see Barnouin et al. (1979), Horton and Rish (1981)). However, no satisfactory results have been obtained. It appears that it would be difficult not to consider the linear-quadratic sum in Morison's equation, since it gives reliable results outside the KC range of about $8 < KC < 25$. Thus it is preferable to attempt to improve the existing equation rather than to devise new ones.

Morison's equation was proposed as a tentative solution to a complex problem. The equation does not consider the complex interaction between flow and structure in a time-dependent flow. The assumptions not directly considered with Morison's equation are the effects of separation, strength of vortices, wake width, transverse forces, spanwise correlation (Chapter 5.2.2), unsteadiness of the force (only considered in the variation of u and $\frac{\partial u}{\partial t}$), orbital motion, free surface effects, flow history which influences the flow around the cylinder and which may also cause cycle to cycle variation, roughness, etc., etc. Thus one cannot expect that two time-invariant averaged coefficients together with a linear-quadratic force

equation will represent the time dependent force, particularly when a small number of pronounced vortices characterize the flow, as is the case in KC range of about $10 < KC < 25$. As will be seen in Chapter 7, both C_D and C_M exhibit large variations during any given wave cycle.

Improved wave force calculation, giving fewer limitations and greater power of prediction requires physical insight into the coupled interaction between time dependent flows and structures. A three-dimensional numerical model which accounted for the development and motion of vortices would be ideal. However, this meets with numerous difficulties. Since no satisfactory fluid-mechanical methods have been developed, even for the simplest oscillating flow, to give the position of the mobile separation, to describe the wake, to account for the time dependent boundary layer and to model the rate of decay of circulation, the use of a numerical model is not yet possible.

This leaves us with two possible methods for improving Morison's equation in the drag and inertia dominated regions. The first possibility is to improve Morison's equation by analysing the residue between measured and calculated force as has been done by Keulegan and Carpenter (1958) and by Sarpkaya (1981a,b). The second is to incorporate the effects of vortex shedding and wake return on the inline and transverse forces. Work along such lines has been carried out by Sarpkaya (1976a, 1981b), Bearman et al. (1981, 1984) and Verley (1982). Here the main problem is to quantify the random nature of vortex shedding. The lack of consistent spanwise correlation also makes the variability of the transverse forces difficult to describe. Only the first of these two possible means of improving Morison's equation is accounted for below.

Keulegan and Carpenter

In the paper by Keulegan and Carpenter (1958), where the

first systematic Fourier averaged drag and inertia coefficients and KC were performed and introduced, improvements of Morison's equation were considered. In fact the original purpose of the authors was to improve Morison's equation for a truer representation of force when considering the coefficients constant throughout the wave cycle.

Keulegan and Carpenter assumed that the flow varied harmonically and that the velocity variation through the cycle was given by

$$u = -u_m \cos \omega t \qquad \ldots (2.18)$$

where

u_m = maximum velocity

$\omega = \frac{2\pi}{T}$

T = wave period

Substituting Eqs. (2.14), (2.18) and $\theta = \frac{2\pi t}{T}$ into Morison's equation (Eq. (2.7)) gives

$$\frac{F}{\rho u_m^2 D} = \frac{\pi^2}{2KC} C_M \sin\theta - \frac{C_D}{2} |\cos\theta| \cos\theta \qquad \ldots (2.19)$$

As accounted for in Appendix 3, the coefficients are calculated from Eq. (2.19) by considering the first component in the Fourier analysis. The coefficients thus obtained are averaged over the wave cycle. With the use of these Fourier averaged coefficients the residue is calculated between the measured force and the one given by Eq. (2.19). The residue (ΔR) has the value

$$\Delta R = A_3 \sin 3\theta + A_5 \sin 5\theta + \ldots + B_3' \cos 3\theta + B_5' \cos 5\theta + \ldots \qquad \ldots (2.20)$$

Like the drag and inertia coefficients, A_3, B_3', A_5 and B_5' were also found to be functions of KC.

Eq. (2.19) may now be written

$$\frac{F}{\rho u_m^2 D} = \frac{\pi^2}{2KC} C_M \sin\theta - \frac{C_D}{2} |\cos\theta|\cos\theta + \Delta R \quad ..(2.21)$$

where C_M and C_D are constant.

By evaluating the residue (ΔR) and combining it with Morison's equation a considerable improvement of the wave force calculation is obtained. The obvious disadvantage of using a residue ΔR as given by Keulegan and Carpenter is that the force calculations now require more than two force coefficients. To be able to account for most of the phenomena governing the KC range of $10 < KC < 25$, six coefficients probably have to be used, namely C_D, C_M, A_3, B_3', A_5 and B_5'. Bearing in mind the difficulties of obtaining a consistent set of C_D and C_M values, the determination of, say, six coefficients for the parameters characterizing time dependent flow is a very difficult task.

Sarpkaya

Sarpkaya (1981a,b) revised Eq. (2.21) by relating the coefficients of the additional terms of the residue to the C_D and C_M coefficients. Through a spectral analysis of the residue Sarpkaya showed the varying degree of importance of harmonics from 2 through 15. The author found that the third and fifth harmonics were far more important than the remaining ones. Consequently the modification of Morison's equation achieved by minimizing the residue should involve the third and the fifth harmonics. This finding justified to some extent the assumption of Keulegan and Carpenter of flow symmetry ($F_{(\theta)} = -F(\theta+\pi)$) and the use of just odd harmonics of the fundamental.

Sarpkaya was able to show unique functions of the residue

involving the third and the fifth harmonics to KC for both smooth and rough cylinders. The ranges of KC and Re studied were about 4 to 100 and $3 \cdot 10^3$ to $1.5 \cdot 10^6$, respectively.

The revised Morison's equation was written

$$\frac{2F}{\rho D u_m^2} = \frac{\pi^2}{KC} C_M \sin\theta - C_D |\cos\theta| \cos\theta + T_3 + T_4 \quad \ldots (2.22)$$

where

T_3 = term including third harmonics

and

T_4 = term including fifth harmonics

In Eq. (2.22) T_3 and T_4 decrease rapidly for KC smaller than about 7 and larger than about 20.

Outside this region where mainly drag or inertia forces are predominant, Eq. (2.22) reduces to the original two-term Morison's equation.

Sarpkaya found the prediction of Eq.(2.22) to be as good as if experimental values had been used. The author clearly states that no functional relationship representing the residue can provide a better correlation between the measured and calculated force. However, the usefulness of a four-term Morison equation as given in Eq. (2.22), is somewhat restricted. The equation is based on experiments conducted in planar oscillating harmonic flow, where the spanwise coherence of vortices is as perfect as possible. In general, a deviation from two-dimensional flow results in decreasing correlation length which smoothens the effects of the vortex shedding and makes the prediction of the original Morison's equation more credible. From a practical point of view the modified Morison equation should be restricted to three terms because of all uncertainties introduced by three-dimensional flow.

In summary, Morison's equation, proposed as an approxi-

mate solution, works quite satisfactorily in the drag and inertia dominated regions. The large deviation present in the KC range of about 8 to 25 may be minimized by improving Morison's equation with additional terms as proposed by Sarpkaya and by Keulegan and Carpenter. Because of all phenomena behind the wave force in separated flow, and because Morison's equation works as well as it does, it is unlikely that an entire new equation will replace it in the foreseeable future.

3. THE MEASURING ARRANGEMENTS

The aim of this chapter is to give a general survey of the experimental setup. A short presentation is given of how the experiments were arranged. For further information about the accuracy of the measurements see Appendix 2.

The chapter begins with a description of the wave tank and the cylinder itself. Thereafter the experimental equipment, such as pressure transducers and different types of gauges, are described. Then follows a discussion about the data processing system and the pressure synchronization with its wave train averaging technique. The chapter is concluded with a description of the system for measuring water velocity, partly developed in our hydraulics laboratory.

3.1 Wave tank and cylinder

The experiments were carried out in a wave tank 80 m long, 2.0 m wide, and with a maximum water depth of 1.0 m, see Fig. 3.1. The wave generator in the tank consists of a flat plate constrained to go parallel with the bottom in a harmonic motion. The construction allows for an amplitude of motion near the bottom from virtually nil to as great as that near the surface.

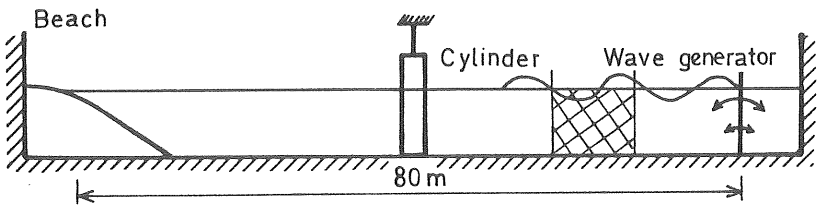

Figure 3.1 Elevation of the wave tank with beach, experimental cylinder and wave generator. (Not to scale).

With this wave generator it was possible to produce regular waves with wave lengths of between 1 and 11 m. The downstream end of the tank has an energy absorbing beach designed to minimize reflection.

The vertical circular cylinder was placed in the middle of the wave tank, 38.5 m from the wave blade. The cylinder shown in Fig. 3.2 has a diameter of 0.3 m and a height of 1.0 m. It is made of steel, and was designed to give a slightly negative gravity force.

Experimental arrangement

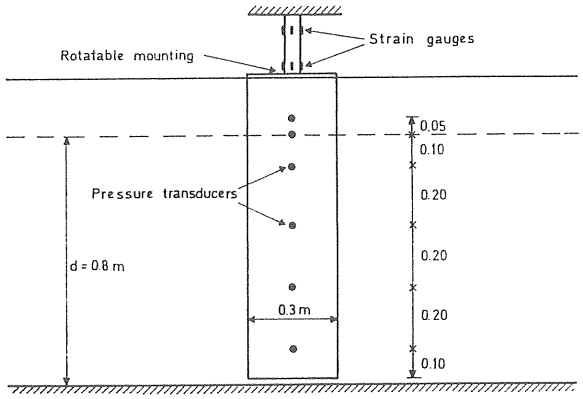

Figure 3.2 The cylinder with the transducers.

The cylinder was hung up in a gauge cantilever. The bottom of the cylinder was placed as close as possible to the bottom of the wave tank without touching it.

3.1.1 Gauge cantilever

The cantilever was equipped with strain gauges at two elevations and in two directions, see Fig. 3.2. The cantilever was clamped to a stiff heavy frame mounted across the top of the wave tank.

The system described above (cylinder and cantilever) can be regarded as a beam clamped in one end. A force acting on the cylinder results in a greater bending moment at the upper pair of strain gauges than at the lower pair. On the basis of the distance between the pairs of strain gauges, they were calibrated so that the magnitude and line of action of the force acting on the cylinder could be assessed, see Chapter 6.1.3.

The cantilever was made of solid aluminium, as a compromise between the need to minimize the motions at the free end of the cylinder and to receive as large electrical signals as possible. For the design force (± 500 N), the maximum amplitude of the free end of the cylinder was measured to be 0.0025 m. Since the maximum force in the test runs was about 1/5 of the design force it was judged that this motion had very little effect on the hydrodynamic forces.

3.2 Pressure measurements

In order to measure the pressure distribution above the still water level, the transducers had to:

- be able to work in two media (water-air)
- respond very fast to changes in pressure
- be small in order not to disturb the flow and to obtain the pressure at a specific point.

Pressure transducers that met the requirements with a diameter of 3.84 mm were found.

For practical reasons the cylinder was equipped with six such pressure transducers. The transducers were mounted flush with the surface in a vertical line, see Fig. 3.2. Depending on the water depth, the uppermost pressure transducer was placed 0.05 or 0.15 m above the still water level. In all the experiments, one of the transducers was placed exactly at the still water level.

The pressure distribution for the whole circumference of the cylinder was measured by rotating the cylinder through 22.5 degree increments between experiments, see Fig. 3.3. With 22.5 degree increments, 16 experiments were required to determine the pressure distribution around the cylinder,

which was obtained at six levels. The total wave force on the cylinder was then obtained by integrating the pressure distribution over the depth and the circumference of the cylinder, see Chapter 6.

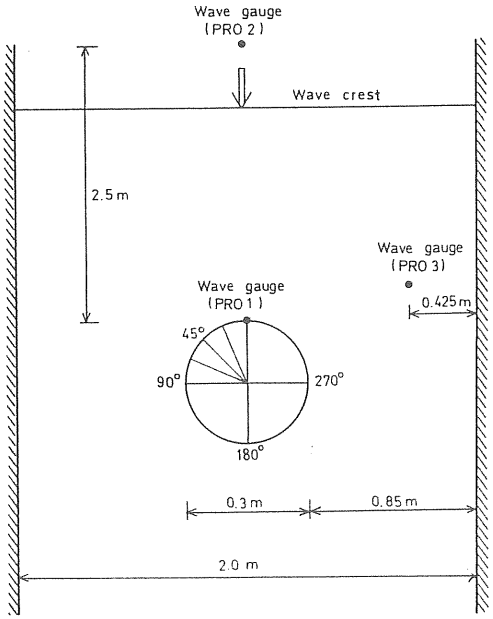

Figure 3.3 The pressure distribution was obtained by rotating the cylinder in 22.5 degree increments. The positions of the wave gauges are also shown. (Not to scale).

The accuracy of integration of the pressure distribution depends on the reproducibility of the chosen wave, as the circumferential distribution is gathered from separate experiments. To obtain the best possible agreement among the different experiments it became very important to start the recording at the corresponding wave in each wave train, see Fig. 3.4.

It also became very important to have a completely calm water surface before the next run was started, despite this the individual waves in a wave train were found to vary somewhat. However, the wave length was found to be almost constant. The problem concerning the varying waves was solved by averaging four to six waves in a wave train,

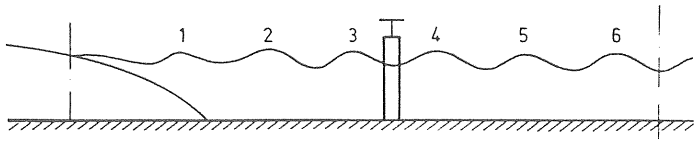

Figure 3.4 Schematic illustration of an advancing wave train.

assuming a constant wave length. As an initial parameter for this averaging procedure one wave gauge (PRO3) was used, see Fig. 3.3. For further details about the wave train averaging and integration technique, see Chapter 3.5.2.

3.3 Wave gauges

To be able to obtain the pressure distribution near the water surface the cylinder was equipped with a wave gauge (PRO1). It was placed very close to and slightly to one side of the line of pressure transducers, see Fig. 3.3. The wave gauge consisted of four parallel thin wires (ø = 0.2 mm) made of stainless steel. It was estimated that these thin wires would not have any significant effect on the water flow near the pressure transducer.

This wave gauge made it possible

- to obtain a good picture of the pressure distribution near the water surface, when the signal of the uppermost submerged transducer was used together with the measured water level, see Chapter 6.

- to handle the problems of signal offset that occurred when the pressure transducers went from one media to another (air-water), see Appendix 2.

This wave gauge always made it possible to define when the relative pressure was zero, i.e. when the pressure transducers were in air. The pressure above the uppermost submerged transducer was assumed to decrease linearly up to the water level measured. For further details, see Chapter 6.

Two additional wave gauges were used. One was used (PRO3) as a start parameter for the averaging procedure described in Chapter 3.5.2. This wave gauge was placed in line with the front of the cylinder, facing the wave generator, see Fig. 3.3. The last wave gauge (PRO2) was placed 2.5 m in front of the cylinder. It was used to obtain a picture of the undisturbed wave.

3.4 The recording system

The assembly of the data processing equipment for the experimental study, see Fig. 3.5, is described below. The data were recorded on a Compucorp 625M-II desk computer and transferred to an IBM 3081 computer. A graphic terminal was placed in the laboratory and connected to the IBM-computer. This arrangement made it possible:

- to obtain a relatively fast check on the reliability of the measured data by using the graphic display

- to arrange handling and storage of recorded data

- to have great flexibility during the assessment and data processing.

Using a graphic display is especially valuable, as it may be the only realistic way of checking large amount of data. Instead of searching for single anomalous values it is possible to watch for deviations in the displayed graphs which, of course, is much easier.

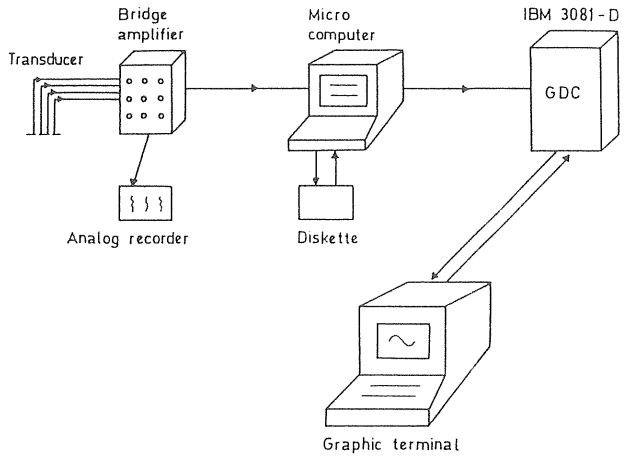

Figure 3.5 Schematic illustration of data processing system.

Furthermore, the use of a graphic display is an excellent tool during the processing and calculating stages. Trends in the data could easily be visualized as they developed during processing.

The signals from the gauges were amplified and fed into the microcomputer, where they were stored on a diskette. After one measuring cycle the data were sent to the central computer (GDC). They were then processed and the results could be shown on the graphic screen.

A Compucorp 625 was used as the recording unit. Altogether 13 channels were used: six for the pressure transducers, three for the wave gauges and four for the strain gauges on the gauge cantilever. The maximum rate of sampling, when 13 channels were used, was 0.021 s. With a maximum recording time of 27 seconds, (6 waves with a period of 4.2 s) 16,700 data points were recorded.

3.5 Pressure synchronisation

All the data in the experimental study were averaged before being used in the calculations. This was necessary

since financial constraints made it impossible to measure all the variables simultaneously, because the individual waves in a wave train varied slightly, see Figs. 3.6 a-c.

As there are numerous flow modes, pressure distribution may differ significantly among different experiments at the same phase in the wave, see Chapter 5. For this reason, extensive efforts must be made to obtain as good correspondence as possible between the different runs.

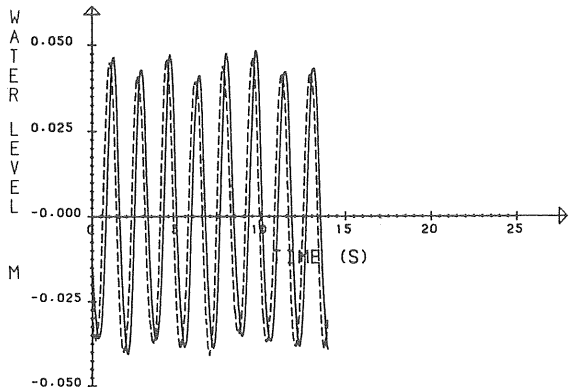

Figure 3.6 a WAVE PROFILE. Wave A. "Deep water"
——— PRO1 - water level at 180° on the cylinder according to Fig. 3.3.
---- PRO3 - water level beside the cylinder.

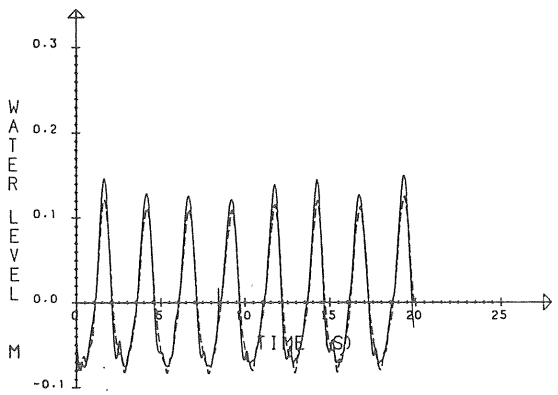

Figure 3.6 b WAVE PROFILE. Wave B. "Transitional water depth"
——— PRO1 - water level at 0° on the cylinder according to Fig. 3.3.
---- PRO3 - water level beside the cylinder.

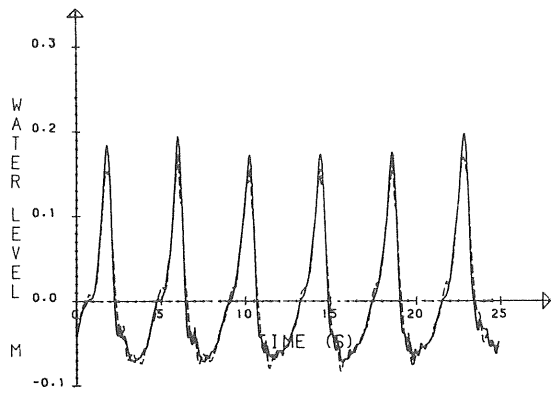

Figure 3.6 c WAVE PROFILE. Wave C. "Shallow water".
——— PRO1 - water level at 22.5° on the cylinder according to Fig. 3.3.
---- PRO3 - water level beside the cylinder.

One way to obtain this correspondence is to have a reference pressure. Then the pressure distribution at different times and at other points can be examined and selections made through conditional averaging. In this selection the resulting pressure distribution corresponds to a single flow mode, as if the distribution had been obtained simultaneously.

Here, good correspondence was brought about by ensuring as constant a flow environment as possible. This was done through measuring the "corresponding" sequences of waves in the wave train and thereafter calculating a wave averaged from those which were measured.

Perhaps the best test of the reliability of using the wave train averaging technique is a comparison between the force obtained from the integrated pressure with that obtained from the strain gauge cantilever, i.e. a comparison of two completely different techniques used for getting the force in the same wave. The wave forces obtained

fit one another well and the total differences between the absolute values did not exceed 4.0% for any of the waves included in the experimental program. This is not absolute proof of reliability, but the good agreement between the two techniques indicates good accuracy. For further details, see Chapter 6 and Appendix 2.

3.5.1 Generating waves

Before describing how the pressures measured in different wave trains were correlated to one another, a few words about the generation of waves are in order. When generating waves over a calm water surface, only a finite number of waves in a wave train can be used. First it is necessary to exclude the first waves arriving at the cylinder, see Fig. 3.4, as it takes a couple of wave-cycles to get waves with approximately constant heights and forms. Second, it is not possible to maintain a constant wave "climate" in the wave tank because, in spite of a good wave-absorbing beach, there are small reflected waves which interfere with the undisturbed waves at the cylinder. The cylinder and the tank wall also cause reflected waves. Finally, there is a sloping mean water level along the tank because of some net transport of energy towards the beach.

3.5.2 Wave train averaging technique

One of the wave gauges (PRO3) was used for correlation of the pressure measured along the verticals in different experiments, Fig. 3.3. This wave gauge was placed in line with the front (facing the wave generator) of the cylinder.

Each experiment began with a completely calm surface. The wave generator was turned on, but the recording was not started until after the excluded waves had passed the cylinder. For the same type of wave train the data recording started on the corresponding wave trough in the wave train. After this, up to 8 waves were recorded with the

microcomputer and transmitted to the central computer. The same procedure was repeated until the pressure distribution for the whole circumference was known.

As the microcomputer scanned over all the channels with a preset and constant time interval, and because the wave length was almost constant, about the same number of data points per wave cycle were measured. As the wave gauge was calibrated to give a zero output signal at the still water level, it was easy to determine whether the water surface was above or below the still water level.

The first positive values found in the data series were then added to the first positive values in the next wave and so on, see Fig. 3.7.

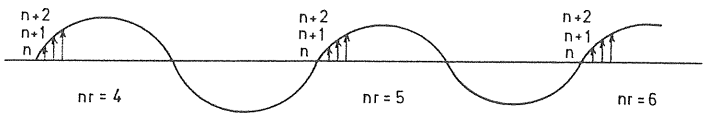

Figure 3.7 Schematic illustration of the wave train averaging technique.

The total was then divided by the number of waves. Because the number of data points per recorded wave was almost constant, no more than three values at the end of the trough were considered less good than the rest. The number of recorded data points per cycle for the waves included in the experimental program was between 62 and 200 (T = 1.3 - 4.2 s).

Examples of some data measured and calculated using the wave train averaging technique corresponding to the data given in Fig. 3.6 are shown in Appendix 1.

3.6 The equipment for measuring water velocities

During the evaluation process it was observed that the wave kinematics, e.g. horizontal particle velocity and acceleration, obtained from different wave theories, varied considerably, see Chapter 4.

In order to study all the variables that enter the formula for calculating wave forces, it is necessary to know the "true" velocity and acceleration. The "true" velocity is especially important since it is used in a quadratic term in the established formula, i.e. Morison's equation, see Chapter 2. Therefore a second test run was carried out in order to measure the undisturbed water velocities in the waves without the cylinder.

During the search for suitable equipment to measure the velocity it was found that the equipment available for this kind of experiment was too expensive or inadequate. For this reason we developed our own equipment.

The technique used was based on a Kent micropropeller which has been examined and employed at ISVA, Techn. Univ. of Denmark, for mean current and turbulence measurements, see Fig. 3.8.

The propeller has five blades. Each time a propeller blade passes a point on the mounting frame, an electric pulse is created. The velocity meter gives an analogue output, which is suitable only for measuring steady or slowly varying flow.

The same type of micropropeller has been used, with good accuracy by Pedersen (1969), Wiuff (1977) and Basco et al. (1982) to measure non-stationary oscillating velocity (recorded analogously or by counting the number of blade passages per unit of time). Pedersen found a frequency response better than 10 to 20 Hz for a 10 mm, 5 bladed propeller in oscillating water. As reported by Basco et al. the startup time for a 5 mm, 3 blade propeller was also well below 20 ms.

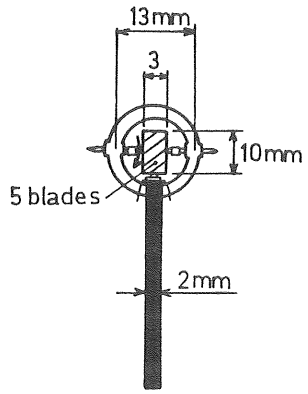

Figure 3.8 Schematic illustration of the micro-propeller current meter.

When the propeller comes above the wave trough, surface tension is sufficient to stop the propeller instantly, as water droplets adhere to the blades. This, plus the good dynamic response, permits measurements of the velocities in the crest section of oscillatory waves.

Wiuff investigated the complex problem of the time response of a propeller in a fluctuating velocity field. He compared the dynamic behaviour of an Armstrong propeller and the micropropeller used (10 mm, 5 bladed) which is smaller and lighter. He found no significant difference in their dynamic behaviour. This fact may be explained by the relatively slow changes in velocities in oscillating water waves. The propeller follows such slow changes easily. All high frequencies are of course filtered out, as the blade passage frequency establishes an upper limit, but this is unimportant as most of the energy is concentrated at low frequencies.

Wiuff also concluded that the uncertainty in measuring the velocity with the 5 bladed propeller is constant, about 2 mm/s and independent of the actual velocity. The propeller used was calibrated for velocities from 0.04 m/s up to 1.00 m/s. In relation to these velocities the

estimated maximum error is ±1% to ±5%, see Appendix 2.

3.6.1 Modified velocity meter

To be able to measure the oscillating horizontal particle velocity, we used the micropropeller described above but exchanged the instrument from an analogue to a digital one. In our system the time interval between the passages of two propeller blades was measured. Calibration curves were established by moving the propeller at a known velocity in stagnant water, see Appendix 2.

As mentioned above, an electrical pulse is created each time a propeller blade passes a point on the mounting frame. The method of treating this electrical pulse is shown schematically in Fig. 3.9.

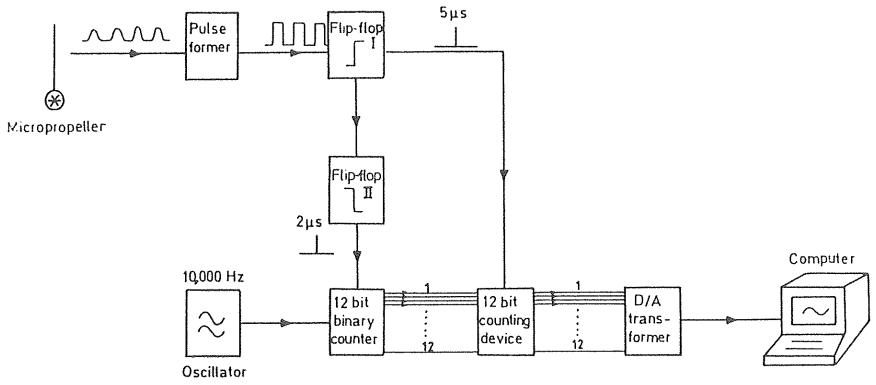

Figure 3.9 Schematic diagram of digitalized velocity records.

An oscillator with a frequency of 10,000 Hz was used as a clock. A 12 bit binary counter was also used, i.e. 4096 positions were available. This means that the maximum time difference between two blades passing a point on the mounting frame is 0.4096 s, which corresponds to a velocity well below the lowest calibrated measurable velocity of 0.04 m/s.

The pulse formed from the micropropeller is fed to flip-flop I which is affected on the positive edge. The output signal from flip-flop I, which is very short (5 μs), is used to make the counting device read the actual status of the 12 bit binary counter. The same pulse feeds flip-flop II, which is affected on the negative edge. The output signal from flip-flop II (2 μs) is therefore always later than the output signal from flip-flop I and is used to set the binary counter to zero. The oscillator, which gives a signal of 10,000 Hz, then refills the binary counter.

To be able to read the actual status of the counting device with the recording unit (microcomputer) a Digital/-Analogue transformer had to be used. This D/A transformer gave an output voltage of zero to 2.5 V, where 2.5 V indicated that the counting device was full, i.e. that 0.4096 s or more had gone by since the last propeller blade passed the trigger point. This analogue signal was then recorded analogously as described in Chapter 3.4, at set time intervals. A more detailed description of the measuring equipment is given by Moberg, Bergdahl and Carlsson (1986).

The modified velocity meter only gave the magnitude and not the direction of the water velocity, see Figs. 3.10 a-c. The direction of the water velocity was obtained by measuring the wave profile simultaneously, using a wave gauge placed in line with the velocity gauge, see Fig. 3.11.

This wave gauge had two functions. First, as described in Chapter 3.5.2, it gave the starting signal for the wave train averaging procedure. Second, it was used to obtain the velocity signal in phase, see Figs. 3.12 a-c. To achieve this in phase, a small computer program was run with the water level as a trigger unit.

As mentioned, the micropropeller was calibrated by moving the propeller at a known velocity in stagnant water. This

was done for velocities from 0.04 m/s up to 1.00 m/s. As seen from Figs. 3.10 a-c it was only possible to measure velocities greater than 0.04 m/s, owing to the changes in

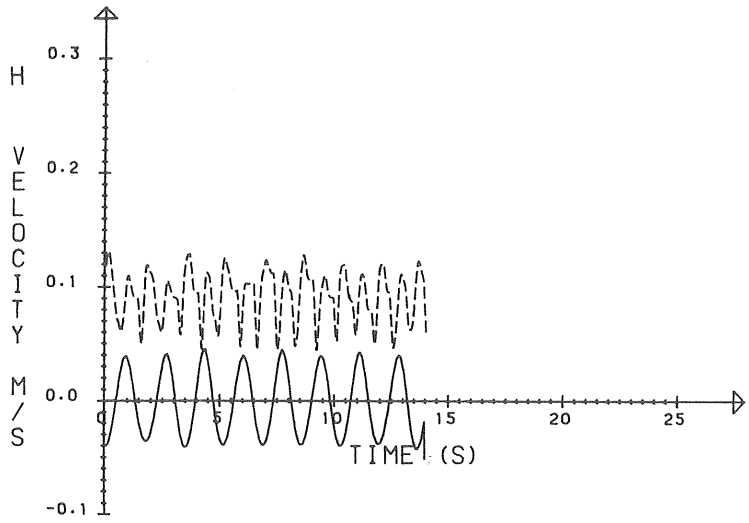

Figure 3.10 a Wave A "Deep water". Measured velocity at 0.7 m below still water level. —— Water level (m). ---- Horizontal velocity.

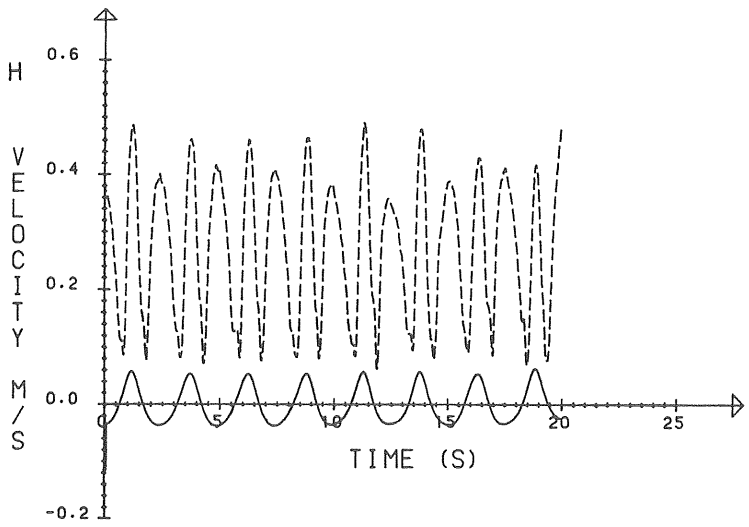

Figure 3.10 b Wave B "Transitional water". Measured velocity at 0.1 m below still water level. —— Water level (m). ---- Horizontal velocity.

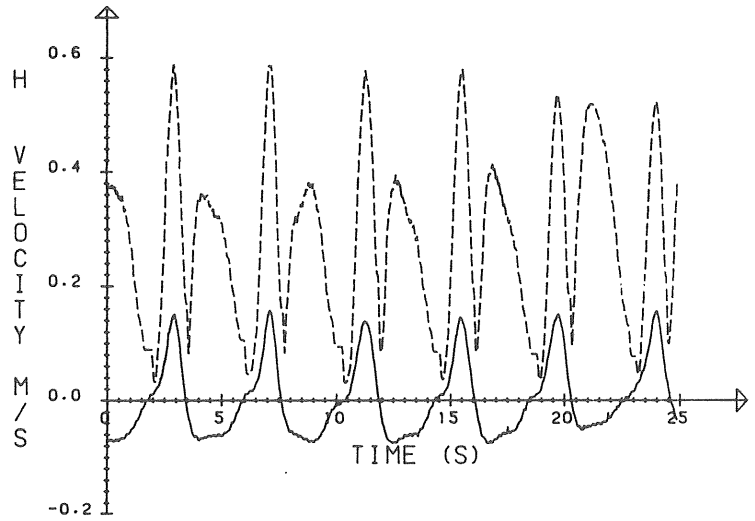

Figure 3.10 c Wave C "Shallow water". Measured velocity at 0.4 m below still water level.
—— Water level. ---- Horizontal velocity.

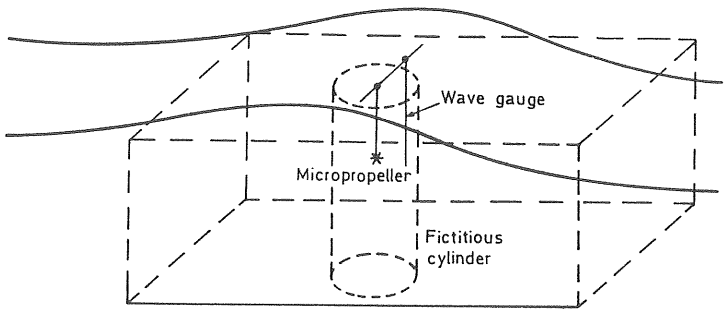

Figure 3.11 Schematic illustration over arrangement of the kinematic measuring set up in undisturbed flow.

direction of rotation. Furthermore, the wave train averaging technique filters the velocity records, as can be seen in Figs. 3.12 a-c. This did not restrict the usefulness of the technique. The significant trough and crest velocities and their time variations could be measured well.

Calculated data were substituted for the data near the zero crossing which were missing. This was done by fitting a smooth curve through the reliable velocity data on both sides at the zero crossing point, see Figs. 3.12 a-c.

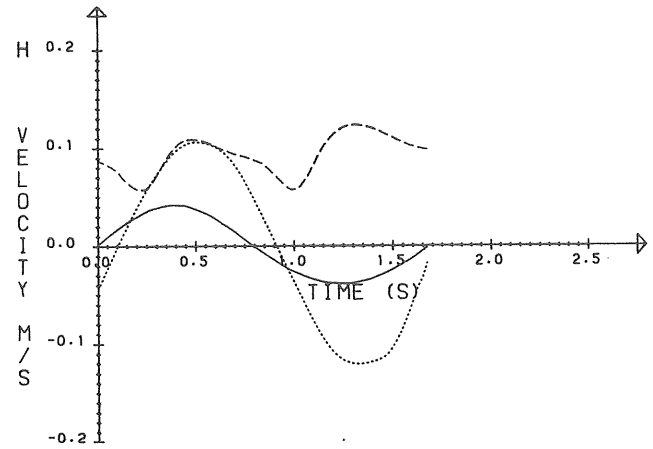

Figure 3.12 a Wave A "Deep water." Measured velocity at level -0.70 m according to the wave train averaging technique. ——— Water level. ---- Horizontal velocity. ..... Corrected for direction and smoothed around the zero crossings.

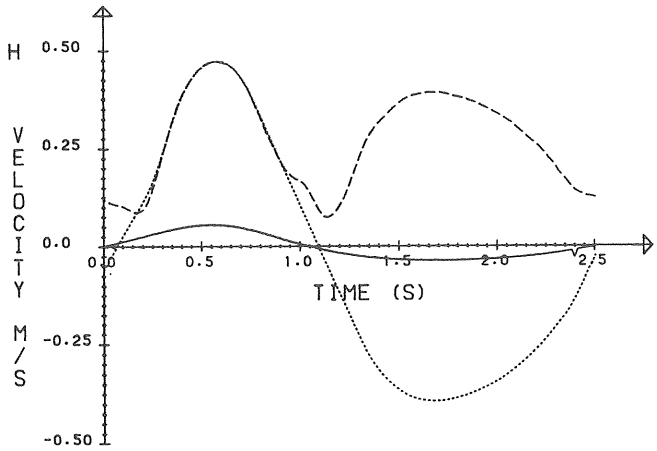

Figure 3.12 b Wave B "Transitional water." Measured velocity at level -0.10 m according to the wave train averaging technique. ——— water level. ---- Horizontal velocity. ..... Corrected for direction and smoothed around the zero crossings.

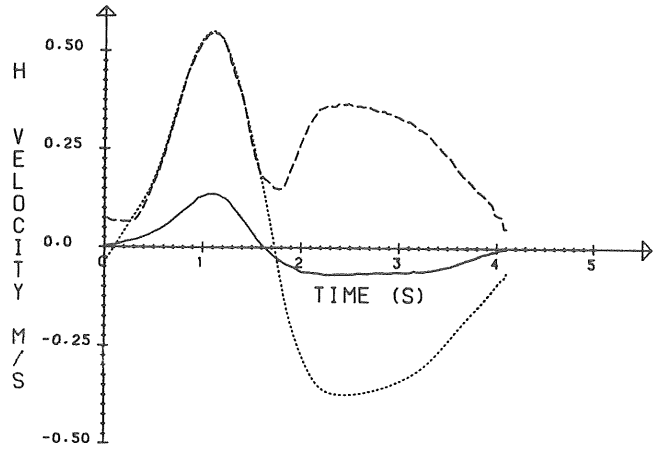

Figure 3.12 c Wave C "Shallow water". Mean velocity at level -0.40 m according to the wave train averaging technique. ——— Water level. ---- Horizontal velocity. .... Corrected for direction and smoothed around the zero crossings.

4. WAVE KINEMATICS

As mentioned in Chapter 1, one of the main purposes of the experiments was, to investigate the mass and drag coefficients in Morison's equation. By comparing measured wave form, measured particle velocities and "measured" accelerations with those from five theories it was found that a substantial part of the disagreement between the presented coefficient values may be explained by the fact that the velocities and the accelerations calculated from some of these theories differ significantly from measured values, see Chapter 7.

The purpose of this chapter is not to penetrate the different theories in detail, but rather to discuss the validity of the wave theories studied compared with "real" water waves. Since a vertical cylinder was studied, only the horizontal components are accounted for.

The chapter begins with assumptions made when applying the theories of water particle motions on progressive waves. Kinematics given by 1st, 2nd, 3rd and 5th order theory according to Stokes and according to the cnoidal theory are studied. Their validity based on theoretical as well as experimental grounds are discussed. The chapter is concluded with a check of the reliability of measured velocity, followed by results and recommendations.

4.1 Assumptions made in wave theories

Ocean waves are complex phenomena, difficult if not impossible to describe correctly in mathematical terms. Typically, a sea state comprises waves of all sizes, lengths and directions. Usually they are the result of disturbances from winds of different intensities and directions. In this report, however, only regular plane waves are discussed. The following assumptions are made:

- the waves are unidirectional and can be described as two-dimensional

- the waves have a defined monochromatic frequency
- the waves maintain a permanent form, height and period
- there is no underlying current
- the fluid is homogeneous, incompressible and nonviscous (frictionless)
- the flow is irrotational
- the waves propagate over a smooth horizontal bed in water of constant depth.

The pressure due to the wind is neglected. The pressure at the upper surface of the fluid is hereby assumed to be constant.

The most severe restrictions in the assumptions may be that there is no underlying current, that the depth is constant and that the wave train is two-dimensional with a permanent form.

The purpose of the wave theories is to describe the motions of water particles, the pressure fluctuations and the profile of the water surface. The equations for these often take the form of infinite series. The theory which only incorporates the first term of the series is called linear, and is the simplest to deal with.

When the wave is travelling in shallow water, or for steep waves, other theories which include second, third and fifth order terms are used. For very shallow water the cnoidal wave theory may be more satisfactory.

4.2 Validities of wave theories

At the evaluation stage it was observed that the wave kinematics from the various wave theories were substantially different.

To study the coefficients of the equation for calculating wave forces, it is necessary to know the true velocity and acceleration. However, the measured "true" velocity and acceleration showed that none of the wave theories studied was satisfactory.

Comparisons of the various theories can be conducted on theoretical as well as experimental grounds.

4.2.1 Comparisons based on theory

Dean (1970, 1974) compared several wave theories on a theoretical basis. His analytical evaluation was based on the degree to which a theory satisfies the governing equations. Since the Laplace equation and the bottom boundary condition are met by all the theories considered, the ability to fit the kinematic and dynamic free surface boundary conditions was used as the criterion of validity. The theories compared included first order wave theory, Stokes' third and fifth order theory, first and second order cnoidal theory, solitary and the stream function theory.

Dean found the first order cnoidal, linear (Airy) and fifth order theories most suitable in the areas shown in Fig. 4.1. The stream function theory is valid in almost the whole band shown in the figure.

In Fig. 4.1 it is seen that fifth order theory (Stokes V) provides the best fit for deep water. First order (Airy) theory provides the best fit in a part of the transitional and shallow water ranges. Finally the first order cnoidal wave provides the best fit in the shallow water range.

Dean pointed out, however, that the analytical validity does not guarantee that the theory necessarily represents the features of natural waves well. He also suggested that this kind of comparison may be biased in favor of the lower order theories.

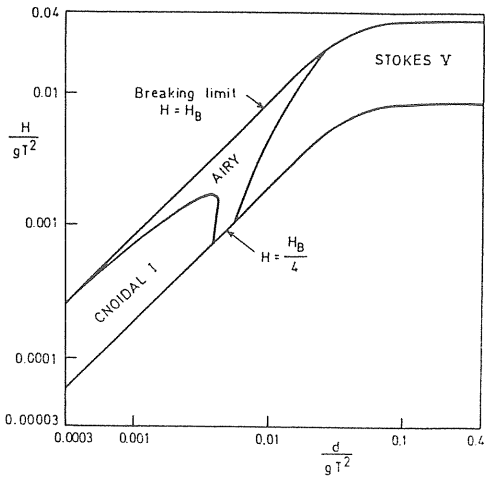

Figure 4.1 Ranges of periodic wave theories providing best fit to dynamic free surface boundary condition (from Dean 1970).

Le Méhauté (1976) presented a figure very similar to Dean's graph. Le Méhauté's graph shows approximate limits of the validity of various wave theories, see Fig. 4.2.

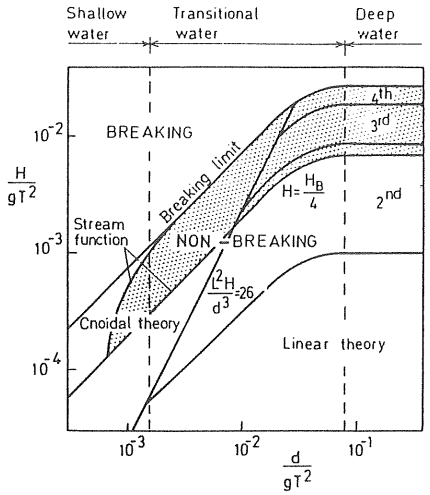

Figure 4.2 Ranges for various wave theories as presented by Le Méhauté (1976).

Le Méhauté's investigation was strictly qualitative, but the figure still show that cnoidal wave theory is preferred for shallow water while Stokes' high order theories are preferred for the deeper water ranges.

4.2.2 Comparisons based on experiment

The preferability of one wave theory over another, on theoretical grounds, is not necessarily reflected in better agreement when the theories are compared with real waves. The suitability of a particular wave theory may even depend on which characteristics are being compared. Since Dean only investigated how well the boundary conditions were met in his theoretical comparison, his comparison does not tell us how well the theories describe the wave kinematics. This leads to the conclusion that an experimental verification is the only real measure of accuracy.

Le Méhauté, Divoky and Lin (1968) reported a series of experiments where the velocity field under the crest of large amplitude shallow water waves was examined and compared with various wave theories. The kinematics were determined photographically through observation of buoyant particles suspended in the water. When comparing the measured maximum particle velocity with velocities from Stokes' first, second, third, fifth order theories and with cnoidal theory, no theory was found to be exceptionally accurate. The most acceptable description of the maximum particle velocity for the range examined ($0.0015 < d/gT^2 < 0.024$) was given by cnoidal theory.

Iwagaki and Sakai (1969) investigated the vertical distribution of horizontal velocity under the wave crest and time variation during the wave period by tracing the motion of hydrogen bubbles and the use of hot film anemometers. Stokes' third order theory and hyperbolic wave theory (a special case of cnoidal theory) gave the closest prediction of velocities in deep water and shallow water, respectively. However, the authors noted that the third order theory may give values of the horizontal particle velocity that are too small at the water surface in the region $T\sqrt{g/d} \geq 10$.

Chakrabarti (1980b) compared laboratory generated waves with several wave theories through measured velocities,

dynamic pressures, wave lengths and variation of the wave forms. The measured maximum averaged velocity and pressure under the crest were used in the comparison. In deep water, the linear wave theory was found to describe the water particle dynamics and kinematics quite well. Stokes' third order theory was found to be valid for higher waves in intermediate water depths. In general, the ninth order irregular stream function theory was found to agree reasonably well with the test data. The profile and pressure measurements correlated well, while the correlation of the velocities was only fair. The author states that the obtained data were limited and also good for only one water depth. Electromagnetic velocity probes were used.

Bullock and Short (1985) compared water particle velocities for generated regular waves, measured with a laser anemometer, with Stokes' first, second and fifth order theories. Errors of over 10% are possible in the amplitude of the first harmonics of velocity components. Relatively larger errors must be expected if free second harmonic waves are generated by the wave blade. In addition there is a "drift" in the water particle motion causing a non-zero mean horizontal velocity at a fixt point. Bullock and Short found that the mean velocity may reach 20% of the amplitude of the first harmonic. The authors concluded that discrepancies between measured and predicted values cannot be wholly attributed to the limitations of a particular theory, but are also a function of the experimental arrangement. Consequently, when accuracy is important, prediction of velocities should be based on measurements.

Obviously, an experimental verification of the different wave theories is a difficult task. The errors in the experiments have led to the result that the validity cannot always be definitely proven or disproven. Evaluations have normally been made for orbital velocities, particularly those occurring under the wave crest. The correspondence between theoretical and measured wave profiles has

also been investigated concurrently and used as a parameter of reliability for the wave theory studied.

As mentioned earlier, it was found that the wave kinematics from the various wave theories were substantially different. This fact led to the carrying out of a second test run, in order to measure "real" velocities and accelerations. When calculating the coefficients C_D and C_M both the "true" measured kinematics and those obtained from the best fitting wave theory were used, see Chapter 7. When choosing the best fitting wave theory, the following criteria were used:

closeness to measured

- surface profile
- velocity and acceleration as well as to the extreme values (maximum/minimum).

The result of this evaluation is presented in Table 4.1, the development of which is described below.

The most common and simplest way of checking the validity of a wave theory is to see how well the profile corresponds to the measured profile. Evaluation by surface profile is shown in Figs. 4.3 a-c. As seen in Fig. 4.3 b, the measured wave profile is closely described by all theories except first order theory. For deep water conditions, exemplified by wave A (Fig. 4.3 a) even first order theory predicts the profile fairly well. The assumptions for the basic equation of the theory are fulfilled here. The basic assumption is that the wave height is much smaller than both the wave length and the water depth.

For shallow water, represented by wave C (Fig. 4.3 c), there were no solutions from Stokes' second and third order. Stokes' fifth order gave a solution, but as seen from Fig. 4.3 c the wave profile contained small unrealistic fluctuations.

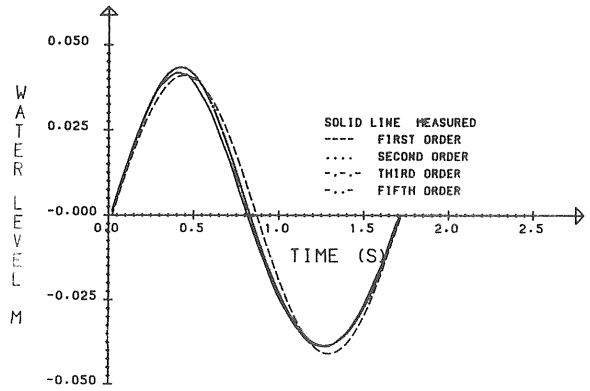

Figure 4.3 a WAVE PROFILE. Wave A. "Deep water".

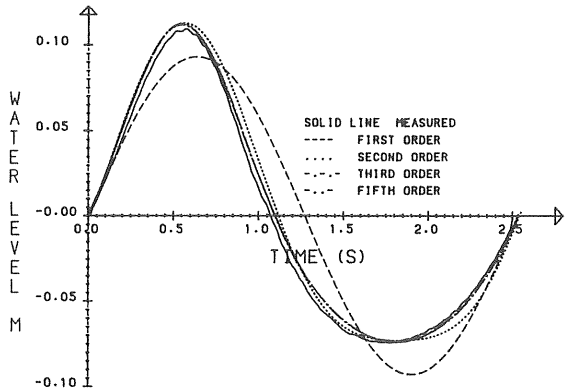

Figure 4.3 b WAVE PROFILE. Wave B. "Transitional water".

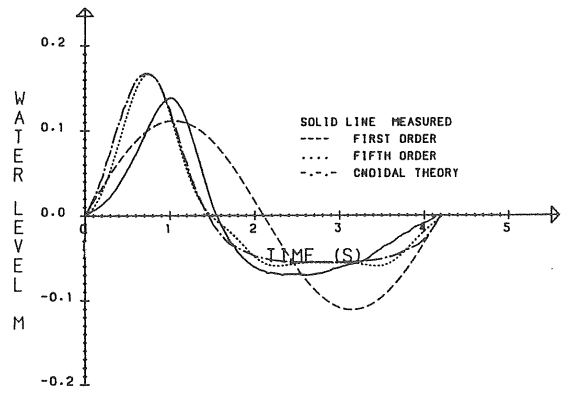

Figure 4.3 c WAVE PROFILE. Wave C. "Shallow water".

Ranking according to closeness to the experimental surface profile is listed in Table 4.1. The ranking is sometimes subjective, based on ocular inspection. But for most waves in the experimental program the ranking was unproblematical. Wave B may be seen as an example. For this wave, only the first order theory gives a poor fit, which places it at the end of the ranking list. Studying the figure more closely, one also observes that the second order theory differs slightly from the others. The two best theories were the fifth and third order theories, which could not be distinguished from one another for this wave. Theories that could not be distinguished are underlined in the table.

A verification based only on comparing the wave profiles is far from sufficient, especially when the theories are used for wave force calculations. In this case the accuracy of particle velocity and acceleration are the quantities of greatest importance.

The horizontal particle velocity was measured with a micropropeller as described in Chapter 3.6. The velocity was basically measured at the same levels as the pressure probes, see Figs. 3.2 and 4.4. Note that two water depths, 0.7 and 0.8 m were used. As two to three pressure probes were placed in or above the still water level, the velocity distribution in the crest was also measured. Additional measurements were made near the water surface for some steep waves included in the experimental program.

Table 4.1 Ranking of theories according to closeness to wave profile, horizontal velocity and horizontal acceleration. Wave characteristics for waves included in the experimental program, listed after increasing Keulegan-Carpenter number (KC), taken in S.W.L.

	Wave Characteristics													Ranking according to closeness to exp.results			
Wave	KC	H_m	T_s	d_m	L_m	H/gT^2	d/gT^2	HL^2/d^3	$\frac{H}{L}$	HL/d^2	$\frac{d}{L}$	$\frac{H}{d}$	$350(d/gT^2)^{3/2}$	Wave profile	Horizontal part velocity	Horizontal part acceleration	Chosen theory
														1234	1234	1234	
A	1.0	0.082	1.70	0.8	3.90	0.0029	0.0281	2.4	0.0210	0.50	0.205	0.1025	1.658	5321	5123	1532	5
B	4.2	0.186	2.53	0.8	6.54	0.0030	0.0130	15.5	0.0284	1.90	0.122	0.2325	0.519	5321	5231	2531	5
C	9.0	0.223	4.20	0.7	10.70	0.0013	0.0040	74.4	0.0208	4.87	0.065	0.3186	0.089	C51	C51	C51	C(5)
D	1.1	0.038	4.20	0.8	11.43	0.0002	0.0046	9.7	0.0033	0.68	0.070	0.0475	0.109	5321	5321	2531	5
E	1.2	0.062	2.53	0.8	6.51	0.0010	0.0127	5.1	0.0095	0.63	0.123	0.0775	0.501	5321	5132	5123	5
F	1.3	0.048	3.36	0.8	8.98	0.0004	0.0072	7.6	0.0053	0.67	0.089	0.0600	0.214	5321	5321	5321	5
G	1.8	0.198	1.30	0.8	2.67	0.0119	0.0482	2.8	0.0742	0.83	0.300	0.2475	3.701	5321	1523	1523	5
H	2.2	0.190	1.70	0.8	3.98	0.0067	0.0282	5.9	0.0477	1.18	0.217	0.2375	1.657	5321	5231	5231	5
I	4.8	0.146	3.36	0.8	9.15	0.0013	0.0072	23.9	0.0160	2.09	0.087	0.1825	0.214	2531	2531	2531	5
J	5.1	0.118	4.20	0.8	11.64	0.0007	0.0046	31.2	0.0101	2.15	0.069	0.1475	0.109	5321	5321	5321	5
K	8.1	0.274	3.36	0.7	9.00	0.0025	0.0063	64.7	0.0304	5.03	0.078	0.3914	0.175	C51	5C1	C51	C(5)
L	8.3	0.350	2.53	0.7	6.52	0.0056	0.0111	43.4	0.0537	4.66	0.107	0.5000	0.409	C51	5C1	C51	C(5)
M	11.0	0.334	4.20	0.7	12.02	0.0020	0.0040	111.5	0.0317	7.29	0.065	0.4771	0.089	C	C	C	C

1st, 2nd, 3rd, 5th order theories according to Stokes.
Cnoidal theory (first order).

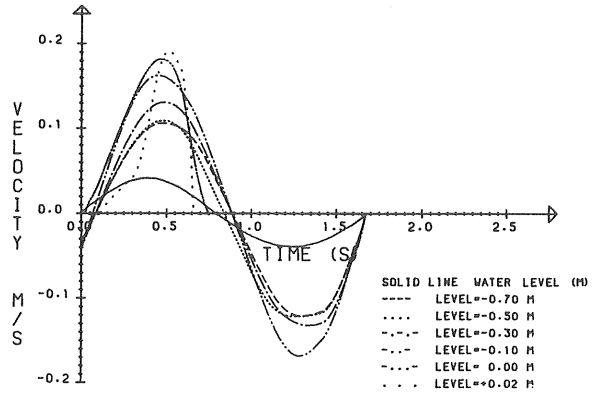

Figure 4.4 a VELOCITY-MEASURED. Wave A. "Deep water".

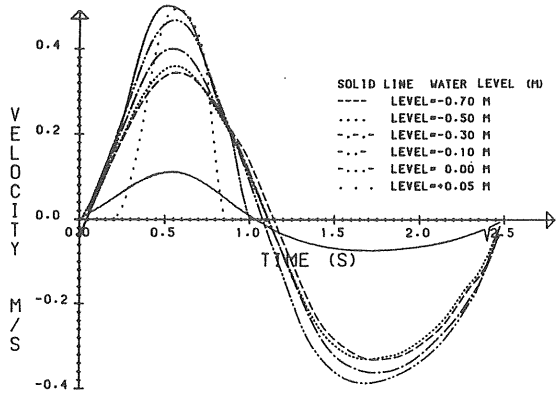

Figure 4.4 b VELOCITY-MEASURED. Wave B. "Transitional water".

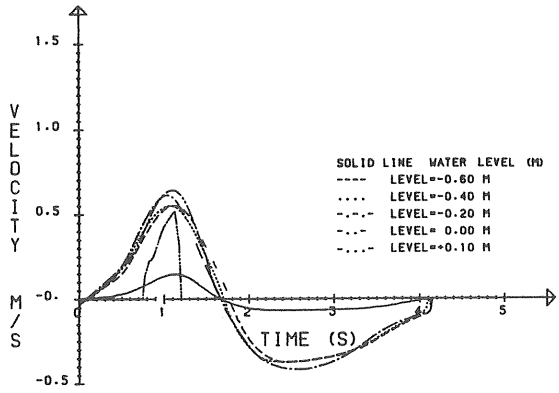

Figure 4.4 c VELOCITY-MEASURED. Wave C. "Shallow water".

A comparison between measured velocity and velocity given by different theories at various depths is shown in Figs. 4.5 a-c. For this comparison two criteria were established. First, how well the velocity corresponds to the measured velocity. Second, how close the measured maximum velocity was to that given by the theories for a crest or trough situation.

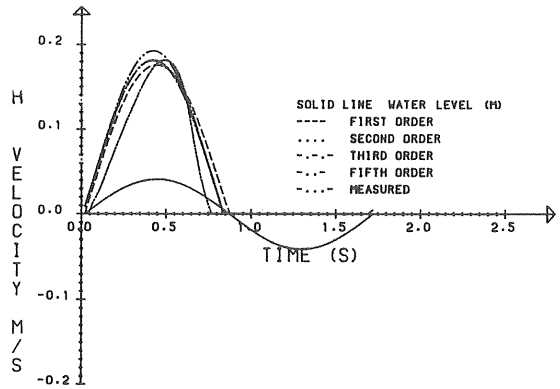

Figure 4.5 a Wave A. "Deep water". Velocities at the still water level. Measured and according to theories.

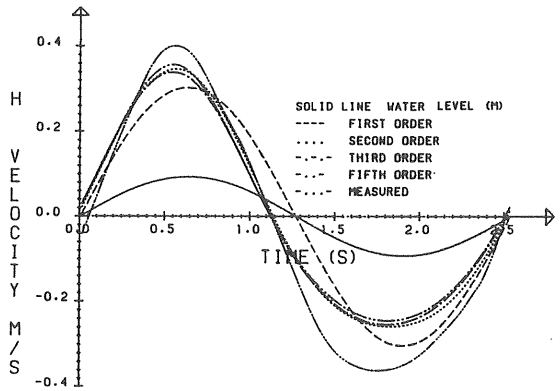

Figure 4.5 b Wave B. "Transitional water". Velocities at 0.30 m below the still water level. Measured and according to theories.

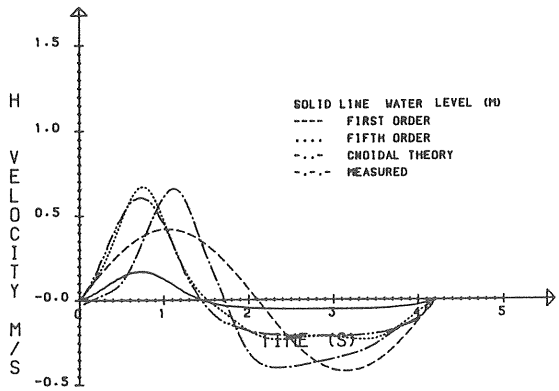

Figure 4.5 c Wave C. "Shallow water". Velocities at 0.1 m below the still water level. Measured and according to theories.

Measured acceleration was calculated from the velocity records by studying the successive change in velocity. The acceleration $\dot{u}_n$ in time step n was calculated as $\dot{u}_n = (u_{n+1} - u_{n-1})/2\Delta t$, where Δt is the chosen time step and where $u_{n\pm1}$ are velocities at point of times n+1 and n-1, respectively.

The horizontal particle acceleration calculated from the measured velocity is shown in Figs. 4.6 a-c.

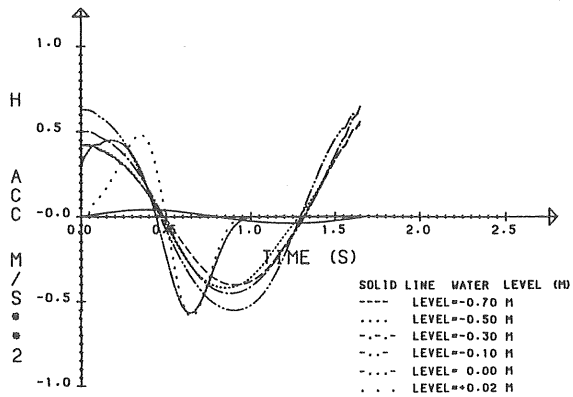

Figure 4.6 a ACCELERATION-"MEASURED". Wave A. "Deep water".

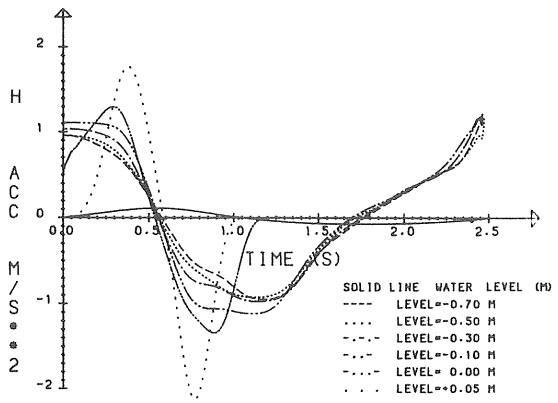

Figure 4.6 b ACCELERATION-"MEASURED". Wave B. "Transitional water".

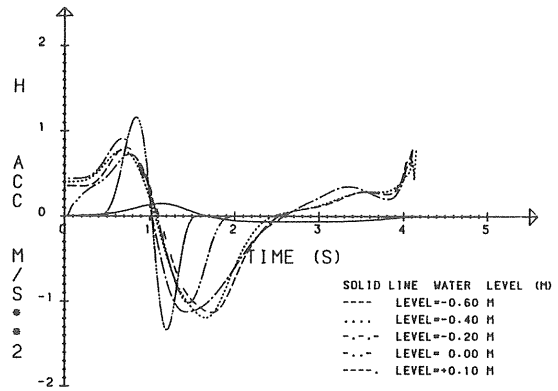

Figure 4.6 c ACCELERATION-"MEASURED". Wave C. "Shallow water".

A comparison between measured acceleration and acceleration given by different theories was made in the same way as for the velocity shown. As the acceleration was obtained from the measured velocity by calculating the numerical derivative, the criteria of closeness to wave profile and velocity were given greater weight.

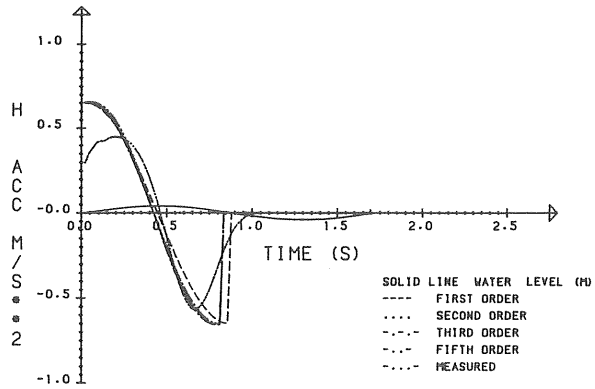

Figure 4.7 a Wave A. Acceleration at the still water level. Calculated and according to theories.

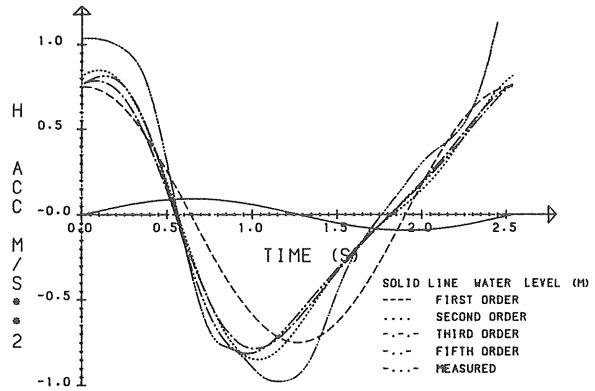

Figure 4.7 b Wave B. Acceleration at 0.30 m below the still water level. Calculated and according to theories.

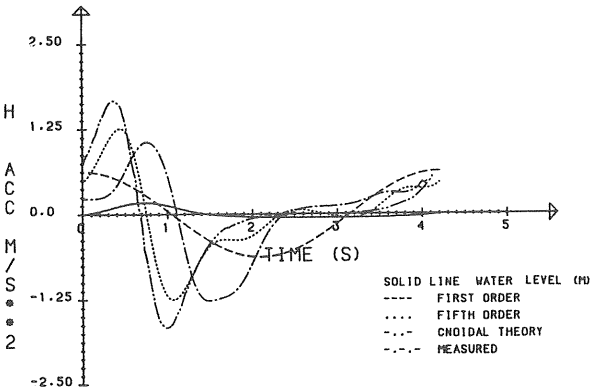

Figure 4.7 c Wave C. Acceleration at 0.10 m below the still water level. Calculated and according to theories.

4.2.3 Estimates of velocity with the use of stagnation pressure

Examination of Figs. 4.4-4.7 gives rise to the question of the reliability of the measuring system. An error analysis for the measuring system is given in Appendix 2, but it is shown in the text below that the measured velocity is close to the "true" velocity.

The measured horizontal particle velocity received from the micropropeller was checked by using the Bernoulli equation together with the measured pressure distribution given in Appendix 1.

By assuming potential unidirectional flow in the wave crest and wave trough and solving the Bernoulli equation using the pressure difference (Δp) between the stagnation point on the front (back) of the cylinder and the points of 90^{o} or 270^{o}, the corresponding water velocity could be obtained, see Fig. 4.8. As given by potential theory, de-

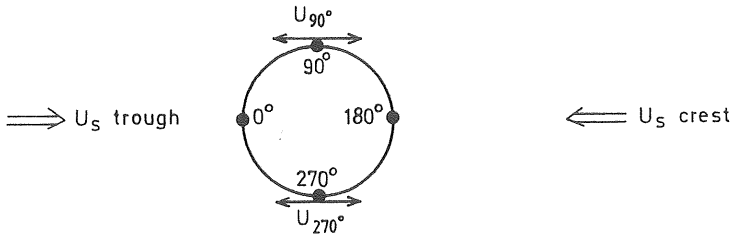

Figure 4.8 Schematic illustration of associated velocities and points of pressure when evaluating the corresponding velocity by use of Bernoulli equation.

scribed in Chapter 5.1.2, the velocity along the surface of the cylinder is given by $U_T = 2U_s \sin \theta$. The velocity U_s is the "free stream velocity" and U_T the velocity close to and tangential to the surface of the cylinder. Thus the Bernoulli equation gives

$$U_s = \sqrt{\Delta p / 2\rho} \qquad \ldots (4.1)$$

Figs. 4.9 a-k show the maximum horizontal particle velocities at different depths for both a crest and trough situation. The measured velocity in the undisturbed wave is compared with the velocity according to Eq. (4.1) and that given by fifth order and cnoidal theories.

The effect of the free surface (Chapter 5.3), the separation of the boundary layer (Chapter 5.1.3 - 5.1.4) and the vortices swept past the cylinder (Chapter 5.2.2) makes the potential theory inapplicable. Also, especially for the shorter waves, the surface curvature affects the pressure. However, in most cases the correspondence is rather good between the measured velocities and velocities calculated using Eq. (4.1) while, as shown, the theories do not fit measured values well in all situations.

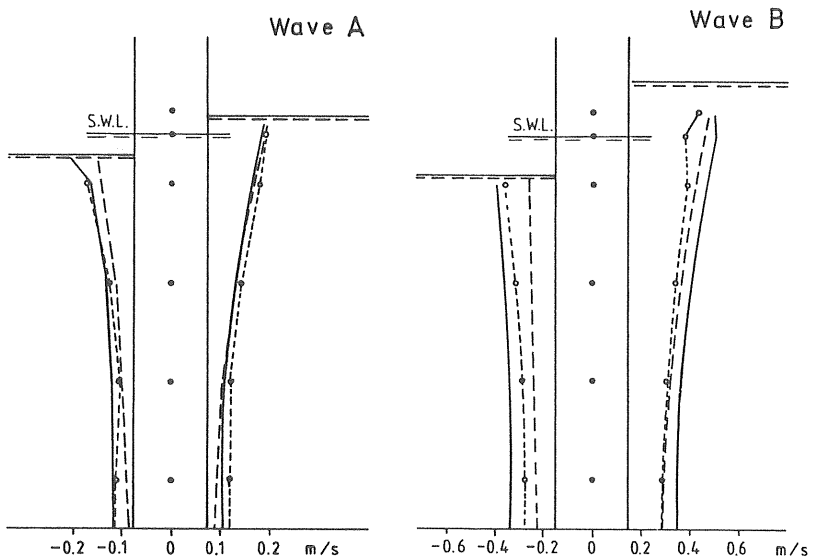

Figure 4.9 a-b Maximum horizontal particle velocity for the crest and trough.
—— measured velocity without cylinder;
---- fifth order theory;
--o-- calculated from stagnation pressure.

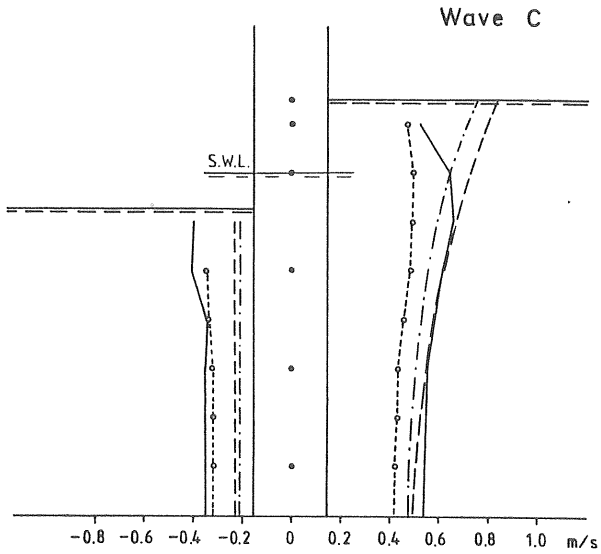

Figure 4.9 c Maximum horizontal particle velocity for the crest and trough.
——— measured velocity without cylinder;
--- fifth order theory; -·-· cnoidal theory;
--o-- calculated from stagnation pressure.

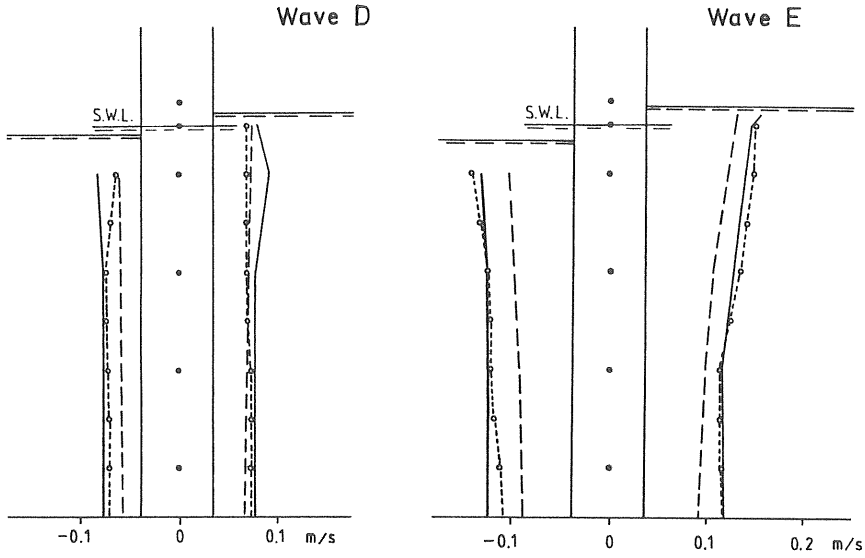

Figure 4.9 d-e Maximum horizontal particle velocity for the crest and trough.
——— measured velocity without cylinder;
--- fifth order theory:
--o-- calculated from stagnation pressure.

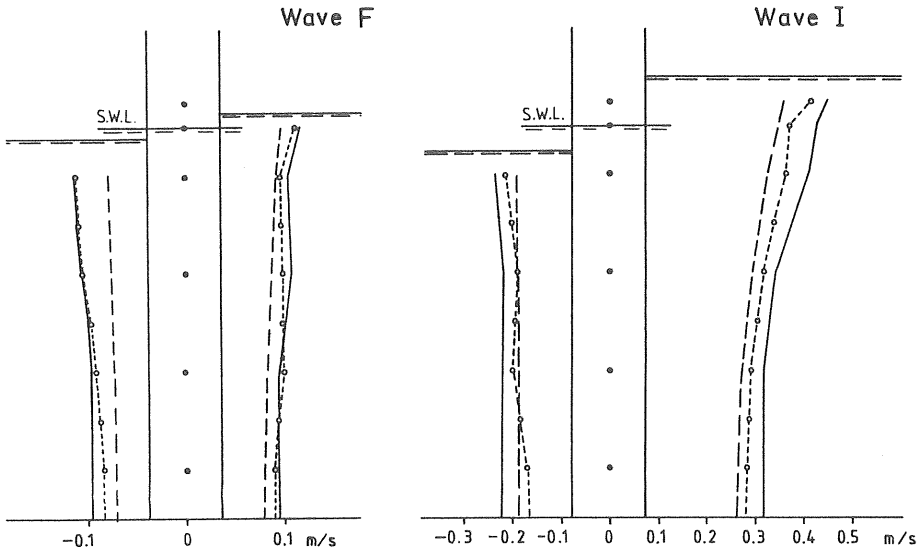

Figure 4.9 f-g Maximum horizontal particle velocity for the crest and trough.
——— measured velocity without cylinder;
--- fifth order theory:
--o-- calculated from stagnation pressure.

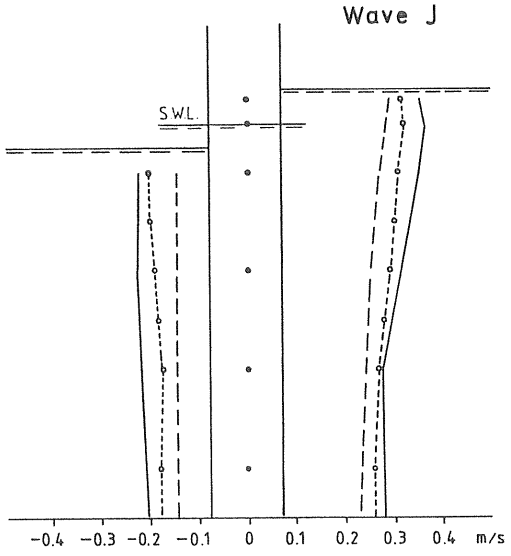

Figure 4.9 h Maximum horizontal particle velocity for the crest and trough.
——— measured velocity without cylinder;
--- fifth order theory;
--o-- calculated from stagnation pressure.

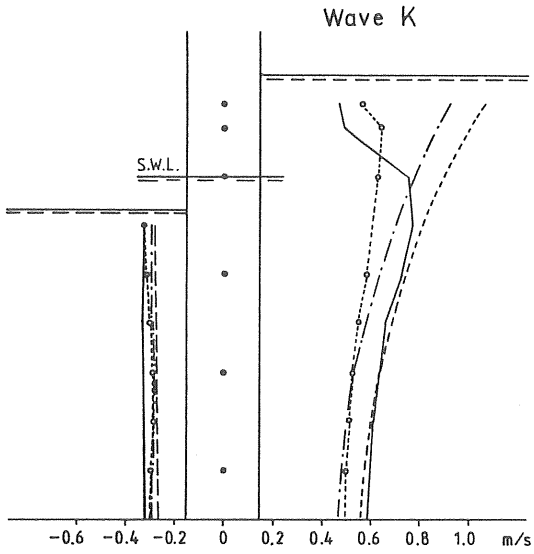

Figure 4.9 i Maximum horizontal particle velocity for the crest and trough.
——— measured velocity without cylinder;
--- fifth order theory;
-•-• cnoidal theory;
--o-- calculated from stagnation pressure.

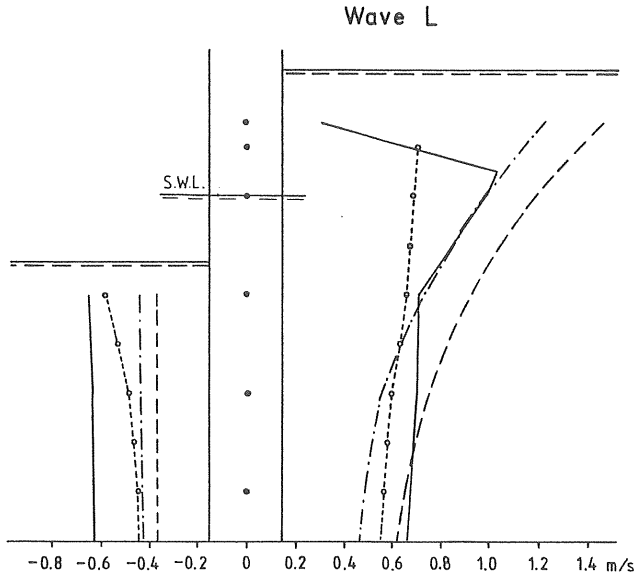

Figure 4.9 j Maximum horizontal particle velocity for the crest and trough.
——— measured velocity without cylinder;
--- fifth order theory; -•-•cnoidal theory;
--o-- calculated from stagnation pressure.

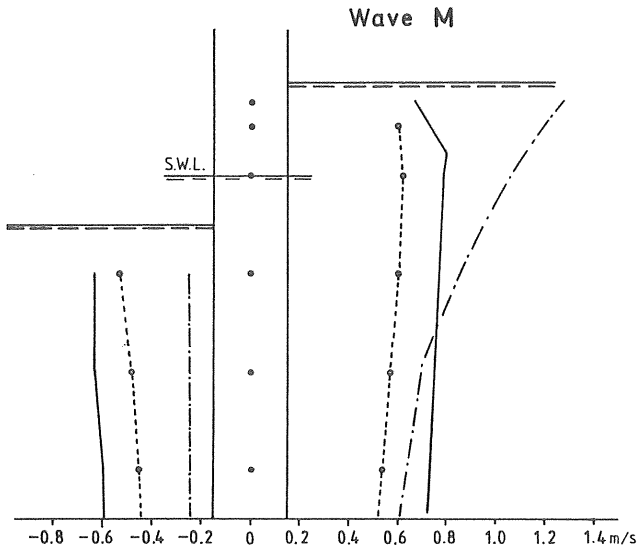

Figure 4.9 k Maximum horizontal particle velocity for the crest and trough.
——— measured velocity without cylinder;
--- fifth order theory; -•-•cnoidal theory;
--o-- calculated from stagnation pressure.

4.2.4 Results

As the main purpose of the experimental program was to investigate wave forces and pressure distribution and not to evaluate the wave theories, the data gathered was not sufficient to reject or prefer any one theory. However, a qualitative comparison can be made, where the validity could be checked for waves included in the experimental program.

This comparison was divided into two steps. First, an investigation was made as to whether there was any relation which could state if one theory or several theories were preferable for certain ranges of suitability. The second question studied was if any ranges of suitability could be obtained, to compare these theories suitable for the respective ranges.

When plotting the waves included in the experimental program in Le Méhauté's diagram (Fig. 4.2), a very good indication was obtained for the range of suitability of cnoidal wave theory. Measured waves with a "shallow water look" were all in the area of the plot restricted by the breaking limit for the wave and the line given by $L^2 \cdot H/d^3 = 26$, see Fig. 4.10. The term "shallow water look" means a wave with a steep-narrow crest and with a long flat trough.

The area of validity for the cnoidal theory given by Le Méhauté's diagram also corresponds with the area recommended by Isaacsson (1978), see Fig. 4.10. Isaacsson gives the relation $H/d > 350(d/gT^2)^{3/2}$, which may be written $H/gT^2 > 350(d/gT^2)^{5/2}$, for which the cnoidal theory is superior. This relation was established on the basis of the mass transport near the seabed throughout a wave cycle.

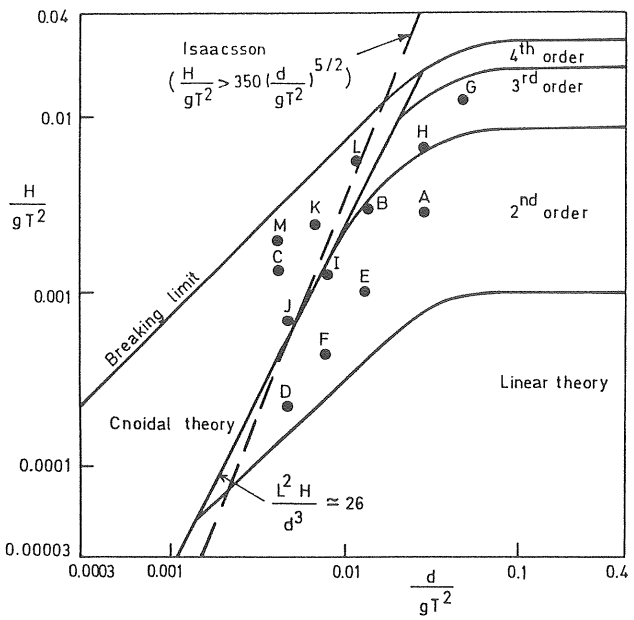

Figure 4.10 Waves included in the experimental program and relation given by Isaacsson (1978) plotted in Le Méhauté diagram.

Other limits for different theories are shown in Table 4.2, but no or little correspondence with waves included in the experimental program was found.

Nor could the criteria of limits for Stokes' 1st to 4th order theories in Le Méhauté's diagram be verified.

The next step after establishing a relation stating whether one theory or several theories were preferable to others for certain ranges was to compare the theories in these respective ranges. In Table 4.1 the ranking according to closeness to measured wave profile, horizontal particle velocity and acceleration for the different theories is shown. It was found that the fifth order theory was best, except for shallow water where the cnoidal theory is preferable.

Third and second order theories were found to work rather well, too, but as the fifth order theory was found to be more accurate, these theories were not chosen for further investigation. When a less sophisticated theory than the fifth order theory is to be considered, the first order theory predicts the velocity fairly well and is easy to handle.

To check the error given by first and fifth order theories, the maximum horizontal particle velocity for crest and trough was compared with the measured velocities, see Figs. 4.11 a-c and the corresponding ones in Appendix 1. The cnoidal theory was also checked for the waves in shallow water. In these figures the maximum theoretical velocity was plotted as the percentage of deviation from the measured corresponding velocity.

From Figs. 4.11 a-c and those in Appendix 1 it is seen that the theories studied usually underestimate the velocities under the still water surface, while there is a tendency for velocities above the still water surface to be overestimated. It is also seen that the first order

Table 4.2 Criteria of limits for different theories given by different authors. Wave characteristics given in Table 4.1.

Limits for validity	Deep water theory is applicable	Cnoidal theory is applicable	Correspondence to waves included in the experimental program
Isaacsson			
Cnoidal theory is superior when $H/d > 350\ (d/gT^2)^{3/2}$		C,J,K,L,M	Good
Le Méhauté			
Cnoidal theory is superior when $HL^2/d^3 > 26$		C,J,K,L,M	Good
ISVA			
Cnoidal theory is meaningless when $d/L > 0.13$	A,G,H		
Stokes' theory is applicable when $HL^2/d^3 < 15$	A,D,E,F,G,H		
Cnoidal gives better results when $HL^2/d^3 > 15$ and $d/L_o < 0.1$ when $L_o = gT^2/2\pi$		B,C,I,J,K,L,M	Fair
Cnoidal and Stokes theories are meaningless when $HL^2/d^3 > 15$ and $d/L_o > 0.1$			
Laitone			
Cnoidal theory is meaningless when $L < 5\ d$		B,C,D,E,F,I,J,K,L,M	Poor
First order theory is applicable when $d/L > 0.2$	A,G,H		
Stokes' theory superior when $d/L > 1/8 - 1/10$	A,B,E,G,H,L		
Stokes' third order is appliacable when $d/L > 0.2$	A,G,H		
Fenton			
Cnoidal theory is applicable when $L/d > 8$		B,C,D,E,F,I,J,K,L,M	Fair
Silvester			
Do not use Stokes' theories when $d/L < 0.1$		C,D,F,I,J,K,M	Poor

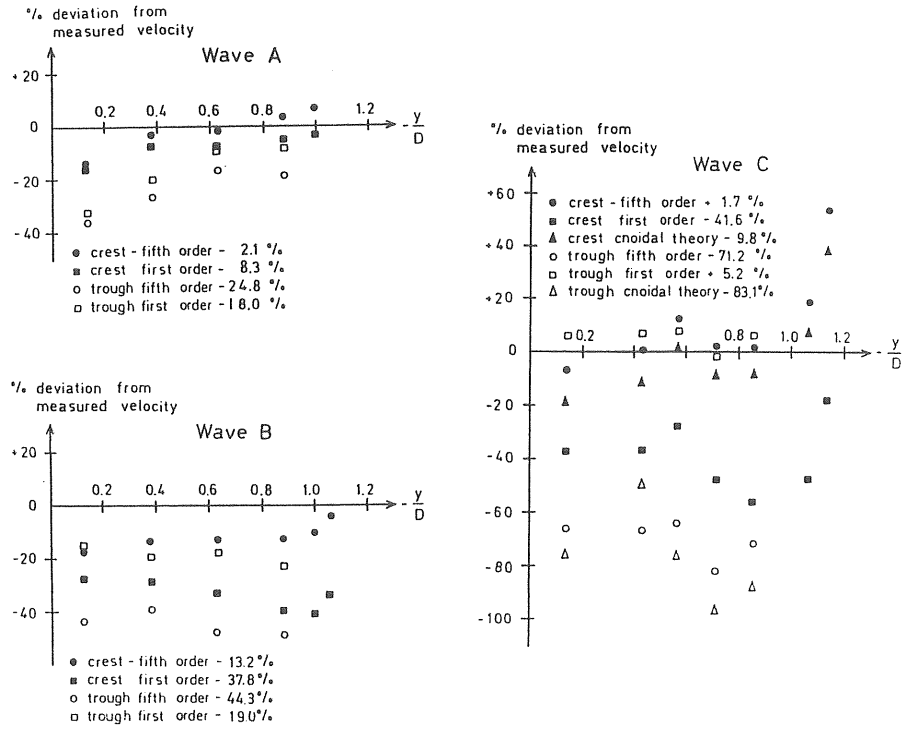

Figure 4.11 a-c Deviation for first, fifth order and cnoidal theories when compared with measured maximum horizontal velocities.

theory for most cases predicts the velocity better for a trough situation than both fifth order and cnoidal theories.

An attempt to indicate validity in percentage is shown in Table 4.3. The mean percentage deviation from measured maximum particle velocity from the still water surface to the bottom is presented.

An interesting feature of waves C, K, L and M, which are typical shallow water waves, can be seen in Figs. 4.9 and 4.11, and the corresponding figures in Appendix 1. The assumption of an exponentially increasing velocity above the still water level for the theories seems to be correct,

except for waves in extremely shallow water where, instead of an exponentially increasing velocity profile, a decreasing velocity profile was measured.

Table 4.3 Mean percentage deviation from measured maximum velocity for waves included in the experimental program. Only values from the still water level and deeper are incorporated.

Mean percentage deviation					
Fifth order**		First order		Cnoidal theory**	
crest	trough	crest	trough	crest	trough
-13	-36	-28	-21	-14	-46

* excluding wave M

** respective range of suitability

Use of a constant or a decreasing velocity profile from the still water level seems to be justified for waves C, K, L and M.

For very shallow water, as represented by wave M, an almost constant velocity profile was measured, see Fig. 4.9 k. This feature is not described by the cnoidal theory. For high HL/d^2 (above 7 to 10), which denotes very shallow water, it seems to be justified to use the velocity at the still water level all the way down to the bottom.

In summary, none of the theories studied could be considered as an outstanding tool for the prediction of wave kinematics, at least not for the steep waves included in the experimental program. The wave theories studied usually underestimate the velocity under the still water level, and overestimate velocities above the still water level. While

the fifth order, cnoidal, second and third order theories describe the maximum velocity fairly well for a crest situation, the first order theory in most cases, gives the closest value for the maximum velocity in a trough situation. Furthermore, none of the theories describes the phase of the velocity as a function of depth, although the phase is known to change for steep waves in deep water. Nevertheless, the fifth order theory gives the most reliable results. For more shallow water the cnoidal theory is superior, as indicated in Fig. 4.2 or when $H/d > 350(d/gT^2)^{3/2}$. However, the cnoidal theory was found to overestimate the acceleration near and above the still water level. It was also found that the cnoidal theory overestimates the velocity above the still water level. Instead of an exponential increase, a decrease in velocity was found.

4.2.5 Recommendations

For want of accurate velocities and accelerations from either measurements or by theories, it is recommended that calculations should be standardized. The first step for obtaining the nominal wave kinematics is to choose a wave theory suitable for the application. By using the Le Méhauté diagram (Fig. 4.2) or the relation $H/d > 350 \cdot (d/gT^2)^{3/2}$ given by Isaacsson, the range of suitability is obtained. If the studied wave is to be considered a shallow water wave, the cnoidal theory should be used. Otherwise, the fifth order theory is recommended.

If only the order of magnitude is needed, the linear theory, which gives fairly good results and is easy to work with, can be used.

It is also recommended that the exponential increase for the velocity and acceleration above the still water level for the cnoidal theory be changed to a constant or a decreasing one.

5. TIME DEPENDENT SEPARATED FLOW

Wavy flow around a vertical cylinder is a complex phenomenon. In addition to the effects of the free surface, the orbital motion of the fluid particles gives rise to a three-dimensional time dependent flow. The exponential decay of the particle velocity along the vertical cylinder is a further complication.

The key to the explanation of time dependent separated flow is the understanding of the formation, growth and motion of vortices. As the problem of separated flow around a bluff body remains theoretically unresolved, observation of experiments is still indispensible.

For a vertical cylinder subjected to oscillating waves, the flow not only accelerates from and decelerates to zero but changes direction during each cycle as well. The vortices which are a result of separated flow, formed during the first half of the flow period, may be pulled back to the cylinder during the second half of the period, interfering with the flow. Furthermore, the separation points make large fluctuations. The boundary layer around the cylinder may also change from fully laminar to partially or fully turbulent. The Reynolds number (Re) may also range from subcritical to postcritical over a given wave cycle.

The purpose of this chapter is to investigate the above-mentioned flow phenomena. The chapter begins with the most elementary flow situation, planar steady flow. As this flow situation could be used to describe the basic phenomena for wavy flow, it is described in detail.

In connection with the planar steady flow, phenomena such as separation and separation bubble, boundary layer, vortex shedding and effects of roughness are accounted for. The potential theory, which can be used to describe flow patterns around structures is also described. Thereafter, planar oscillating flow is discussed. The chapter is con-

cluded with a section on wavy flow around a vertical cylinder. Among other things the effects of the free surface are discussed.

5.1 Steady flow past a circular cylinder

When water flows past a circular cylinder, several completely different flow patterns are possible. In some cases the flow pattern may look like the flow of an ideal non-viscous fluid. In other cases the viscous effects characterize the flow completely, in which case the flow pattern is much more complex. As an illustration we can study the most elementary flow situation, namely planar steady flow.

The flow around a smooth cylinder is characterized by the Reynolds number, Re. The major regimes as compiled by Lienhard are shown in Fig. 5.1. Note that there are other definitions as well as sub-divisions of the different flow regimes, see e.g. Norberg (1987).

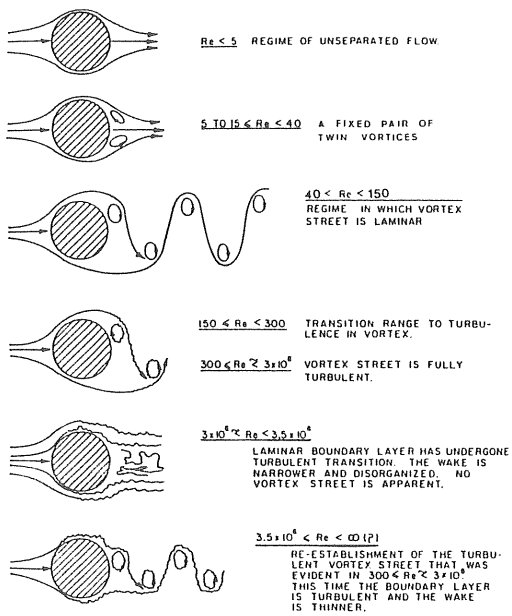

Figure 5.1 Regimes of fluid flow across a circular cylinder (from Lienhard, 1966 with changes).

At low Re, less than 5, the flow does not separate and consequently no vortices are produced. As Re is increased a pair of symmetrical fixed vortices are formed behind the cylinder. As Re is further increased (up to about 40), the vortices elongate in the streamwise direction until a vortex breaks away and a periodic wake and staggered vortex street are formed. Up to a Re of approximately 150, laminar vortices are produced. In the subcritical regime defined at about $300 < Re < 2 \cdot 10^5$ the boundary layer remains laminar but the vortex street becomes turbulent. The shedding of vortices occurs here, at a well defined frequency. As Re is increased into the critical ($2 \cdot 10^5 < Re < 5 \cdot 10^5$) and supercritical regimes ($5 \cdot 10^5 < Re < 3 \cdot 10^6$), dramatic changes in the flow take place. The boundary layer becomes partly turbulent and the flow is characterized by the disorganized vortex shedding. As the post-critical regime is reached at about $Re > 3 \cdot 10^6$ the boundary layer becomes successively more turbulent and the vortex shedding is re-established at a well defined frequency. These flow regimes and the underlying physics are further discussed in this chapter. For a recent critical discussion of different regimes the reader is referred to Farell, 1983.

5.1.1 Impulsively started flow

The photographs in Fig. 5.2 show the flow at different times after a cylinder has been made to move rapidly and then kept at a constant velocity. Fig. 5.2 a shows the flow pattern just after the cylinder has been made to move. It is seen that the flow pattern is almost symmetrical fore and aft of the cylinder. Fig. 5.2 b is taken close to the instant at which separation has begun at the downstream stagnation point. Fig. 5.2 c-d show that the point of separation has moved a considerable distance upstream and also shows the successive growth of the symmetrical vortices. Finally, Fig. 5.2 f shows the flow pattern after a long time. Here the vortices are shed one at a time from alternate sides.

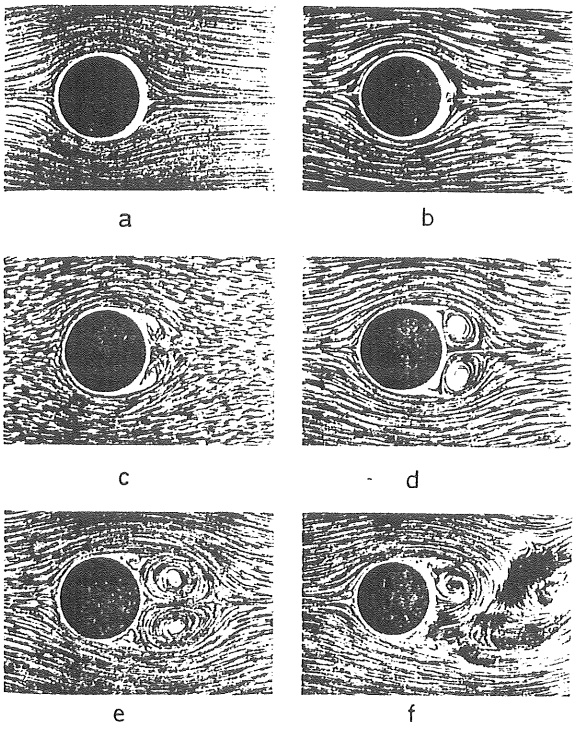

Figure 5.2 Impulsively initiated steady flow (Batchelor 1970, from Prandtl 1927).

Fig. 5.2 a-f demonstrates that the flow pattern is not only dependent on the free stream velocity, which is identical in the figures, but is also dependent on time until a finite state is established.

As shown in Fig. 5.2 a, the water behaves largely as potential flow with the exception of a thin boundary layer which has been developed by the shear between the water and the cylinder surface. The flow pattern changes successively until a periodic shedding of the vortices is obtained. The vortices are shed alternately from one side or the other, causing a transversal alternating force. Thus a time dependent force has appeared although the mean velocity has been kept constant.

Before we describe the steady flow past a cylinder, potential theory is accounted for. This theory describes the flow of a nonviscous fluid but may give us some hints on the behaviour of real viscous flows.

5.1.2 Potential flow

The flow pattern for an ideal flow past a cylinder is described in potential theory. The velocity components at a point are defined as the derivatives of the velocity potential ϕ. In the x and z directions they are

$$u = -\frac{\partial \phi}{\partial x} \qquad \ldots (5.1a)$$

$$w = -\frac{\partial \phi}{\partial z} \qquad \ldots (5.1b)$$

As is discussed later in this chapter, the flow field of a real viscous fluid around a body can be divided into three regions. Close to the body there is a thin layer in which the viscous effects are large. Outside this thin layer, with the exception of the wake, the viscous effects are almost negligible. Knowledge of nonviscous fluid behaviour is therefore useful in predicting or analysing the behaviour of viscous flows.

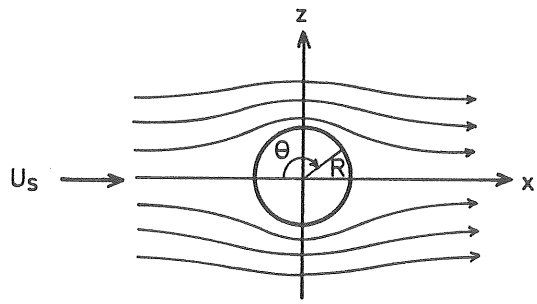

Figure 5.3 Flow pattern for flow past a circular cylinder.

By combining the velocity potential for a rectilinear flow with that of a dipole, which describes the influence of the cylinder, the flow pattern for flow past a circular

cylinder is obtained, see Fig. 5.3. The velocity potential for the combined flow is

$$\phi = -U_s x - U_s \frac{R^2 x}{x^2 + z^2} \qquad \ldots (5.2)$$

The velocity U_s is known as the free stream velocity, and is not affected by the cylinder, and R is the radius of the cylinder studied.

The velocity components at an arbitrary point may be obtained by differentiating Eq.(5.2).

In the x- and z-directions we obtain

$$u = -\frac{\partial \phi}{\partial x} = U_s + U_s R^2 \frac{(z^2 - x^2)}{(x^2 + z^2)^2} \qquad \ldots (5.3)$$

and

$$w = -\frac{\partial \phi}{\partial z} = \frac{U_s R^2 2xz}{(x^2+z^2)^2} \qquad \ldots (5.4)$$

respectively.

At any point in the flow the total velocity U is obtained by

$$U = \sqrt{\left(\frac{\partial \phi}{\partial x}\right)^2 + \left(\frac{\partial \phi}{\partial z}\right)^2} \qquad \ldots (5.5)$$

From Eqs. (5.3-5.5) one obtains the relation valid along the surface of the cylinder.

$$U_T = 2 U_s \sin\theta \qquad \ldots (5.6)$$

From Eq. (5.6) it is seen that the tangential velocity (U_T) at the surface is zero at the front and the back of the cylinder ($\theta = 0, \pi$). It is also seen that a maximum velocity of twice the free stream velocity is obtained at

$$\theta = \frac{\pi}{2} \text{ or } \frac{3\pi}{2}.$$

From the flow pattern and the Bernoulli equation the pressure variation throughout the flow may be obtained.

The Bernoulli equation is given by

$$-\frac{\partial \phi}{\partial t} + \frac{u^2}{2g} + \frac{p}{\rho g} + d = \text{constant} \qquad \ldots (5.7)$$

where p is the pressure, ρ is the density, g is the acceleration of gravity and d is the level. For constant d, ρ and t we obtain

$$\frac{u^2}{2g} + \frac{p}{\rho g} = \text{constant} \qquad \ldots (5.8)$$

The resultant force of the fluid on the surface of the cylinder is obtained by integrating the pressure distribution (Eq. (5.8)). The flow is laterally symmetrical around the structure and the velocities at θ and $(\pi - \theta)$ are equal, see Eq. (5.6). This leads to the finding that the pressures at those points are also equal and thus, that the resultant force is equal to zero (d'Alembert's paradox, see e.g. Batchelor, 1970). This is a consequence of the assumptions of potential flow where viscosity and separation are neglected. Nevertheless, potential theory is a useful tool for discussing general flow features.

5.1.3 Separation of flow

Separation is one of the key phenomena to describing flow past a bluff body such as a cylinder. As discussed, the flow of an ideal fluid past a body results in no force. A real fluid, however, cannot slip on a solid boundary, and consequently momentum is lost.

In real flow streamlines deviate from the body somewhere at its sides. This is called separation. The result is usually the formation of vortices.

Flow separation is caused by viscosity. For this reason, it is often described as boundary layer separation. Addi-

tional prerequisites for flow separation are increasing pressure in the streamwise direction (cylindrical bodies) and also enough fluid and a sufficiently long period of time, as exemplified in Fig. 5.2.

Separation and production of vortices may be understood by studying the flow around a circular cylinder, as shown in Fig. 5.4.

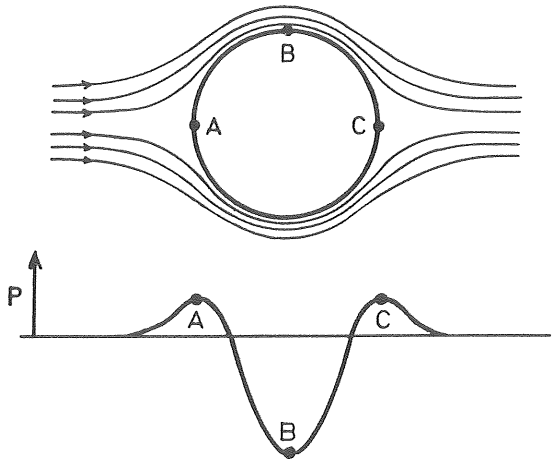

Figure 5.4 Ideal flow and pressure distribution (p) around a circular cylinder.

In an ideal fluid the fluid is accelerated downstream from A to B and decelerated from B to C. As the fluid flows towards the forward face, the pressure in the fluid rises from the free stream pressure to the stagnation pressure at A. As the fluid downstream from A accelerates to its maximum velocity at B, the pressure decreases according to Eq. (5.8).

The reverse takes place along B to C so that the fluid arrives close to C at the same velocity as it had close to A.

For real viscous flow the ideal or potential flow could be applied outside the boundary layer and wake where the flow is almost irrotational. Within the boundary layer,

however, large viscous effects are present. On its path from A to C the fluid loses much of its kinetic energy. And as the fluid in the boundary layer remains under the same pressure field as that existing outside the boundary layer, there is not enough kinetic energy left to overcome the positive pressure gradient, and so the fluid stops and the pressure gradient forces it to change direction away from the cylinder surface.

The point at which the flow separates is defined by $(\partial u/\partial y)_{y=0} = 0$ in the local coordinate system given in Fig. 5.5. Simultaneously the shear stress becomes zero, i.e. the viscous force vanishes at the point of separation. However, this definition is not applicable to all separation situations, for instance the separation associated with periodic shedding of vortices from a circular cylinder. The definition only yields an estimation of the mean separation point (line). For further discussion see e.g. Taneda, 1980.

Because of the positive pressure gradient downstream of the separation point, a backward flow occurs, as shown in Fig. 5.5.

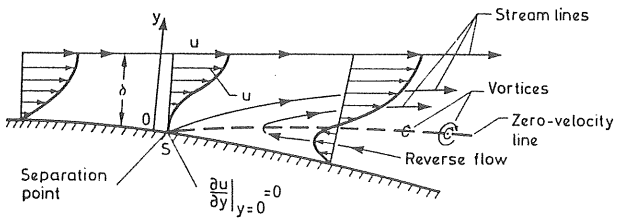

Figure 5.5 Velocity profile near the separation point (Chang, 1970).

As a consequence of the reverse flow, the boundary layer thickens considerably and vortices are introduced. These vortices grow and are finally transported away with the flow.

The importance of separation may be understood in terms of the fact that the flow pattern is completely governed

by the existence and position of the separation points, see Fig. 5.6.

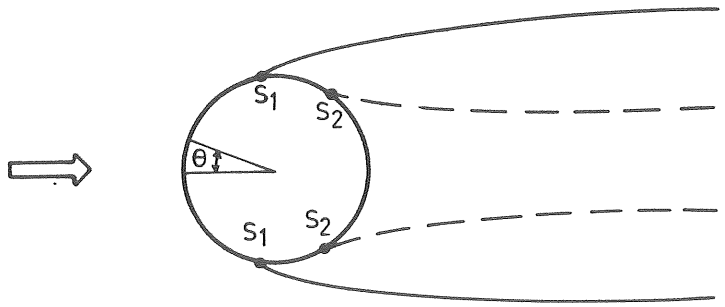

Figure 5.6 Schematic illustration of subcritical and critical wake region. ——— subcritical flow, ------- critical flow.

Points S_1 and S_2 in Fig. 5.6 are designated as the separation points for subcritical and critical flow, respectively. The drag coefficient for the critical flow is about 1/4 of that for the subcritical flow. A periodic force is also generated when the vortices are shed alternately from each side of the cylinder.

The flow around the cylinder also depends on the roughness of the cylinder and the intensity of the turbulence present in the ambient flow, as is discussed later in this chapter.

5.1.4 Boundary layer

The boundary layer is defined as the area in which the viscous effects become important. The boundary layer includes a thin region in front of the separation points on the cylinder.

As the force on a circular cylinder is caused mainly by the pressure (Re > 300), the positions of the separation points and the pressure distribution in the boundary layer are clearly important.

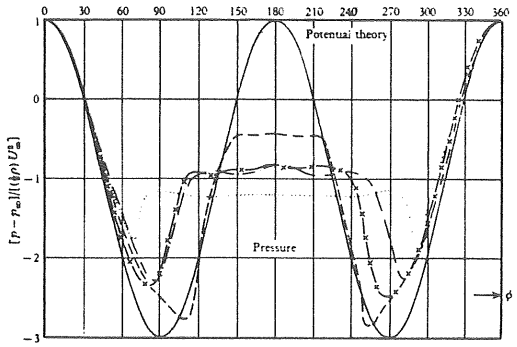

Figure 5.7 Pressure distribution around a circular cylinder at various Reynolds numbers, ..., Re = $1.0 \cdot 10^5$; -.-, Re = $2.6 \cdot 10^5$; --, Re = $8.5 \cdot 10^5$ -x-, Re = $3.6 \cdot 10^6$. (Achenbach, 1968).

In Fig. 5.7 the pressure distribution around a cylinder for various Re is shown as measured by Achenbach (1968). The pressure distribution according to potential theory is also shown.

Fig. 5.8 shows the variation of the drag coefficient with the Reynolds number. From this figure at least four different flow regimes may be discerned, namely subcritical, critical, supercritical and postcritical flow.

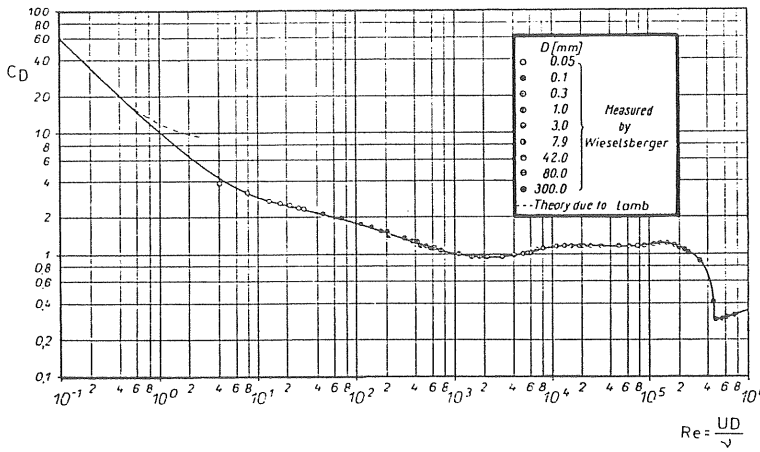

Figure 5.8 Drag coefficient for a smooth circular cylinder as a function of Re (Schlichting, 1968).

The subcritical flow regime comprises the regime where the Reynolds number is about $300 < Re < 2 \cdot 10^5$. Flow around a circular cylinder in this regime is shown schematically in Fig. 5.9 a.

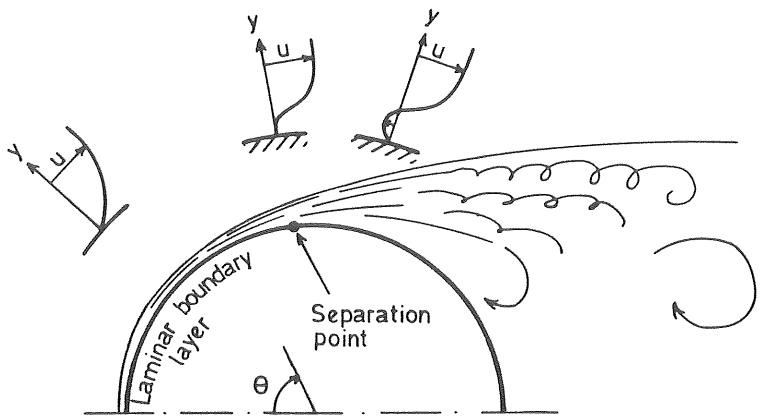

Figure 5.9 a Schematic illustration of a steady flow past a circular cylinder at subcritical Re. The approximate velocity variation within the boundary layer is also shown.

For a circular cylinder in this regime the whole boundary layer remains laminar but the vortex street becomes turbulent some distance downstream. Compared to a turbulent boundary layer, a laminar boundary layer has less resistance to separation because the exchange within the boundary layer (outer/inner region) and between the boundary layer and the outer region is small, and therefore the momentum transfer from the surrounding flow to the laminar boundary layer is also small.

In a turbulent boundary layer, however, the vigorous momentum exchange results in a large energy flux from the surrounding flow. Consequently the fluid particles may advance further towards a positive pressure gradient and shear before they separate from the body.

Fig. 5.9 a shows that the flow is attached to the surface from the stagnation point forward to an angle of about 80^o

before the separation takes place. The figure also shows that the separated flow, which is still laminar, becomes turbulent some distance downstream of the cylinder where a transition from laminar to turbulent flow thus takes place, see e.g. Bloor, 1964.

As the Reynolds number increases into the critical regime at about $2 \cdot 10^5 < Re < 5 \cdot 10^5$, a dramatic reduction of the drag coefficient takes place. A gradual increase of Re from $2 \cdot 10^5$ has the effect of moving the area with the turbulent separated flow gradually closer to the separation point, see Fig. 5.9 b.

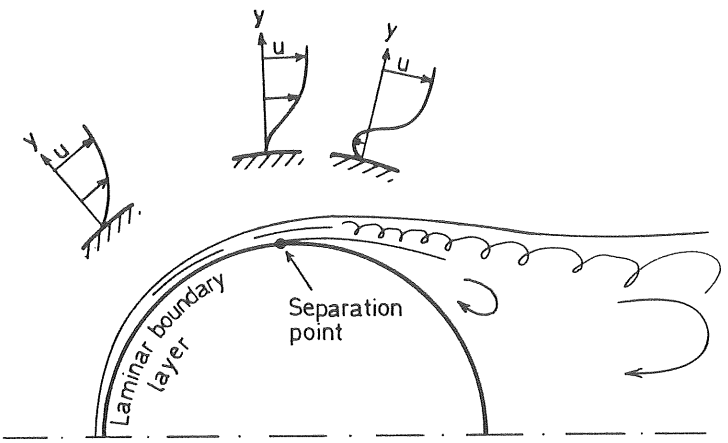

Figure 5.9 b Schematic illustration of a steady flow past a circular cylinder at about Re = $2 \cdot 10^5$. The approximate velocity variation within the boundary layer is also shown.

As the exchange of momentum become more vigorous the turbulent flow affects the laminar boundary layer in such a way that it becomes increasingly capable of resisting the adverse pressure gradient and boundary shear, and thus the flow separates further downstream.

At a Re of about $3 \cdot 10^5$ to $5 \cdot 10^5$ the transition has reached the surface of the body, which results in a reattachment of the separated flow, see Fig. 5.9 c.

As seen from Fig. 5.9 c there are now two separation points,

one in the laminar (S_1) and one in the turbulent boundary layer (S_2). Between the laminar separation point and the reattachment point (R) a "separation bubble" of circulating flow is produced.

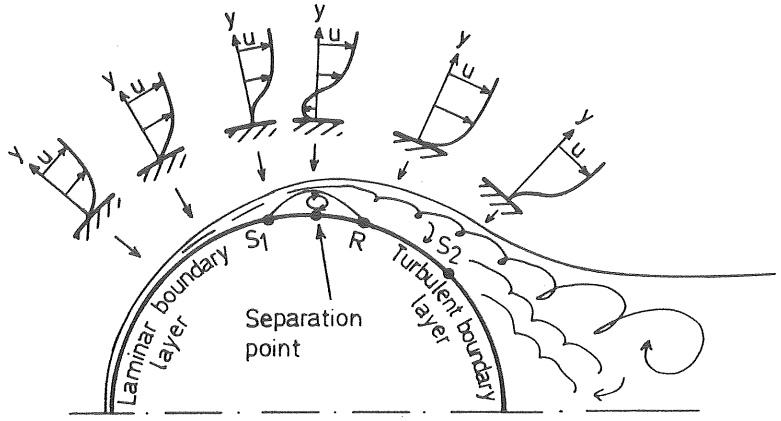

Figure 5.9 c Schematic illustration of a steady flow past a circular cylinder at about Re = $5 \cdot 10^5$. The approximate velocity variation within the boundary layer is also shown. S_1 and S_2 are laminar and turbulent separation points respectively. R is the reattachment point.

The momentum transfer of energy to and in the turbulent boundary layer results in separation first at about 120° to 140°. It should be noted that owing to small disturbances the separation bubble may arise only at one side - with a resultant skewness of the flow.

In the supercritical regime at about $5 \cdot 10^5 < Re < 3 \cdot 10^6$ the separation bubble is gradually dissolved. When the transition has extended far enough, at about Re = $3 \cdot 10^6$ the first separation point (S_1) vanishes and the separation bubble disappears, see Fig. 5.9 d.

The processes and phenomena occuring in the (super)critical regime have not been fully clarified. For recent experimental investigations the reader is referred to e.g. Schewe, 1986.

In the postcritical region, defined as the area where Re

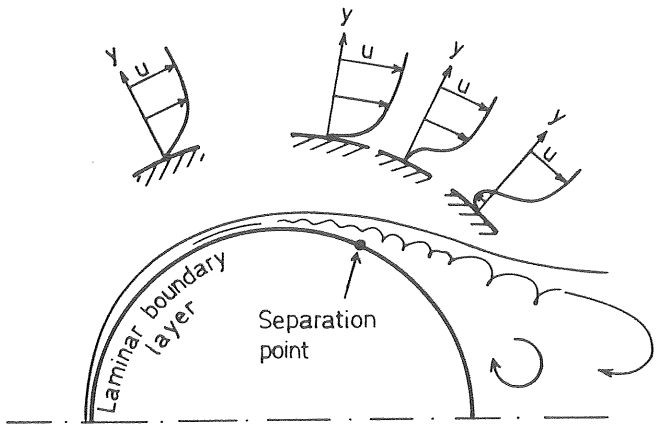

Figure 5.9 d Schematic illustration of a steady flow past a circular cylinder at postcritical Reynolds number. The approximate velocity variation within the boundary layer is also shown.

is greater than about $3 \cdot 10^6$, the transition moves further upstream. The angle of the turbulent separation point also becomes smaller. The reason for this is that in spite of an increased momentum transfer, the thickness of the boundary layer also increases, with correspondingly increased energy loss. When the transition appears at the point of minimum pressure, the position of the separation point is finally stabilized at an angle of about 110° - 120°.

Little is known about what happens at very high Reynolds number. Probably the flow is similar to that which characterizes the postcritical regime.

Finally, measurements made by Achenbach (1968) may illustrate how the separation point moves along the cylinder surface with increasing Re.

In Fig. 5.10 at least three of the four defined flow regimes can be distinguished. From about 80° in the subcritical regime, the separation angle suddenly rises at about $Re = 3 \cdot 10^5$. The separation point shifts from about 95° to 135°-140°. The postcritical regime is reached when the separation bubble vanishes at $Re = 1.5 \cdot 10^6$. The separation then occurs in the range of about 115° to 120°.

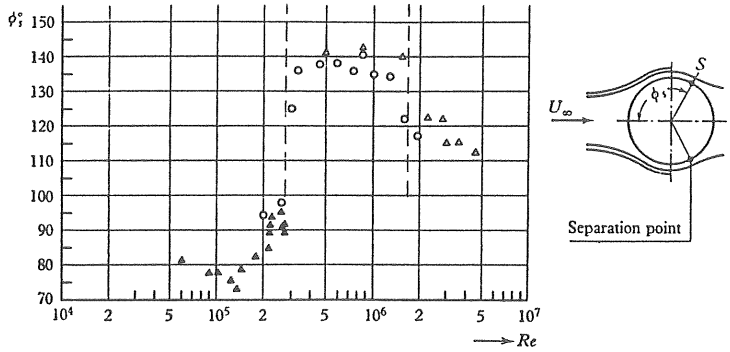

Figure 5.10 Position of separation point. (Achenbach, 1968).

5.1.5 Separation bubble

A separation bubble is likely to be formed if a laminar shear layer separates under a weak pressure gradient and goes turbulent soon after separation. The Reynolds number must be sufficiently high to give a nearly complete transition to turbulence before the shear layer has moved too far from the surface. Reattachment of the separated flow occurs if the relatively small entrainment flow into the underside of the separated shear layer is larger than the available reversed flow from far downstream. If this is the case the shear layer sucks itself back onto the surface, see Fig. 5.11.

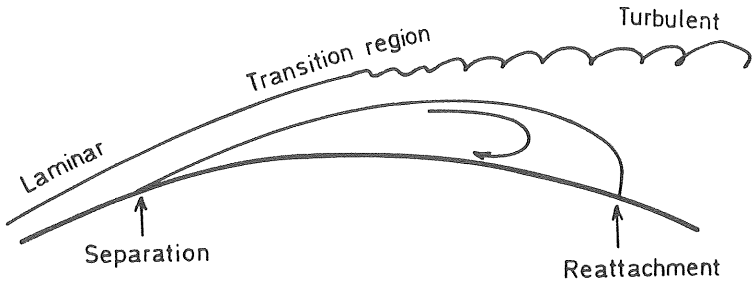

Figure 5.11 Transitional separation bubble.

A laminar reattachment is rare because the entrainment rate is not strong enough to overcome the adverse press-

ure gradient. Reattachment for an initially turbulent layer is also rare. Thus the entrainment rate is larger than in laminar flow, and so is the pressure gradient required to produce separation. A separation bubble can be observed for the case of a smooth surface according to Achenbach (1968) in a range of $3 \cdot 10^5 < Re < 1.5 \cdot 10^6$. However, it is restricted to a narrow flow range if the surface is rough.

Depending upon the length of the bubble the pressure distribution near the bubble changes just slightly. For airfoils, the existence of such bubbles are of great importance. The collapse of a bubble could result in a sudden increase of drag and a loss of lift force.

5.1.6 Boundary layer thickness

As a viscous fluid flows along a solid boundary first the laminar boundary layer thickens, and then after the transition the turbulent boundary layer thickens, as seen in Figs. 5.9 a-d. The boundary layer thickness may be expressed in several ways. One definition refers to the thickness δ of the region of retarded flow. Since the velocity variation within the boundary layer asymptotically approaches the free stream velocity, δ_{99} is usually defined as the distance where $U = 0.99\ U_s$. The distance by which the external flow stream lines are displaced in the y-direction by the existence of a boundary layer is called the displacement thickness δ^*. According to Fig. 5.12 this definition makes area A equal to B, so that (A+C) equals area (B+C).

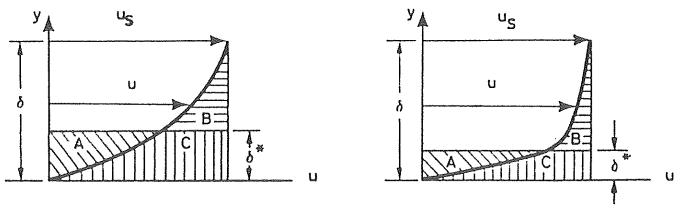

(a) Laminar boundary layer (b) Turbulent boundary layer

Figure 5.12 Boundary layer displacement thickness.

Another physically meaningful thickness is the momentum thickness (δ_θ), which is the thickness of a layer of external stream carrying a momentum flux equal to the reduction in momentum flux caused by the presence of the boundary layer. The definition given above may be used to describe the rate of momentum transferred to the retarded flow near the surface. This is expressed by the ratio of displacement thickness to momentum thickness by the shape factor (S_f) defined by $S_f = \delta^*/\delta_\theta$.

No more extensive discussion of steady boundary layer flow is given here. However, it should be mentioned that for calculations of the laminar and turbulent shear layers in a pressure gradient, the methods of Thwaites and Head may be used. An excellent description of momentum transfer in boundary layers is given by Cebeci and Bradshaw 1977, where complete Fortran programs for the various methods are given.

5.1.7 Vortex shedding

The separation of flow around a circular cylinder discussed in the previous pages, concerns average behaviour over time. Actually, flow separation is an unstable phenomenon, as the separation points are moving back and forth along the surface.

In the subcritical and postcritical regimes there is a strong connection between vortex shedding and the resulting alternating force. The predominant frequency of vortex shedding (f_s) and the free stream velocity (U_s) is given by

$$f_s = \frac{SU_s}{D} \qquad \ldots (5.9)$$

where D is the cylinder diameter and S the Strouhal number given in Fig. 5.13. According to Norberg 1987, the Strouhal number for $200 \leq Re \leq 3 \cdot 10^5$ is given by $S = 0.20 \pm 0.015$.

In the critical - supercritical regimes the shedding fre-

quency may be defined in terms of the dominant frequency in a broad-banded spectrum.

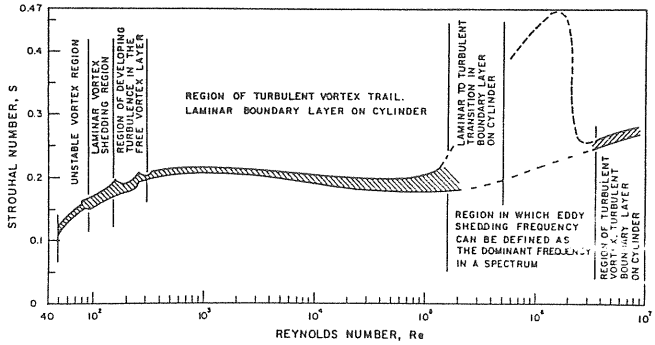

Figure 5.13 The Strouhal-Reynolds number relationship for circular cylinders (Lienhard, 1966).

5.1.8 Roughness effects and free stream turbulence

Surface roughness has a major impact on the flow around a circular cylinder. This is mainly caused by the roughness, which introduces disturbances that cause an early transition. The positions and value of the minimum drag coefficient are also strongly affected by the cylinder roughness, as is the Strouhal number.

In Fig. 5.14 a the drag coefficient (C_D) is shown as a function of the Reynolds number with the surface roughness as a parameter (k_s/D).

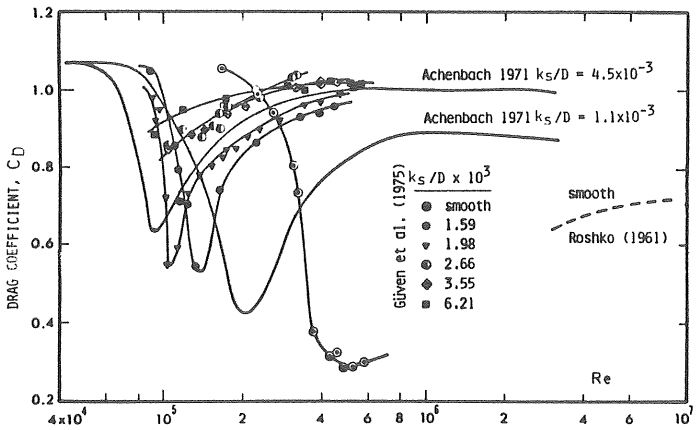

Figure 5.14 a Drag coefficient for rough cylinders as a function of the Reynolds number. (Sarpkaya and Isaacson, 1981).

In the subcritical regime, where the boundary layer is laminar, roughness has no effect on the drag. The Reynolds number is called critical at the positions of minimum drag. In Fig. 5.14 a it can be seen that the critical Re decreases with increasing roughness. The range of Re for which the drag is considerably reduced also decreases with increased roughness. Note that the critical Re also is defined as the point where C_D = 0.7 (Bearman and Morel, 1983).

The actual critical Reynolds number for a given surface roughness is given by Achenbach and Heinecke (1981) as

$$Re_{crit} = \frac{6000}{(k_s/D)^{1/2}} \qquad \ldots (5.10)$$

The postcritical regime is found where the C_D is almost constant.

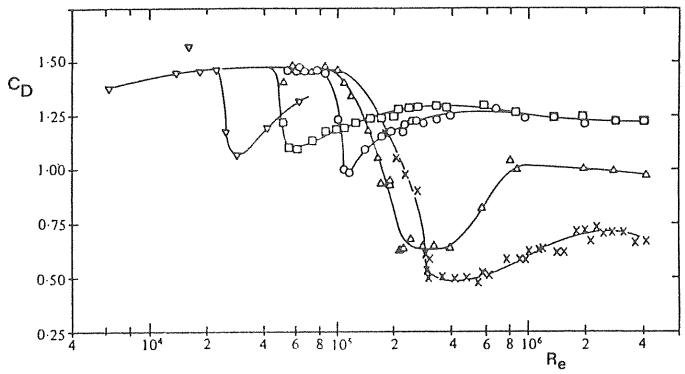

Figure 5.14 b Drag coefficient for cylinder at various surface roughness parameters k_s/D:

x, smooth; $\frac{1}{5}$ Δ, $75 \cdot 10^{-5}$; $\frac{1}{5}$ o, $300 \cdot 10^{-5}$;
□, $900 \cdot 10^{-5}$; ∇, $3000 \cdot 10^{-5}$.
(Achenbach and Heinecke, 1981).

As can be seen from Fig. 5.14 b increased C_D is obtained with increased relative roughness. For $k_s/D > 300 \cdot 10^{-5}$ the C_D coefficient levels out at about 1.2.

Fig. 5.15 shows the angular position of boundary layer separation at various roughness parameters. From this figure the phenomena in the critical-to-postcritical region may be clarified.

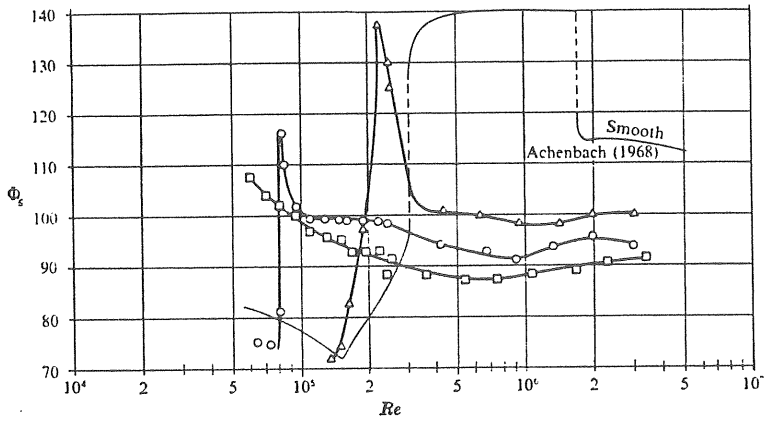

Figure 5.15 Circular cylinder in cross-flow. Angular position of boundary layer separation at various roughness parameters. k_s/D: Δ, $110 \cdot 10^{-5}$; O, $450 \cdot 10^{-5}$; □, $900 \cdot 10^{-5}$ (Achenbach, 1971).

The importance of angular position of boundary layer separation on the Strouhal number is also clarified by Figs. 5.15 and 5.16. With increasing roughness the Strouhal number is reduced, as seen in Fig. 5.16. For a very raw surface the Strouhal number levels out and is almost constant over the whole range of Reynolds numbers.

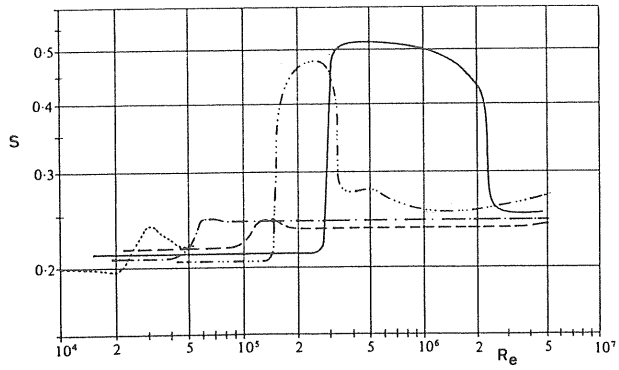

Figure 5.16 Circular cylinder: Strouhal number vs. Reynolds number at variable surface roughness conditions. ——, smooth; -·-·-, $k_s/D = 75 \cdot 10^{-5}$; — —, $k_s/D = 300 \cdot 10^{-5}$; -·-·-, $k_s/D = 900 \cdot 10^{-5}$; -----, $k_s/D = 3000 \cdot 01^{-5}$. (Achenbach and Heinecke, 1981).

The Reynolds number where the critical regime starts is also strongly affected by the free stream turbulence present in the ambient flow. An increased free stream turbulence intensity results in a lowering of the critical Re. However, as reported by Bearman and Morel 1983, the resulting effect on drag is not easily predictable. Occasionally free stream turbulence acts to increase as well as to decrease drag. At other times free stream turbulence has no effect at all. However, when it does change the drag the effect always increases with increasing intensity.

5.2 Planar oscillating flow

There are fundamental differences between harmonically oscillating flow and steady flow around a circular cylinder. In an oscillating flow the fluid reverses direction and consequently the vortices shed in the previous half cycle are swept back, affecting the flow around the cylinder. Furthermore, this reversed flow causes the separation points to undergo large fluctuations, thus changing the magnitudes of the fluid induced forces.

In spite of these differences, the study of steady flow is very useful for developing ideas about the flow processes. Physically, many aspects of the flow processes involved are similar which helps to obtain a better understanding of oscillating flow.

Considerable progress has been made in the understanding of three-dimensional wave-induced flow around structures by carrying out experiments in planar harmonic flows. The wave-induced flow is henceforth called wavy flow. Wake reversal is a particularly common feature of both planar harmonic and wavy flow and the vortex motions observed indicate that planar oscillating flow should be fairly representative of wavy flow.

As regards motion geometry, the harmonic planar oscillatory flow can be considered the simplest type of oscillat-

ing flow. This flow is obtained by either oscillating the cylinder in still water or oscillating the flow around a fixed cylinder.

The most important parameter governing oscillating flow is the Keulegan-Carpenter number KC

$$KC = u_m T/D$$

where u_m is the maximum velocity during a cycle
T the period of the cycle
and D the diameter of the cylinder.

Sarpkaya found that the force coefficients depend not only on KC but also on a frequency parameter β

$$\beta = Re/KC = D^2/T\nu$$

where ν is the kinematic viscosity.

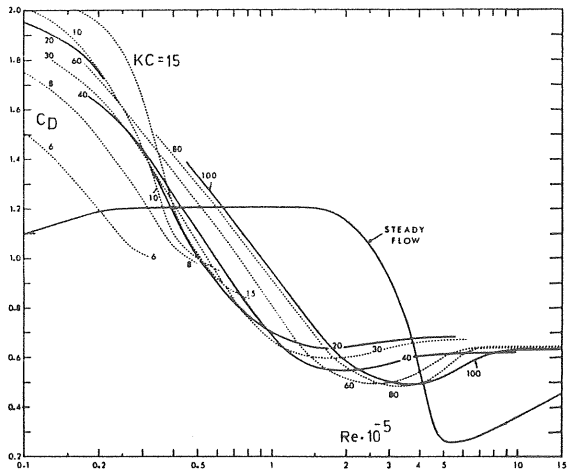

Figure 5.17 C_D verses Reynolds number for various values of KC (Sarpkaya and Isaacson, 1981).

In Fig. 5.17 the C_D coefficient as a function of Reynolds number is shown with KC as a parameter. It can be seen that the critical Re decreases with decreasing KC. The range of reduced drag coefficient is also greater for smaller KC. Furthermore the oscillating flow has increased the

drag coefficient at the critical Re and finally amplified the drag coefficients in the subcritical region.

The increased drag coefficient at decreased critical Re is caused by an earlier transition in the boundary layer. As described above, the transition depends on the surface roughness, the intensity of turbulence in the ambient flow and also on how the experiments were performed. As the low drag coefficient at the critical Re for a steady flow is mainly caused by the existence of a separation bubble, its formation and extent are very sensitive to these factors. The increase of the drag coefficient in the subcritical regime is mainly caused by vortices and large scale turbulence in the vicinity of the cylinder. The influence of vorticity may be divided into two parts, the growth of new vortices and the passage of vortices from the previous cycle.

During the initial stage of the cycle, the growth of the vortices is so rapid that the vortices grow much larger than their steady state size before they separate. Sarpkaya and Isaacson (1981) demonstrates that the drag coefficient for an impulsively initiated flow may initially exceed the steady state value by up to 30 procent.

The influence of vorticity is most pronounced when the duration of the flow in one direction is relatively short, which is the case at low KC. This effect is discussed in greater detail in the next section.

5.2.1 Separation in oscillating flow

If it were possible to predict the point of separation for oscillating flow around a cylinder it would also be possible to explain the pressure distribution around it and hence the forces. The free stream turbulence in the ambient flow and the complex behaviour of vortices shed in the previous cycle strongly affect the separation of the boundary layer.

A simplified study by Grass and Kemp (1979) may be used to describe the separation phenomena in oscillating flow. Their study shows that the angle of separation varies regularly through each half cycle of oscillation, see Fig. 5.18.

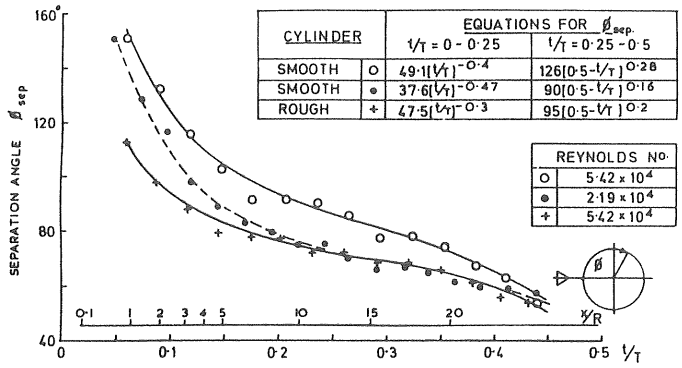

Figure 5.18 Variation of the separation angle over a half cycle for smooth and rough cylinders at a KC of 38 (Grass and Kemp, 1979).

The study is based on flow visualization for oscillatory flow past smooth and rough cylinders with data chosen from Sarpkaya. According to Fig. 5.17, for the chosen Re ($0.219 \cdot 10^5$ and $0.542 \cdot 10^5$) and KC (38), the flow over the smooth cylinder should be in the subcritical and in the critical regimes, respectively.

The planar oscillatory flow was simplified so that each half cycle was considered as an independent event. This is analogous to a cylinder accelerating from at rest in still water to a point of maximum velocity and then slowed down with increasing deceleration to a zero velocity at the end of each half cycle. In reality, as discussed in the next section, the cylinder moves into a highly disturbed flow field left over from preceding half cycles.

The study also shows that initially an unseparated potential-like flow is obtained. Separation occurs very early and usually in the region close to the downstream stagnation point. The separation point then moves very quickly

upstream round the cylinder as is seen in Fig. 5.18. In the deceleration stage the pressure gradient on the flow forces the fluid particles to leave the surface at the upstream face of the cylinder, which reduces the angle of separation still further. This results in a progressively increased width of the wake region during the half cycle.

If Sarpkaya's results (Fig. 5.17) are compared with the results of Grass and Kemp, a passage from the subcritical to the critical region which would approximately increase the separation angle by 10^{o} throughout the cycle, would result in a drop of the C_D coefficient from about 1.6 to 1.0.

5.2.2 Vortex trajectories

The key to time dependent separated flow is the understanding of the formation, growth and history of motion for vortices. As the problem of separated flow about a bluff body remains theoretically unresolved one must still rely on the observation of experiments.

The fact that the vortices formed return to the cylinder when the flow or the cylinder reverses (in still water) is important. Specific repeatable vortex shedding patterns are found to occur within different ranges of KC.

For small KC, below 3, there are no pronounced vortex patterns. Small vortices with very little or no influence may be present. At a KC of about 4, symmetrical vortex pairs form at flow reversal as shown in Fig. 5.19.

In picture (1) the vortices from the previous half cycle are split up as the cylinder moves downwards and each vortex generates a secondary vortex of the opposite sign as seen in picture (2). These two pairs quickly move away from the cylinder and can be seen in the top corners of pictures (3) and (4). As the cylinder reverses, a new set

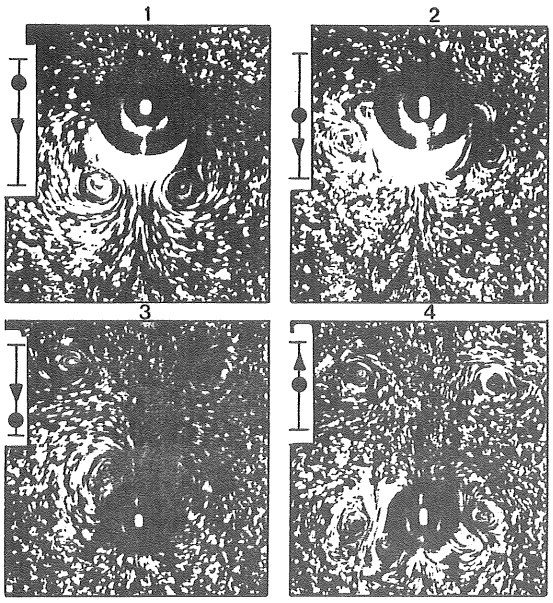

Figure 5.19 Symmetrical vortex shedding for KC of about 4. Arrows refer to the cylinder motion (Williamson, 1985).

of vortices are formed, ready to undergo the same process. This can be seen at the bottom of picture (4). As the vortices are shed symmetrically, no transverse force is generated.

In the KC range of 4 to about 7, the vortices increase in strength, but behave essentially as described above. However, a small transverse force is now present, caused by asymmetrical flow. This slightly asymmetrical flow has been noted by Williamson (1985) to be caused by the fact that, due to small disturbances in the flow, the vortex pairs do not form simultaneously when the flow reverses.

Another stable vortex shedding pattern is established for KC somewhere between about 7 and 15. This regime may be termed the transverse vortex shedding regime because the majority of the vortex activitity takes place on only one side of the cylinder. Fig. 5.20 shows the flow at various stages in this KC regime.

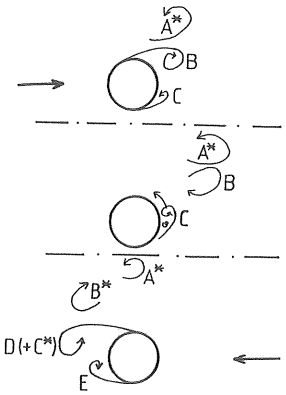

Figure 5.20 Vortex shedding pattern for 7<KC<15. * indicates a vortex that has been shed in a previous half cycle (Bearman, 1985).

In the first sketch showing the flow passing from left to right vortex A* which was formed and shed during the last half cycle, is being convected back to the cylinder. The influence of vortex A* at an early stage in the half cycle causes higher velocities over the top of the cylinder. Vortex B thus grows stronger than vortex C. At the end of the half cycle vortex C is forced back over the top of the cylinder by the field of the stronger vortex, B. In spite of the fact that some of the vorticity of vortex C has probably vanished, the remaining parts of vortex C initiate shedding in the next half cycle. As the vorticity of vortex C* has the same sign as the new vortex D it mixes with and strengthens vortex D as indicated by D(+C*) in the lower sketch. Regarding the transverse force, vortex C, travelling to the other side of the cylinder causes a force downward in the figure, of opposite sign as that created by vortex B when it returns.

One more full vortex is shed every time KC is increased by roughly 8. The vortex shedding pattern for 15 < KC < 24 and 24 < KC < 32 is shown in Fig. 5.21 a-b.

In the range 15 < KC < 24 the returning vortex A* forms a pair with vortex B before the end of a half cycle and the

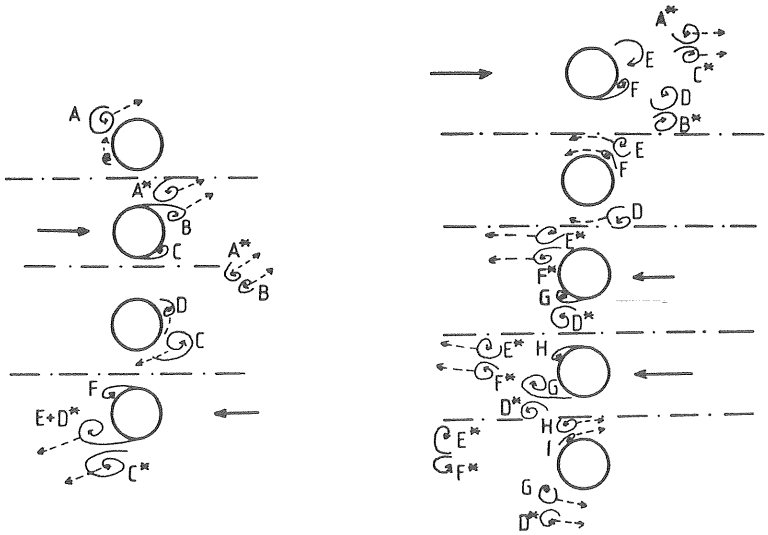

Figure 5.21 a-b Vortex shedding pattern for 15<KC<24 resp. 24<KC<32. * indicates a vortex that has been shed in a previous half cycle (Bearman, 1985).

two move away at an angle of about 45 degrees. During this event vortex C continues to grow. When the flow reverses, vortex D is forced back under the cylinder by the field of the stronger vortex, C. The vortex pair formed (C* and E+D*) are transported away in the diametrically opposite direction of the pair in the previous half cycle. The vortex shedding pattern for 24 < KC < 32 is essentially as described for the range 7 < KC < 15, but with three instead of one vortex shed per half cycle. For further details see Bearman (1985) and Williamson (1985).

For KC above about 30, Bearman et al. (1981) and others show that the transverse force could be described quite adequately by a quasi-steady model.

To further complicate the vortex trajectoring there is a spanwise correlation of shedding. Measurements of transverse force using load cells attached to each end of the cylinder show that the force from either end may be in phase, while at other times it may be 180^{o} out of phase.

Bearman (1985) and Bearman et al. (1981) show that the correlation length may be no more than 3 or 4 diameters, see Fig. 5.22.

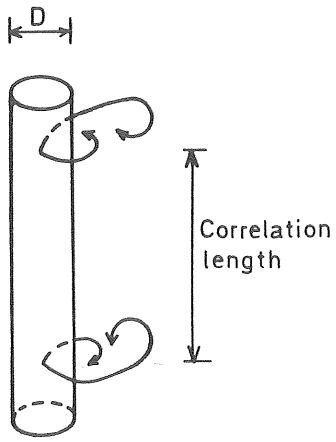

Figure 5.22 Spanwise correlation of the vortex shedding.

Bearman states that the precise cause of the phase switching is not clear but it may be due to different modes of shedding occurring on different parts of the cylinder.

5.3 Wavy flow

The experiments with cylinders in planar harmonic flow described above are more easily observed and reproduced than experiments with a cylinder in waves, "wavy flow". It is therefore important to note the differences between the two types of flow.

For wavy flow, the undisturbed paths of the water particles are ellipses instead of straight lines. For wavy flow there is also an exponential decay of the particle velocity from the water surface and downwards. Especially for steep waves, then, there is no harmonic variation of the kinematics during the wave period. Unlike planar oscillating flow, which is usually produced in a closed conduit, there also is the effect of the free surface for wavy flow.

The advantage of wavy flow experiments is that both the undisturbed water paths and free surface effects are correctly

modelled. Furthermore, experimental data from regular waves can be used to predict forces on a vertical cylinder in irregular waves, as confirmed by Bearman, Chaplin et al. (1985). The disadvantages are that it is difficult to obtain realistic Re, and that the kinematics must be measured separately or evaluated from a suitable wave theory.

What is the effect of the elliptic motion of the water particles in wavy flow on shallow water, compared to the effect of the straight motion in planar oscillating flow? Deep below the still water level, one might suspect that the flow pattern outside the boundary layer around the cylinder to the separation points, would be described by potential theory. But are there any ellipticity effects on the flow above this level up to the water surface? So far, the phenomena have not been fully understood, but some observations have been made. Both Williamson (1985) and Bearman (1985) conclude that the wake reversal is a feature of the two and the three-dimensional oscillating flow, and that the vortex motion observed at low Re indicates that the two-dimensional flow should be representative of some of the vortex motion around vertical cylinders in waves.

However, the correlation of shedding over a distance of only two cylinder diameters was found by Bearman, Chaplin et al. As also shown by Gaster (1969), a deviation from two-dimensionality may result in weaker and less regular shedding. Bearman, Chaplin et al. (1985) measured loads on both a vertical and a horizontal cylinder in the post-critical region. For both orientations they concluded that the loading coefficients show little or no influence of the ellipticity of the water particles over the range examined. It is thus possible to conclude that the two-dimensional flow represents the wavy flow from the ellipticity point of view fairly well. The small influence observed is probably due to a destabilization of the boundary layer, which results in the critical region being reached at smaller Re.

How the free surface affects the flow around a vertical cylinder for oscillating flow is seldom discussed in literature. In order to gain a better understanding of the phenomenon, experiments were carried out by Nilsson and Nilsson (1985). They measured the water particle velocities and the flow direction around a vertical circular cylinder in wavy flow. The same measuring equipment as described in Chapter 3 and by Moberg, Bergdahl and Carlsson (1986) was used.

The maximum velocity below the wave crest and the flow direction around the cylinder were measured. The measuring points were situated between 30 and 150 mm from the cylinder surface and at 0.1 m and 0.3 m below the still water level ($Re \cong 10^5$). By comparing the measured values with the ones given by potential theory, the following conclusions concerning the flow direction could be drawn. First, the flow angle to the free stream direction in front of the cylinder was about 5 to 10 degrees greater than that given by theory. Secondly, the flow direction was not tangential at the middle of the cylinder (90^o). Finally, the flow direction at the back of the cylinder was more aligned with the free stream direction. These deviations were especially pronounced for points close to the cylinder surface.

Concerning the comparison between measured maximum velocity and that given by potential theory, the following characteristics were observed. Firstly, the velocities at the middle of the cylinder were smaller than predicted by potential theory. This discrepancy decreases with increased depth and with increased distance from the cylinder surface. Secondly, a higher maximum velocity was recorded at 135 degrees than was measured at 45 degrees, which results in fore and aft asymmetry of the flow pattern. Finally, velocities measured at the front of the cylinder were considerably smaller than those given by the potential flow.

Fig. 5.23 shows the percentage deviation, compared to potential theory, of maximum velocity as a function of

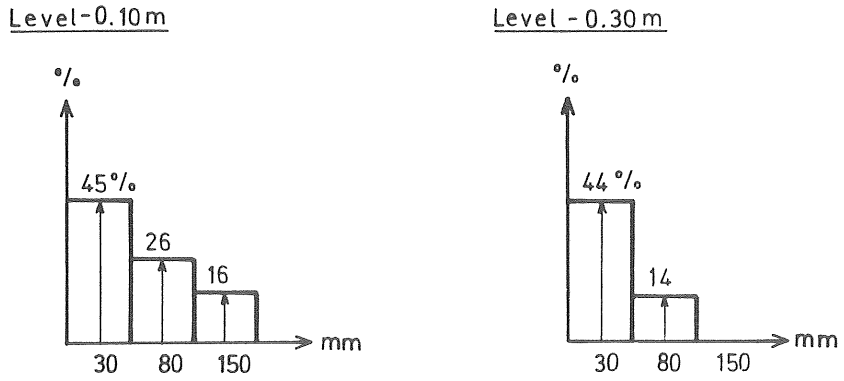

Figure 5.23 Measured deviation in maximum horizontal velocity in front of the cylinder (0^{o}), given as percent, compared with potential theory, as a function of radial distance from the cylinder surface 0.1 and 0.3 m below still water level (Nilsson & Nilsson, 1985). These data correspond to wave J, whose characteristics are given in Table 4.1.

radial distance from the stagnation point at the front of the cylinder. As can be seen, the deceleration is substantially greater than that given by potential theory, which must result in a greater area of nearly stagnant water in front of the cylinder.

The main conclusion which can be drawn from the observations is that the boundary layer thickens on the up-wave face of the cylinder near the free water surface. This thicker boundary layer consists of the ordinary boundary layer (see Chapter 5.1) together with a layer retarded by the cylinder. This amplified boundary layer results in an asymmetrical flow pattern around the cylinder which affects the pressure distribution considerably, and consequently affects the resulting forces. The phenomena caused by the free water surface are referred to as "free surface effects".

5.3.1 Free surface effects

The effects of the free surface, so far, have not been fully understood, even for stationary flow. The descrip-

tion in this chapter is mainly taken from two papers, one by Mori (1984) and one by Takekuma and Eggers (1984). These papers investigate the bow wave phenomenon around blunt ship bows in stationary flow. However, their observations are probably also applicable to wavy flow, since the phenomena reported are supported by the observations made by Nilsson and Nilsson (1985) and by findings in the present study.

The free surface effects are mainly due to separation on the free surface, under which a shear layer develops. The reason for this shear flow is the free-surface curvature. The free surface effects, which may also be called the bow wave phenomena are very important, since they may contribute to much of the total resistance to forward motion in case of full ship forms or, as in the case of a circular cylinder in waves, affect the flow pattern considerably.

The bow wave is considered to consist of three regions with significantly different flow characteristics, as shown in Fig. 5.24.

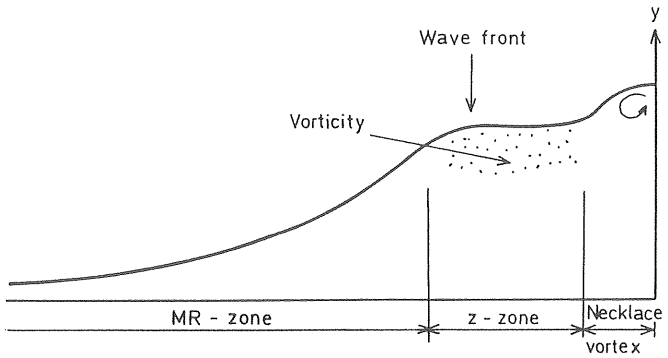

Figure 5.24 Schematic illustration of different flow regions for a bow wave.

The MR-zone is the part of the bow wave ahead of the blunt body where the free surface is stable and rises monotonously with a concave curvature. Through a sharp change of curvature the flow enters the horseshoe-like

z-zone, where the free surface flow may be turbulent. In the immediate vicinity of the bow a necklace vortex with a reversed flow at the free surface develops. The name necklace vortex is illustrative, because around a ship at full speed it looks like a necklace of pearls.

Mori photographed and measured wave patterns and profiles around two vertical cylinders, one of which was circular (D=0.42 m) and one of which had an elliptic section (beam = 0.3 m). Fig. 5.25 a-d shows the different flow regions and how they are affected by different speeds and shapes.

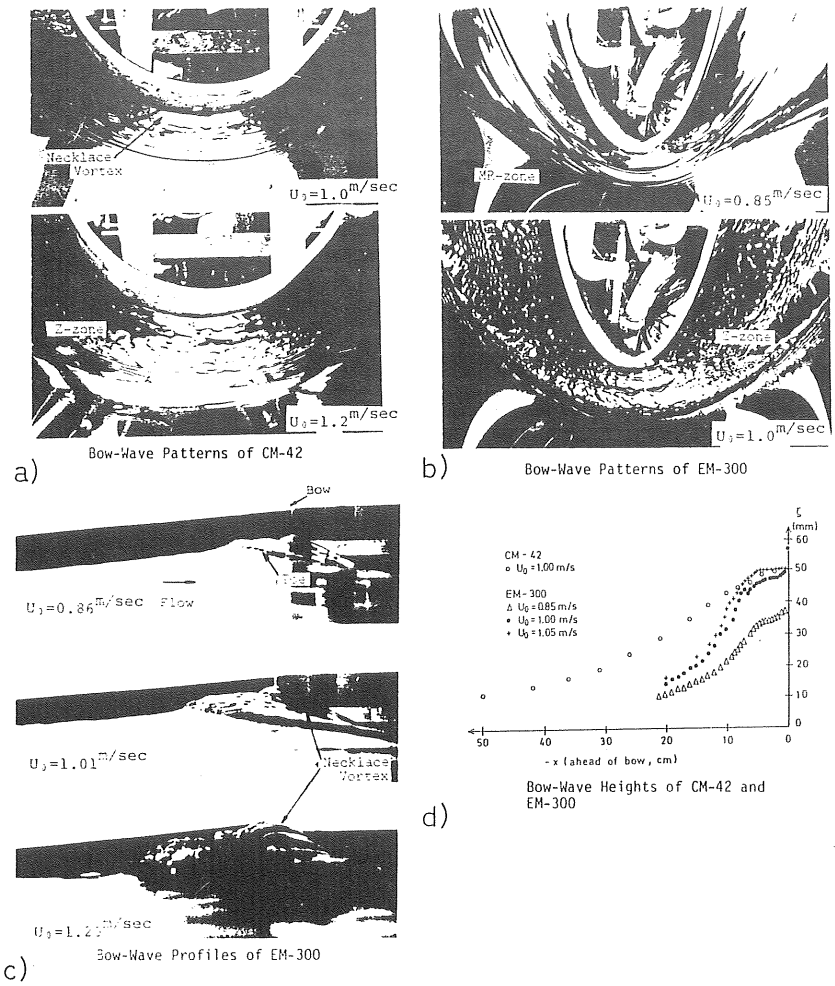

Figure 5.25 a-d Wave patterns and profiles around a circular and elliptic cylinder (Mori, 1984).

The wave-front is clearly distinguished surrounding the bow, with capillary waves ahead of it. It is seen that the surface of the plateau-like elevation becomes rather turbulent beyond a certain velocity.

Close to the body accumulated vorticity around the bow can be observed as a necklace vortex. It can also be observed that the wrinkles, due to turbulent fluctuations are less intense for the circular cylinder than for the elliptical one at the same speed.

On the other hand, the necklace vortex of the circular cylinder seems larger and more intense. Mori suggests that the turbulent flow may be generated at the wave front (toe), which then probably plays the role of a trigger for the turbulence transition. A sharp change of curvature is then followed by a rapid change of vorticity. Mori also concludes that the deceleration of the approaching velocity in the proximity of the bow is responsible for the formation of the upstream necklace vortex. Fig. 5.25 d now offers an explanation of the differences between the circular and elliptical cylinders reported above. As the free surface ahead of the circular cylinder has less curvature, the approaching velocity in the proximity of the bow must be greater than for the elliptical cylinder. This results in a larger and more intense necklace vortex for the circular cylinder.

The approaching velocity and its deceleration rate are important factors for the inception of the free surface instability. It is assumed that the vorticity generated in the free surface shear layer is one of the sources of vortex motion of the necklace vortex. The formation of the necklace vortex may be explained on the basis of the amplification of vorticity in the free surface shear layer through vortex stretching as the particles flow downstream and wrap around the cylinder.

The existence of a shear flow on the free surface has been

shown clearly by Takekuma and Eggers, who used dye particles placed in front of the bow, as seen in Fig. 5.26. They also observed that the intensity of the shear layer and the vorticity increased with increasing speed.

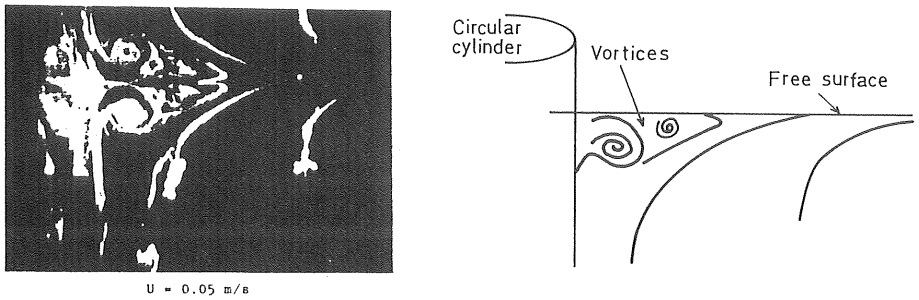

Figure 5.26 Shear flow and vortices observed by flow visualization for a circular cylinder. (Takekuma and Eggers, 1984).

By measurements of mean velocities Mori also concluded that there is also a velocity defect in the MR-zone. No reverse flow was observed in the z-zone.

The effect of the decelerated flow on the free surface of the bow wave is clearly explained in a study by Kayo and Takekuma (1981). They produced an artificially strengthened shear flow in front of the model by covering the free surface with a thin vinyl sheet and towing it at the same speed as the model itself. The artificially strengthed shear flow caused an expanded region of breaking - as can be seen in Fig. 5.27 - which caused increased resistance for the ship model.

On the other hand, by accelerating the free surface toward the ship model by using an air jet, the shear layer and the wave breaking were reduced, as was the ship resistance.

One realistic and efficient way of reducing the shear flow is to use a bulb protruding underwater. Such a bulb accelerates the water, which decreases vortical motions and consequently reduces the bow wave. Flow visualization of

this phenomena on a circular cylinder, with and without a bulb, is shown in Fig. 5.28.

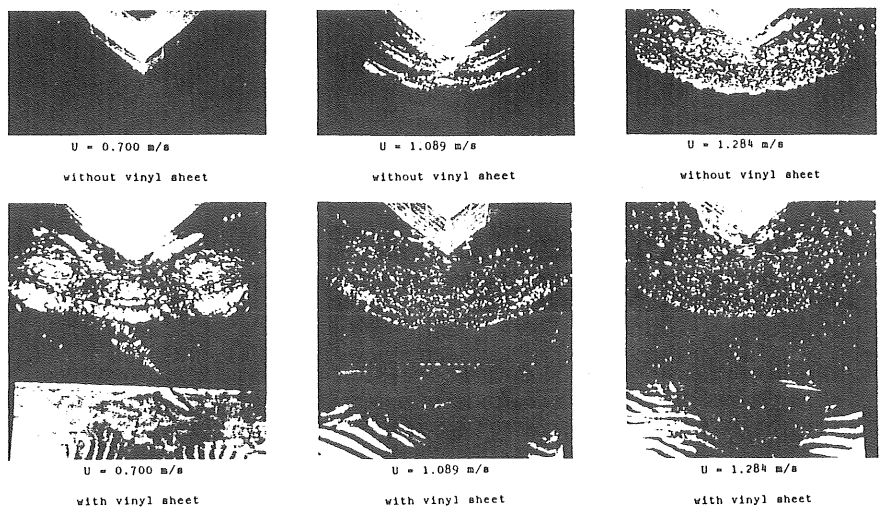

Figure 5.27 Effect of an artificial increase of shear flow (Kayo and Takekuma, 1981).

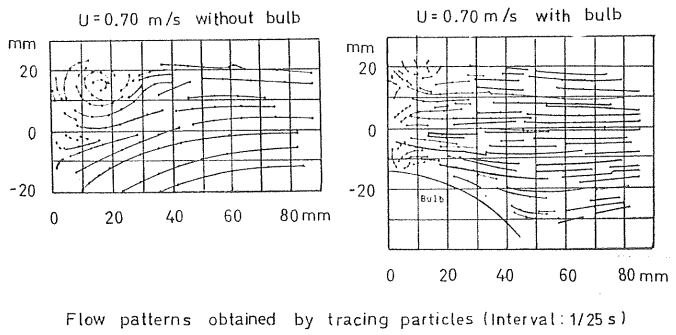

Figure 5.28 Flow field in front of a vertical circular cylinder with and without a bulb (Takekuma and Eggers, 1984).

In summary, the following are the main conclusions that can be drawn from stationary flow studies of the free surface effects

- The existence of a shear flow on the free surface has a significant effect on the occurrence of wave breaking.

- The turbulence intensity of the sub-breaking wave is closely related to the free surface curvature, the velocity defect in the free surface shear layer and the deceleration rate.

- The free surface affects the flow pattern around the cylinder considerably.

5.3.2 Time-dependent separated wavy flow - observations and conclusions

It is not possible, on the basis of the experimental data gathered, to draw general conclusions concerning the effect of the free surface for a time dependent separated wavy flow. However, some of the phenomena observed may help us to get an idea of what further work is needed.

To begin with, the work done by Nilsson and Nilsson (1985) clearly shows that, as a result of the free surface effects, there is a retarded layer in front of the cylinder. This retarded layer observed may be treated as a part of the boundary layer since the viscous effects are large. By measuring the velocity, its direction and the pressure distribution around the cylinder, it was established that the free surface effects result in an asymmetrical flow around the cylinder. Disregarding the effects of the separated flow, this asymmetrical flow results in a greater flow angle to the free stream direction at the front and a more aligned direction at the back of the circular cylinder. From this one can conclude that the explanation of wavy flow is found at both the front and the back of the vertical cylinder. The flow in the front plays a paramount role since it very much influences the flow pattern at the back.

An additional study of the free surface effects was performed by taking a series of photographs of the water surface. These photos were taken from below through the glassed wall of the wave tank up towards the water sur-

face. Two cameras were used which photographed the surface around the cylinder simultaneously, at about 70 and 110 degrees from the wave tank longitudinal direction.

Fig. 5.29 shows the flow pattern at the surface for a crest situation. In the photos, a horseshoe-like flow around the cylinder can be distinguished. This flow should represent the previously described z-zone. Also, between 112.5^{o} and 135^{o} some kind of separation is seen. The necklace vortex may be seen in the left photo. Inside the horseshoe-like zone and probably in connection with the prolonged necklace vortex, there is a deflection of the water surface downward and inward against the cylinder. This phenomenon may be more clearly observed in Fig. 5.30 which shows the measured pressure distribution and the corresponding water level from the front stagnation point to the back of the cylinder. The water level of the waves was measured alongside the cylinder, halfway between the cylinder surface and the wave tank wall. The local water level at the cylinder is lower than the corresponding level for the bypassing wave, from about 20 degrees all the way around to the back stagnation point.

By studying the pressure distribution in Fig. 5.30 it can be observed that from having been rather symmetrical (potential-like flow) at deep levels, the pressure distribution near the water surface is considerably affected.

The pressure distributions measured around the cylinder for a crest situation are shown in Figs. 5.31 and 5.32. Seen together with measured distribution in steady flow without free surface effects, see Fig. 5.7, it is possible to observe a larger measured pressure of up to about 40 degrees near the surface for the wavy flow. (In Fig. 5.7 the measured pressure follows the distribution according to potential theory). A difference at the position of minimum pressure may also be observed. These decrepancies are probably due to the free surface effects, i.e. amplified retardation in front of the cylinder with corresponding changed flow pattern.

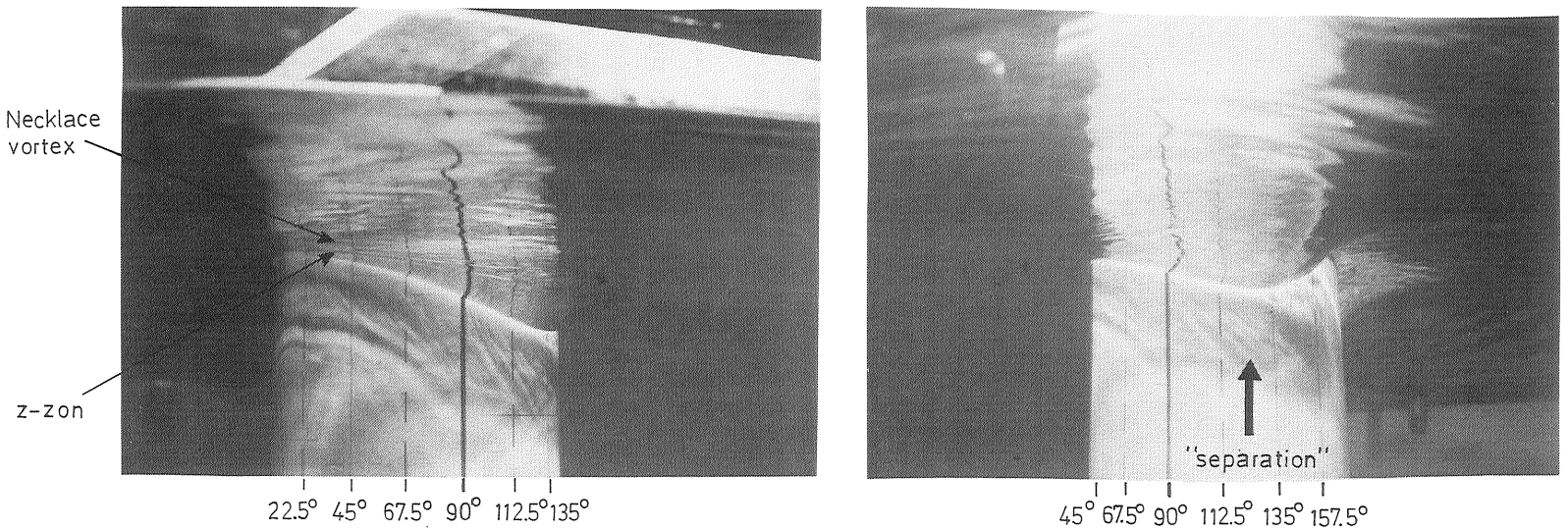

Figure 5.29 Wave C. "Shallow water". Flow pattern around the cylinder at a crest situation. Each camera is at about 70° from the wave tank's longitudinal direction. Photos are taken simultaneously. The main full line represents 90 degrees. Every additional line indicates 22.5 degrees.

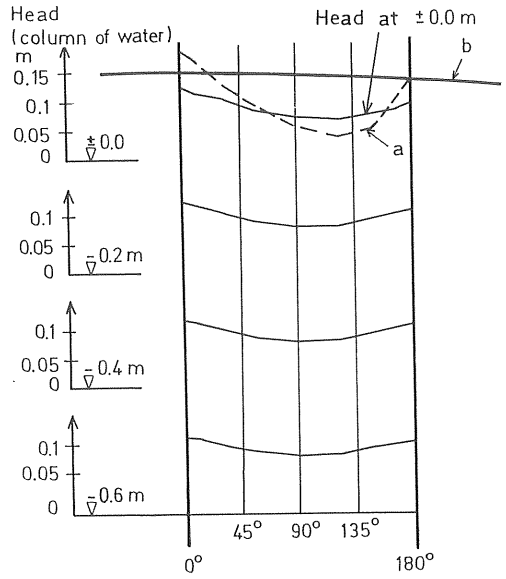

Figure 5.30 Wave C. Measured pressure distribution and corresponding water levels in a crest situation

a) ---- water level at the cylinder surface
b) ——— water level alongside the cylinder.

The flow pattern photographed, corresponding to Figs. 5.31 and 5.32, is shown in Fig. 5.33 for the moments during a wave cycle indicated in the small sketch in the bottom right hand corner. From the photos the angle of separation was estimated, as indicated in Fig. 5.34.

Disregarding the fact that the estimated separation angles are considerably higher than those given by Grass and Kemp (different flow regimes, non-harmonic flow, etc.), there seems to be relatively little variation throughout the half-cycle here. This is probably due to two effects, the highly disturbed flow field left from the preceding half cycle and the asymmetrical flow pattern caused by the free surface giving a variation of separation angle.

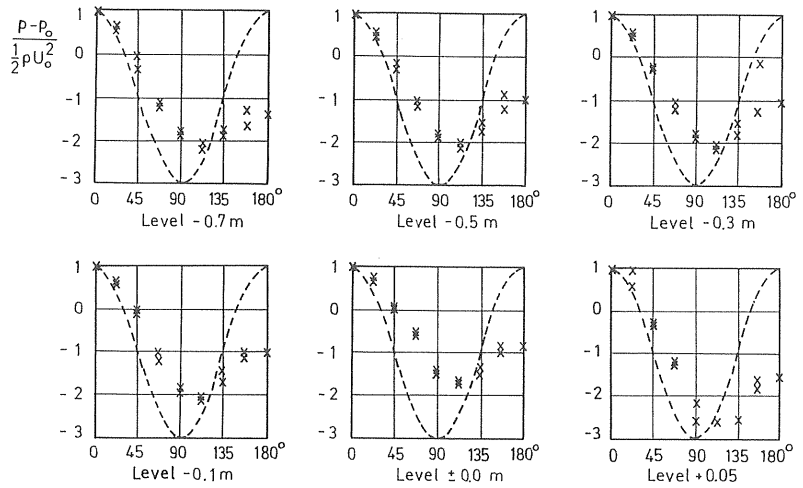

Figure 5.31 Wave B. Transitional water depth. Pressure distribution around the circular cylinder at various depth for a crest situation. U_o and p_o are the measured horizontal free stream velocity and pressure at infinity (calculated). x - measured pressure, --- potential flow pressure. Re = 0.31 - 1.49·10^5.

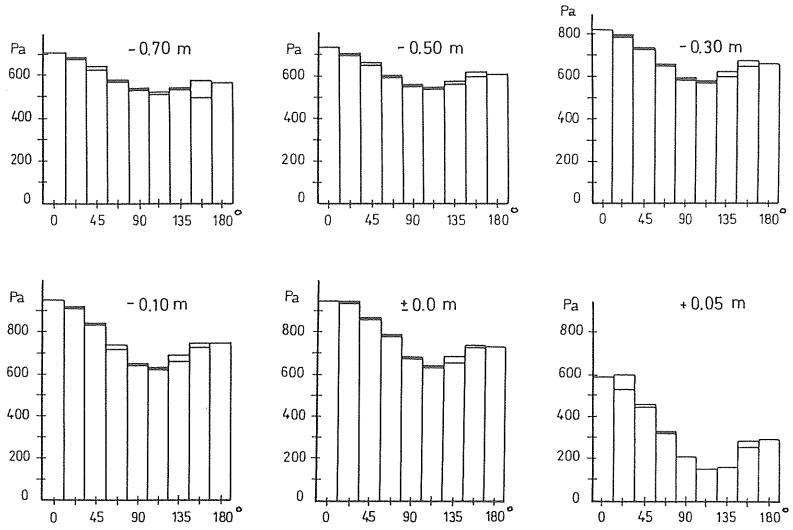

Figure 5.32 Total pressure distribution around the circular cylinder at various depth for a crest situation (corresponds to Fig. 5.31).

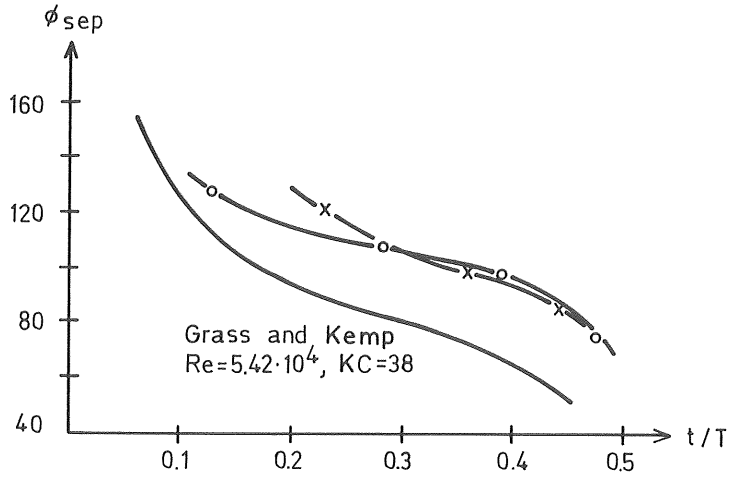

Figure 5.34 Wave B. Estimated variation of the separation angle, at the water surface over a half cycle, at a KC of 4 and a Re of $1.5 \cdot 10^5$ (maximum at the still water level). x indicates a crest situation. O indicates a trough situation.

To be able to study the effects of the free surface on the pressure distribution (changed flow pattern with resultant local water level near the cylinder), the wave length should be sufficiently long to minimize the influence of the surface curvature. The velocity should also be sufficiently high, so that the effect of the free surface grows larger as the velocity of the incident flow increases, Mori (1984). Furthermore, a particle velocity as constant with depth as possible is to be preferred, as the effects on the pressure distribution may then be neglected.

Wave M met these requirements. This wave, with a period of 4.2 sec., has a sufficiently high horizontal velocity at the crest situation. Wave M also has an almost constant velocity profile, as shown in Fig. 4.9 k. However it must be stressed that a significant transverse force was present, and that wave M was also extreme in the sense that it was close to the limit of what could be generated in

the wave tank. Therefore, scatter can be expected in the pressure distribution derived from the 16 almost equal but separate experiments.

Figs. 5.35 a-b, 5.36 and 5.37 show the effect of the free surface on the pressure distribution. Fig. 5.35 a shows the pressure at the front (0^{o}) and at the back (180^{o}) for a crest situation (maximum water level). Fig. 5.35 b also shows the difference between the front and back pressure of Fig. 5.35 a. Finally, Figs. 5.36 and 5.37 show the circumferiential normalized pressure distribution defined in the figure caption and the total pressure distribution, respectively.

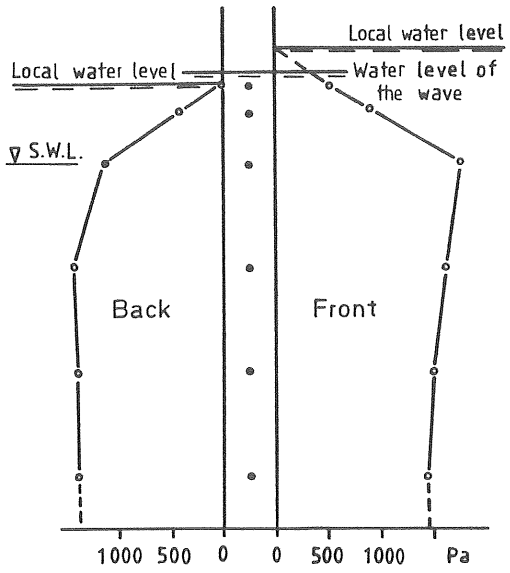

Figure 5.35 a Wave M. Pressure distribution at the front (0^{o}) and back (180^{o}) for a crest situation.

In spite of small vertical decay of velocity along the cylinder of wave M it can be observed in Figs. 5.35-5.37 that the pressure distribution, from having been quite symmetrical (potential-like flow) at deep levels, changes quite dramatically near the water surface. It can also be

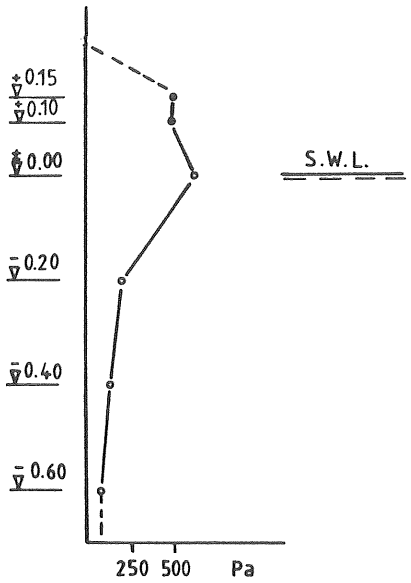

Figure 5.35 b Wave M. Difference in pressure between 0^{o} and 180^{o}.

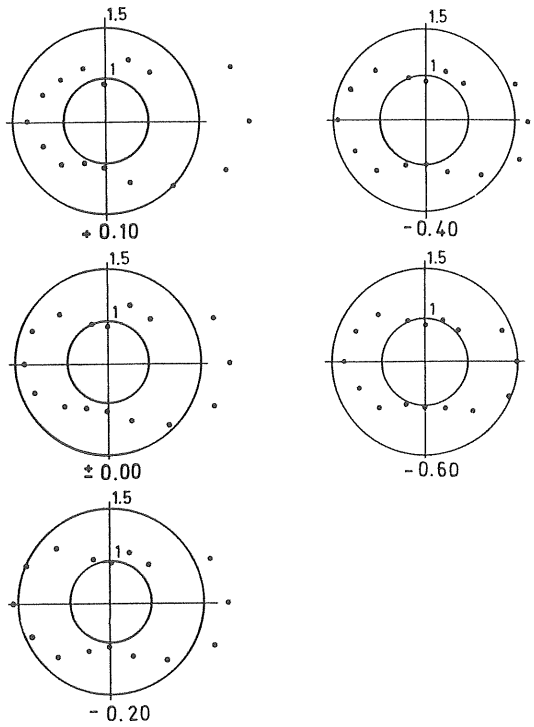

Figure 5.36 Wave M. Circumferential normalized pressure distribution. Obtained by dividing actual pressure by (p 90^{o} + p 270^{o})/2.

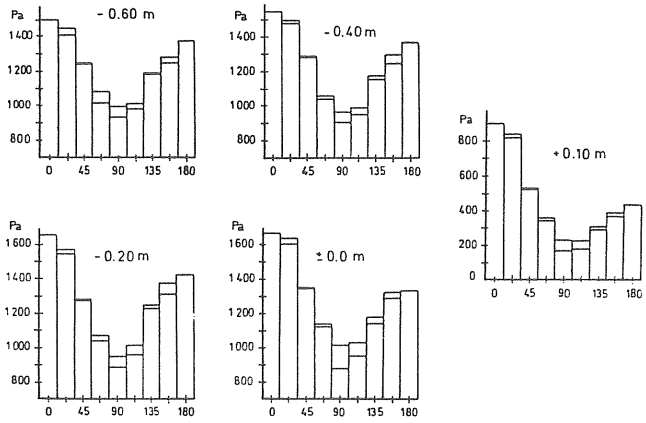

Figure 5.37 Wave M. Total pressure distribution around the circular cylinder at various depths.

observed that the free surface affects the flow at quite a distance below the S.W.L. For the studied crest situation the influence was noticeable as deep as about the distance of one wave's height below the water surface.

In conclusion, the explanation of time dependent separated flow lies in the understanding of the formation, growth and motion of vortices. Morison's equation works quite satisfactorily outside a KC range of about 7 to 30. Few if any, just slightly asymmetrical vortices are found for KC less than about 7. At KC greater than about 30 the flow is characterized by many vortices. However, their individual effects even out, which makes quasi-steady models quite adequate for the description of transverse force. The large deviation present in the KC range of about 7 to 30 using Morison's equation is caused by a small number of pronounced vortices.

Furthermore, free surface effects result in an amplified asymmetrical flow pattern around the cylinder close to the free surface as compared to the pattern at deeper levels which affects the pressure distribution and consequently the resulting net pressures and forces, as well as the value of the force coefficients, as is shown in Chapter 7.

The free surface effects are important because the influence increases as the velocity of the incident flow increases. Clearly, force coefficients used for integration of force along the cylinder should take the effect of the free surface into consideration.

6. PRESSURE DISTRIBUTION AND MEASURED FORCE

The aim of this chapter is to review measured pressure and measured force.

The relative importance of pressure and shear forces are briefly noted, after which the measuring of force and the calculation of integrated pressure are accounted for. The wave train averaging technique and integration are also tested by comparing the force obtained from integrated pressure with the mean of the measured force.

The chapter is concluded with a discussion of measured transverse forces.

6.1 Calculation of wave force

All the data were averaged before they were used in evaluations. This was necessary because the individual waves in a wave train varied slightly, see Figs. 3.6 a-c, and because the circumferential pressure distribution had to be calculated from different but almost equal experiments. Good correspondence was brought about by measuring the "same" sequence of waves in the beginning of the wave train and then calculating an averaged wave. Methods are accounted for in Chapter 3.

Pressure distributions corresponding to waves A, B and C are given in Appendix 1.

6.1.1 Viscous shear

Wave forces on a slender vertical cylinder may be divided into two components, i.e. the inertia force and the drag force. Generally, the inertia force comes into being on the basis of the pressure gradient caused by the relative and absolute acceleration of the ambient flow. The other component, the drag force, arises from the viscosity of the flow as described in the previous chapter.

Two types of forces act over the surface of the body in a viscous flow. These surface forces are the pressure and the shear forces, the later also known as skin friction. Over any infinitesimal area of the body surface, the pressure force is normal to that area while the viscous shear force is parallel or tangential to that area. When the force from the integrated pressure distribution is calculated, the contribution of the shear force is not included.

It can be shown that the maximum contribution of the shear force to the total force is small (Re > 300). The average contribution of the shear force in the experimental study was estimated to be 0.1%.

Note that the shear force still is very important for the development of the boundary layer and the positions of the points of separation, which, in turn, affects the size of the wake and the pressure differences within it.

6.1.2 Force per unit length

The net pressure per unit length is calculated by totalling the pressure distributions given in Appendix 1. In the direction of wave propagation the force per unit length is calculated by

$$F(K,LE) = \sum_{N=1}^{16} PRE(K,LE,N) \cdot \cos\theta_N \cdot R \cdot d\theta \qquad \ldots \quad (6.1)$$

where F = force at a certain level
PRE = pressure
K = chosen time step
LE = specific level
N = number of the increment given in Fig. 3.3
θ_N = the angle of the pressure probes for increment N
R = radius of cylinder
and $d\theta$ = increment of angle.

The force per unit length at the different levels of measurement is shown in Figs. 6.1 a-c and in Appendix 1.

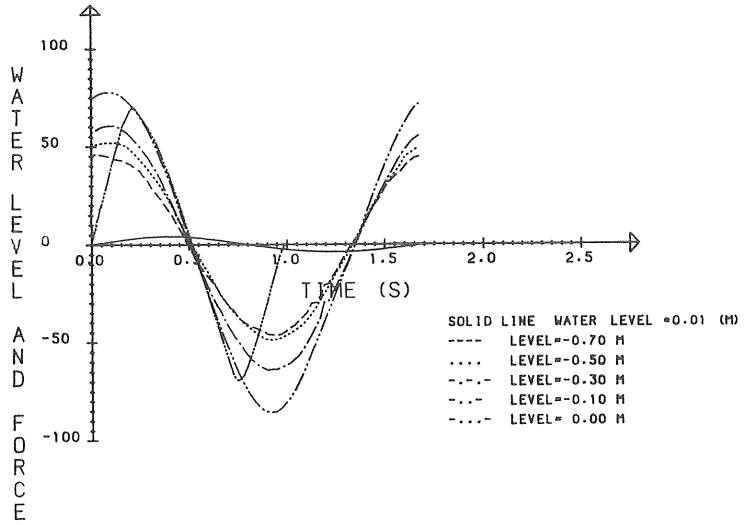

Figure 6.1 a Wave A. "Deep water". Force per unit length at the different levels of measurement (N/m).

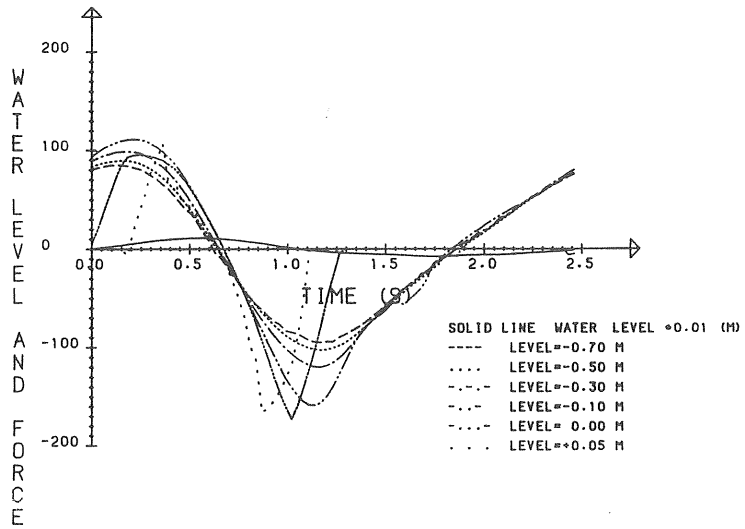

Figure 6.1 b Wave B. "Transitional water depth". Force per unit length at the different levels of measurement (N/m).

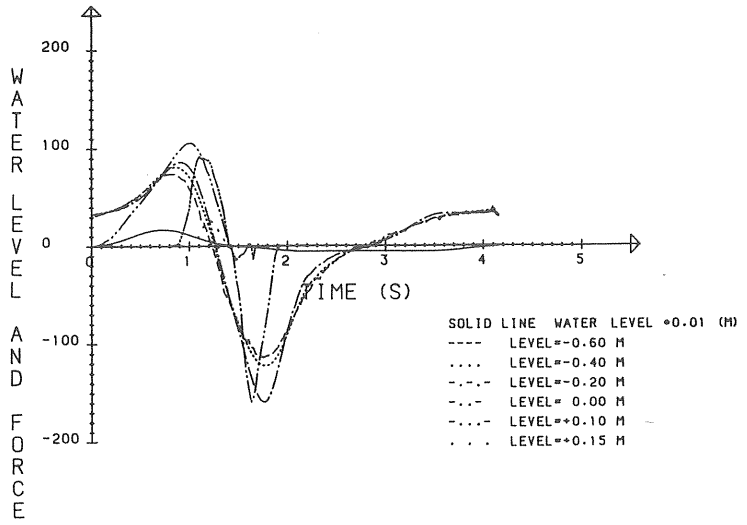

Figure 6.1 c Wave C. "Shallow water". Force per unit length at the different levels of measurement (N/m).

Fig. 6.1 a-c show that the forces are more or less dominated by the inertia component. The maximum force occurs approximately where the water surface is at its steepest, i.e. at the time of maximum acceleration. However, for some waves, the contribution of the drag force becomes large near the surface, noticibly at wave B and C. Figs. 6.1 b-c also show that the forces at the wave trough are of about the same magnitude at all depths for transitional and shallow water, indicating that the velocity varies slowly with depth. These observations are sustained by the measured kinematics, given in Figs. 4.4 and 4.9.

6.1.3 Measured force and integrated pressure

A good test of the wave train averaging technique (Chapter 3) is a comparison between the force obtained from the integrated pressure and the force obtained from the strain gauge cantilever.

If the distance between the pairs of strain-gauges is

known, the resulting force (F) and its line of action (x_o) can be measured, see Fig. 6.2.

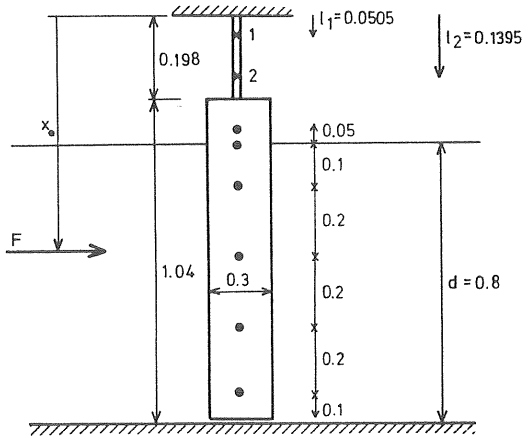

Figure 6.2 The cylinder. If the distance between the pairs of strain gauges is known, the magnitude and line of action of the force can be measured.

The force and its line of action, in either the longitudinal or transverse direction, are given by

$$F = \frac{M_1 - M_2}{(l_2 - l_1)} \qquad \ldots \quad (6.2)$$

$$x_o = \frac{M_1 + F \cdot l_1}{F} \qquad \ldots \quad (6.3)$$

where M_1 and M_2 are moments at the distance of l_1 and l_2 respectively, measured from the heavy beam mounted across the wave tank, see Fig. 6.2.

By integration of the total pressure distribution, the time dependent force on the cylinder is given by

$$F = \int_0^{2\pi} \int_{-d}^{\eta} PRE \cdot \cos\theta \cdot R \cdot dY \cdot d\theta \qquad \ldots \quad (6.4)$$

where d = water depth
η = elevation of water level
and Y = vertical coordinate

The calculation of the total force from the pressure is shown schematically in Fig. 6.3. The circumferential pressure at six levels along the cylinder is known, as indicated by PRE1 to PRE6 in Fig. 6.3. At the bottom of the cylinder a ficticious pressure (PREB) is calculated by assuming a linear decrease for the pressure distribution. We get

$$PREB = PRE6 - ((PRE5 - PRE6)/y_6) \cdot y_7 \qquad \ldots \quad (6.5)$$

where PREB, PRE6, PRE5, y_6 and y_7 are defined in Fig. 6.3.

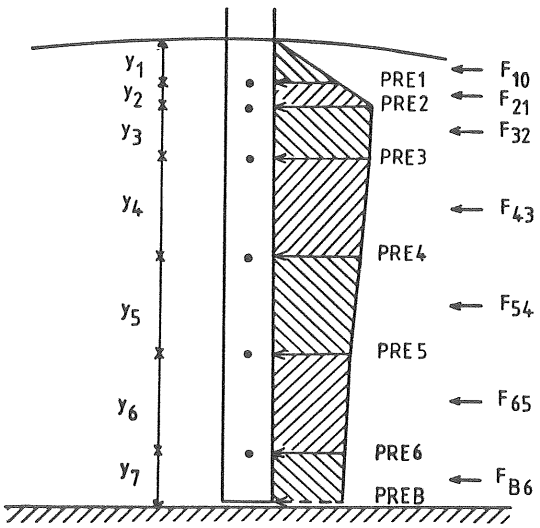

Figure 6.3 Wave B. Schematic illustration of the technique for obtaining total force from integrated pressure distribution.
The pressure distribution shown corresponds to maximum instantaneous pressure in a crest situation at the front of the cylinder (0°).

The force (F_{B6}) acting on the circle segment with the height y_7 and a set increment of 22.5 degrees is given by

$$F_{B6} = ((PREB + PRE6)/2) \cdot y_7 \cdot 2\pi R \cdot \frac{22.5}{360} \quad \ldots \quad (6.6)$$

Correspondingly, we obtain

$$F_{65} = ((PRE6 + PRE5)/2) \cdot y_6 \cdot 2\pi R \cdot \frac{22.5}{360} \quad \ldots \quad (6.7)$$

The same technique was used for obtaining the force all the way up to the water surface.

Near the water surface the uppermost submerged pressure transducer was used together with the water level (PRO1) measured at the cylinder, see Chapter 3. With this wave gauge it was always possible to define when the relative pressure was zero, i.e. when the pressure transducer was in air. The force (F_{10}) above the uppermost submerged transducer was calculated by using the measured water level (PRO1) as

$$F_{10} = (PRE1(PRO1-y_2)/2) \cdot 2\pi R \cdot \frac{22.5}{360} \quad \ldots \quad (6.8)$$

The pressure was hereby assumed to decrease linearly up to the water surface. The measured pressure distribution for crest situations, when several transducers were submerged, indicates that this was permissible. As an example, it is possible to study the pressure distribution and water level given in Figs. 5.35 a and 6.3.

A comparison between the force obtained from the integrated pressure with the force obtained from the strain gauge cantilever is shown in Figs. 6.4 a-c and Appendix 1.

The forces obtained fit one another well for the waves studied, as can be seen in Fig. 6.4, which indicates good accuracy of the technique used.

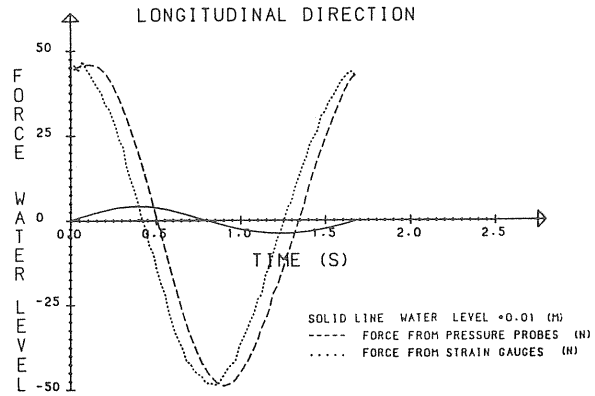

Figure 6.4 a Wave A. Comparison between measured force and integrated pressure.

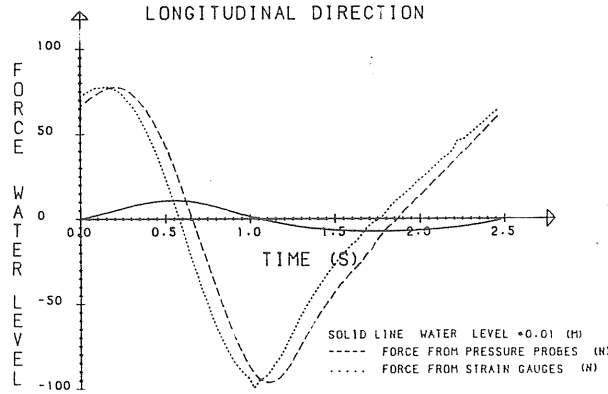

Figure 6.4 b Wave B. Comparison between measured force and integrated pressure.

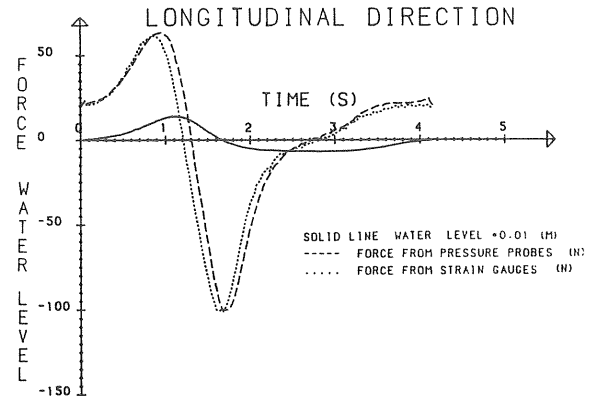

Figure 6.4 c Wave C. Comparison between measured force and integrated pressure.

Concerning the phase angle between the two forces evaluated in Fig. 6.4, it is emphasized that the force from the integrated pressure is the one in phase with the real force. The phase shift for the force obtained from the strain gauge cantilever was caused by the electronics of the equipment used, see Appendix 2. Only the force from the integrated pressure was used for further processing. The force from the strain gauge cantilever was thus only used to check the reliability of the wave train averaging technique. However, the bending moments were used to analyse the transverse force, as is discussed in the next section.

6.2 Transverse force

The range of Keulegan-Carpenter numbers (KC) was between $1 < KC < 11$ in the experiments. According to experiments in harmonic planar flow, the transverse force can be divided into the following regimes (Williamson, 1985 and Bearman, 1985. See also Chapter 5.2.2).

- $KC < 3$. No pronounced vortices exist and consequently there are no transverse forces.

- $KC = 4$. Symmetrical vortex shedding. Consequently no transverse forces exists.

- $4<KC<7$. Slightly asymmetrical flow which causes a small transverse force.

- $7<KC<15$. A majority of the vortex activity takes place only on one side of the cylinder, which results in a pronounced transverse force. This regime may be termed the transverse vortex shedding regime.

As the factors behind transverse forces are highly random, as is discussed later in this section, the use of the

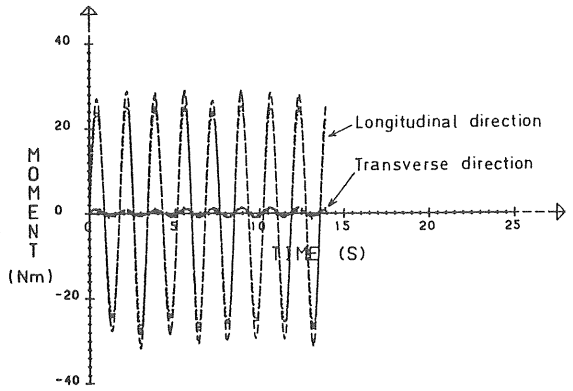

Figure 6.5 a Wave A. "Deep water". Moment at a distance of l_1 and l_2 in the longitudinal and transverse directions. KC = 1.0.

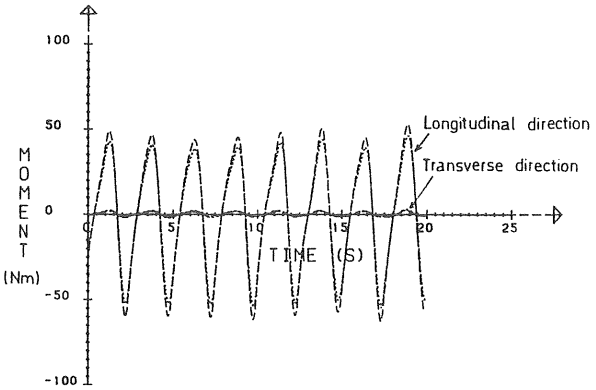

Figure 6.5 b Wave B. "Transitional water depth". Moment at a distance of l_1 and l_2 in the longitudinal and transverse directions. KC=4.2.

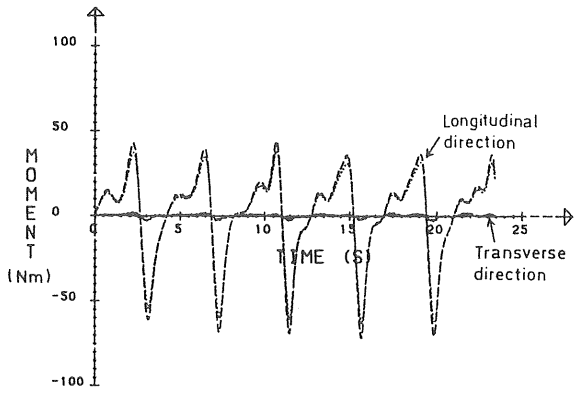

Figure 6.5 c Wave C. "Shallow water". Moments at a distance of l_1 and l_2 in the longitudinal and transverse directions. KC=9.0.

wave train averaging technique is not satisfactory. Instead, bending moments in the cantilever are used to analyse the transverse force. The forces in either the longitudinal or transverse direction may be obtained with Eq. (6.2).

From Figs. 6.5 a-c, it may be observed that small transverse forces are present. However, the flow regimes according to Williamson (1985) and Bearman (1985) indicates that no transverse forces should be present for wave A (KC=1.0) and that pronounced transverse forces could be expected for wave C (KC=9).

Table 6.1 may be used to clarify the observations. The table shows the calculated and observed number of oscillations per wave cycle for the transverse force. The Strouhal-Reynolds number relationship is used, see Fig. 5.13. The ratio of the transverse to the longitudinal forces is also given. As may be seen, there is a small transverse force present even for waves with KC less than 4, which may be due either to, a wavy flow introduced, asymmetrical flow, or a possible constant small inclination of the cylinder to the loadline.

In spite of the fact that the observed number of oscillations differs from the calculated number at low KC, the Strouhal-Reynolds number relation (using maximum velocity in the S.W.L.) tends to hold for wavy flow (KC < 11, Re < $2 \cdot 10^5$). For planar oscillating flow Sarpkaya (1976a) gave the frequency ratio (f_r) of the dominant lift frequency (f_s) to the flow frequency versus Re and KC, see Fig. 2.7. Defining the Strouhal number (S) in terms of the maximum velocity (u_m) during the cycle, $S = f_s \cdot D/u_m = f_r/KC$, Sarpkaya found that S was more or less constant at 0.22 for KC larger than about 14. However, in the KC region between 5 and 14, the author showed an almost linear decrease from ≅ 0.4 to ≅ 0.15 of S. Further, in the post-critical region S rose to about 0.3.

Table 6.1 Calculated and observed number of oscillations per wave cycle for the transverse force. The Strouhal number (S) is defined in terms of the maximum velocity (u_m) during the cycle, taken in the S.W.L. Order of the transverse to the longitudinal forces is also given. Keulegan-Carpenter number (KC) taken in S.W.L.

			Number of oscillations per wave cycle		Ratio of the transverse to the longitudinal forces
Wave	KC-number	Strouhal-No S	Calculated $f_s \cdot T$	Observed $f_s \cdot T$	
A	1.0	0.18-0.20	0.19-0.21	1	≅1/22
B	4.2	0.18-0.24	0.75-1.00	1	≅1/25
C	9.0	0.18-0.26	1.64-2.37	2	≅1/20
D	1.1	0.18-0.20	0.20-0.23	1	≅1/30
E	1.2	0.18-0.20	0.22-0.25	1	≅1/26
F	1.3	0.18-0.20	0.24-0.26	1	≅1/20
G	1.8	0.18-0.22	0.33-0.40	1	≅1/17
H	2.2	0.18-0.22	0.40-0.49	1	≅1/27
I	4.8	0.18-0.22	0.86-1.05	1	≅1/20
J	5.1	0.18-0.22	0.91-1.12	1	≅1/15
K	8.3	0.18-0.28	1.50-2.34	2	≅1/15
L	8.3	0.18-0.31	1.50-2.59	2	≅1/21
M	11.0	0.18-0.28	1.98-3.07	2	≅1/3-1/30

In spite of the fact that there were four waves with KC greater than 7, there was just one wave with a significant transverse force. For this wave (M) with KC=11 the transverse vortex shedding regime was reached.

The random behaviour of vortex shedding and the corresponding transverse forces may also be exemplified by wave M. In Figs. 6.6 a-c the moments are shown for three different but almost equal experiments. As may be seen, the transverse force varies for those experiments from almost zero to about 1/3 of the force in the longitudinal direction. As may also be seen in Figs. 6.6 b-c, the transverse force in one experiment may be 180 degrees out of phase with that in another experiment.

In summary, the Strouhal-Reynolds number regimes for vortex shedding tend to hold even for wave flow. However, wavy flow results in weaker and less regular shedding.

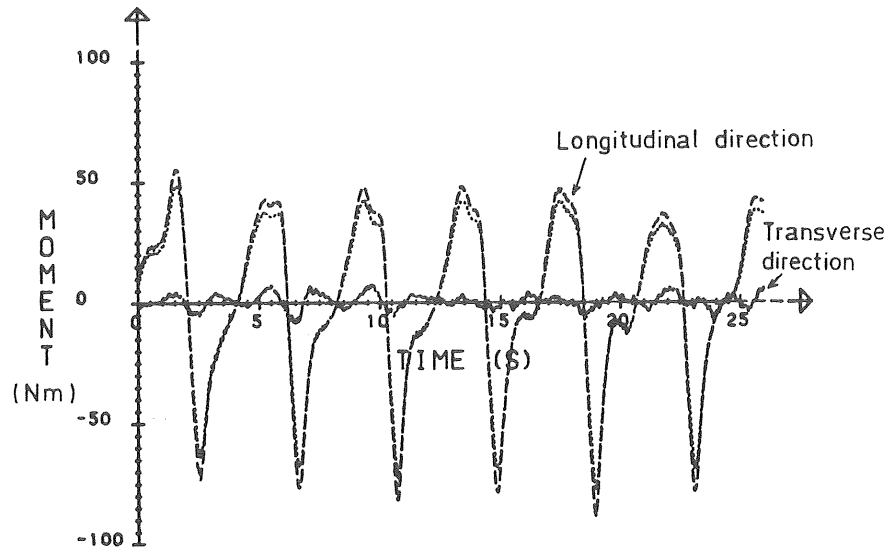

Figure 6.6 a Wave M. Moments at a distance of l_1 and l_2 in the longitudinal and transverse directions as given in Fig. 6.2.
KC = 11. Small transverse force.

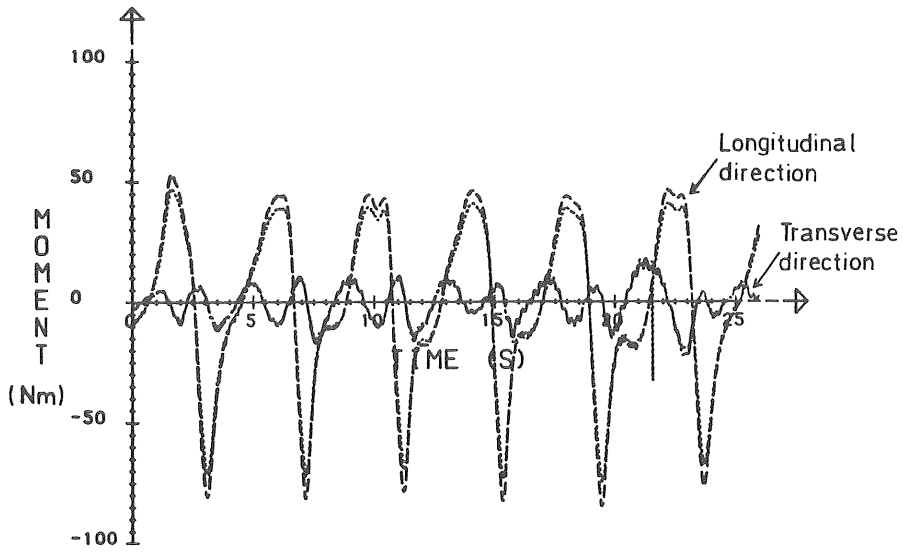

Figure 6.6 b Wave M. Moments at a distance of l_1 and l_2 in the longitudinal and transverse directions as given in Fig. 6.2.
KC = 11. Pronounced transverse force.

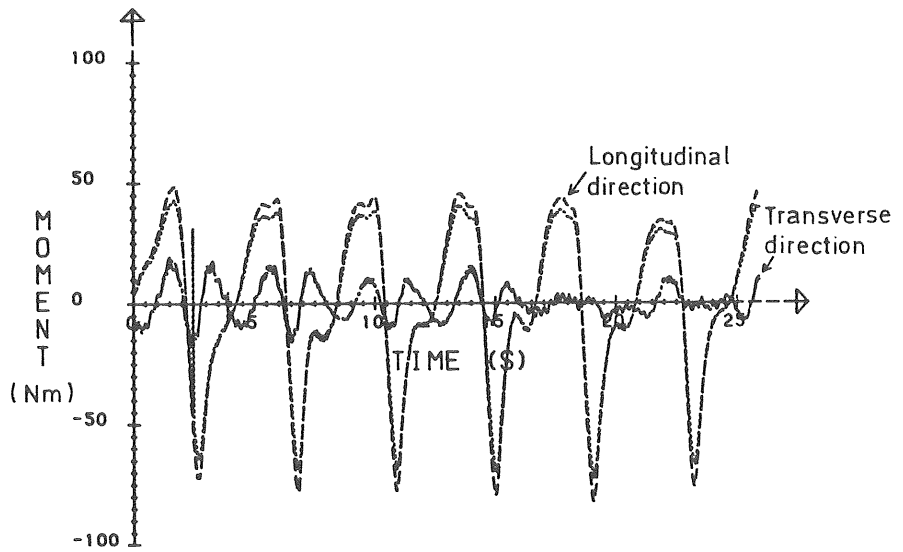

Figure 6.6 c Wave M. Moments at a distance of l_1 and l_2 in the longitudinal and transverse directions as given in Fig. 6.2. KC = 11. Pronounced transverse force in antiphase with the force shown in Fig. 6.6 b.

7. FORCE COEFFICIENT

Using drag and inertia coefficients as functions of the Keulegan-Carpenter number (KC) and the Reynolds number (Re) is one way of compensating for phenomena present in separated time-dependent flow. This gives a truer representation of the force predicted by Morison's equation. However, values of force coefficients found in the literature exhibit substantial scatter. Besides the fact that two coefficients can hardly account for all conditions in time-dependent flow, there are several other factors that influence the values of the coefficients, such as the effects of the experimental technique, the quality of the kinematics used, and the way the coefficients were evaluated.

The purpose of this chapter is to analyse different calculation procedures as well as to present results of evaluation using the methods chosen. The importance of using correct force coefficients is exemplified. It is shown that a prerequisite for good wave force calculation is the availibility of force coefficients that ensure correct maximum forces. Otherwise, the magnitude and the phase of the force may be in poor agreement with measurements.

The values of force coefficients given in literature are usually time-invariant, but are averaged over whole periods. However, it is recognized that the instantaneous values of the coefficients are not constant throughout the wave cycle, as is noted by Sarpkaya and Isaacson 1981. In reality both C_D and C_M exhibit large variations during a given cycle. For this reason the instantaneous time-varying values of C_D and C_M are studied here.

7.1 Time varying force coefficients

Two time-invariant averaged coefficients together with a linear quadratic force equation (Morison's eq.) cannot be

expected to represent a time-dependent separated flow. However, previous efforts have primarily been focused on the problem of determining those time-invariant averages. They only lead to estimates of the force, which is dependent on the KC, the relative roughness k_s/D etc. and on the particular wave theory with respect to which they are calibrated. Clearly, time invariant force coefficients have little physical significance, since in reality both C_D and C_M exhibit large variations during a given cycle.

To gain more information about the behaviour of the force coefficients and the physics behind Morison's equation, the time-varying coefficients are studied.

The time-varying $C_{D(\theta)}$ and $C_{M(\theta)}$ values are solved from two equations. By assuming the values to be constant within a small time interval (Δt), the C_D and C_M values between two force data points n and n+1 become

$$C_{D(n)} = \frac{2(F_{n+1}\,\dot{u}_n - F_n\,\dot{u}_{n+1})}{\rho A(\dot{u}_n|u_{n+1}|u_{n+1} - \dot{u}_{n+1}|u_n|u_n)} \qquad \ldots \quad (7.1)$$

and

$$C_{M(n)} = \frac{F_{n+1}|u_n|u_n - F_n|u_{n+1}|u_{n+1}}{\rho V(\dot{u}_{n+1}|u_n|u_n - \dot{u}_n|u_{n+1}|u_{n+1})} \qquad \ldots \quad (7.2)$$

where

F = instantaneous total force
u_n = - " - velocity
$\dot{u}_n$ = - " - acceleration
ρ = density of water
A = characteristic area
V = immersed volume

Figs. 7.1 - 7.3 show the time-varying force coefficients at chosen levels along the cylinder. These coefficients

were determined by the use of integrated pressure and measured velocities and accelerations. The chosen time steps vary from 0.022 to 0.030 sec. For the sake of clarity, no values outside the range of $0 < C_D, C_M < 3.5$ are plotted.

After studying Figs. 7.1 - 7.3 several observations may be made. First, both $C_{D(\theta)}$ and $C_{M(\theta)}$ exhibit large variations during a given cycle. This variation is particularly pronounced for wave C, representing shallow water conditions, which may in part be explained by its asymmetrical shape and the presence of stronger vortex activity (KC about 7). There is also a large increase in $C_{D(\theta)}$ at zero - crossings (0, $\cong\pi$, 2π) due to the fact that the velocity vanishes at about these points.

Secondly, neither $C_{D(\theta)}$ nor $C_{M(\theta)}$ is symmetrical around the wave crest ($\sim\pi/2$) and wave trough ($\sim 3\pi/2$), i.e. acceleration and deceleration flows with corresponding velocities and accelerations do not result in identical forces on the cylinder. Furthermore, neither $C_{D(\theta)}$ nor $C_{M(\theta)}$ are equal for wave crest and wave trough. This indicates that a crest and a trough situation are two different events, demanding separate analyses. An averaging technique such as the method of least squares, applied over the whole wave cycle, would hereby give less accurate force coefficients, at least for waves B and C.

Figs. 7.1 - 7.3 also show that the force coefficients vary with depth. This variation is mainly due to the fact that the velocity decreases with depth, thereby changing the KC, see Table 7.1. This may also cause different flow regimes to occur along the cylinder (changed Re). Also, there is the effect of the free surface, which affects the force coefficients near the free surface and the possible influence of the orbital shape of the water particles (Ω).

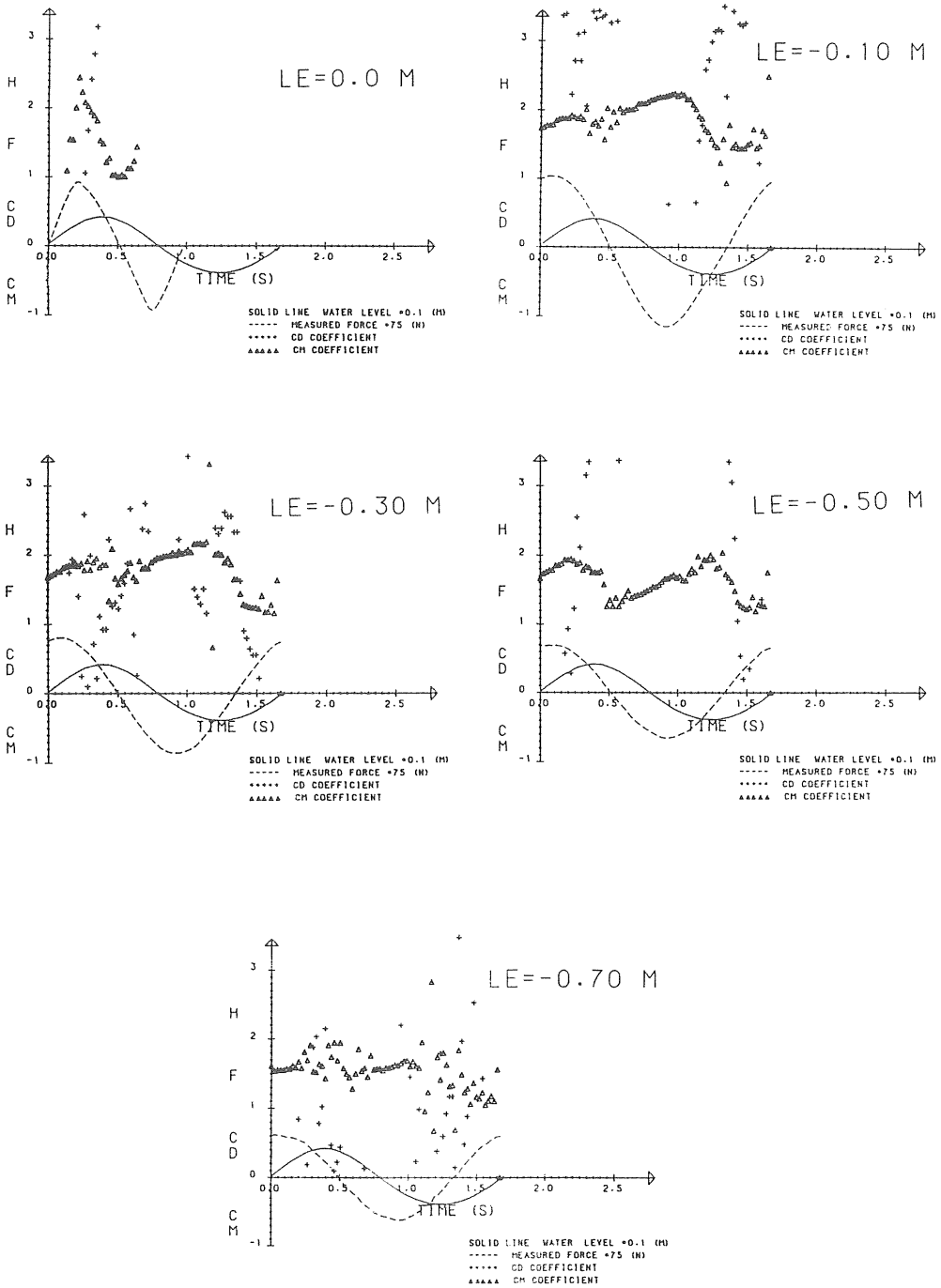

Figure 7.1 a-e Wave A. "Deep water". Time-varying force coefficients along the cylinder. Coefficients determined from measured velocity and "measured" acceleration.

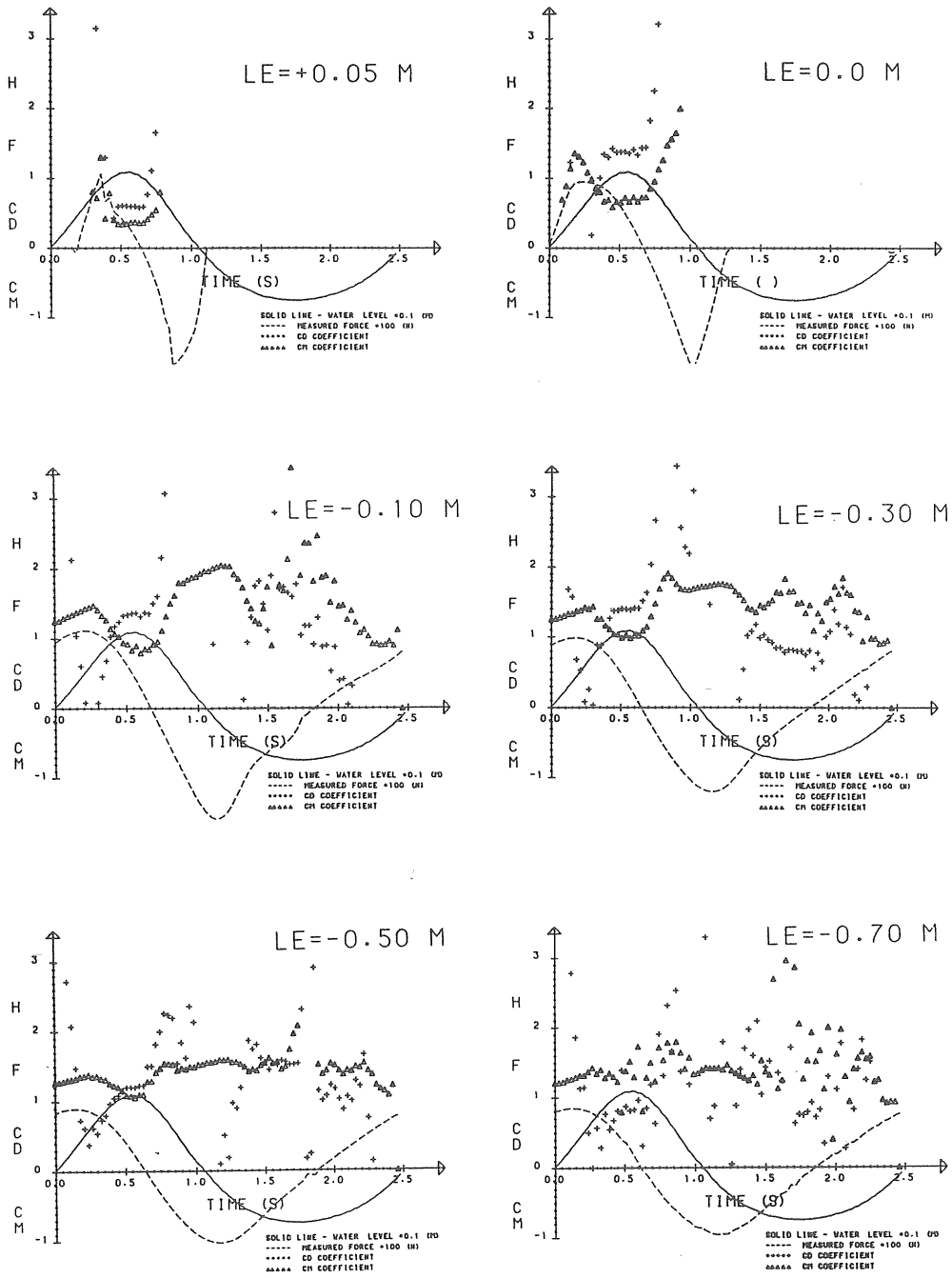

Figure 7.2 a-f Wave B. "Transitional water". Time-varying force coefficients along the cylinder. Coefficients determined from measured velocity and "measured" acceleration.

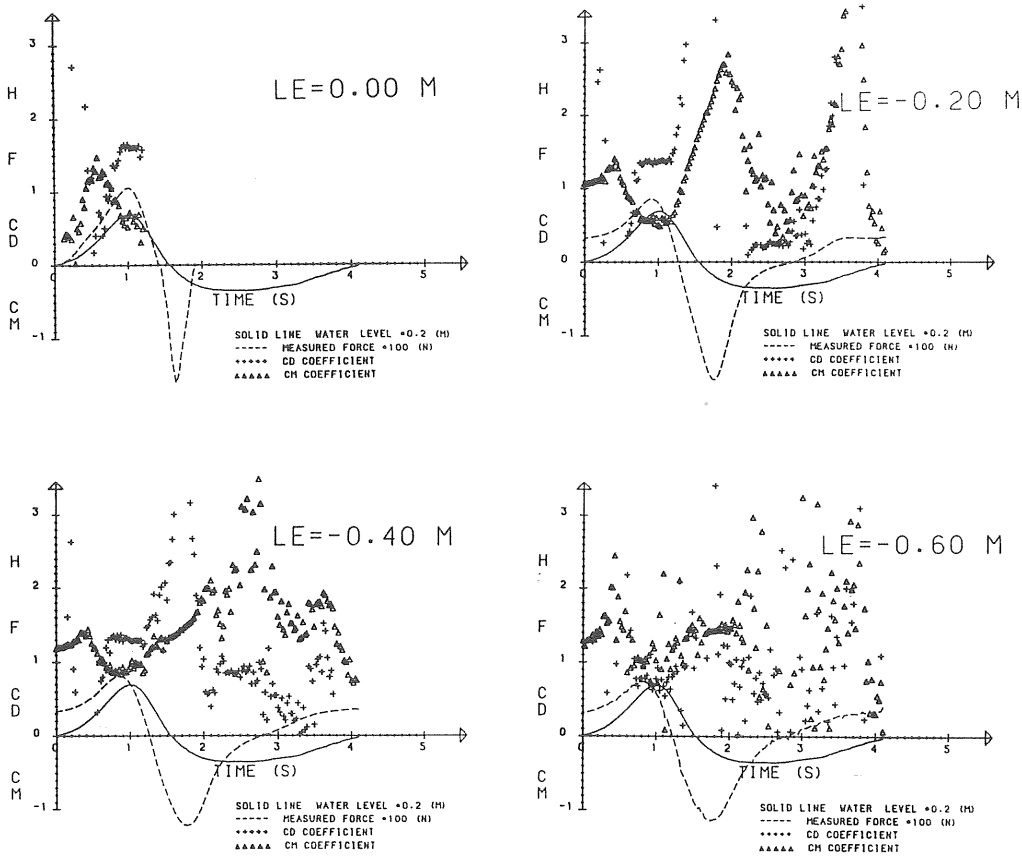

Figure 7.3 a-d Wave C. "Shallow water". Time-varying force coeffients along the cylinder. Coefficients determined from measured velocity and "measured" acceleration.

Furtheron, the difference in absolute values between the half cycles becomes smaller, the obvious reason being that disturbances at the surface (such as waves) have less effect at greater depths.

Finally, Figs. 7.4 - 7.7 show force coefficients calculated from fifth and cnoidal theories. These plots correspond to the ones shown in Figs. 7.1-7.3. Note that both fifth and cnoidal theories are used for wave C. To attain

Table 7.1 Parameters characterizing the force coefficients. Determined from measured velocity. The r.m.s. orbital shape parameter (Ω) is calculated from fifth order theory.

Level	+0.05	0.00	-0.10	-0.30	-0.50	-0.70
Wave A						
β = 52417						
Crest/trough						
$Re \cdot 10^5$	-	0.54/-	0.48/0.50	0.39/0.39	0.32/0.36	0.31/0.36
KC	-	1.0/-	0.9/1.0	0.7/0.7	0.6/0.7	0.6/0.7
Ω (r.m.s)	-	0.86/-	0.81/0.80	0.68/0.65	0.47/0.43	0.06/0.01
Order of drag to inertia force	-	-	1/6/1/6	1/12/1/10	((1	((1
Wave B						
β = 35224						
Crest/trough						
$Re \cdot 10^5$	1.47/-	1.49/-	1.39/1.15	1.19/1.08	1.07/0.98	1.02/0.98
KC	4.2/-	4.2/-	3.9/3.3	3.4/3.1	3.0/2.8	2.9/2.8
Ω (r.m.s)	0.69/-	0.66/-	0.61/0.57	0.48/0.43	0.32/0.26	0.14/0.07
Order of drag to inertia force	-	1/2/-	1/2/1/4	1/3/1/6	1/3/1/4	1/4/1/5
Level	+0.15	+0.10	0.00	-0.20	-0.40	-0.60
Wave C						
β = 21216						
Crest/trough						
$Re \cdot 10^5$	-	1.54/-	1.90/-	1.82/1.24	1.63/1.11	1.62/1.11
KC	-	7.3	9.0/-	8.6/5.8	7.7/5.2	7.7/5.2
Ω (r.m.s)	-	0.61/-	0.55/-	0.42/0.26	0.28/0.17	0.13/0.05
Order of drag to inertia force	-	-	1.6/1/-	1.5/1/1/6	1/1/1/7	1/2/1/7

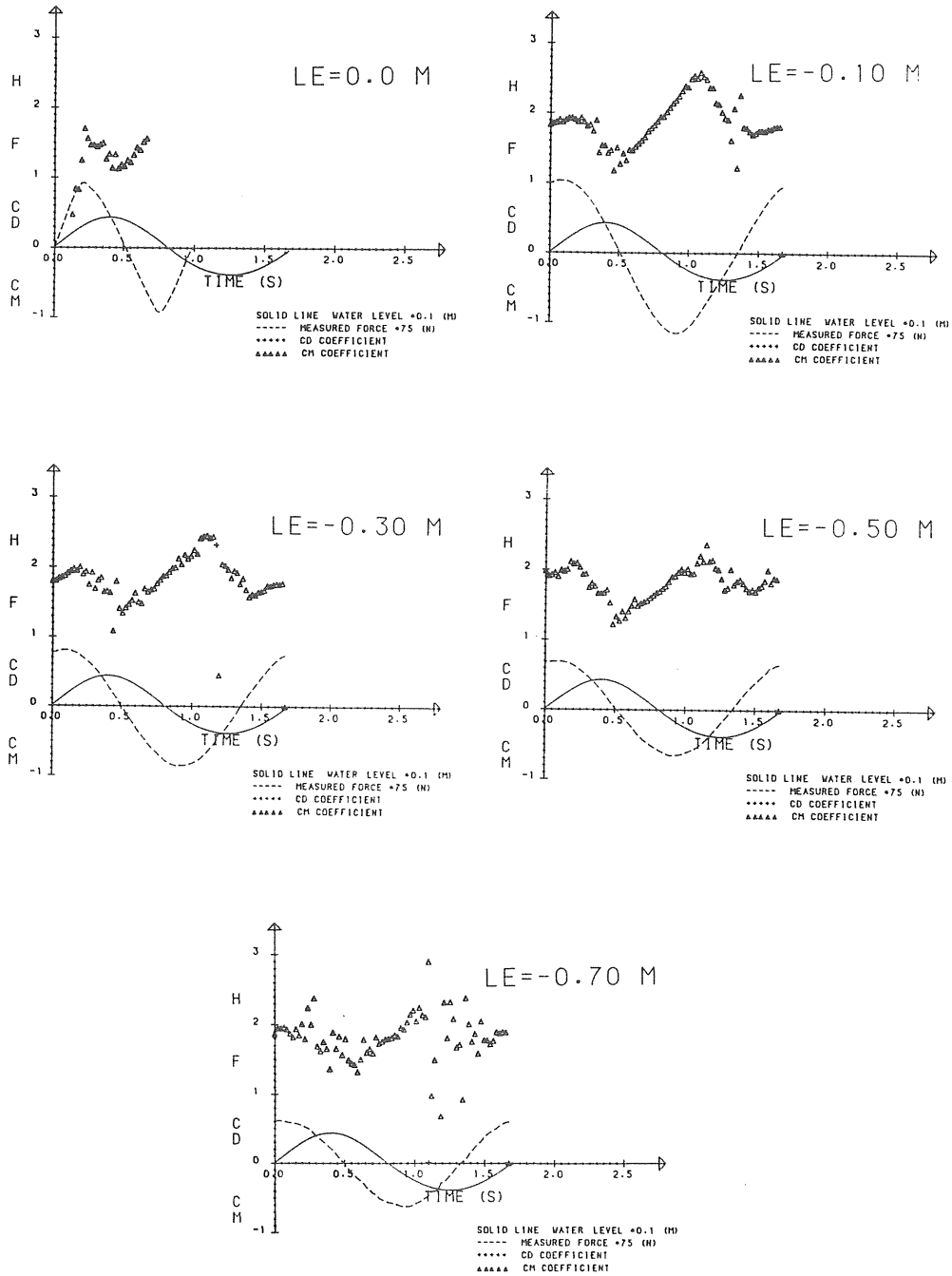

Figure 7.4 a-e Wave A. "Deep water". Time-varying force coefficients along the cylinder. Coefficients determined using kinematics from fifth order theory.

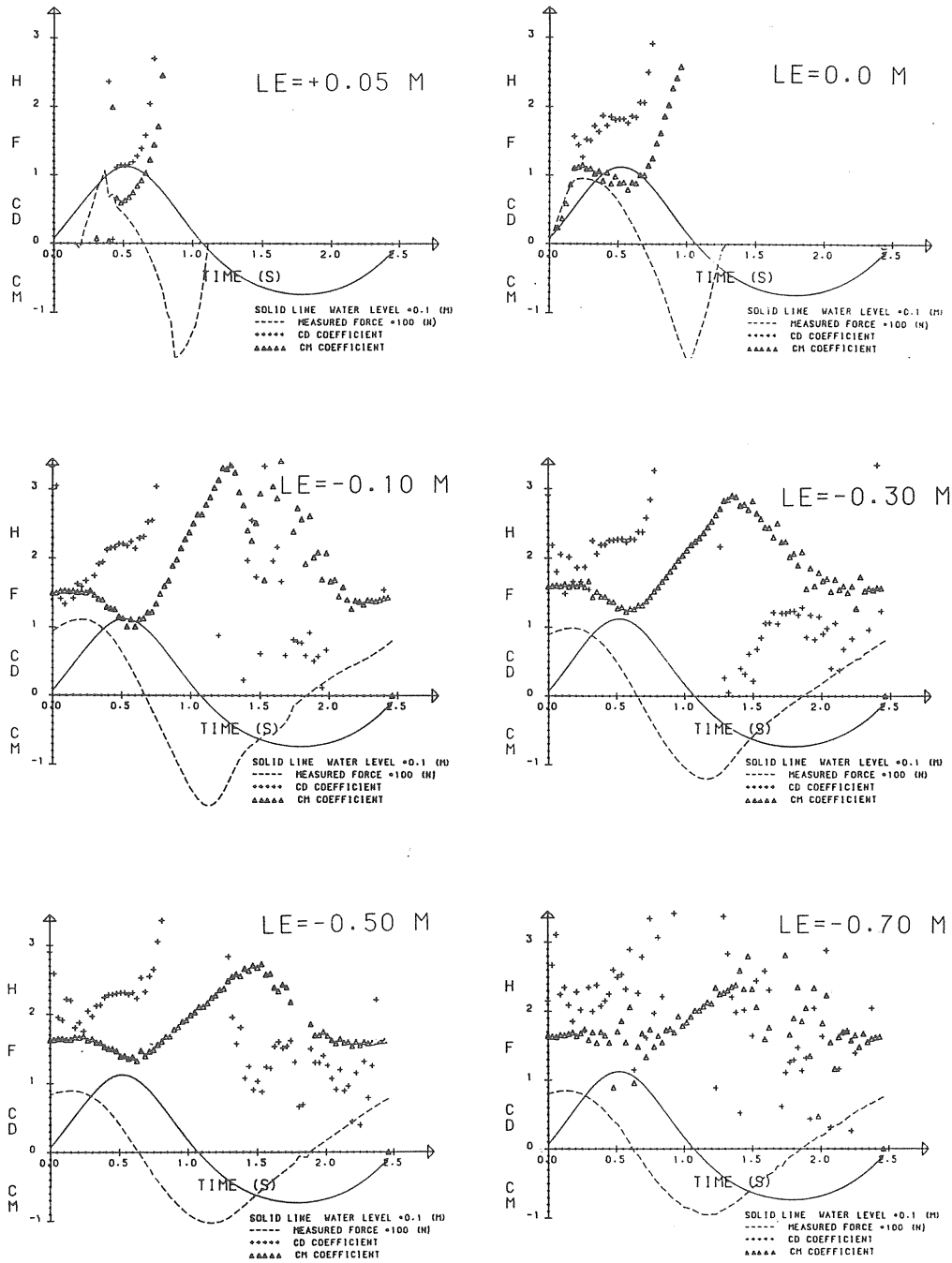

Figure 7.5 a-f Wave B. "Transitional water". Time-varying force coefficients along the cylinder. Coefficients determined, using kinematics from fifth order theory.

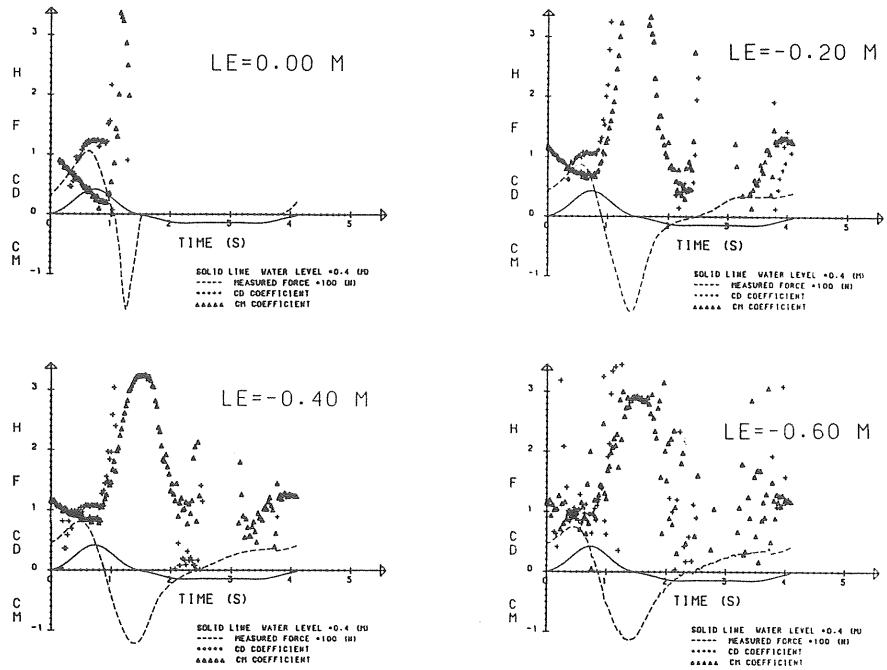

Figure 7.6 a-d Wave C. "Shallow water". Time-varying force coefficients along the cylinder. Coefficients determined, using kinematics from fifth order theory.

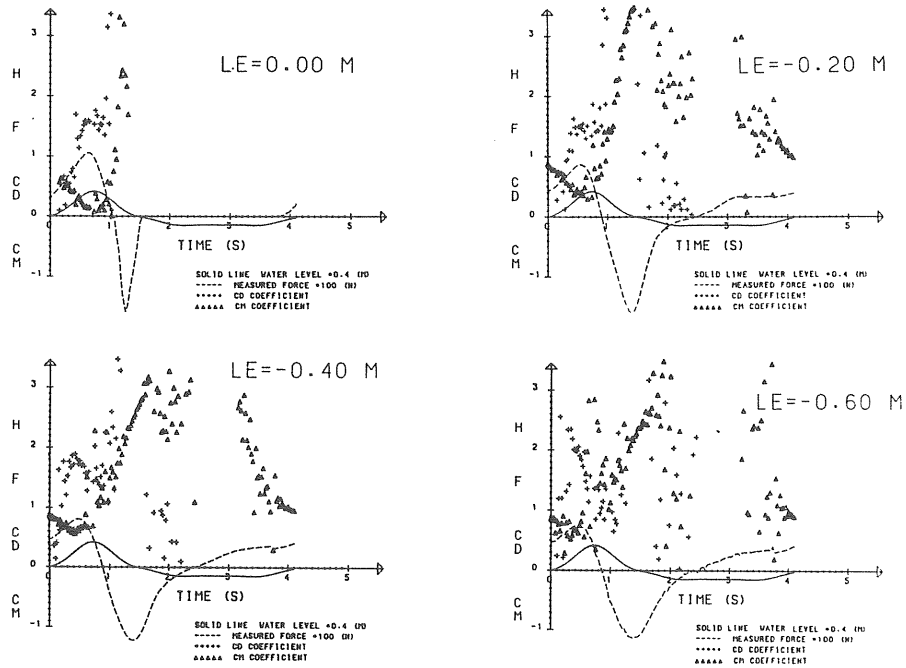

Figure 7.7 a-d Wave C. Time-varying force coefficients along the cylinder. Coefficients determined, using kinematics from cnoidal theory.

better reliability of the force coefficients a phase shift between measured force and kinematics as given in theories was introduced (only performed for wave C in the experimental program). A phase shift of 0.375 sec. was needed for maximum measured velocities to coincide with velocities given by fifth and cnoidal theories, see Fig. 4.5 c.

After studying Figs. 7.4 - 7.7 and comparing these figures with Figs. 7.1 - 7.3 it becomes clear that the kinematics used may affect the value of calculated force coefficients to a substantial extent. Consequently, the chosen wave theory may greatly affect the values of calculated wave force.

7.1.1 Quality of drag and inertia force components

The range of attained maximum Keulegan-Carpenter numbers (KC) was $1 < KC < 11$ at the still water level. Based on linear theory, Eq. (2.17) shows that the inertia force dominates when KC is less than about 8, i.e. $F_{M\ max} \geq 2 \cdot F_{D\ max}$. The actual proportion of measured drag to inertia forces is shown in Figs. 7.8 a-f. These figures show the total measured force as well as the instantaneous drag and inertia force components (F_D resp. F_M), calculated by the use of $C_{D(\theta)}$ and $C_{M(\theta)}$. The use of instantaneous force coefficients in Morison's equation yields an in-line force identical to that measured. As was predictable, Fig. 7.8 and Table 7.1 show that the inertia force is the dominating force component. It is only the shallow water waves (in the experiments) that have drag force components greater than or of the same order as the inertia force components. The shallow water waves are represented by waves C, J, K, L and M in the experimental program. The drag and inertia forces may also be of the same order in a wave crest while the inertia force dominates in the trough of the same wave. This is seen for wave C, which indicates that wave crests and troughs are different cases, demanding separate analyses.

As is discussed in Chapter 7.6 experimental errors and the inapplicability of Morison's equation tend to affect one or the other of the force coefficients. Therefore, waves in the experimental program with the lowest KC can be expected to have contaminated drag coefficients.

Figs. 7.8 a,b and Table 7.1 show that wave A is totally inertia dominated (about 10 to 1), with a poor quality drag coefficient, as expected. They are therefore omitted when establishing the C_D relationships presented below.

7.2 Time invariant force coefficients - evaluative approaches

There is no ultimately satisfactory method for evaluating force coefficients. Frequently used methods include the Fourier-averaging technique and the method of least squares. Evaluation of the coefficients for maximum velocities and accelerations, maximum and zero forces and short segments of the wave where the data are judged to be good are also used. The methods given below may be regarded as time-invariant averages for the particular wave and section of the cylinder on which the forces were measured. They may be used to obtain the force coefficients for each wave, half the wave cycle or smaller parts of the wave cycle.

7.2.1 Fourier-averaging technique

The first systematic evaluation of the Fourier-averaged drag and inertia coefficients was made by Keulegan and Carpenter (1958). Assuming a harmonic flow, $F(\theta) = -F(\theta+\pi)$ and only odd harmonics, the force (F) in terms of Fourier series may be written

$$\frac{F}{\rho u_m^2 D} = A_1\sin\theta + A_3\sin3\theta + A_5\sin5\theta + \ldots + B_1\cos\theta + B_3\cos3\theta + B_5\cos5\theta + \ldots \quad \ldots (7.3)$$

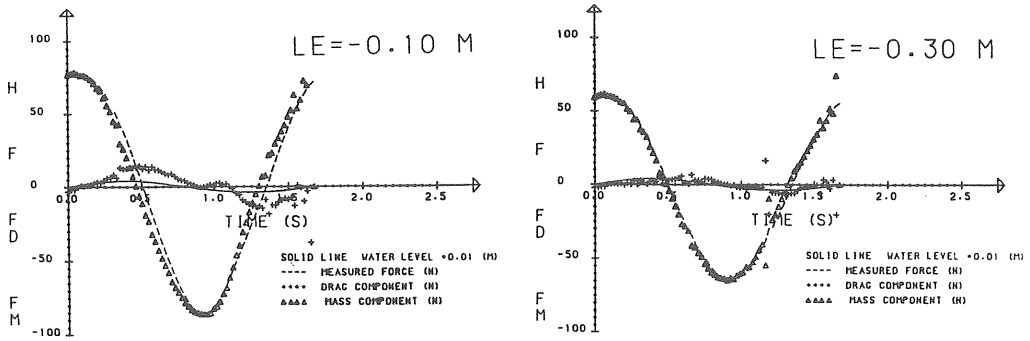

Figure 7.8 a,b Wave A. Force components at 0.1 m and 0.3 m below the still water level. Calculated from measured kinematics and use of time-varying force coefficients.

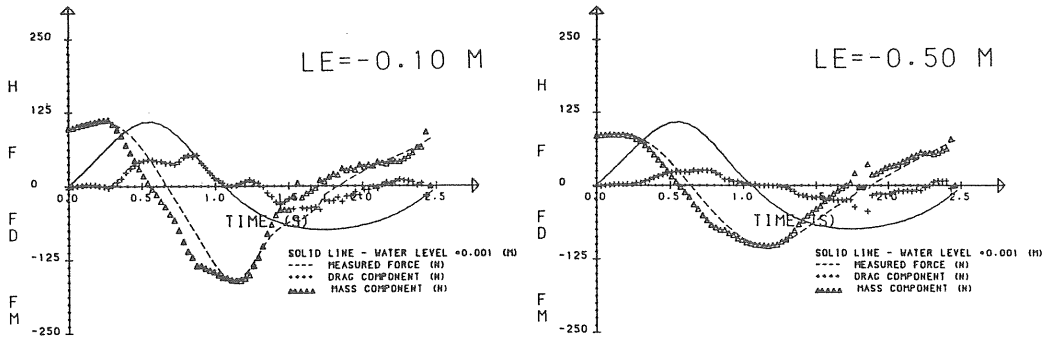

Figure 7.8 c,d Wave B. Force components at 0.1 m and 0.5 m below the still water level. Calculated from measured kinematics and use of time-varying force coefficients.

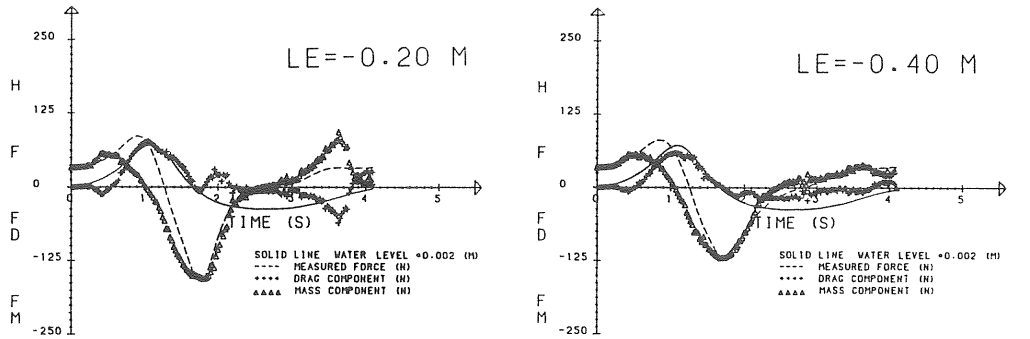

Figure 7.8 e,f Wave C. Force components at 0.2 m and 0.4 m below the still water level. Calculated from measured kinematics and use of time-varying force coefficients.

where

ρ = density of water

u_m = maximum velocity

D = diameter of cylinder

T = wave period

$\theta = \frac{2\pi \cdot t}{T}$

Studying the first Fourier component, we get

$$C_M = \frac{2}{\pi^3} \frac{u_m T}{D} \int_0^{2\pi} \frac{F \sin\theta}{\rho u_m^2 D} d\theta \quad \ldots \quad (7.4)$$

and

$$C_D = -\frac{3}{4} \int_0^{2\pi} \frac{F \cos\theta}{\rho u_m^2 D} d\theta \quad \ldots \quad (7.5)$$

respectively.

The Fourier averages of C_D and C_M presented are restricted to harmonically oscillating flow. Also note that the Fourier-averaging technique does not guarantee that the maximum calculated force is equal to the maximum measured force. For further information about the Fouirer-averaging technique, see Appendix 3.

7.2.2 Method of least squares

The drag and inertia coefficients (C_D, C_M) may also be determined by using the method of least squares. This procedure involves a minimization the sum of the squares of the errors, or rather the difference between the measured force and the force calculated using Morison's equation.

The method of least squares does not garantee that the maximum calculated force is equal to the maximum force. However, it can be applied for assymmetrical waves, as either measured kinematics or kinematics chosen from a wave theory can be used. For further information about the method of least squares, see Appendix 3.

7.2.3 Method of maximum velocities and accelerations

The drag and inertia coefficients may also be calculated by using the force at the points corresponding to maximum velocities and accelerations. This method may yield reliable results for C_D and C_M in the drag and inertia dominated regions, respectively. However, the method is not recommended when the drag and inertia forces are of equal importance and highly dependent on flow history.

7.2.4 Method of zero and maximum forces

Another way of evaluating the drag and inertia coefficients is to write Morison's equation, one for the zero force, and one for the maximum (or minimum) force together with corresponding velocities and accelerations. The method ensures that maximum measured and calculated forces coincide. However, a small fluctuation in the force maximum or in the kinematics at the time of zero force may result in a large differences in the inertia coefficient in the drag dominated flow regime and large differences in the drag coefficient in the inertia dominated regime.

7.2.5 Method of short segments

A frequently used method for determining the coefficient of interest is to select points only from that segment of the wave where the data are best conditioned. For this purpose a decision must be made regarding the length of each segment. An averaging procedure as the method of least squares may then be used on the selected segment.

A slightly different approach may be used on data obtained mainly in either the drag or inertia dominated region. One of the force coefficients is determined in the region where this force component dominates. Holding this value fixed, the best value of the other force coefficient is found by trial calculations.

7.3 Time invariant force coefficients - results of calculations

Calculation of the time invariant coefficients has been made by the methods of least squares, maximum velocities and accelerations, zero and maximum forces, and short segments. The values of the force coefficients according to these methods are given in Appendix 1.

The Reynolds number (Re) and orbital shape parameter (Ω) obtained are $0.3 \cdot 10^5 < Re < 2.3 \cdot 10^5$ and $0.03 < \Omega < 0.86$, respectively. The parameter values are based on the local vertical distribution of maximum velocity (in and below the S.W.L.). In the ranges studied no obvious dependence of force coefficients on Reynolds number or orbital shape parameter was found. This may be attributed to the limited number of experiments or the limited range of studied Re - based on maximum velocity during each half cycle. This is in agreement with the results by Bearman, Chaplin et al. 1985.

KC is the most important parameter governing the total force on a vertical cylinder. It has been common practice to calculate KC using the velocity at the still water level. Such a practice does not take into account the vertical distribution of the force in wave crest and trough.

In the following context a local KC is used, calculated by using the maximum velocity in wave crest and trough at the different levels. In cases where the coefficients have been evaluated from a whole period, using the method of least squares, the averaged value of the local KC from wave crest and trough is used.

Note. Because of the limited number of data points, the mean curves presented may only be used for internal comparison.

7.3.1 Time invariant force coefficients according to measured velocities

Tables A1.1 a-d (Appendix 1) show the force coefficients evaluated according to the method of least squares applied over a whole wave period, over the wave crest and over the wave trough. The method was also used over 60 degree segments around the maximum, zero and minimum velocity respectively. The relative error according to the method is shown in connection with each group of force coefficients. The error has been obtained through the root mean squared error as expressed in Eq. (A3.19) (Appendix 3) to the maximum measured force in the interval studied. The coefficients calculated according to the method of maximum velocities and accelerations and according to zero and maximum force are also given.

The orbital shape parameter (Ω) is defined as the ratio of r.m.s. vertical velocity to r.m.s. horizontal velocity (fifth order theory). Re and KC are calculated using the vertical distribution of the maximum velocity in the wave crest and the wave trough. The frequency parameter β = Re/KC is constant along the cylinder for a wave. The obtained β ranges between $21.2 \cdot 10^3 < \beta < 68.5 \cdot 10^3$.

Inertia coefficients

Fig. 7.9 shows the inertia coefficients below the still

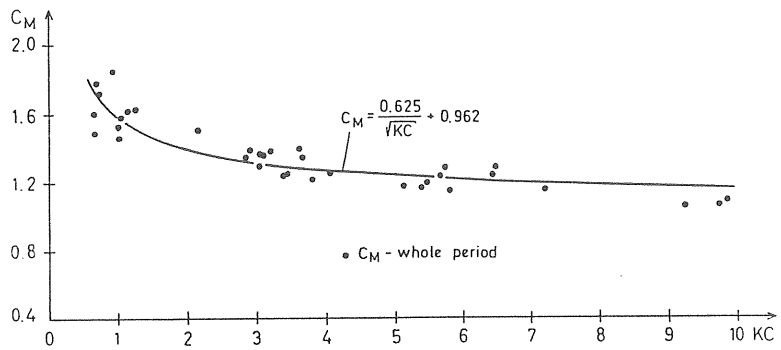

Figure 7.9 C_M versus KC below the still water level along the vertical cylinder. Method of least squares is used, applied over the whole period. KC are calculated by averaging local KC from wave crest and trough. Measured velocity.

water level calculated according to the method of least squares, applied over the whole period. Data from all levels below the still water level are included. Fig. 7.10 also shows the inertia coefficients calculated according to the method of least squares. However, the inertia coefficients are calculated here according to the method of least squares applied with local KC at the wave crest and the wave trough, respectively. In spite of a larger scatter (twice as many data points) the curves calculated by regression have almost the same coefficients as given in Fig. 7.9.

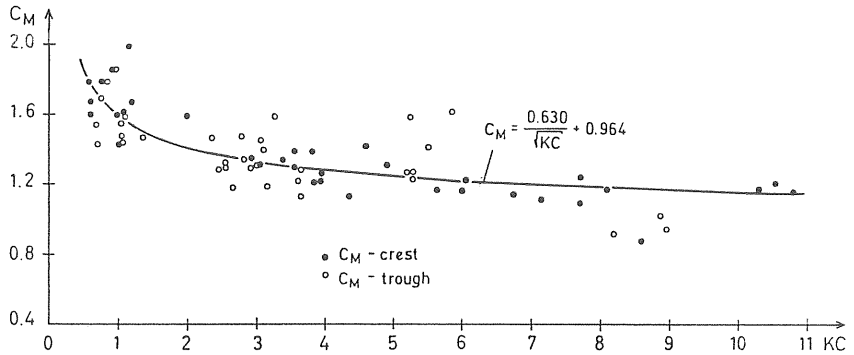

Figure 7.10 C_M versus KC below the still water level along the vertical cylinder. Method of least squares is used, applied at wave crest and trough. Local KC are used. Measured velocity.

Fig. 7.11 shows the least squares averaged inertia coefficient applied over 60 degree segments around maximum, zero and minimum velocity respectively. C_{M60}° applied around zero velocity yields somewhat larger values. However, C_{M60}° applied around maximum/minimum velocity yields just slightly smaller values than the ones given by the least square method applied over the whole wave period and over the crest/trough.

Fig. 7.12 shows the inertia coefficients calculated according to the methods of maximum velocities and accelerations and also according to the method of zero and maximum forces. Both values are given in the figure, and the scatter is indicated by an interval. Pairs of C_M-values with a greater difference than 0.9 were discarded.

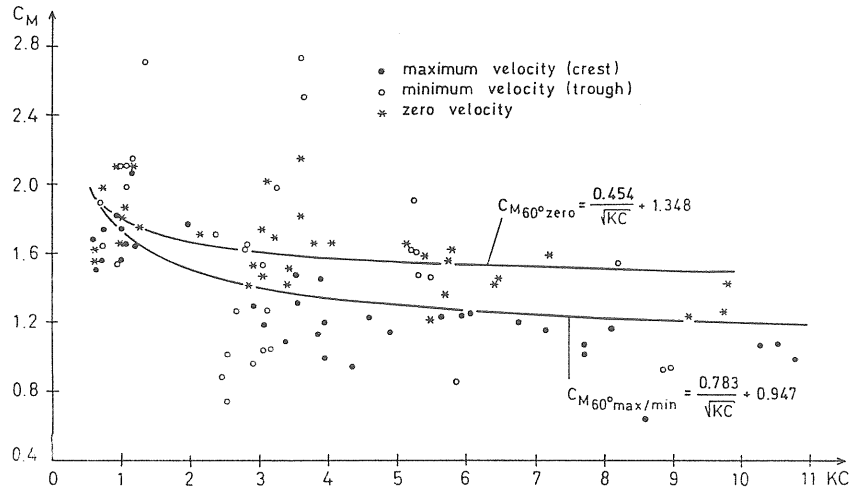

Figure 7.11 C_M versus KC below the still water level along the vertical cylinder. Method of least squares is used applied over 60 degree segments around maximum, zero and minimum velocity. Local KC are used. At zero velocity, an averaged KC is used calculated from local KC at wave crest and trough. Measured velocity.

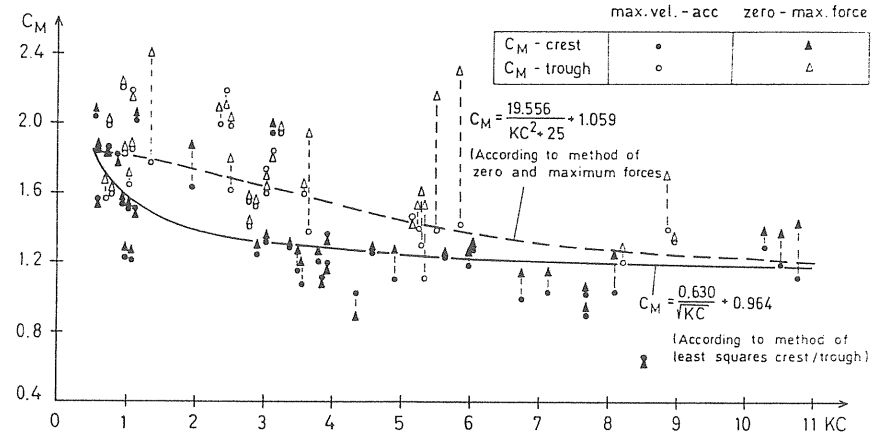

Figure 7.12 C_M versus KC below the still water level along the cylinder. Method of maximum velocities and accelerations and of zero and maximum forces are used. Local KC are used. The criterion of maximum scatter according to the two methods were set at 0.9. Measured velocity.

With reference to Figs. 7.9-7.12 some observations may be made in the range of KC studied. To begin with, there is

a general decrease of the C_M coefficient with increasing KC. In the case of the method of least squares, curves calculated by regression gradually approach constant values. However, with the methods of maximum velocities and accelerations and of zero and maximum forces the C_M values stay at a somewhat higher level up to a KC of about 3 before approaching the values generated by the method of least squares.

The almost identical mean curves through data points from the method of least squares indicates that the wave crest and wave trough are two different events that can be described by the use of a local KC.

Drag coefficients

The maximum attained KC was 11. In consequence, reliable inertia coefficients are anticipated, but the drag coefficients may be contaminated by errors from various sources as is discussed in Chapter 7.6. In summary, the number of useful data points for establishing the C_D-KC relationship is small compared to the number used for the inertia coefficient, especially in the lower region of KC. Furthermore, the scatter may be expected to be greater for the C_D-KC relationship than for the C_M-KC relationship.

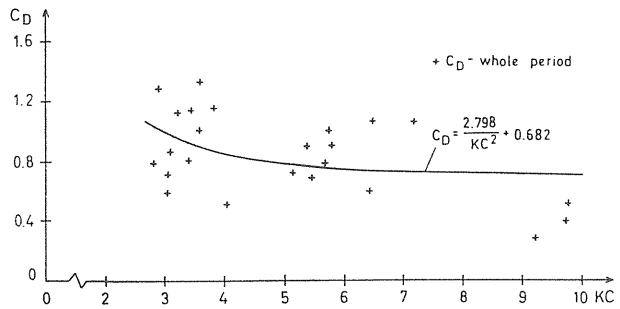

Figure 7.13 C_D versus KC below the still water level along the vertical cylinder. Method of least squares is used, applied over the whole period. KC are calculated by averaging local KC from wave crest and trough. Measured velocity.

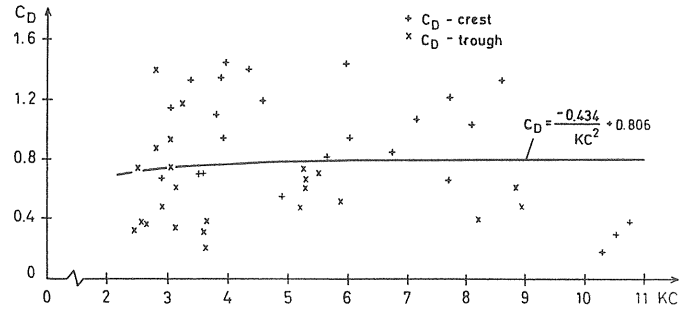

Figure 7.14 C_D versus KC below the still water level along the vertical cylinder. Method of least squares is used applied at wave crest and trough. Local KC are used. Measured velocity.

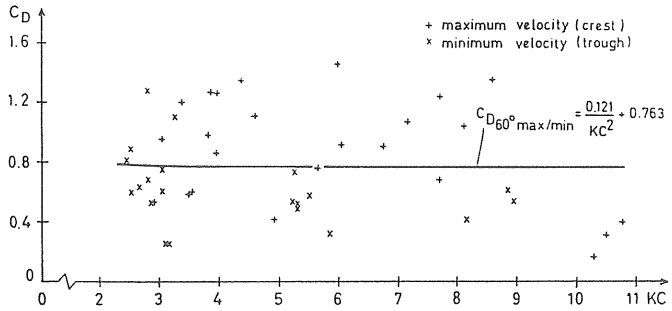

Figure 7.15 C_D versus KC below the still water level along the cylinder. Method of least squares is used applied over 60 degree segments around maximum and minimum velocity. Local KC are used. Measured velocity.

With reference to Figs. 7.13-7.16 some observations may be made in the KC range studied. Particularly Fig. 7.16 indicates that the C_D decreases with increasing KC up to a KC of about 4. The discarded C_D values in this region also show greater rather than smaller values than C_D values at higher KC. For a KC greater than about 4 no stable trends were found for the regressed curves.

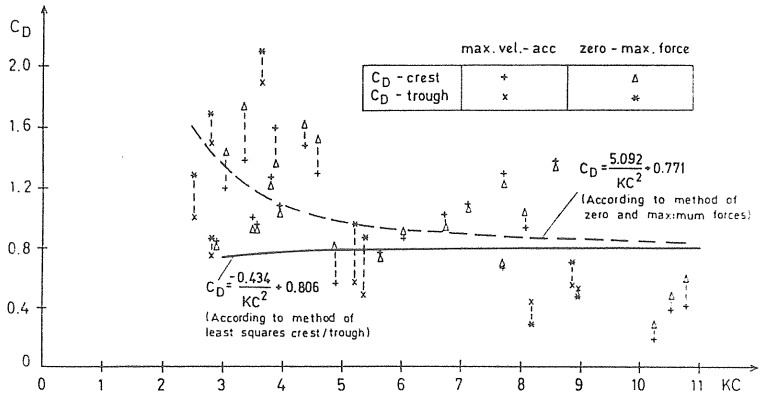

Figure 7.16 C_D versus KC below the still water level along the cylinder. Method of maximum velocities and accelerations and of zero and maximum forces are used. Local KC are used. The criterion of maximum scatter according to the two methods were set at 0.4. Measured velocity.

7.3.2 Time invariant force coefficients according to calculated kinematics

In this section the C_M, C_D-KC relationship according to kinematics from fifth order and cnoidal theories are presented. Figures presented correspond to and are calculated in the same way as those in Chapter 7.3.1. Tables may be found in Appendix 1.

Inertia coefficients

In Figs. 7.17-7.19 approximately the same trends for the C_M-KC relationship as according to measured kinematics are shown. That is, a general decrease at the C_M coefficient which gradually approaches a constant value with increasing KC. In this case, too, the methods of maximum velocities and accelerations and of zero and maximum forces give somewhat higher values up to a KC of about 3. Further, as for the case of measured velocities, almost

identical regression curves were obtained through the data points, indicating that wave crests and troughs are two different types of events that can be described by the use of a local KC and with the use of fifth order and/or cnoidal wave theories. However, the time invariant inertia coefficients with calculated kinematics give both a somewhat higher C_M value and increased scatter throughout the KC-range attained.

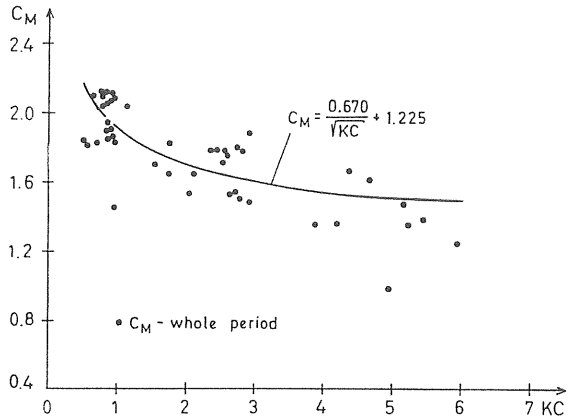

Figure 7.17 C_M versus KC below the still water level along the vertical cylinder. Method of least squares is used, applied over the whole perod. KC calculated by averaging local KC from wave crest and trough. Kinematics according to fifth and cnoidal theories. Wave M is excluded.

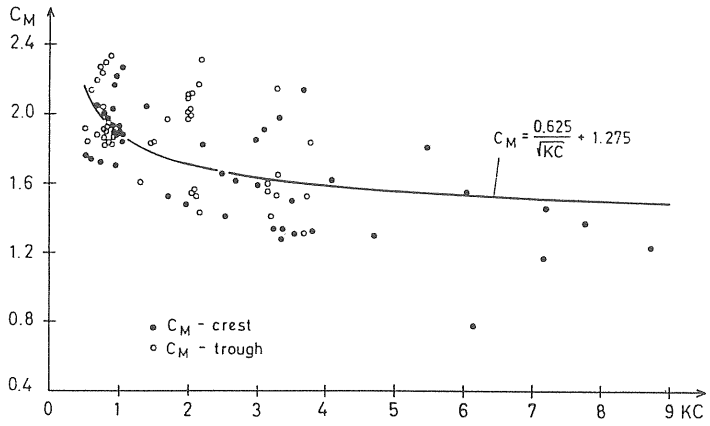

Figure 7.18 C_M versus KC below the still water level along the vertical cylinder. Method of least squares is used applied at wave crest and trough. Local KC are used. Kinematics according to fifth and cnoidal theories. Wave M is excluded.

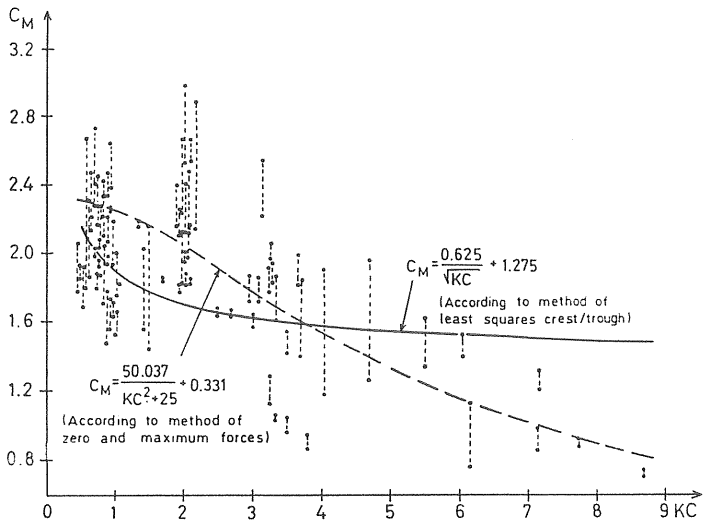

Figure 7.19 C_M versus KC below the still water level along the cylinder. Method of maximum velocities and accelerations and of zero and maximum forces are used. Local KC are used. The criterion of maximum scatter according to the two methods were set at 0.9. Kinematics according to fifth and cnoidal theories. Wave M is excluded.

Drag coefficients

It was only possible to use C_D values from five waves, calculated according to the method of least squares. As

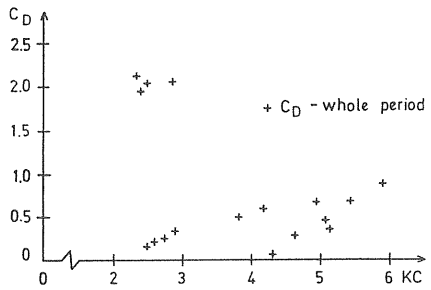

Figure 7.20 C_D versus KC below the still water level along the vertical cylinder. Method of least squares is used applied over the whole period. KC calculated by averaging local KC from wave crest and trough. Kinematics according to fifth and cnoidal theories. Includes waves B, C, I, K and L.

seen in Figs. 7.20-7.22 there still is great scatter for the C_D coefficient calculated using kinematics according to fifth order and cnoidal theories. Thus it was not possible to establish any reliable C_D-KC relationship.

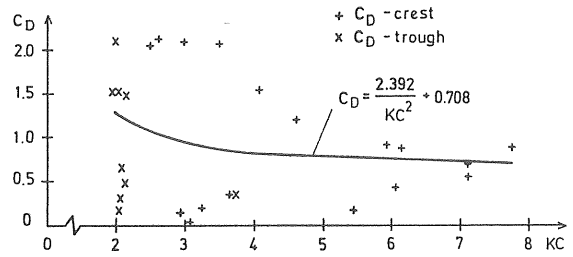

Figure 7.21 C_D versus KC below the still water level along the vertical cylinder. Method of least squares is used applied at wave crest and trough. Local KC are used. Kinematics according to fifth and cnoidal theories. Includes waves B, C, I, K and L.

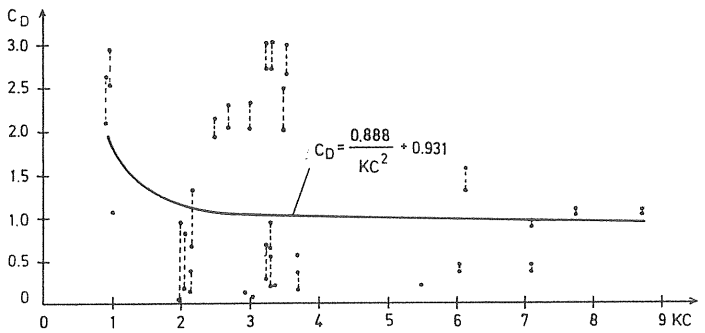

Figure 7.22 C_D versus KC below the still water level along the cylinder. Method of maximum velocities and acceleration and of zero and maximum forces are used. Local KC are used. Criterion of maximum scatter according to the two methods were set at 0.9. Kinematics according to fifth and cnoidal theories. Includes waves B, C, I, K and L.

7.3.3 Effects of the free surface on time-invariant force coefficients

The effect of the free surface is described and discussed in Chapter 5.3. Its effects on the time invariant force coefficients at the still water level are seen if Figs. 7.23-7.26 are compared to Figs. 7.10, 7.12, 7.14 and 7.16 which have been drawn up on the same basis. Data for the waves studied are given in Table A1.1e.

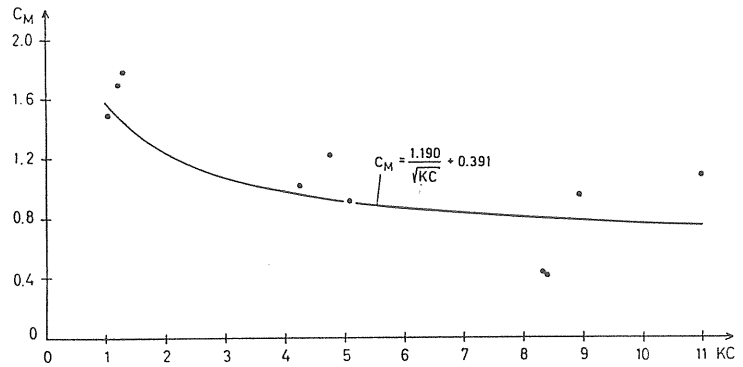

Figure 7.23 Effect of the free surface on the C_M-KC relationship at the still water level. Method of least squares is used, applied at wave crest. Local KC are used. Measured velocity.

Too few data points were available to establish any reliable relationships. However, disregarding the magnitude of C_M, Figs. 7.23-7.24 show approximately the same trends for the C_M-KC relationship as the ones evaluated for levels below the still water level. Furthermore, Figs. 7.23-7.26 show that the effect of the free surface is to increase the C_D coefficient as well as to decrease the C_M coefficient throughout the range of KC. Measurements above the S.W.L. are not presented in Figs. 7.23-7.26. However, measurements indicate that trends reported for the C_M-KC relationship become even more pronounced above the S.W.L.

These observations are contrary to the conclusions drawn by Törum (1985), as obtained in the drag dominated regimes

(KC > 25 in S.W.L.). The author states that the C_M values increase from the S.W.L. up to the water surface, while the C_D values tend to stay uniform all along the cylinder, up to the surface area. Törum's observations may be explained by the fact that kinematics from Stokes' 2nd order theory were used instead of measurements. As reported in Chapter 4, the studied theories have tendency to overestimate velocities above the still water level. Furthermore, instead of an exponentially increasing velocity, a decreasing velocity profile was measured above the S.W.L. for waves on very shallow water.

From Morison's equation (Eq. (2.7)) it may be seen that the use of an erroneously high velocity, for a force, results in a decreased C_D coefficient. Furthermore, Sarpkaya and Isaacson (1981) noted counter-variation of C_D and C_M consequently results in increased C_M-values. (The counter-variation of C_D and C_M is a consequence of the use of Morison's equation with time-invariant force coefficients and not a fluid mechanical phenomenon). However, Törum was aware of the limitation of the theory used (Stokes' 2nd order) and recommended further analysis to be concentrated on water-wave kinematics.

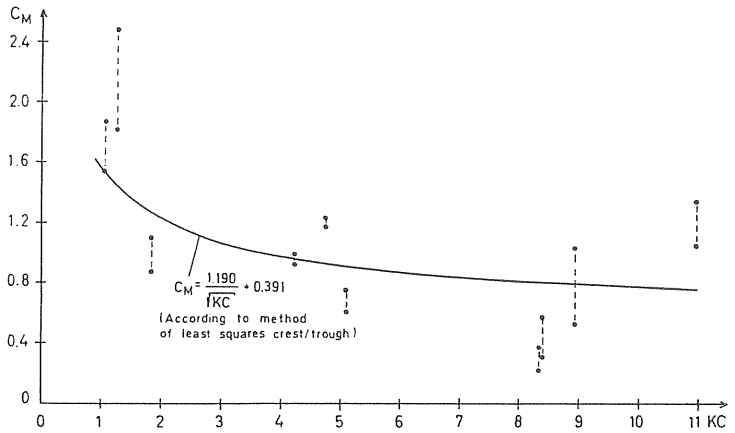

Figure 7.24 Effect of the free surface on the C_M-KC relationship at the still water level. Methods of maximum velocities and accelerations and of zero and maximum forces are used. Local KC are used. Measured velocity.

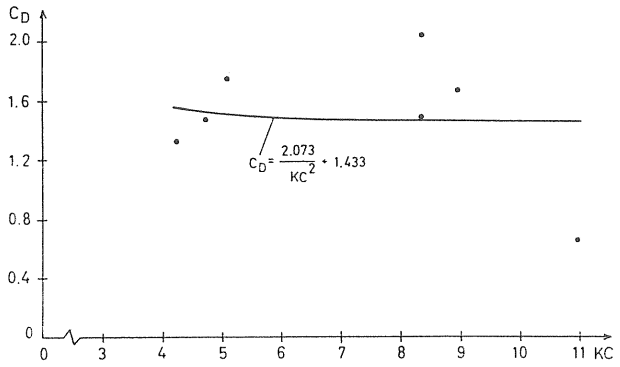

Figure 7.25 Effect of the free surface on the C_D-KC relationship at the still water level. Method of least squares is used, applied at wave crest. Local KC are used. Measured velocity.

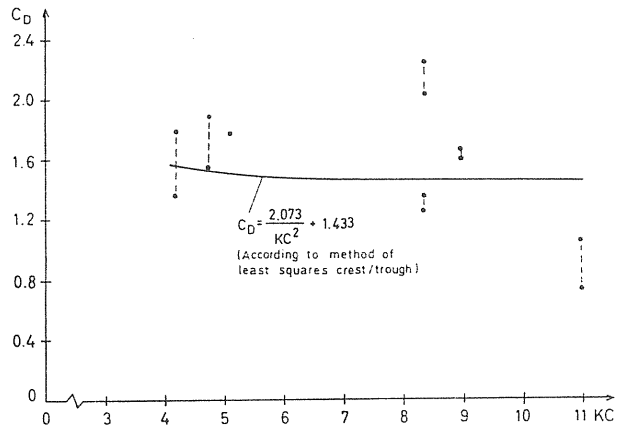

Figure 7.26 Effect of the free surface on the C_D-KC relationship at the still water level. Methods of maximum velocities and accelerations and of zero and maximum forces are used. Local KC are used. Measured velocity.

7.4 Importance of correct force coefficients

As an example of the importance of using correct force coefficients, Figs. 7.27 and 7.28 may be examined. The figures compare the total force calculated by using Morison's equation with fifth order or cnoidal wave theories and the total force obtained from the integrated pressure.

In both cases the total force is obtained from calculated sectional force, as described in Chapter 6.1.3.

Figs. 7.27 a-d show the comparison between total forces on the vertical cylinder and total forces obtained from the integrated pressure. Force coefficients according to the method of zero and maximum forces are used and applied in crests and wave troughs (given in Table A1.2). This method of calculation ensures that maximum measured and calculated sectional forces coincide. As seen, there is good correspondence between "measured" and calculated total forces. However, in reality, it is impossible to choose "correct" force coefficients, and one has to rely on graphs such as those presented by Sarpkaya and Chakrabarti.

Figs. 7.28 a-d, which correspond to those given in Figs. 7.27 also compare "measured" and calculated total forces. However, in this case the force coefficients were set in accordance with a realistic engineering point of view, i.e. using force coefficients given in graphs evaluated from the method of least squares and with local KC and the effect of the free surface incorporated.

Yet, notwithstanding, Figs. 7.28 a-d show that both the magnitude and the phase of the force are in poor agreement with measurements. Total force from waves on deep and transitional water, represented by waves A and B are fairly well predicted. However, the agreement between "measured" and calculated forces in shallow water (represented by wave C) using fifth order or cnoidal wave theories is poor.

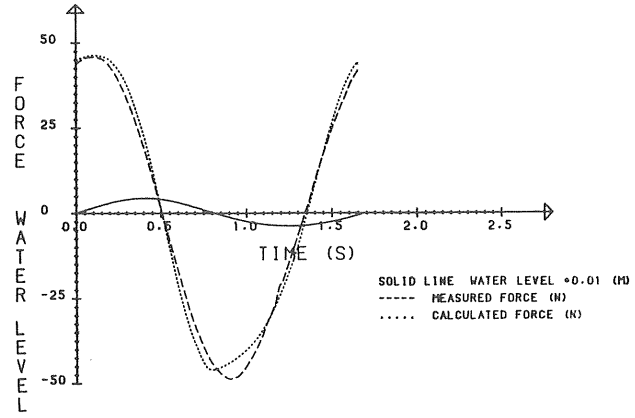

Figure 7.27 a Wave A. Total wave force. "Deep water" (fifth order theory).

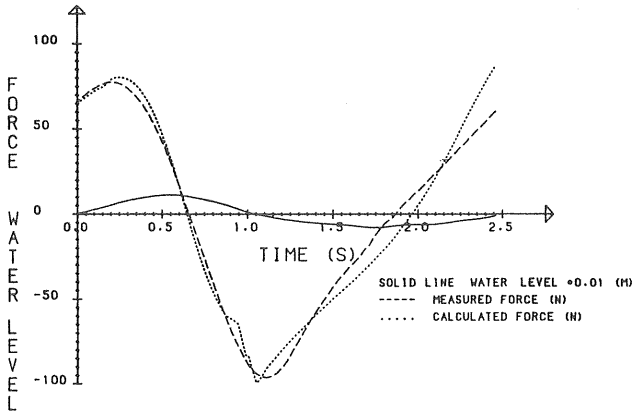

Figure 7.27 b Wave B. Total wave force. "Transitional water depth" (fifth order theory).

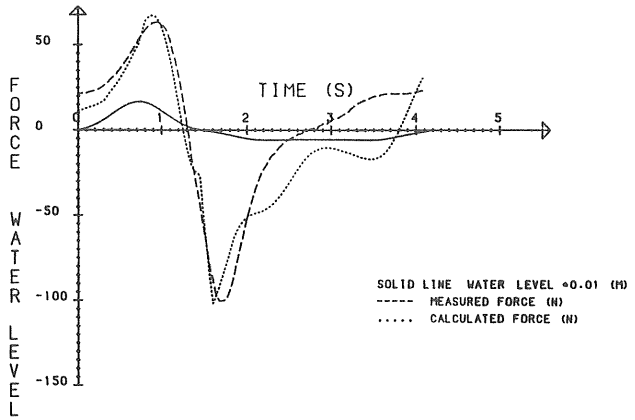

Figure 7.27 c Wave C. Total wave force. "Shallow water" (fifth order theory).

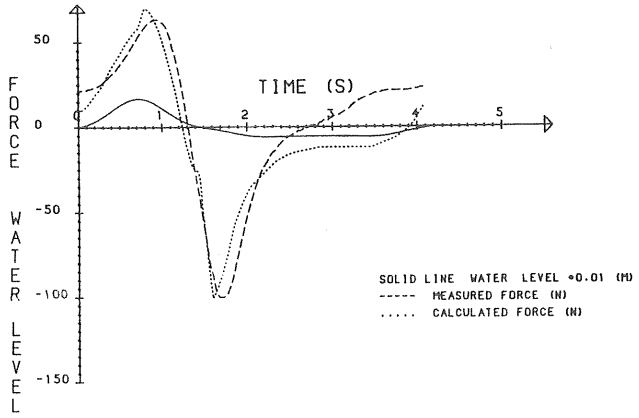

Figure 7.27 d Wave C. Total wave force. "Shallow water" (cnoidal theory).

Figs. 7.27 a-d. Comparison between total force on the vertical cylinder calculated using Morison's equation (fifth order or cnoidal theories) and the total force obtained from the integrated pressure (measured force). Force coefficients set according to the method of zero and maximum forces and using local KC.

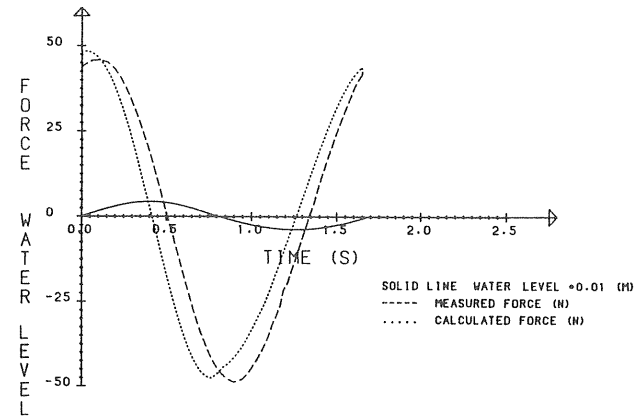

Figure 7.28 a Wave A. Total wave force (fifth order theory).

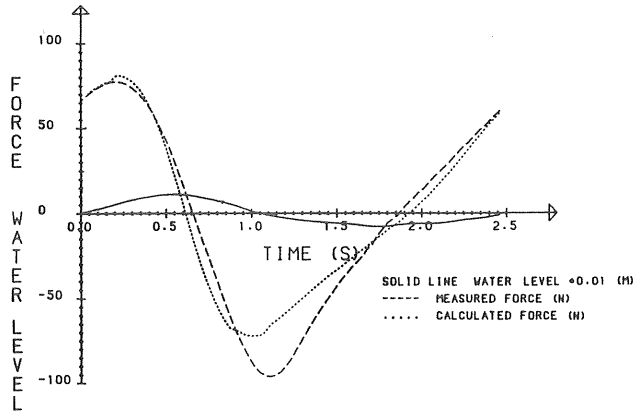

Figure 7.28 b Wave B. Total wave force (fifth order theory).

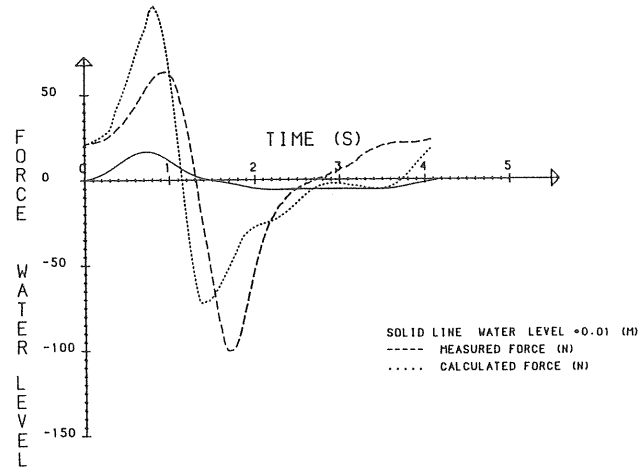

Figure 7.28 c Wave C. Total wave force (fifth order theory).

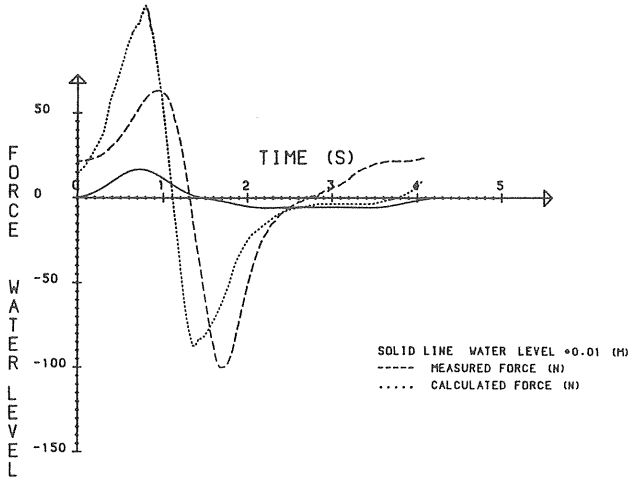

Figure 7.28 d Wave C. Total wave force (cnoidal theory).

Figs. 7.28 a-d. Comparison between total force on the vertical cylinder calculated using Morison's equation (fifth order or cnoidal theories) and the total force obtained from the integrated pressure (measured force). Force coefficients set according to the method of least squares and using local KC.

7.5 Comparison of results

The mean curves representing the C_D, C_M-KC relationships established in the previous chapters may only be used for comparison. As pointed out, only a limited number of data points was available.

Figs. 7.29-7.30 a,b show C_D, C_M-KC relations calculated from the present experiment and relations from Bearman, Chaplin et al., (1985), Chakrabarti (1980) versus various values of β-values and the Reynolds number given by Sarpkaya (1976a, 1985). In planar oscillatory flow Sarpkaya has shown that loading on a circular cylinder is dependent on β. However, in agreement with the findings of Bearman, Chaplin et al., no obvious dependence of the force coefficients on β was found in this study. Chakrabarti was also unable to show any dependence on the β-values.

The limited range of Re, and also the scatter in results attributed to this. Both the results of Bearman, Chaplin et al. and the present tests are based on wavy flow and involve β-number of about the same order. Consequently, these tests should be the most readily comparable.

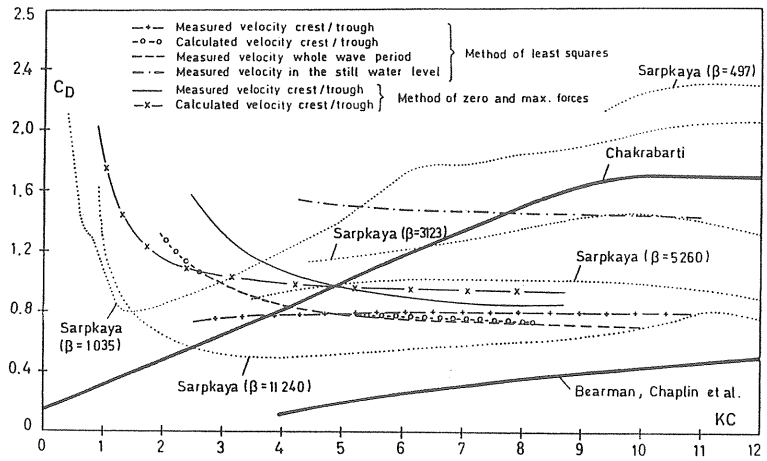

a C_D-KC relationship

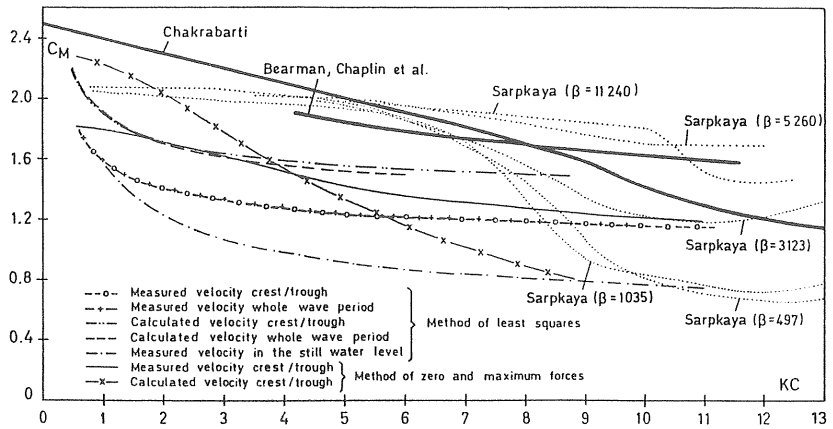

b C_M-KC relationship.

Figure 7.29 a-b Comparison of experiments by Bearman, Chaplin et al. (1985), Chakrabarti (1980) and present experiments versus various values of β-values, given by Sarpkaya (1976a, 1985). (β = Re/KC).
Bearman, Chaplin et al.; $2 \cdot 10^4 < \beta < 5.49 \cdot 10^4$
Chakrabarti ; $200 < \beta < 0.33 \cdot 10^4$
Present test ; $2.1 \cdot 10^4 < \beta < 6.9 \cdot 10^4$

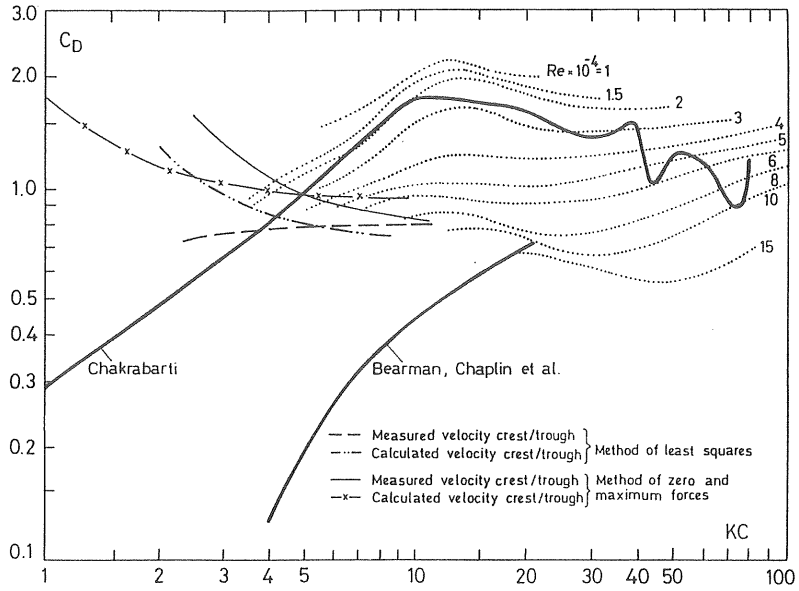

a C_D-KC relationship

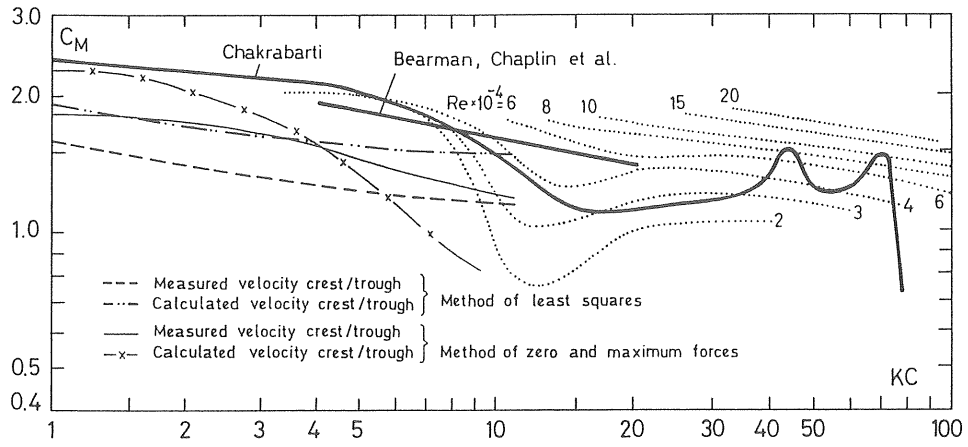

b C_M-KC relationship

Figure 7.30 a-b Comparison of experiments by Bearman, Chaplin et al. (1985), Chakrabarti (1980) and present experiments versus various values of the Reynolds number, given by Sarpkaya (1976a).
Bearman, Chaplin et al.; $14.6 \cdot 10^4 < Re < 50.5 \cdot 10^4$
Chakrabarti ; $2 \cdot 10^4 < Re < 3 \cdot 10^4$
Present test ; $3 \cdot 10^4 < Re > 23 \cdot 10^4$

As noted in Chapter 7.3, the almost identical mean curves for both the C_D and the C_M-KC relationship indicate that wave force calculation may be improved by the use of the local KC.

Furthermore, the method of least squares gives a general decrease of the C_M coefficient, which gradually approaches a constant value. The values of C_M coefficients, especially the one evaluated from measured velocities, are small compared to results form the other investigators. This may be because the acceleration was obtained from the measured velocity by calculating the numerical derivative. Furthermore, the missing velocity data near the zero crossing was replaced with calculated data. Another possible explanation is that all levels of measurements under the S.W.L. were included, i.e. there is a possibility of influence from the free water surface.

However, the method of zero and maximum forces yields C_M-values of about 2 for both calculated and measured kinematics in the lower half of the KC region studied.

Finally, somewhat the same trends were observed for the force coefficients at the S.W.L. as below the S.W.L. However, the effect of a free surface is to increase the C_D coefficient as well as to decrease the C_M coefficient throughout the KC range attained. Obviously, good wave force calculations should consider such effects.

7.6 Sources of uncertainty

Although a large number of laboratory and field experiments have been conducted to establish the drag and inertia coefficients there is a wide scatter in reported coefficients.

From the physical insights gained in Chapter 5, it becomes clear that there has to be some bias in data interpretation. For instance, a given flow may change from the sub-

critical to the postcritical flow regime for a given time alongside the cylinder. This variation in velocity along the cylinder may make the separation points undergo large fluctuations and cause the vortices to separate from the surface at different moments in time along the cylinder. This also means that the correlation length varies with depth. A further complication is the fact that the vortices are swept back and forth and that a possible current influences those movements greatly. Consequently, it is important to distinguish between force coefficients obtained from planar harmonical flow, two-dimensional waves and an ocean environment.

The drag and inertia coefficients obtained from two identical waves may not be the same. The force acting on the cylinder depends not only on the wave under consideration but also on the previous waves. Consequently, consideration of the effect of the previous flow history on the kinematics of the flow and hence on the force coefficients is necessary. Usually a representative cycle is obtained by overlaying all the data cycles of measurements in a run and then averaging these overlaid cycles.

As has been shown, the choice of kinematics in the wave force calculations is responsible for a substantial part of the scatter of reported force coefficients. One of the reasons for the consistency of Sarpkaya's results is that his kinematics are established rather precisely. In other works, velocities and accelerations were often not measured but calculated on the basis of the measured water level. It has only lately become possible to perform simultaneous measurements of wave forces and water velocities. An additional source of uncertainty about the kinematics in wave force calculations is that the velocity (u) is taken as the horizontal component, and, furthermore, that the convective acceleration terms are often ignored. It is then assumed that the total acceleration is equal to the local acceleration, i.e. that $\frac{du}{dt} = \frac{\partial u}{\partial t}$. However, the force from the convective acceleration terms is small only when the wave steepness is moderate, see Appendix 2.

The results are also affected by the way in which the experiments are performed. The force acting on the cylinder may be deduced either through measurements of the force on the entire cylinder, on segments or at specific levels along the cylinder. In the first case the total force is obtained through force measurements at both ends or from the bending moments acting at one end of the cylinder. In this case there is the least certainty in the calculated force coefficients. Here it may be as correct to use velocities and accelerations at the surface as at a suitable point along the cylinder. In any case, the calculated coefficients represent quantities averaged over both time and space. In the second case both the force and the kinematics of the flow are more precise. However, the experiments are usually restricted because of the use of a very limited number of instrumental force sections. Also, the sections with finite lengths (0.2-0.3 m) are subjected to some extent to the same limitations as with force measurements on the entire cylinder. Consequently, measurements at specific levels along the cylinder are preferred.

Usually, the experimental data are better suited for the determination of one or the other of the coefficients. If the drag forces dominate then the data are better for determining the drag coefficient while the inertia coefficient may be contaminated by the errors of various sources noted earlier. Conversely, if the inertia force dominates then the inertia coefficient is the most accurate coefficient. If the drag and inertia forces are of the same order of magnitude and the general quality of the data is good then reasonable resolution in both coefficients can be expected.

7.7 Concluding remarks

The Reynolds numbers (Re) attained ranges between $0.3 \cdot 10^5$ and $2.3 \cdot 10^5$ the orbital shape parameters (Ω) between 0.03 and 0.86 and the Keulegan-Carpenter numbers (KC) between 1 and 11.

In the Reynolds number range studied no obvious dependence of the Reynolds number on the force coefficients was found. Nor did the orbital shape parameter seem to have any marked effect. A possible reason for this may be the limited range of Re and the limited amount of data. However, these observations are in agreement with those of Bearman, Chaplin et al. 1985.

The values of force coefficients given in literature are usually time-invariant and averaged over whole wave cycles. Consequently, these coefficients have little physical significance, because in reality both C_M and C_D exhibit large variations during a given cycle.

When establishing the C_M, C_D-KC relationship at levels of measurements below the still water level it was found that the variation of force coefficients was mainly caused by the fact that the velocity decreases with depth. Mean curves through data points obtained from the method of least squares with the use of local KC (defined as noted above) applied over whole wave cycles or half cycles (wave crest or trough) were found to yield almost identical results. This was the case for measured velocities as well as for velocities given by fifth and cnoidal theories.

Clearly, and especially for waves in shallow water, wave force calculations may be improved by considering wave crests and troughs as two different types of events characterized by velocity decreasing with depth and by using local KC.

There is some scatter among results based on different evaluation approaches. However, clear trends with regard to the C_M-KC relationship were found. The method of least squares gave a general decrease of the C_M coefficient which gradually approaches a constant value with increasing KC. However, for the methods of maximum velocities and acceleration and of zero and maximum forces the C_M values remain at a somewhat higher level up to a KC of about 3.

These trends were observed at the C_M coefficients calculated from measured velocity as well as from velocities from fifth and cnoidal theories. However, the C_M coefficients calculated from wave theories generally yield somewhat higher values (about 0.3) throughout the KC range attained.

The inertia force was the dominant component in the KC range attained, which meant that there was comparatively larger scatter for the C_D coefficient and a smaller number of useful data points. No stable trends were found for the C_D coefficients. However, the methods of maximum velocities and accelerations and of zero and maximum forces indicate that values of the C_D increse when the KC is smaller than about 4.

Obviously, the used kinematics is one of the most important factors influencing the value of evaluated force coefficients. Consequently the chosen wave theory, with set force coefficients may greatly influence the values of calculated wave forces.

It was possible to study the effect of the free surface on the force coefficients at (and above) the still water level. Approximately the same trends for the coefficients, as calculated by the method of least squares, maximum velocities and accelerations and of zero and maximum forces as reported for points below the still water level were observed. However, the effect of the free surface is to increase the C_D coefficient as well as to decrease the C_M coefficient throughout the KC range attained.

Finally, Figs. 7.9-7.26 show that the method of calculation influences the values of force coefficients. The influence and consequences of using erroneous force coefficients has been exemplified. It was shown that the prerequisite for good wave force calculation is having force coefficients that ensure correct maximum forces. Otherwise, the magnitude and the phase of the force may be in poor agreement with measurements.

8. THE USE OF r.m.s. FORCE COEFFICIENT

In a practical situation it is difficult (if not impossible) to choose correct force coefficients. Consequently the calculated force may be out of phase. The use of a single root mean square force coefficient ($C_{Fr.m.s.}$) which does not consider the phase may then be justified.

Results obtained by Bearman, Chaplin et al. (1985) correspond well with the present test and indicate that the use of $C_{Fr.m.s.}$ is a promising way of calculating the $F_{r.m.s.}$. In this chapter it is shown that it is possible to relate $u_{r.m.s.}$ calculated by the use of fifth order or cnoidal theories and $F_{r.m.s.}$ to the maximum force in crest and wave trough, respectively. With 95 percent confidence the ratio between measured force and the true mean of predicted force was found to be within 0.988 ± 4.5% for crest situations and within 0.941 ± 5.8% for trough situations for all waves in the experimental program.

8.1 R.m.s. force

In order to avoid decomposition into drag and inertia components several investigators have used a root mean squared in-line force coefficient $C_{Fr.m.s.}$ defined as

$$C_{F_{r.m.s.}} = \frac{2\,F_{r.m.s.}}{\rho D (u_{r.m.s.})^2} \qquad \ldots (8.1)$$

where $F_{r.m.s.}$ = r.m.s. value of in-line force
ρ = density of water
D = diameter
and $u_{r.m.s.}$ = r.m.s. value of horizontal velocity

The force coefficient $C_{Fr.m.s.}$ as defined in Eq. (8.1) has been used by Bearman, Chaplin et al. (1985), confirming that regular wave data can be used to predict forces in random waves. Stansby et al. (1983) and Chakrabarti (1985) used $C_{Fr.m.s.}$ to investigate the influence of the orbital shape parameter (Ω), see Chapter 2.

The use of $C_{Fr.m.s.}$ obscures the time dependence of the force and hence the physics of the problem. The use of $C_{Fr.m.s.}$ may consequently only be justified for estimation of the magnitude of forces.

Figs. 8.1 a,b show $C_{Fr.m.s.}$ evaluated from the present test and plotted versus the local KC, using measured velocities in Fig. 8.1 a, and velocities calculated from fifth order and cnoidal theories in Fig. 8.1 b. $C_{Fr.m.s.}$ from whole wave cycles as well from crests and wave troughs below the still water level along the cylinder are given. A regression curve of the form $x = (a/y)+b$ has been calculated on the basis of the findings of Bearman, Chaplin et al. (1985). Their KC interval stretched from KC = 2.6 to 21. The regression curve is plotted in Figs. 8.1 a and b together with the results of the present test. The curve has been extrapolated for values below KC = 2.6.

The present $C_{Fr.m.s.}$ values from measured and calculated velocities evaluated over whole cycles as well from crests and wave troughs are in good agreement with the findings of Bearman, Chaplin et al. This agreement indicates that the $C_{Fr.m.s.}$-KC relationship established in the present tests or according to Bearman, Chaplin et al. may be used together with Eq. (8.1) to calculate the r.m.s. force in crest and wave trough. Furthermore, the $C_{Fr.m.s.}$-KC relationship established in the still water level given in Figs. 8.2 a,b also show good agreement. However, the consistency is weaker because of the limited number of data points.

Table 8.1 gives the 95 percent confidence interval of the ratio between $F_{r.m.s.}$ values from the present test (from measured force) to calculated $F_{r.m.s.}$ values given by the relations in Fig. 8.1 b. All levels of measurement below the still water level are incorporated. The confidence level of the ratio between $F_{r.m.s.}$ values from the present test and the results from Bearman, Chaplin et al. are also given. The standard deviation of the ratio is also

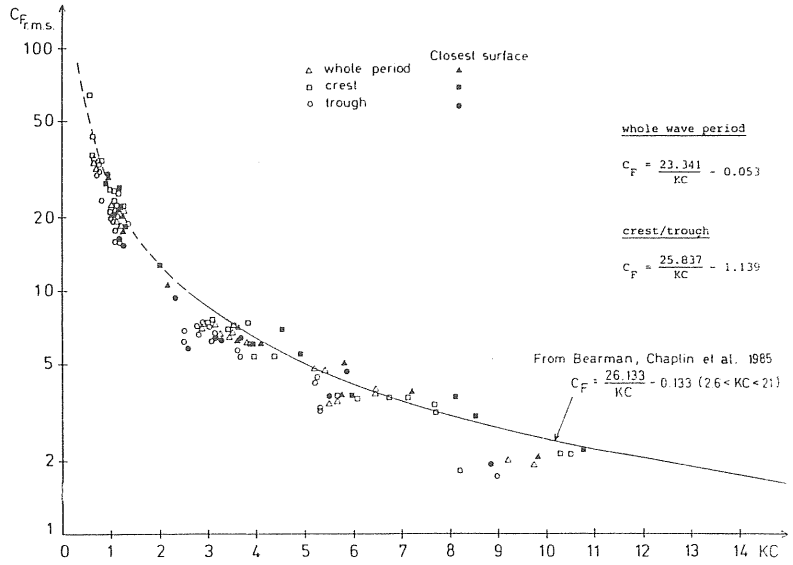

Figure 8.1 a Variation of CFr.m.s. with KC below the S.W.L. Measured velocities. Values from whole wave cycles as well from crests and wave troughs are shown. Values from the level of measurement situated uppermost under the S.W.L. are indicated.

given in the table. The standard deviation may be seen as a measure of the quality of an individual measurement while the 95% confidence interval can be seen as a measurement of the quality of the regression curve.

An alternative form of the root mean squared in-line force coefficient $C_{Fr.m.s.}$ is obtained by using Eq. (2.7) - assuming the horizontal velocity to be given by $u = a\omega \cos \omega t$. It may be shown that

$$C_{F_{r.m.s.}} = \frac{2\, F_{r.m.s.}}{\rho\, D\, a^2 \omega^2} = \sqrt{\frac{1}{2}\left(\left(\frac{\sqrt{3}}{2} C_D\right)^2 + \left(\frac{\pi^2 C_M}{KC}\right)^2\right)} \quad \ldots \quad (8.2)$$

where a = wave amplitude

and $\omega = \frac{2\pi}{T}$

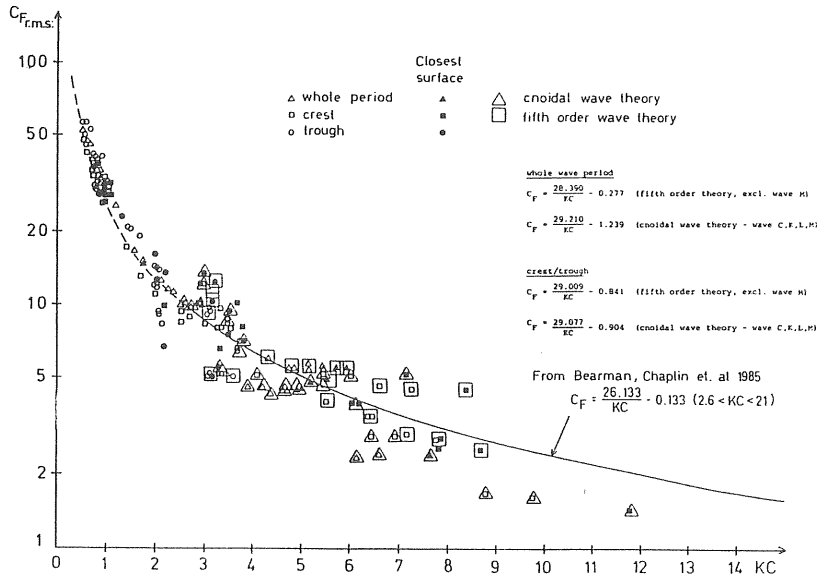

Figure 8.1 b Variation of CFr.m.s. with KC. Velocities calculated from fifth order or/and cnoidal theories below the S.W.L. along the vertical cylinder. For shallow water waves CFr.m.s. values are presented from both fifth order and cnoidal theories, indicated by an extra symbol. Values from whole wave cycles as well from crests, and wave troughs are shown. Values from the level of measurement situated uppermost under the S.W.L. are indicated.

The $C_{Fr.m.s.}$ as given in Eq. (8.2) has been used, e.g. by Sarpkaya (1976a) and Hogben (1979).

Introducing $a^2\omega^2 = u_{max}^2 = 2(u_{r.m.s.})^2$ into Eq. (8.2) and letting KC -> 0 and ∞ gives, with $C_M = 2$ and $C_D = 0.6$,

$$C_{F_{r.m.s.}} = \frac{C_M \pi^2 \sqrt{2}}{KC} = \frac{27.91}{KC} \qquad \ldots \quad (8.3)$$

and

$$C_{F_{r.m.s.}} = C_D \sqrt{3/2} = 0.735 \qquad \ldots \quad (8.4)$$

respectively.

Eq. (8.3) indicates that $C_{Fr.m.s.}$ as calculated both in the present test ($1 < KC < 11$) and in results by Bearman, Chaplin et al. ($2.6 < KC < 21$) should be represented by constant/KC at low KC. Furthermore, Eq. (8.3) gives about the same value for the constant as was calculated in the present experiments and by Bearman, Chaplin et al.

Eq. (8.4) indicates that $C_{Fr.m.s.}$ should approach a value of 0.735 at a high KC. In fact, Sarpkaya (1976a) shows that $C_{Fr.m.s.}$ approaches 0.74 at a KC of about 70 for β between 3000-5300. However, at $\beta = 8370$ the $C_{Fr.m.s.}$ approached a value of 1.0.

Table 8.1 Confidence of the ratio between Fr.m.s. values from present test to calculated Fr.m.s. values given by relations in Fig. 8.1 b (waves on shallow water - cnoidal theory used i.e. wave C, K, L, M) and to results from Bearman, Chaplin et al. (1985). All levels (all waves) of measurements below S.W.L. are incorporated. The standard deviation of the ratio is also given in the table.

Fr.m.s. (measured) to Fr.m.s. (calculated) applied over	Calculated relations from present test (given in Fig. 8.1 b) cnoidal wave theory - waves C, K, L, M		Relations from results by Bearman, Chaplin et al.,	
	95% confidence	S.Dev.	95% confidence	S.Dev.
whole cycle	0.978 ± 3.0%	0.10	0.998 ± 4.4%	0.14
whole cycle ((crest+trough)/2)	0.996 ± 2.1%	0.07	1.032 ± 2.7%	0.09
crest	0.995 ± 5.5%	0.18	1.016 ± 5.9%	0.20
trough	1.004 ± 6.4%	0.21	1.067 ± 6.8%	0.22

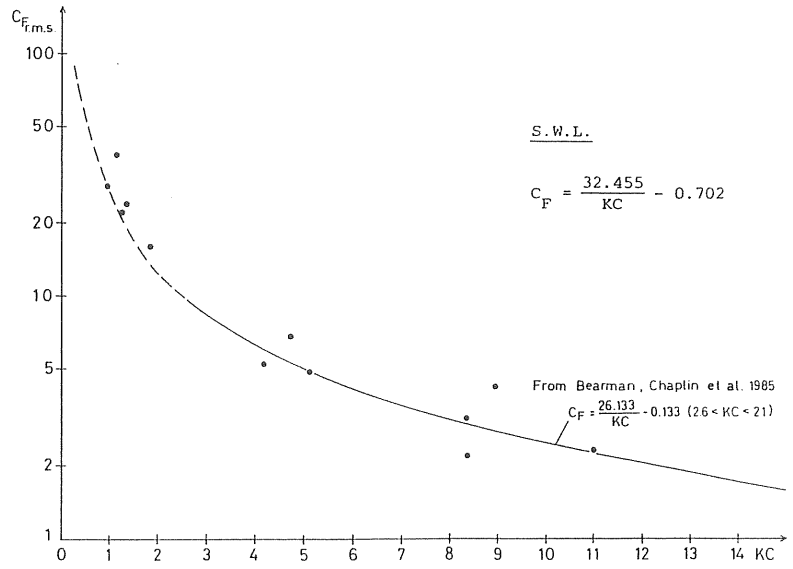

Figure 8.2 a Variation of CFr.m.s. with KC in the S.W.L. Measured velocities.

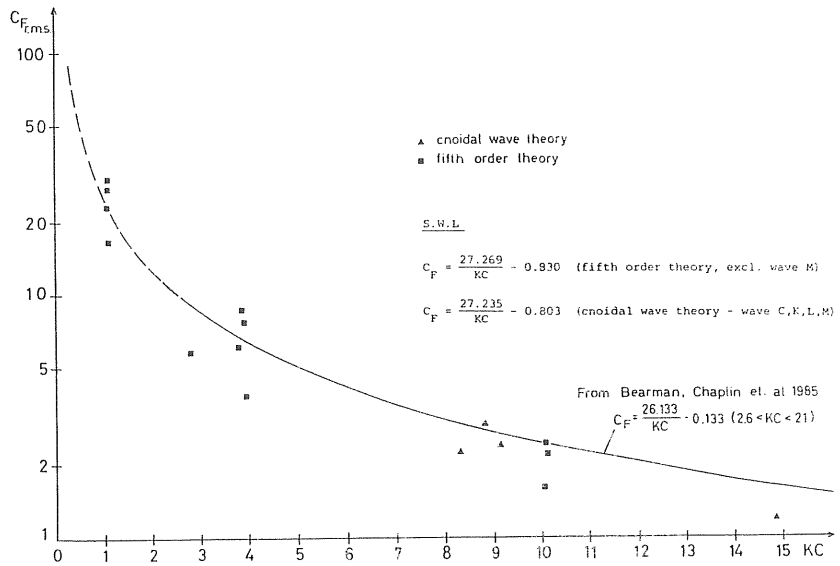

Figure 8.2 b Variation of CFr.m.s. with KC in the S.W.L. Velocities calculated from fifth order or/and cnoidal theories. For shallow water waves CFr.m.s. values are presented from both fifth order and cnoidal theories.

8.1.1 Ratio of r.m.s. force to maximum force

The good agreement between the $C_{Fr.m.s.}$-KC relationship found in the present test with the use of velocities according to fifth order or cnoidal theories and the results of Bearman, Chaplin et al. (1985) carried to an investigation of finding some ratio of r.m.s. force to maximum force.

First order theory gives a ratio of $\sqrt{2}$ between maximum velocity and r.m.s. velocity for whole cycles as well as for crests and troughs, i.e. $u_{max} = \sqrt{2} \cdot u_{r.m.s.}$. For steep waves such as those in the present test, it was found

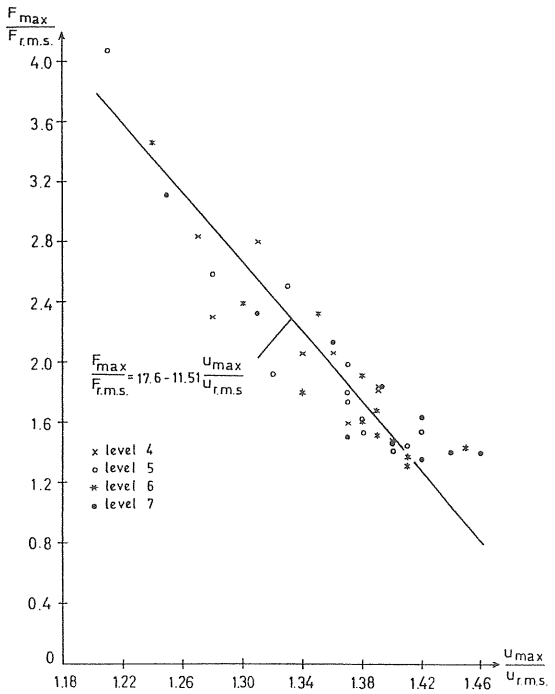

Figure 8.3 a Wave trough. Variation of Fmax/Fr.m.s. with umax/ur.m.s. given by fifth order theory and cnoidal theory (wave K, L). Each symbol represents a certain level of measurements below the S.W.L. With a 95 percent confidence interval the true mean of Fmax/Fr.m.s is within ± 10.1%. (Waves C and M excluded).

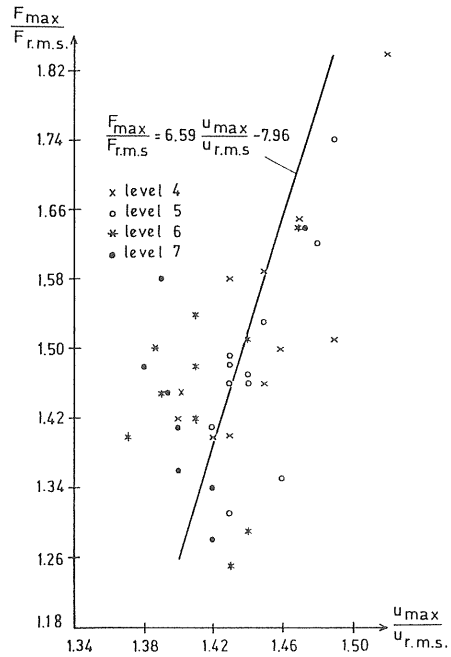

Figure 8.3 b Wave crest. Variation of Fmax/Fr.m.s. with umax/ur.m.s. given by fifth order theory and cnoidal theory (wave K,L). Each symbol represents a certain level of measurements below the S.W.L. With a 95 percent confidence interval the true mean of Fmax/Fr.m.s. is within ±2.9%. (Waves C and M excluded).

that the ratio of $u_{max}/u_{r.m.s.}$ was greater than $\sqrt{2}$ for crests and smaller for wave troughs. Consequently, we investigated whether it was possible to relate the r.m.s. force to the r.m.s. velocity given by fifth order theory or cnoidal theory (on shallow water) in crest and wave trough.

The ratio of $F_{max}/F_{r.m.s.}$ from measurements versus the ratio of $u_{max}/u_{r.m.s.}$ given by fifth order or cnoidal theories is plotted in Figs. 8.3 a,b. The plots indicate linear relations although some scatter is present, and calculated regression lines are drawn in the figures. When plotting $F_{max}/F_{r.m.s.} - \sqrt{2}$ as a function of $u_{max}/u_{r.m.s.} - \sqrt{2}$ it is found that the regression lines pass almost through the origin of the coordinates. Thus it is possible to relate the force, at least for the

mass-dominated waves in the experimental program, to the deviation from the sinusoidally varying velocity.

8.1.2 Method for estimation of maximum forces along a vertical cylinder by the use of $C_{Fr.m.s.}$

An alternative technique for the calculation of the maximum force along a vertical cylinder has been described in the previous pages. A short review of the technique is given below.

1) Choice of wave theory. By the use of the Le Méhauté diagram (Fig. 4.2) or the relation $H/d > 350 \cdot (d/gT^2)^{3/2}$ (Chapter 4.2.4) the range of suitability is obtained. If the wave studied can be considered a shallow water wave, the cnoidal theory is recommended. Otherwise, the fifth order theory should be used.

2) Calculation of local KC along the cylinder, using the maximum velocity given by fifth order or cnoidal theories in wave crest and trough, respectively.

3) Determination of the in-line force coefficient $C_{Fr.m.s.}$. $C_{Fr.m.s.}$ is determined by the use of the relation given in Fig. 8.1 b or by the regression curve calculated on the results by Bearman, Chaplin et al. given in the same figure. Use the local KC in crest and trough along the cylinder. For KC > 30-40 a value between 0.74-1.00 of $C_{Fr.m.s.}$ should be chosen.

4) Calculation of the r.m.s. force ($F_{r.m.s.}$) using Eq. (8.1). $u_{r.m.s.}$ is calculated using fifth order or cnoidal theories applied over wave crest and trough.

5) Calculation of the ratio of u_{max} to $u_{r.m.s.}$ using fifth order or cnoidal theories for wave crest and trough. The ratio of maximum force to $F_{r.m.s.}$ in wave crest and trough along the cylinder may be obtained

by using Fig. 8.4 or by the relations given in Figs. 8.3 a,b.

6) Total maximum force in wave crest and trough is obtained by integration of maximum force along the cylinder.

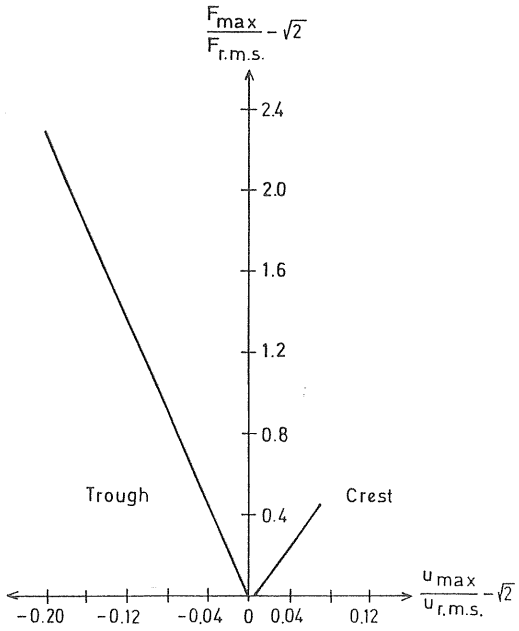

Figure 8.4 Variation of Fmax/Fr.m.s.- $\sqrt{2}$ with umax/ur.m.s.- $\sqrt{2}$. Velocity according to fifth order or cnoidal theories.

The maximum force from all levels of measurements below the S.W.L. for all examined waves was calculated with the use of given relations in Fig. 8.1 b and Fig. 8.4. With a 95% confidence interval the ratio between measured force and the true mean of predicted force was within 0.988 ± 4.5% for crest situations and within 0.941 ± 5.8% for trough situations. The corresponding values determined by using the graph from Bearman, Chaplin et al. are 1.022 ± 4.4% and 1.008 ± 6.5%, respectively. The same confidence intervals with corresponding standard deviations are given in Table 8.2.

Table 8.2 Ratio of maximum measured force to the maximum force calculated using the r.m.s. method. The standard deviation of the ratio is also given.

	Present test ($C_{Fr.m.s.} = \frac{29.077}{KC} - 0.904$)		From Bearman, Chaplin et al. ($C_{Fr.m.s.} = \frac{26.133}{KC} - 0.133$)	
	95% Confidence	S. Dev.	95% Confidence	S.Dev.
crest	0.988 ± 4.5%	0.14	1.022 ± 4.4%	0.14
trough	0.941 ± 5.8%	0.18	1.008 ± 6.5%	0.21

In Table 8.3 the ratio of maximum measured sectional force to the maximum calculated sectional force according to the outlined r.m.s. method and by Morison's equation are given for waves A, B and C. Force coefficients according to the method of least squares and with a local KC. For these three waves it is seen that the method of r.m.s. force gives the closes prediction of maximum force.

Table 8.3 Ratio of maximum measured force to maximum calculated force given by the r.m.s. method and by Morison's equation for waves A, B and C in the experimental program.

	Method of r.m.s.		Morison's eq.	
	Ratio	Total range %	Ratio	Total range %
Wave A (4 levels)				
crest	0.96-1.03	7	0.92-1.01	9
trough	1.05-1.19	14	0.91-1.12	21
Wave B (4 levels)				
crest	0.92-0.99	7	1.04-1.33	29
trough	1.08-1.28	20	1.16-1.49	33
Wave C (3 levels)				
crest	0.75-0.89	14	0.54-0.74	20
trough	0.84-1.03	19	1.14-1.26	12

9. OBSERVATIONS AND CONCLUSIONS

The most important observations and conclusions made during the present investigation are given below. Reference to the relevant chapter is made in conjunction with each section.

9.1 Experimental approach

- The inexpensive technique for measuring instantaneous velocities with a micropropeller was found to work well for oscillating flow. (Chapter 3.6, 3.6.1, 4.2.2, 4.2.3).

- The technique used for measuring the distribution of pressure was fruitful for the studies of wave forces and the physics underlying them. (Chapter 3.2, 3.5, 6.1.2, 6.1.3, and throughout the text).

When determining the force on a structure in waves, two equally important steps can be distinguished. Firstly, it is necessary to know the wave characteristics, such as the velocity field under the wave. Secondly, a method of calculation must be developed and used, relating the actual wave to the force on the structure.

9.2 Wave kinematics

- The experiments performed have shown that it is important to use a relevant wave theory for evaluating the C_D and C_M coefficients in Morison's equation, and that coefficient values obtained from experiments using one wave theory cannot be used when designing with the help of another wave theory. (Chapter 4.2.2, 4.2.4, 7.1, 7.3.1, 7.3.2, 7.4).

- It is recommended to use the Le Méhauté diagram, Fig. 4.2, for classifying the wave. If a shallow water wave is to be studied, the cnoidal wave theory should be

used. Otherwise the fifth order theory is recommended. If only the magnitude of the force is needed and not the phase, the linear theory can be used, with fairly good results. (Chapter 4.2.4, 4.2.5).

- It is also recommended that the exponential increase of velocity and acceleration above the still water level given by theories for waves on shallow water be changed to a constant or a decreasing one. (Chapter 4.2.3, 4.2.4).

9.3 Method of calculation - Morison's equation

- Because of all the facors underlying the wave forces in separated flow, and because Morison's equation works as well as it does, it is unlikely that a new equation will replace it. (Chapter 2.2, 2.2.2, throughout Chapter 5, 7.4).

- However, it is shown that the prerequisite for good wave force calculation is having force coefficients that ensure correct maximum forces. Otherwise both the magnitude and the phase of the force may be in poor agreement with measurements. (Chapter 7.4).

9.4 Wavy flow

- In addition to the effect of the free surface, the orbital motion of the fluid particle gives rise to a three-dimensional time dependent flow. A further complication is the exponential decay of the particle velocity along the vertical cylinder. (Chapter 5.3).

- Especially for steep waves, then, there is no harmonic variation of kinematics during the wave period. (Chapter 4.2.2, 5.3, 7.1).

- Experiments in waves have the advantage that both the undisturbed paths and free surface effects are correctly

modelled. Furthermore, experimental data from regular waves can be used to predict forces on a vertical cylinder in irregular waves, as was confirmed by Bearman, Chaplin et al. 1985. (Chapter 5.3).

- In this study the ranges of attained Reynolds number (Re), orbital shape parameter (Ω) and Keulegan-Carpenter number (KC) were

$$0.3 \cdot 10^5 < Re < 2.3 \cdot 10^5$$
$$0.03 < \Omega < 0.86$$
and $$1 < KC < 11$$

In the above studied Re range no obvious dependence of the force coefficients on the Reynolds number was found. Neither does the orbital shape parameter seem to have a marked effect. These observations are in agreement with those of Bearman, Chaplin et al. 1985. (Chapter 7.3, 7.3.1, 7.3.2, 7.4, 7.5, 7.7).

- Furthermore the relation between Strouhal and Reynolds number for vortex shedding tends to be the same for wavy flow as for steady flow. However, the wavy flow results in weaker and less regular shedding. (Chapter 5.3, 6.2).

9.5 Free surface effects

- The free surface causes a more asymmetrical flow pattern around the cylinder but less variation of separation angles than in planar oscillating flow. This affects the pressure distribution and consequently the resulting net pressure and force considerably. (Chapter 5.3, 5.3.1, 5.3.2, 7.3.3).

- The free surface effects are mainly due to separation on the free surface under which a shear layer develops. The reason for this shear flow is the free-surface curvature. (Chapter 5.3.1).

- The free surface effects are important because the influence increases as the velocity of the incident flow increases. (Chapter 5.3.1).

- Furthermore, the free surface affects the flow at quite a distance below the still water level. For a studied crest situation the influence was noticeable as deep as the distance of one wave height (H) below the water surface. (Chapter 5.3.2).

- Force coefficients calculated at the still water level show approximately the same trends for the C_D, C_M-KC relationships as the ones calculated below the still water level. However, the effect of the free surface is to substantially increase the C_D coefficient as well as to decrease the C_M coefficient throughout the range of KC. (Chapter 5.3.2, 7.3.3, 7.5).

9.6 Improvements of wave force calculations

- Morison's equation works quite satisfactorily in the drag and inertia-dominated regions. The large deviation present in KC range of about 8 to 25 (planar oscillating flow) may be minimized by improving Morison's equation with additional terms as proposed by Sarpkaya. (Chapter 2.2, 2.2.2, 7.1, 7.4, 7.5, 7.7).

- Clearly, and especially for waves in shallow water, wave force calculations may be improved by considering wave crests and troughs as being two different types of events characterized by velocity decreasing with depth, and the use of a local KC. (Chapter 7.1, 7.3, 7.3.1, 7.3.2, 7.3.3, 7.4, 7.5, 7.7).

9.7 R.m.s. force coefficient

- In a practical situation it is difficult to choose correct force coefficents. Consequently, the calculated force may be out of phase, which justify the use of a root mean square force coefficient ($C_{Fr.m.s}$) for the calculation of force ($F_{r.m.s.}$). (Chapter 7.4, 8.1).

- Good correspondence with results of Bearman, Chaplin et al. (1985) indicated that the use of $C_{Fr.m.s.}$ is a promising way for the calculation of $F_{r.m.s.}$. (Chapter 8.1).

- Furthermore, results show that it is possible, with good accuracy, to relate $u_{r.m.s.}$ calculated by the use of fifth order or cnoidal theories and $F_{r.m.s.}$ to the maximum force in crest and wave trough respectively. (Chapter 8.1.1).

- The technique of calculating the maximum magnitude of forces along the cylinder is outlined in Chapter 8.1.2.

LIST OF SYMBOLS

a = wave amplitude

a_n = Fourier coefficients

A = characteristic area

A_n = Fourier coefficients

B_n = - " -

B_n^* = - " -

C_D = drag coefficient

$C_{D(\theta)}$ = time varying drag coefficient, defined by Eq. (7.1)

$C_{Fr.m.s.}$ = r.m.s. in-line force coefficient

C_L = lift coefficient

C_m = added mass coefficient

C_M = mass or inertia coefficient

$C_{M(\theta)}$ = time varying inertia coefficient, defined by Eq. (7.2)

C_M^* = effective inertia coefficient

d = still water depth

$d\theta$ = increment of angle

D = diameter of cylinder

e = distance between cylinder and wall

f = flow frequency

f_r = frequency ratio (= f_s/f)

f_s = frequency of vortex shedding/dominant lift frequency

F = force

F_D = drag component of force

F_L = lift force

F_M = inertia component of force

F_{Mc} = inertia force component due to the convective acceleration

$F_{r.m.s.}$ = r.m.s. value of in-line force

F.S.E. = free surface effects

g = acceleration of gravity

H = wave height

H_s = significant wave height ($H_{1/3}$)

k = wave number (= $2\pi/L$)

k_s = equivalent sand roughness (k_s/D = relative roughness)

K = chosen time step

KC = Keulegan-Carpenter number (= $u_m T/D$)

l = length of cylinder

$l_{1,2}$ = distances, given in Fig. 6.2

L = wave length

L_o = $gT^2/2\pi$

LE = specific level

m_a = added mass

N = number of datapoints or increment

p = pressure

PRE = pressure

PRO = wave profile

R = radius of the cylinder

Re = Reynolds number (= uD/ν)

S = Strouhal number

S_f = shape factor (δ^*/δ_θ)

t = time

t/T = time instant during the wave cycle

T = period of the wave cycle

T_z = average apparent period

u = x-component of the water particle velocity

u_m = maximum horizontal particle velocity

u_n = instantaneous velocity

$\dot{u}_n$ = instantaneous acceleration

u_h = horizontal particle velocity

$u_{r.m.s.}$ = r.m.s. value of horizontal velocity

u_v = vertical particle velocity

U = total velocity

U_s = free stream velocity

U_T = tangential velocity

V = immersed volume

x_o = line of action, given in Fig. 6.2

y_n = defined in Fig. 6.3

Y = vertical coordinate

w = z-component of the fluid velocity

W = width of test section

β = frequency parameter (= Re/KC)

$\partial u/\partial t$ = water particle acceleration

δ = boundary layer thickness

δ_θ = momentum thickness

δ^* = displacement thickness

Δp = pressure difference

ΔR = residue

Δt = time step - interval

ε = root mean squared error

η = instantaneous level of the water surface

θ = angle (= $2\pi t/T$)

θ_N = angle of pressure probes for increment N

ν = kinematic viscosity

ρ = density of water

ϕ = velocity potential

$\emptyset$ = diameter

$\emptyset_{sep}$ = separation angle

ω = angular frequency (= $2\pi/T$)

Ω = orbital shape parameter (= u_v/u_h)

LIST OF FIGURES

LIST OF TABLES

REFERENCES

Achenbach, E. (1968): Distribution of local pressure and skin friction around a circular cylinder in cross-flow up to Re = $5 \cdot 10^6$, J. Fluid Mech., Vol. 34, pp 625-639.

Achenbach, E. (1971): Influence of surface roughness on the cross-flow around a circular cylinder, J. Fluid Mech., Vol. 46, pp 321-335.

Achenbach, E. and Heinecke, E. (1981): On vortex sheddipg from smooth and rough cylinders in the range of Reynolds numbers $6 \cdot 10^3$ to $5 \cdot 10^6$, J. Fluid Mech., Vol. 109, pp 239-251.

Barnouin, B., Mattout, M. and Sagner, M. (1979): Experimental study of the validity domain of some formulae for hydrodynamic forces for regular and irregular flows, in Mech. of Wave Induced Forces on Cylinders, (ed. T.L. Shaw), Pitman, London, pp 393-405.

Basco, D., Svendsen, I. and Christensen, J. (1982): Measurement with a bi-directional micro-propeller current meter, Prog. Rep. No 57, ISVA, Techn. Univ., Denmark, pp 25-32.

Batchelor, G.K. (1970): An introduction to fluid dynamics, Cambridge Univ. Press.

Bearman, P.W. and Graham, J.M.R. (1979): Hydrodynamic forces on cylindrical bodies in oscillatory flow, 2nd Int. Conf. on the Behaviour of Off-Shore Structures, London, pp 309-322.

Bearman, P.W., Graham, J.M.R., Naylor, P. and Obasaju, E.D. (1981): The role of vortices in oscillatory flow about bluff cylinders, Hydrodynamics in Ocean Eng., The Norwegian Institute of Technology, Trondheim, Norway, pp 621-644.

Bearman, P.W. and Morel, T. (1983): Effect of free stream turbulence on the flow around bluff bodies, Prog. Aerospace Sci., Vol. 20, pp 97-123.

Bearman, P.W., Graham, J.M.R. and Obasaju, E.D. (1984): A model equation for the transverse forces on cylinders in oscillatory flows, Applied Ocean Reserach, Vol. 6, No. 3, pp 166-172.

Bearman, P.W. (1985): Vortex trajectories in oscillatory flow, Separated Flow Around Marine Structures, The Norwegian Inst. of Tech., Trondheim, Norway, pp 133-153.

Bearman, P.W., Downie, M.J., Graham, J.M.R. and Obasaju, E.D. (1985): Forces on cylinders in viscous oscillatory flow at low Keulegan-Carpenter numbers, J. Fluid Mech. Vol. 154, pp 337-356.

Bearman, P.W., Chaplin, J.R., Graham, J.M.R., Kostense, J.K., Hall, P.F. and Klopman, G. (1985): The loading on a cylinder in post-critical flow beneath periodic and radom waves, Proc. 4th Int. Conf. on the Behaviour of Off-shore Structures, Delft, pp 213-225.

Bidde, D.D. (1971): Laboratory study of lift forces on circular piles, J. Waterways, Harbors and Coastal Eng. Div., ASCE, Vol. 97, No WW4, pp 595-614.

Bishop, J.R. (1979): R.m.s. force coefficients derived from Christchurch Bay wave force data, NMI Report R62, OT-R-7943.

Bishop, J.R. (1982): Wave force investigations at the second Christchurch, Bay tower, NMI Report No. R177, OT-O-82100.

Bloor, S. (1964): The transition to turbulence in the wake of a circular cylinder, J. FLuid Mech., Vol. 28, pp 290-304.

Borgman, L.E. and Yfantis, E. (1979): Three-dimensional character of waves and forces, Civil Eng. in the Oceans IV, ASCE, pp 791-804.

Bullock, G. and Short, I. (1985): Water particle velocities in regular waves, J. Waterway, Port, Coastal and Ocean Eng., ASCE, Vol. 111, No. 2, pp 189-200.

Cebeci, T. and Bradshaw, P. (1977): Momentum transfer in boundary layers, Hemisphere Publishing Corporation, McGraw-Hill Book Company.

Celik, I. (1980): Mean flow past circular cylinders. Ph.D.thesis, Univ. of Iowa, Iowa City.

Chakrabarti, S.K., Wolbert, A.L. and Tam, W.A. (1976): Wave forces on vertical circular cylinder, J. Waterways, Harbors and Coastal Eng. Div., ASCE, Vol. 102, No WW2, pp 203-221.

Chakrabarti, S.K. (1980a): Inline forces on fixed vertical cylinder in waves, J. Waterway, Port, Coastal and Ocean Div., ASCE, Vol. 106, No WW2, pp 145-155.

Chakrabarti, S.K. (1980b). Laboratory generated waves and wave theories, J. Waterway, Port, Coastal and Ocean Div., ASCE, Vol. 106, No. WW3, pp 349-368.

Chakrabarti, S.K. (1985): Hydrodynamic coefficients and depth parameter, J. Waterway, Port, Coastal and Ocean Eng., Vol. 111, No. 1, pp 123-127.

Chang, P.K. (1970): Separation of flow, Pergamon Press, New York.

Chaplin, J.R. (1985): Morison inertia coefficients in orbital flow, J. Waterway, Port, Coastal and Ocean Engineering, Vol. 111, No. 2, pp 201-215.

Dawson, T.H. (1985): In-line forces on vertical cylinders in deepwater waves, J. Energy Resources Technology, Vol. 107, pp 18-23.

Dean, R.G. (1970): Relative validities of water wave theories, J. Waterways and Harbors Div., ASCE, Vol. 96, No WW1, pp 105-119.

Dean, R.G. (1974): Evaluation and development of water wave theories for engineering application, Vol. I.U.S. Army, Coastal Eng. Res. Center, Spec. Report No. 1, Fort Belvoir, Virginia, pp 121.

Dean, R.G. (1976): Methodology for evaluating suitability of wave and wave force data for determining drag and inertia coefficients, First Int. Conf. on the Behaviour of Off-Shore Structures, Trondheim, pp 40-64.

Dean, R.G., Dalrymple, R.A. and Hudspeth, R.T. (1981): Force coefficients from wave project I and II data including free surface effects, Soc. Pet. Eng. J., Vol. 21, No 6, pp 779-786.

Dean, R.G. and Dalrymple, R.A. (1984): Water wave mechanics for engineers and scientists, Prentice-Hall, Inc., Englewood Cliffs, New Jersey.

Dean, R.G., Törum, A. and Kjeldsen, S.P. (1985): Wave forces on a pile in the surface zone from the wave crest to the wave trough, Separated Flow Around Marine Structures, The Norwegian Inst. of Tech., Trondheim, Norway, pp 75-89.

DnV - Det Norske Veritas (1981): Rules for classification of mobile offshore units, Norway.

Ellix, D.M. (1984): Second order wave loading on vertical cylinders, Ph.D.thesis. City Univ. London.

Evans, D.J. (1969): Analysis of wave force data, OTC Paper NO 1005, Houston.

Farell, C. (1983): Flow around fixed circular cylinders: Fluctuating loads, J. Eng. Mech. Div., ASCE, Vol. 109, No. 4. pp 1153-1156

Fenton, J.D. (1979): A high-order cnoidal wave theory, J.Fluid Mech., Vol. 94, pp 129-161.

Garrison, C.J., Field, J.B. and May, M.D. (1977): Drag and inertia forces on a cylinder in periodic flow, J. Waterway, Port, Coastal and Ocean Division, ASCE, Vol. 103, No WW2, pp 193-203.

Gaster, M. (1969): Vortex shedding from slender cones at low Reynolds numbers, J. Fluid Mech. Vol. 38, pp 565-576.

Gaston, J.D. and Ohmart, R.D. (1979): Effect of surface roughness on drag coefficients, Civil Eng. in the Oceans IV, ASCE, pp 611-621.

Goda, Y. (1964): Wave forces on a vertical circular cylinder, Port and Harbour Technical Research Institute Ministry of Transportation, Rep. 8, pp 1-74.

Grass, A.J. and Kemp, P.H. (1979): Flow visualisation studies of oscillatory flow past smooth and rough circular cylinders, in Mech. of Wave Induced Forces on Cylinders, (ed. T.L. Shaw), Pitman, London, pp 406-420.

Heideman, J.C., Olsen, O.A. and Johansson, P.I. (1979): Local wave force coefficients, Civil Eng. in Oceans IV, ASCE, pp 684-699.

Hogben, N. (1979): The behaviour of stationary objects - theory and experiments, Int. Symp. on Advances in Marine Tech., The Norwegian Inst. of Tech., Trondheim, Norway, pp 305-333.

Honji, H. (1981): Streaked flow around an oscillating circular cylinder, J. Fluid Mech. Vol. 107, pp 509-520.

Horton, T.E. and Rish, J.W. (1981): A study advancing wave-foce methodology - a one-dimensional formulation of the inertial pressure concept, Hydrodynamics in Ocean Eng., The Norwegian Institute of Technology, Trondheim, Norway, pp 585-600.

Isaacson, M. de St. Q. and Maull, D. (1976): Transverse forces on vertical cylinders in waves, J. Waterways, Harbors and Coastal Eng. Div., ASCE, Vol. 102, No. WW1, pp 49-60.

Isaacson, M. de St.Q. (1978): Mass transport in shallow water waves, J. waterway, Port, Coastal and Ocean Div., ASCE, Vol. 104, No. WW2, pp 215-225.

Isaacson, M. de St. Q. (1979): Nonlinear inertia forces on bodies, J. Waterway, Port, Coastal and Ocean Div., ASCE, Vol. 105, No. WW3, pp 213-227.

Isobe, M. (1985): Calculation and application of first-order cnoidal wave theory, Coastal Eng., No. 9, pp 309-325.

ISVA - Institute of hydrodynamics and hydraulic engineering (1974): Sinusoidal and cnoidal gravity waves formulae and tables, Techn. Univ. of Denmark.

Iwagaki, Y. and Sakai, T. (1969): Horizontal water particle velocity of finite amplitude waves, Proc. 12th Coastal Eng. Conf., Washington DC, pp 309-325.

Kayo, Y. and Takekuma, K. (1981): On the free-surface shear flow related to bow wave-breaking of full ship models, J. Soc. of Naval Arch. of Japan, Vol. 149, pp 11-20.

Keulegan, G.H. and Carpenter, L.H. (1958): Forces on cylinders and plates in an oscillating fluid, J. Resurge of the National Bureau of Standards, Vol. 60, No 5, pp 423-440.

Kim, Y.Y. and Hibbard, H.C. (1975): Analysis of simultaneous wave force on water particle velocity measurements, OTC Paper No. 2192, Houston.

Le Mêhautê, B., Divoky, D. and Lin, A. (1968): Shallow water waves - A comparison of theories and experiments, Proc. 11th Coastal Eng. Conf., London, pp 86-107.

Le Mêhautê, B. (1976): An introduction to hydrodynamics and water waves, Springer-Verlag, Düsseldorf.

Lienhard, J.H. (1966): Synopsis of lift, drag and vortex frequency data for rigid circular cylinders, Washington State Univ., College of Eng., Res. Div., Bulletin 300.

MacCamy, R.C. and Fuchs, R.A. (1954): Wave forces on piles - diffraction theory, U.S. Army Corps of Eng., Beach Erosion Board, Tec. Memo. No. 69.

Maull, D.J. and Milliner, M.G. (1978): Sinusoidal flow past a circular cylinder, Coastal Eng., Vol. 2, pp 149-168.

Moberg, G., Bergdahl, L. and Carlsson, B. (1986): Use of correct or nominal water velocities and accelerations in Morison's equation, Int. Conf. on Measuring Techniques of Hydraulics Phenomena in Offshore, Coastal and Inland Waters. London, pp 85-105.

Morison, J.R., O'Brien, M.P., Johnson, J.W. and Schaaff, S.A. (1950): The force exerted by surface waves on piles, Petroleum Trans. Vol. 189, pp 149-154.

Mori, K.H. (1984): Necklace vortex and bow wave around blunt bodies, 15th Sym. Naval Hydrodynamics, Hamburg, pp 303-317.

Nilsson, K. and Nilsson, A. (1985): An experimental and theoretical study of the velocity distribution around a vertical cylinder, MSc Thesis, Rep. 1985:7, In Swedish, Dept. of hydraulics, Chalmers Univ. of Tech., Göteborg, Sweden.

Norberg, C. (1987): Reynolds number and freestream turbulence effects on a flow and fluid forces for a circular cylinder in cross flow, Ph.D. thesis, Chalmers Univ. of Tech., Göteborg.

Ohmart, R.D. and Gratz, R.L. (1979): Drag coefficient from hurricane wave data, Civil Eng. in the Oceans IV, ASCE, pp 260-272.

Olson, R.M. (1980): Essentials of engineering fluid mechanics, Fourth Edition, Harper and Row, Publisher, New York.

Pearcey, H.H. and Bishop, J.R. (1979): Wave loading in the drag and inertia regims - routes to design data, Proc. 2nd Int. Conf. on the Behaviour of Off-Shore Structures, London, pp 631-660.

Pedersen, F.B. (1969): Turbulence measurements by use of micro-propellers, Coastal Eng. Lab./Hydraulics Lab., Prog. Rep. No 18, Tech. Univ. Denmark, pp 11-17.

Ramberg, S.E. and Niedzwecki, J.M. (1979): Some uncertainties and errors in wave force computations, OTC, Paper No. 3597, Houston.

Rodenbusch, G. and Källström, C. (1986): Forces on a large cylinder in random two-dimensional flows, OTC Paper No 5096, Houston.

Sarpkaya, T. (1976a): Vortex shedding and resistence in harmonic flow about smooth and rough circular cylinders at high Reynolds numbers. Rep. No. NPS-59SL76021, Naval Postgraduate School, Monterey, California, pp 183.

Sarpkaya, T. (1976b): In-line and transverse forces on smooth and sand-roughened cylinders in oscillatory flow at high Reynolds numbers, Rep. No NPS-69SL76062, Naval Postgraduate School, Monterey, California, 70 pp.

Sarpkaya, T. (1981a): A critical assessment of Morison's equation, Hydrodynamics in Ocean Eng., The Norwegian Institute of Technology, Trondheim, Norway, pp 447-468.

Sarpkaya, T. (1981b): Morison's equation and the wave forces on offshore structures, Naval Civil Eng. Lab. Report No. CR82008, Port Huenema, California, pp 251.

Sarpkaya, T. and Isaacson, M. (1981): Mechanics of wave forces on offshore structures, Van Nostrand Reinhold, New York.

Sarpkaya, T. (1984): Discussion of Quasi-2-D forces on a vertical cylinder in waves, J. Waterway, Port, Coastal and Ocean Eng., Vol. 110, No. 1, pp 120-123.

Sarpkaya, T. (1985): Past progress and outstanding problems in time-dependent flows about ocean structures, Separated Flow Around Marine Structures, The Norwegian Inst. of Tech., Trondheim, Norway, pp 1-36.

Sarpkaya, T. and Storm, M. (1985): In-line force on a cylinder translating in oscillatory flow, Applied Ocean Research. Vol. 7, No. 4, pp 188-196.

Sarpkaya, T. (1986): Forces on a circular cylinder in viscous oscillatory flow at low Keulegan-Carpenter numbers, J. Fluid Mech., Vol. 165, pp 61-77.

Sawaragi, T., Nakamura, T. and Kita, H. (1976): Characteristics of lift forces on a circular pile in waves, Coastal Eng. in Japan, Vol. 19, pp 59-71.

Schewe, G. (1986): Sensitivity of transition phenomena to small perturbations in flow round a circular cylinder, J. Fluid Mech., Vol. 172, pp 33-46.

Schlichting, H. (1968): Boundary-layer theory, McGraw-Hill Book Co., New York.

Silvester, R. (1974): Coastal engineering, 1, Elsevier Scientific Publishing Company, New York.

Skjelbreia, L. (1959): Gravity waves - Stokes third order approximation - tables of functions, The Eng. Foundation Council on Wave Res., Berkeley, California, pp 337.

Skjelbreia, L. and Hendrickson, J. (1960): Fifth order gravity wave theory, Proc. 7th coastal Eng. Conf., The Hague, pp 184-194.

Stansby, P.K., Bullock, G.N. and Short, I. (1983): Quasi-2-D forces on a vertical cylinder in waves, J. Waterway, Port, Coastal and Ocean Eng., Vol. 109, No. 1, pp 128-132.

Svendsen, I.A. (1974): Cnoidal waves over a gently sloping bottom, Series Paper NO. 6, Inst. of Hydrodyn. and Hydraul. Eng., Tech. Univ. of denmark, 181 pp.

Takekuma, K. and Eggers, K. (1984): Effect of bow shape on free-surface shear flow, 15th sym. Naval Hydrodynamics, Hamburg, pp 387-405.

Taneda, S. (1980): Definition of separation, Rep. Res. Inst. Appl. Mech., Vol. 28, No 89, pp 73-81.

Törum, A. (1985): Wave forces on a pile in the surface zone. Regular, non-breaking waves. Progress report No. 2, Report No. 1.9, MARINTEKNIK, Norway, 93 pp.

Verley, R.L.P. (1982): A simple model of vortex-induced forces in waves and oscillating currents, Applied Ocean Research, Vol. 4, No. 2, pp 117-120.

Wiegel, R.L., Beebe, K.E. and Moon, J. (1957): Ocean wave forces on circular cylindrical piles, J. Hydraulics Div., ASCE, Vol. 83, No. HY2, pp 1199.1 - 1199.36.

Wiegel, R.L. (1964): Oceanographical Engineering, Prentice-Hall, Englewood Cliffs, N.J.

Williamson, C.H.K. (1985): Sinusoidal flow relative to circular cylinders, J. Fluid Mech., Vol. 155, pp 141-174.

Wiuff, R. (1977): Experiments on the surface buoyant jet, Series Paper No. 16, ISVA, Techn. Univ., Denmark, 168 pp.

APPENDIX 1 FIGURES AND TABLES

Examples of some data measured and calculated using the wave train averaging technique.

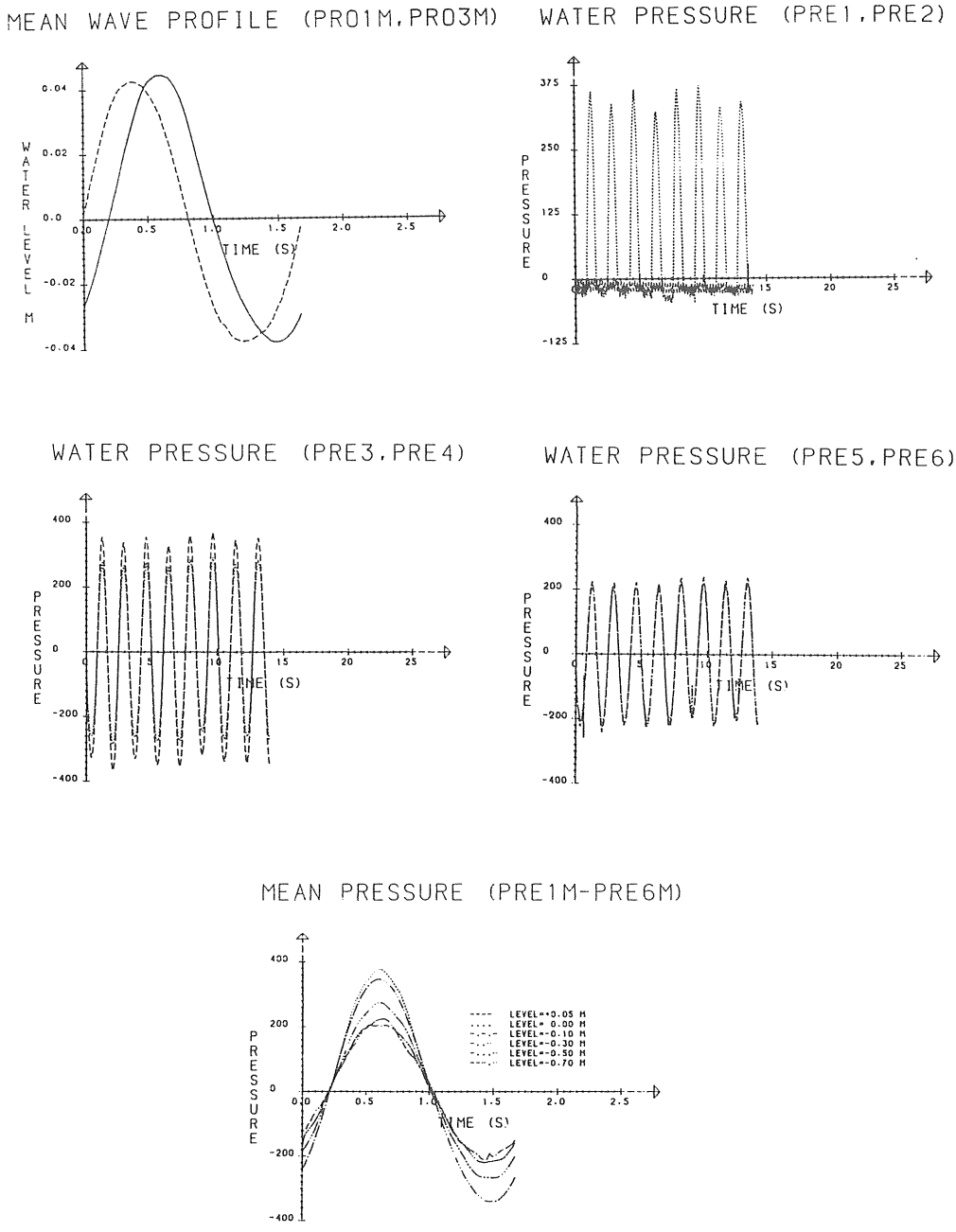

Figure A1.1 a Wave A_6 "Deep water". Water level, pressure (N/m^2) as functions of time at 180^0 on the cylinder according to Figs. 3.3, 3.6, 6.3.

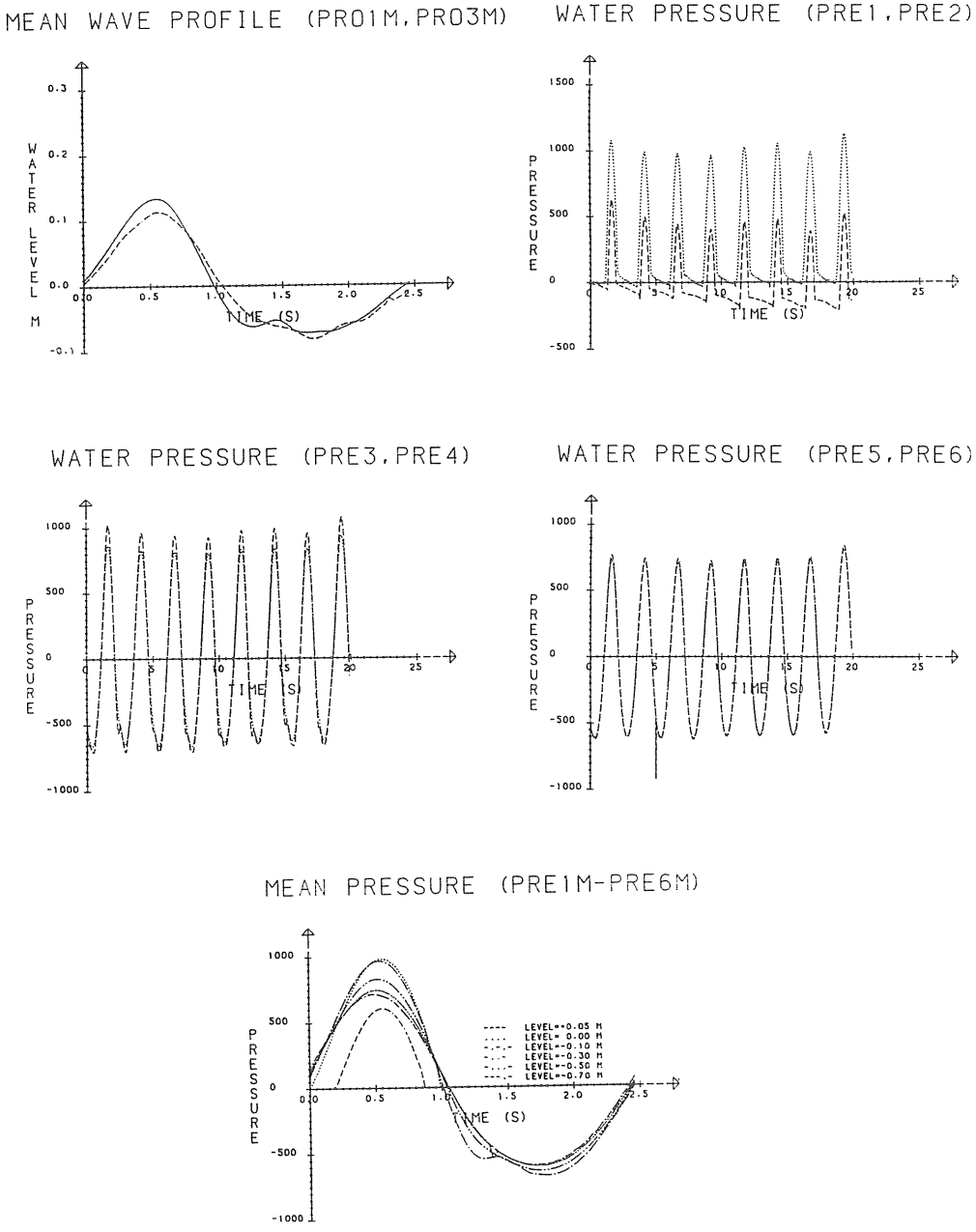

Figure A1.1 b Wave B. "Transitional water depth". Water level, pressure (N/m^2) as functions of time at 0^o on the cylinder according to Figs. 3.3, 3,6, 6.3.

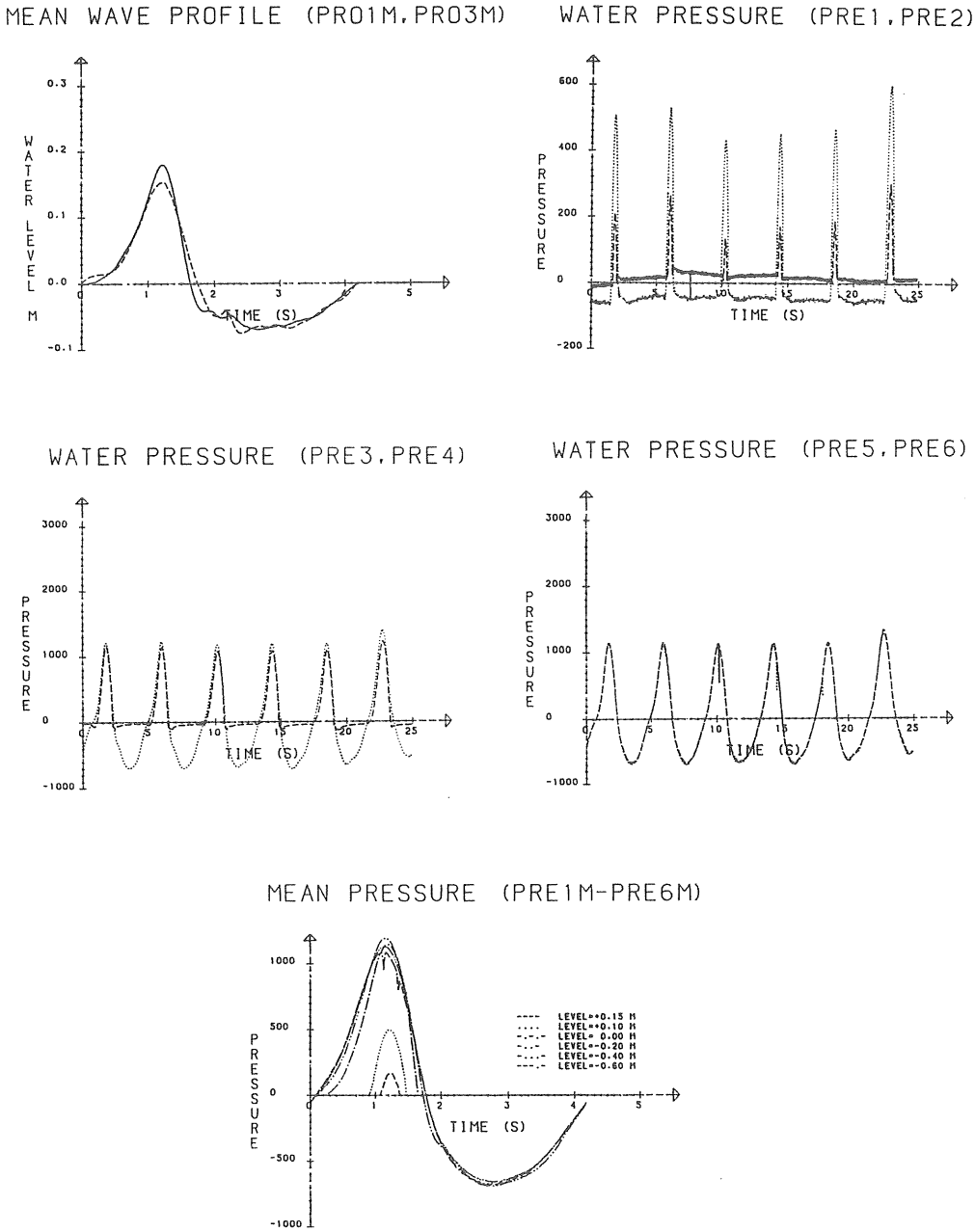

Figure A1.1 c Wave C. "Shallow water". Water level, pressure (N/m^2) as functions of time at 22.5^o on the cylinder according to Figs. 3.3, 3.6, 6.3.

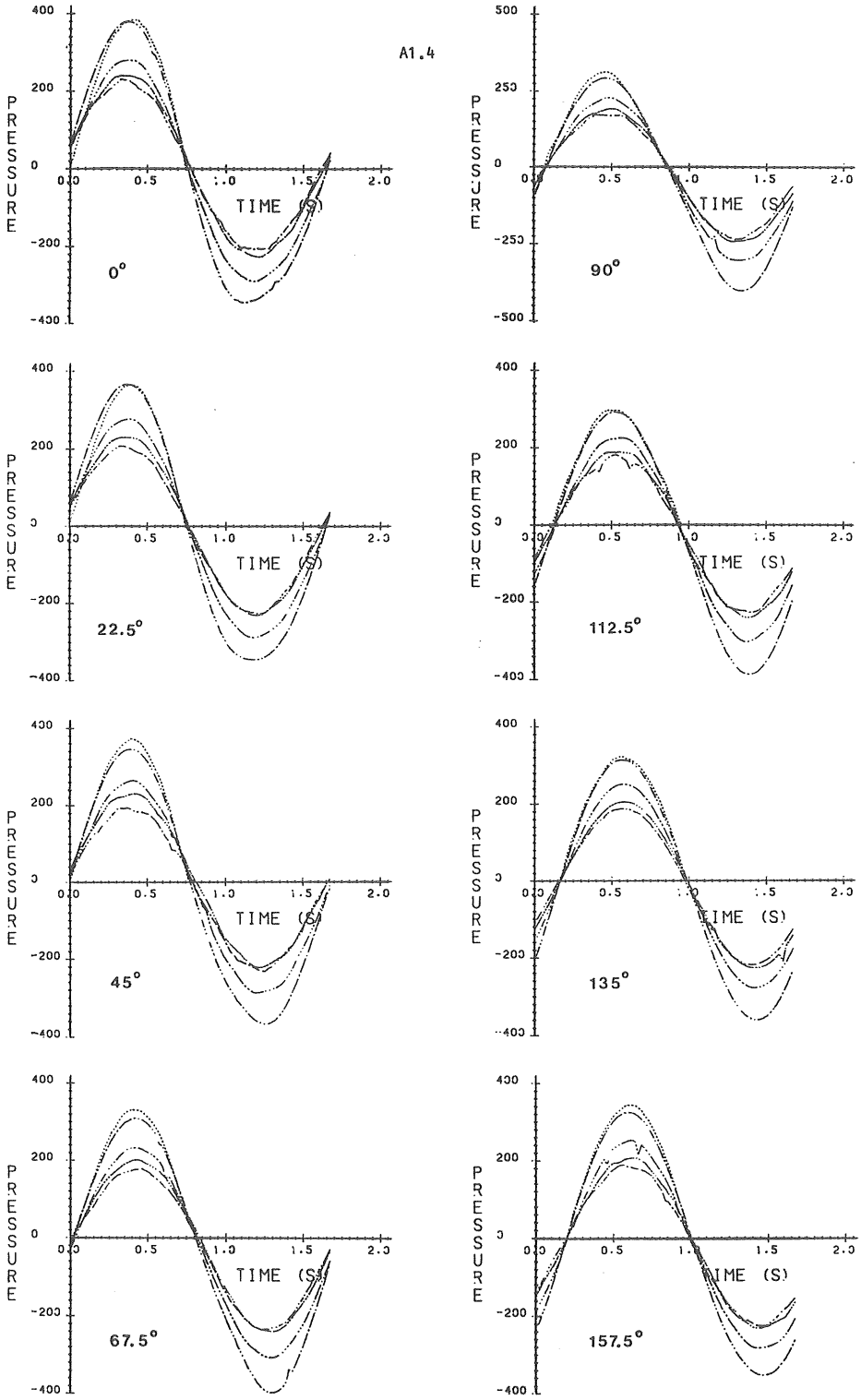

a-h Measured pressure (N/m^2) as functions of time.

.... LEVEL= 0.00 M
-.-.- LEVEL=-0.10 M
-..- LEVEL=-0.30 M
-...- LEVEL=-0.50 M
---.- LEVEL=-0.70 M

continued

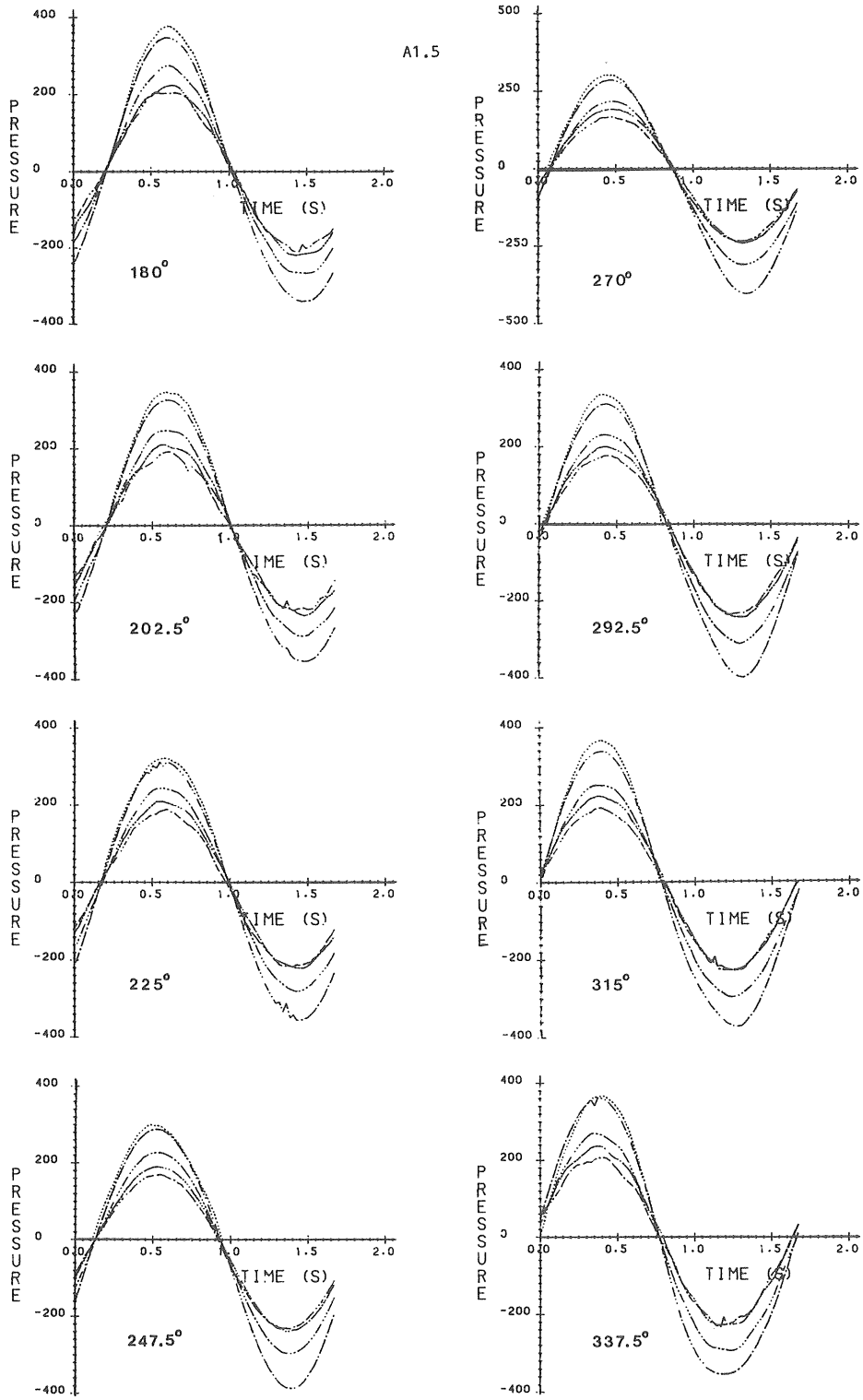

i-p Measured pressure (N/m^2) as functions of time.

Figure A1.2 a-p Wave A. "Deep water".

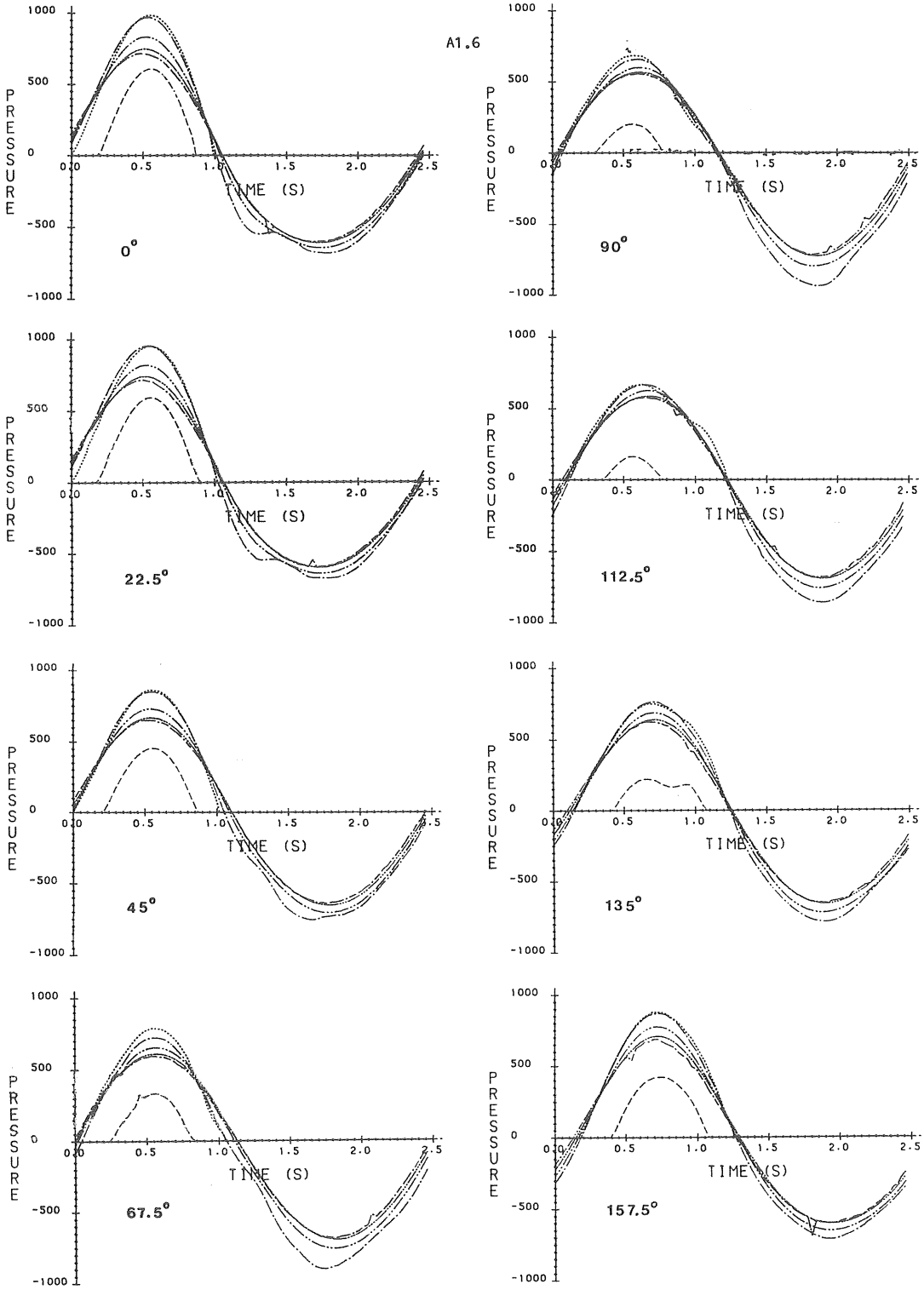

a-h Measured pressure (N/m^2) as functions of time.

continued

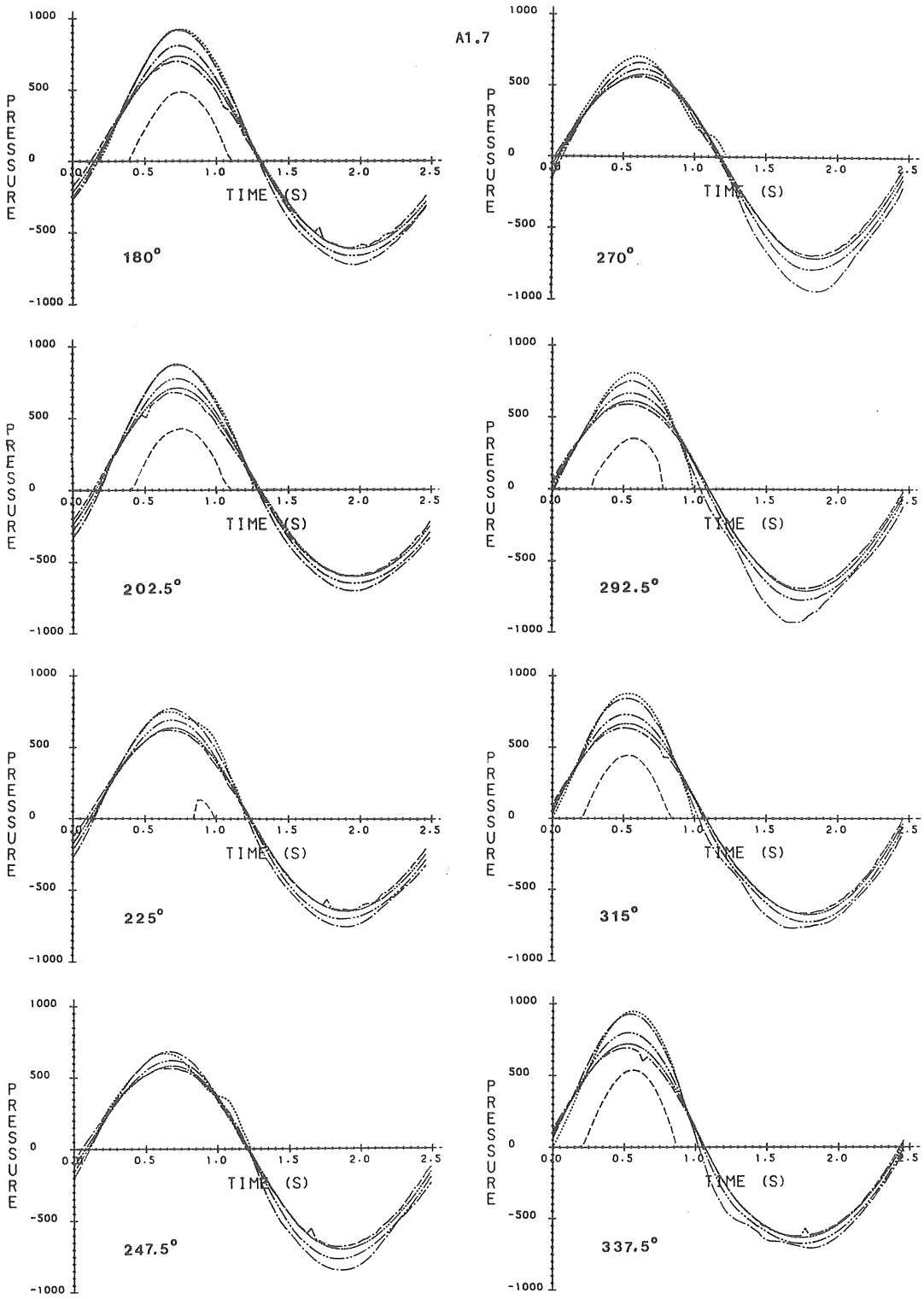

i-p Measured pressure (N/m^2) as function of time.

Figure A1.3 a-p Wave B. "Transition water depth".

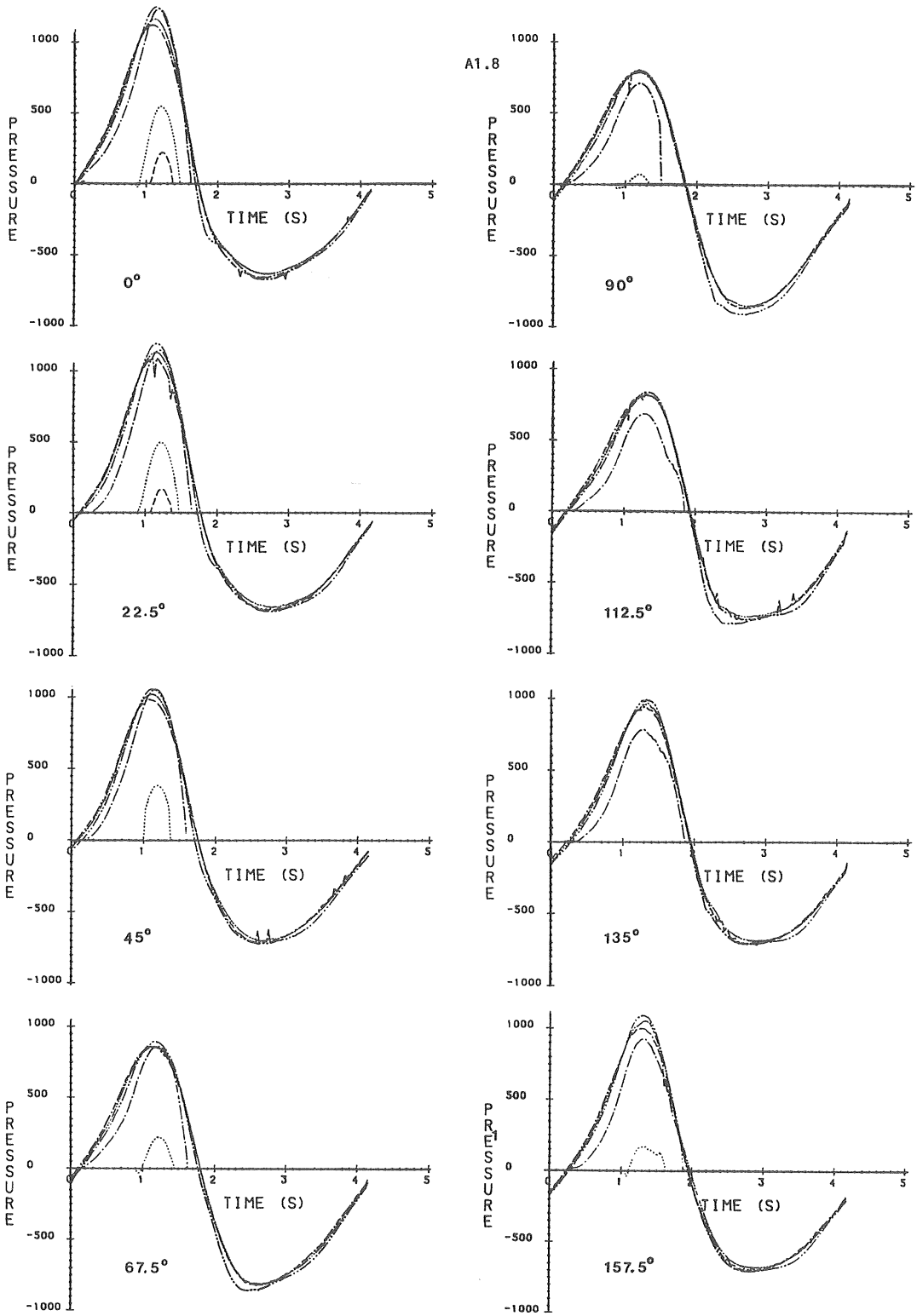

a-h Measured pressure (N/m^2) as function of time.

---- LEVEL=+0.15 M
.... LEVEL=+0.10 M
-.-.- LEVEL= 0.00 M
-..- LEVEL=-0.20 M
-...- LEVEL=-0.40 M
---.- LEVEL=-0.60 M

continued

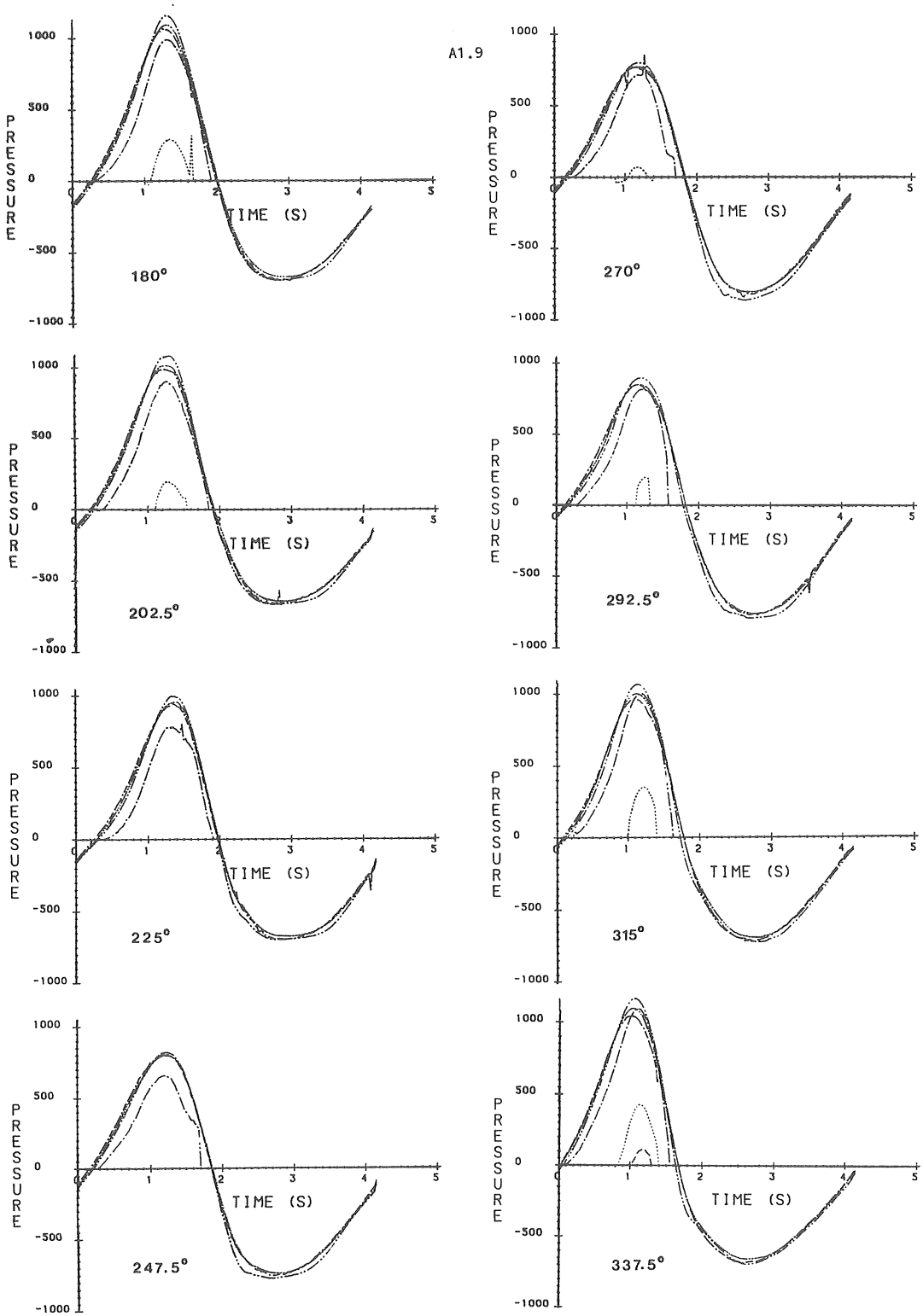

i-p Measured pressure (N/m^2) as function of time.

Figure A1.4 a-p Wave C. "Shallow water".

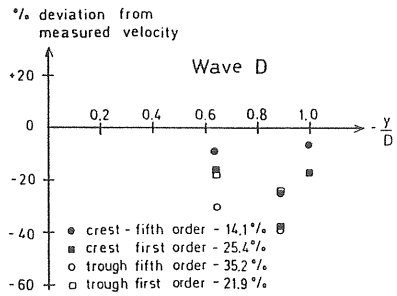

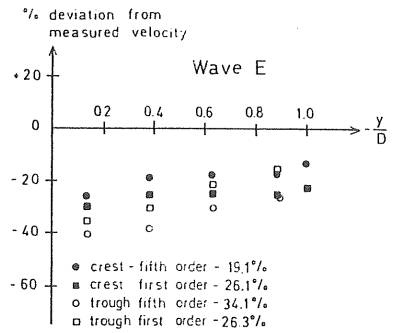

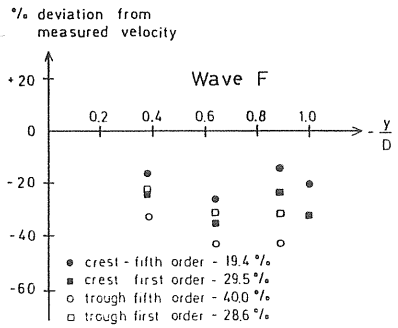

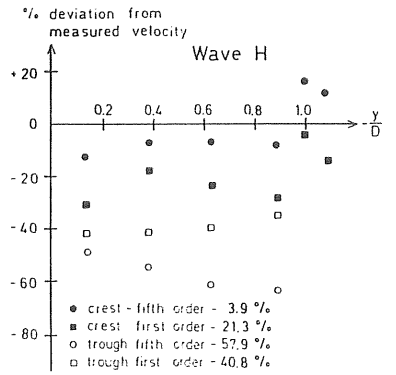

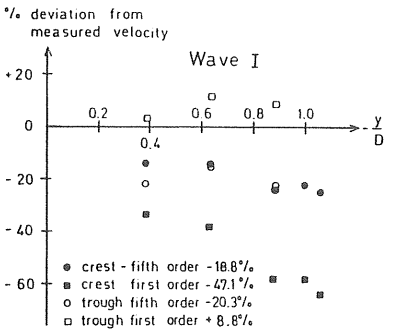

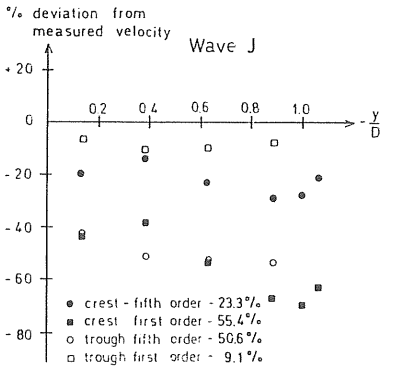

a-f

continued

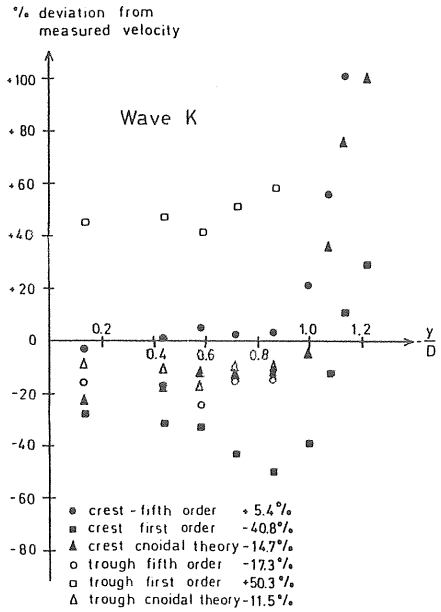

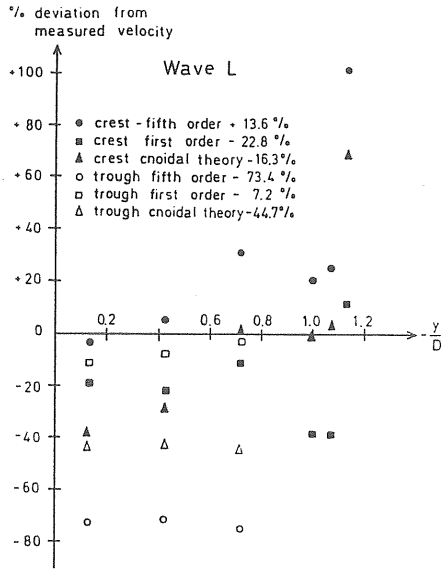

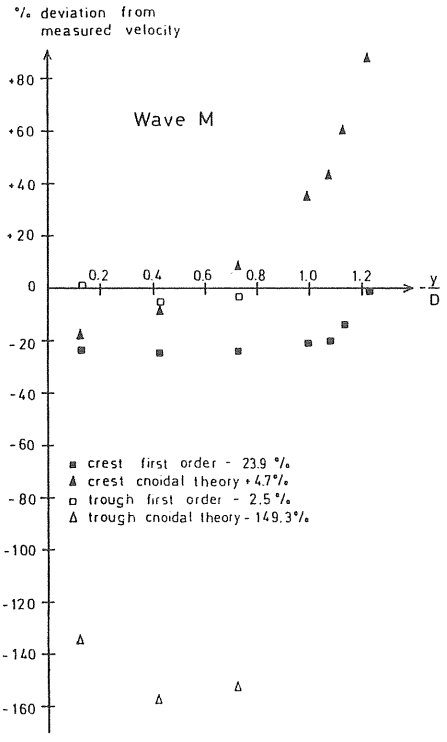

g-i

Figure A1.5 a-i Deviation for first, fifth order and cnoidal theories when compared with measured maximum horizontal velocities.

WAVE FORCE-MEASURED

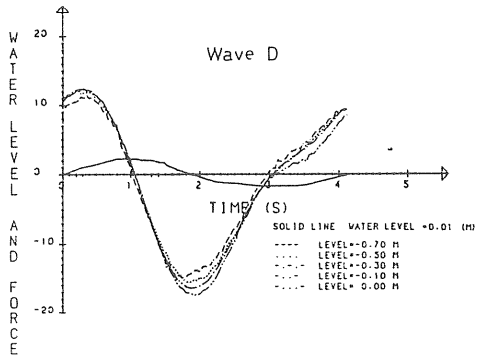

WAVE FORCE-MEASURED

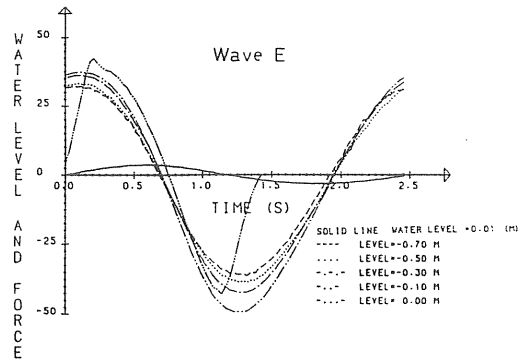

a-b Wave D, E

WAVE FORCE-MEASURED

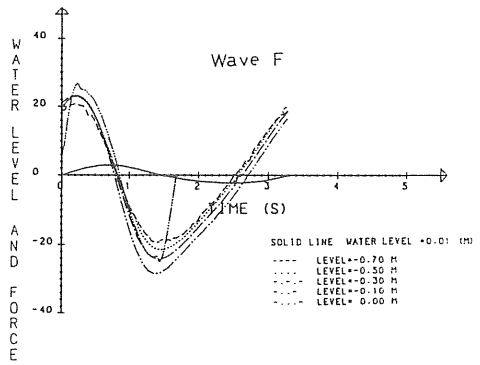

WAVE FORCE-MEASURED

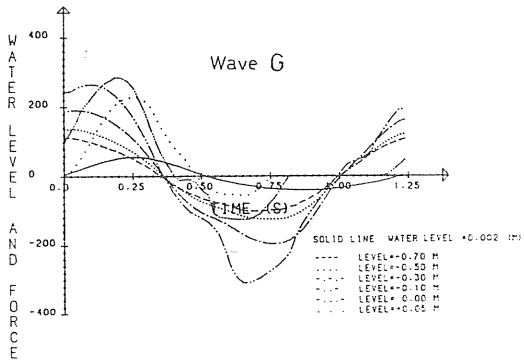

c-d Wave F, G

WAVE FORCE-MEASURED

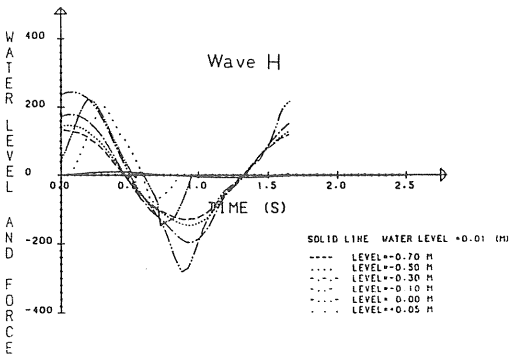

WAVE FORCE-MEASURED

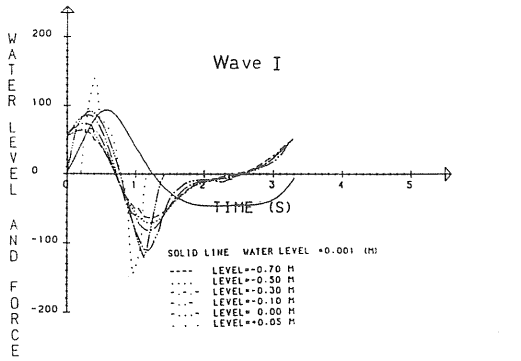

e-f Wave H, I

continued

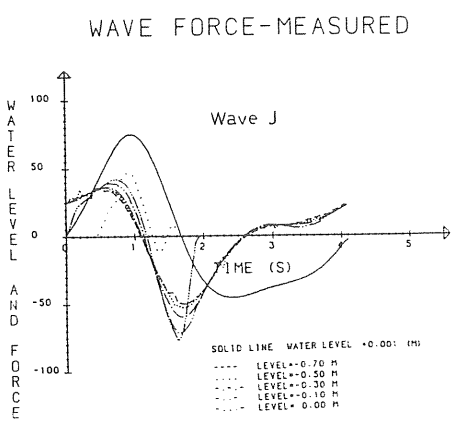

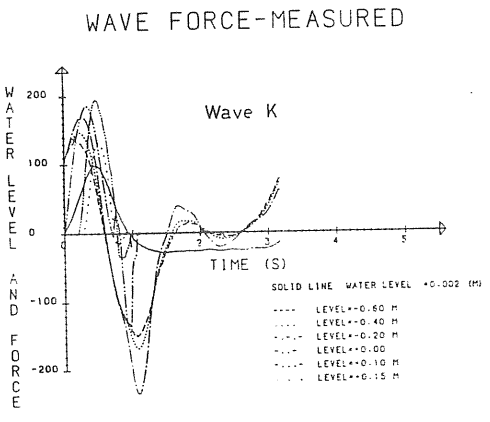

g-h Wave J,K

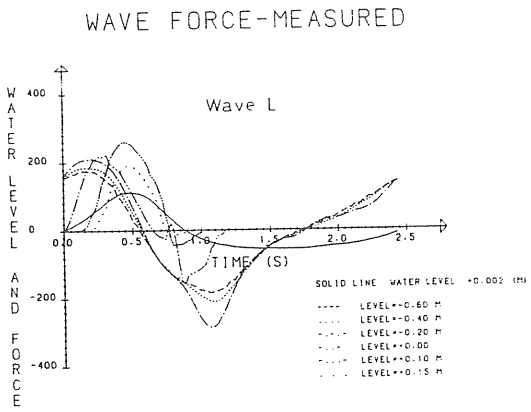

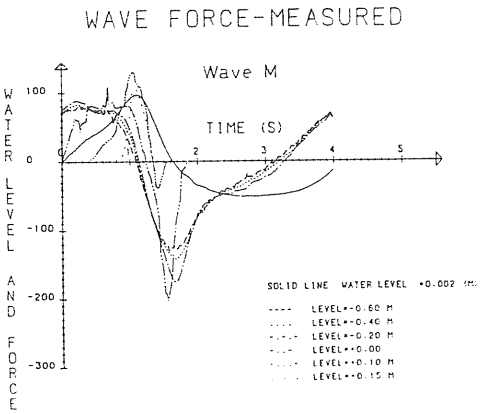

i-j Wave L, M

Figure A1.6 a-j Force per unit length at the different levels of measurements (N/m).

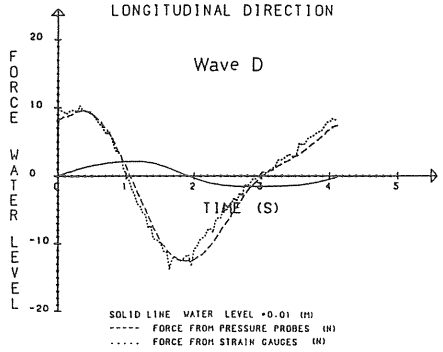

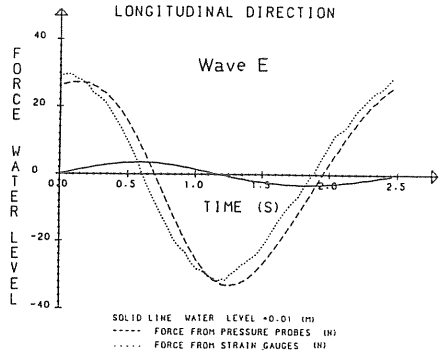

a-b Wave D, E

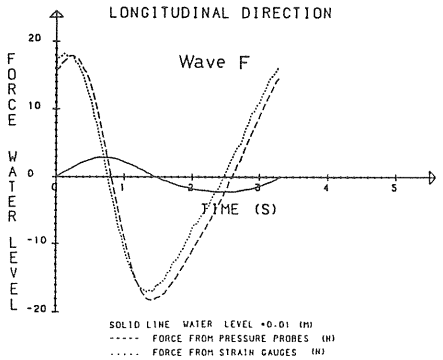

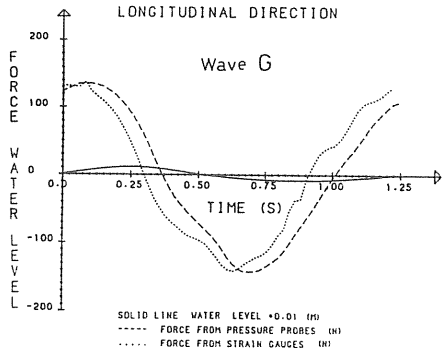

c-d Wave F-G

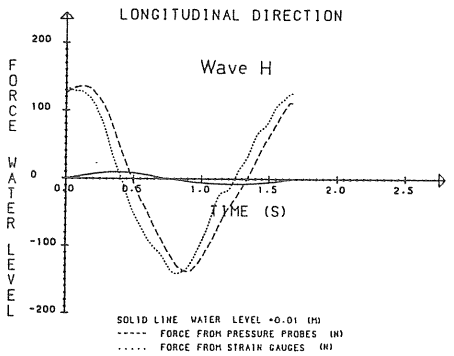

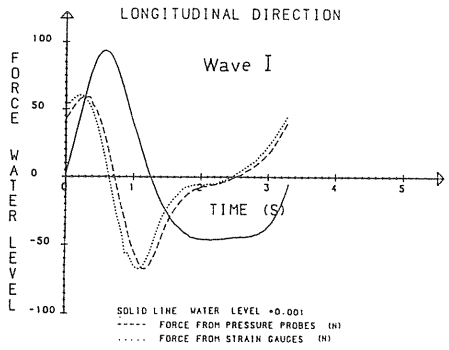

e-f Wave H, I

continued

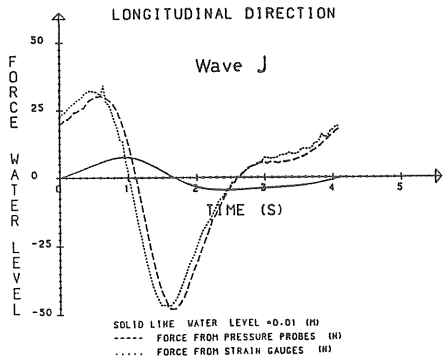

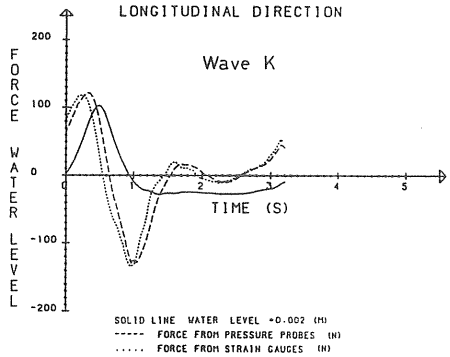

g-h Wave J, K

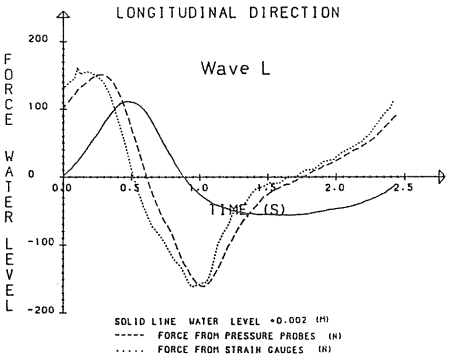

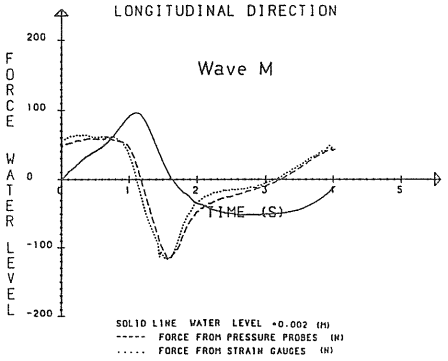

i-j Wave L, M

Figure A1.7 a-j Comparison between measured force and integrated pressure.

Table A1.1 a Time invariant force coefficients at; 0.1 m below S.W.L. for wave A and B,
0.2 m below S.W.L. for wave C.
Drag coefficients given by wave A are not further used. Measured velocity.

Wave	Level - 0.10 m (-0.20 m)				Force coefficients according to methods of																	
					Least squares												Max.vel. and acc.		Zero and max force	
	Ω crest/trough	Re x 10^5 crest/trough	KC crest/trough	β x 10^3		whole period	ε %	crest	ε %	trough	ε %	crest 60°	ε %	trough 60°	ε %	π 60°	ε %	crest	trough	crest	trough
A	0.81/0.80	0.48/0.50	0.92/0.95	52.4	C_D	(3.69	8	3.17	4	4.15	11	3.36	1	3.49	3	3.2	2	3.34	3.14	3.3	4.03)
					C_M	1.85		1.86		1.85		1.82		1.54		2.1		1.85	2.20	1.77	2.21
B	0.69/0.57	1.39/1.15	3.94/3.26	35.2	C_D	1.33	12	1.45	11	1.19	12	1.26	3	1.10	14	0.48	8	1.36	1.60	2.01	2.99
					C_M	1.40		1.26		1.59		0.98		1.98		1.82		1.32	1.96	1.30	1.99
C	0.42/0.26	1.82/1.24	8.57/5.84	21.2	C_D	1.07	17	1.33	13	0.51	16	1.35	5	0.32	6	2.91	19	1.38	0.25	1.34	4.58
					C_M	1.16		0.88		1.61		0.63		0.85		1.59		0.66	1.42	0.61	2.32

Table A1.1 b Time invariant force coefficients at; 0.3 m below S.W.L. for wave A and B
0.4 m - " - for wave C.
Drag coefficients given by wave A are not further used. Measured velocity.

Wave	Level - 0.30 m (-0.40 m)				Force coefficients according to methods of																	
					Least squares												Max.vel. and acc.		Zero and max force	
	Ω crest/trough	Re x 10^5 crest/trough	KC crest/trough	β x 10^3		whole period	ε %	crest	ε %	trough	ε %	crest 60°	ε %	trough 60°	ε %	π 60°	ε %	crest	trough	crest	trough
A	0.68/0.65	0.39/0.39	0.74/0.75	52.4	C_D	(3.28	11	1.71	3	4.56	14	1.55	1	3.11	6	11.1	1	1.31	2.33	1.29	1.26)
					C_M	1.73		1.78		1.69		1.74		1.64		1.98		1.81	1.99	1.82	2.03
B	0.48/0.43	1.19/1.08	3.38/3.05	35.2	C_D	1.12	10	1.33	9	0.93	10	1.20	2	0.75	2	-0.4	3	1.39	0.82	1.74	2.18
					C_M	1.38		1.33		1.45		1.09		1.53		1.68		1.28	1.73	1.32	1.73
C	0.28/0.17	1.63/1.11	7.70/5.24	21.2	C_D	1.06	10	1.21	9	0.73	7	1.24	5	0.74	3	2.52	5	1.29	0.84	1.23	2.00
					C_M	1.29		1.09		1.58		1.01		1.91		1.45		0.93	1.40	0.95	1.54

Table A1.1 c Time invariant force coefficients at; 0.5 m below S.W.L. for wave A and B
0.6 m - " - for wave C.
Drag coefficients given by wave A are not further used. Measured velocity.

Wave	Level - 0.50 m (-0.60 m) Ω crest/trough	Re x 10^5 crest/trough	KC crest/trough	β x 10^3	Force coefficients according to methods of: Least squares												Max.vel. and acc.		Zero and max force	
						whole period	ε %	crest	ε %	trough	ε %	crest 60^δ	ε %	trough 60^δ	ε %	π 60^o	ε %	crest	trough	crest	trough
A	0.47/0.43	0.32/0.36	0.62/0.69	52.4	C_D	(5.24	8	5.89	7	4.92	9	4.98	4	4.08	1	15.1	3	3.78	3.96	5.20	4.75)
					C_M	1.60		1.67		1.54		1.50		1.89		1.55		1.85	1.57	1.86	1.67
B	0.32/0.25	1.07/0.98	3.04/2.78	35.2	C_D	1.29	6	1.15	5	1.40	5	0.96	2	1.26	4	1.53	2	1.20	1.51	1.45	1.69
					C_M	1.39		1.31		1.47		1.19		1.62		1.52		1.31	1.55	1.33	1.57
C	0.13/0.05	1.63/1.12	7.70/5.22	21.2	C_D	0.60	12	0.66	8	0.48	14	0.69	5	0.55	4	1.23	1	0.67	0.57	0.71	0.97
					C_M	1.25		1.24		1.26		1.16		1.64		1.42		1.03	1.44	1.06	1.43

Table A1.1 d Time invariant force coefficients at; 0.7 m below S.W.L. for wave A and B.
Drag coefficients given by wave A are not further used. Measured velocity.

Wave	Level - 0.70 m Ω crest/trough	Re x 10^5 crest/trough	KC crest/trough	β x 10^3	Force coefficients according to methods of: Least squares												Max.vel. and acc.		Zero and max force	
						whole period	ε %	crest	ε %	trough	ε %	crest 60^δ	ε %	trough 60^δ	ε %	π 60^o	ε %	crest	trough	crest	trough
A	0.19/0.13	0.31/0.36	0.60/0.69	52.4	C_D	(1.78	8	0.69	2	2.36	10	0.47	3	1.68	4	2.29	1	0.44	1.17	0.29	0.24)
					C_M	1.49		1.60		1.42		1.68		1.46		1.61		1.57	1.63	1.54	1.66
B	0.14/0.07	1.02/0.99	2.91/2.80	35.2	C_D	0.79	7	0.69	6	0.87	8	0.54	3	0.68	3	-0.6	2	0.83	0.75	0.83	0.86
					C_M	1.35		1.35		1.34		1.30		1.65		1.42		1.25	1.42	1.31	1.42

Table A1.1 e Time invariant force coefficients at the S.W.L. for wave A,B and C.
Drag coefficients given by wave A are not further used. Measured velocity.

Level ±0.00						Force coefficients according to methods of															
						Least squares												Max.vel. and acc.		Zero and max force	
Wave	Ω crest/trough	Re x 10^5 crest/trough	KC crest/trough	β x 10^3		whole period	ε %	crest	ε %	trough	ε %	crest 60^o	ε %	trough 60^o	ε %	π 60^o	ε %	crest	trough	crest	trough
A	0.86	0.54	1.03	52.4	C_D	-		(6.3	21	-		5.36	6	-		-		4.46		7.62)	
					C_M	-		1.49		-		1.21		-		-		1.54		1.88	
B	0.67	1.49	4.23	35.2	C_D	-		1.33	19	-		1.22	2	-		-		1.37		1.80	
					C_M			1.02		-		0.73						1.00		0.94	
C	0.55	1.90	8.96	21.2	C_D	-		1.68	27	-		1.66	4	-		-		1.61		1.65	
					C_M	-		0.96		-		0.56		-		-		1.05		0.54	

Table A1.2 a Time invariant force coefficients at; 0.1 m below S.W.L. for wave A and B.
- " - ; 0.2 m - " - C (fifth order theory).

Wave	Ω crest/trough	Re x 10^5 crest/trough	KC crest/trough	β x 10^3	Level -0.10 (-0.20)	Force coefficients according to methods of: Least squares whole period	ε %	crest	ε %	trough	ε %	crest 60°	ε %	trough 60°	ε %	π 60°	ε %	Max.vel. and acc. crest	trough	Zero and max force crest	trough
A	0.81/0.80	0.50/0.42	0.9/0.8	52.4	C_D	8.94	9	8.38	7	9.90	7	7.77	3	8.67	3	23.9	6	7.4	8.12	9.74	11.86
					C_M	1.85		1.70		2.03		1.55		2.09		1.96		1.85	1.88	1.87	2.29
B	0.69/0.57	1.24/0.77	3.5/2.2	35.2	C_D	2.04	15	2.11	9	1.74	12	1.88	2	0.78	9	5.4	10	2.00	0.53	2.49	4.89
					C_M	1.78		1.50		2.31		1.26		3.03		2.2		1.55	2.16	1.42	2.89
C	0.42/0.26	1.84/0.68	8.7/3.2	21.2	C_D	0.72	22	0.91	40	-1.9	8	0.99	10	0.05	20	1.97	26	1.04	0.45	1.01	4.56
					C_M	1.24		1.23		1.40		0.79		0.81		1.74		0.76	1.60	0.71	3.62

Table A1.2 b Time invariant force coefficients at; 0.3 m below S.W.L. for wave A and B.
- " - ; 0.4 m - " - C (fifth order theory).

Wave	Ω crest/trough	Re x 10^5 crest/trough	KC crest/trough	β x 10^3	Level -0.30 (-0.40)	Force coefficients according to methods of: Least squares whole period	ε %	crest	ε %	trough	ε %	crest 60°	ε %	trough 60°	ε %	π 60°	ε %	Max.vel. and acc. crest	trough	Zero and max force crest	trough
A	0.68/0.65	0.38/0.34	0.7/0.6	52.4	C_D	11.26	7	10.2	5	12.9	7	9.47	2	11.4	3	29.8	5	9.00	11.08	10.65	11.86
					C_M	1.83		1.73		1.95		1.64		2.02		1.90		1.80	1.87	1.89	2.14
B	0.48/0.43	1.06/0.73	3.0/2.1	35.2	C_D	2.04	12	2.13	7	1.77	10	1.83	1	0.87	3	4.71	7	2.03	1.00	2.34	3.48
					C_M	1.78		1.59		2.12		1.42		2.07		2.00		1.65	1.98	1.57	2.48
C	0.28/0.17	1.64/0.67	7.7/3.2	21.2	C_D	0.67	21	0.91	42	-1.8	9	1.00	8	-0.36	10	2.06	19	1.07	0.09	1.04	3.33
					C_M	1.39		1.37		1.55		0.98		1.43		1.87		0.93	1.64	0.89	2.86

Table A1.2 c Time invariant force coefficients at; 0.5 m below S.W.L. for wave A and B.
- " - ; 0.6 m - " - C (fifth order theory).

Wave	Ω crest/trough	Re x 10^5 crest/trough	KC crest/trough	β x 10^3		Force coefficients according to methods of: Least squares whole period	ε %	crest	ε %	trough	ε %	crest 60°	ε %	trough 60°	ε %	π 60°	ε %	Max.vel. and acc. crest	trough	Zero and max force crest	trough
Level -0.50 (-0.60)																					
A	0.47/0.43	0.31/0.29	0.6/0.5	52.4	C_D	13.36	7	14.3	8	12.16	5	13.07	2	11.14	2	30.99	5	12.66	10.49	15.81	15.63
					C_M	1.81		1.74		1.86		1.68		1.97		1.73		1.98	1.69	1.95	1.92
B	0.32/0.25	0.94/0.70	2.7/2.0	35.2	C_D	2.13	10	2.14	4	2.11	9	1.80	1	1.21	6	4.60	6	2.03	0.72	2.3	3.12
					C_M	1.79		1.61		2.02		1.50		2.07		1.96		1.66	1.91	1.62	2.25
C	0.13/0.05	1.52/0.66	7.2/3.1	21.2	C_D	0.45	19	0.71	37	-1.8	10	0.83	9	-0.67	25	2.23	14	0.95	0.08	0.89	2.30
					C_M	1.48		1.46		1.60		1.13		1.62		2.09		0.87	2.22	0.99	2.55

Table A1.2 d Time invariant force coefficients at; 0.7 m below S.W.L. for wave A and B (fifth order theory).

Wave	Ω crest/trough	Re x 10^5 crest/trough	KC crest/trough	β x 10^3		Force coefficients according to methods of: Least squares whole period	ε %	crest	ε %	trough	ε %	crest 60°	ε %	trough 60°	ε %	π 60°	ε %	Max.vel. and acc. crest	trough	Zero and max force crest	trough
Level -0.70																					
A	0.19/0.13	0.28/0.26	0.5/0.5	52.4	C_D	13.06	5	13.57	5	12.48	4	12.47	2	11.57	4	35.7		12.95	11.43	13.80	14.64
					C_M	1.85		1.77		1.92		1.74		1.93		1.83		1.86	1.79	1.94	2.07
B	0.14/0.07	0.88/0.69	2.5/2.0	35.2	C_D	1.95	9	2.05	3	1.75	8	1.70	2	0.92	6	4.35	5	2.15	1.04	1.89	2.49
					C_M	1.79		1.65		1.97		1.61		2.11		1.93		1.64	1.83	1.68	2.14

APPENDIX 2 ACCURACY OF MEASUREMENTS

A2.1 Velocity measurements

Calibrations at constant velocities showed that the propeller moves approximately 6 mm between two pulses. To get good accuracy at high velocities the clock pulse must be set rather high. 10,000 Hz was chosen. Thus, at 0.85 m/s 70 or 71 clock pulses are counted depending on the phase difference between propeller pulses and clock pulses. This error in the digital/analogue converter is ± 0.5 bit. ("True" value in this example is 70.58 "pulses"). Another error is caused by the fact that the reset-pulse can be given at the same moment as a clock pulse. This clock-pulse will then be counted in the next lapse of time.

In Table A2.1 the estimated maximum errors in velocity for a continuously submerged propeller at constant velocity are given for the range of velocities used. It should be pointed out that these faults are very much smaller than those experienced if the propeller is maltreated or dirty. The propeller must therefore be recalibrated often and be protected against damage and dirt.

Table A2.1 Estimated maximum error in velocity measurement due to propeller (constant ± 2 mm/s) and velocity meter (D/A ± 1.5 bit). Noise on output (< 2 mV). Values in brackets relate to cases when the total error cannot be considered independent and random.

Velocity (m/s)	Noise on output %	D/A %	Propeller %	Inaccuracy %	Total %
1.00	±0.04	±2.5	±0.2	±0.2	±2.5 (±2.9)
0.50	±0.04	±1.3	±0.4	±0.2	±1.4 (±1.9)
0.25	±0.04	±0.6	±0.8	±0.2	±1.0 (±1.6)
0.10	±0.04	±0.3	±2.0	±0.2	±2.0 (±2.5)
0.04	±0.04	±0.1	±5.0	±0.2	±5.0 (±5.3)

Fig. A2.1, shows calibration curves for the propeller. The observed small nonlinearity was considered during processing. Furthermore, Fig. A2.2 shows possible error introduced by variation of propeller angle to the free stream direction.

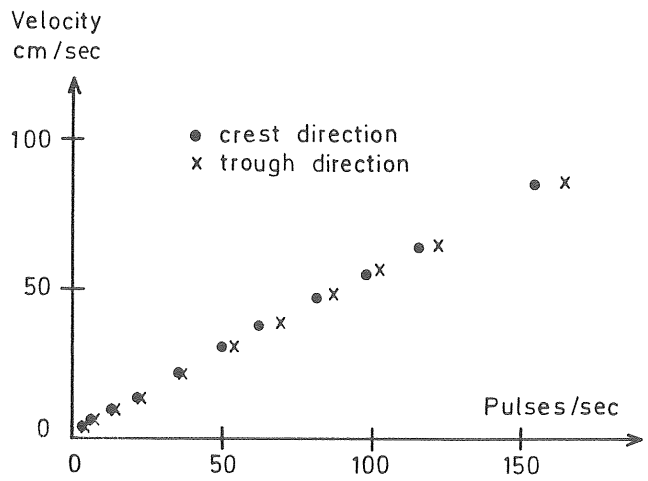

Figure A2.1 Calibration curves for 10 mm diameter, 5-bladed propeller - aligned with the free stream direction (90°), constant velocities.

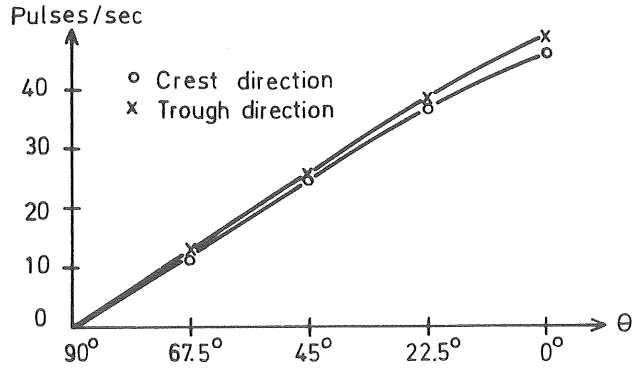

Figure A2.2 Calibration curves for a 10 mm diameter 5-bladed propeller - variation of propeller angle (θ) to the free stream direction, constant velocity (0.28 m/s).

A2.2 Wave gauges

Two ordinary resistive wave gauges (PR02, PR03) were used for measuring the water level, ϕ = 3 mm (Danish Hydraulic Institute). Also, a special wave gauge (PR01) was built to measure the water level at the cylinder surface close to the vertical line of pressure transducers. This wave gauge was also resistive but was made of four thin (ϕ = 0.2 mm) wires of stainless steel.

Table A2.2 Estimated maximum error in water level measurements of full scale output (FSO). Values in brackets relate to cases when the total error cannot be considered independent and random.

	Noise on output ((4 mV) %	Linearity (better than) %	D/A (±0.5 bit) %	Inaccuracy (±0.1 mm) %	Total %
PR02, PR03	±0.08	±0.5	±0.01	±0.04	±0.51(±0.63)
PR01	±0.08	±1.5*	±0.01	±0.04	±1.50(±1.63)

*) combined linearity and hysteresis

Table A2.2 shows the estimated total error for PR02, PR03 and PR01 respectively.

In addition to the error presented, there is the influence of miniscus of water which becomes larger the thicker the wires of the wave gauges are.

For PR02 and PR03 the error introduced was estimated to be ±0.5 mm (±0.1%). However, disregarding a small introduced phase shift, the relatively slow changes at maximum/minimum water level make the influence of miniscus of water negligible.

A2.3 Pressure measurements

The distribution of pressure was measured with six pressure transducers, mounted flush with the cylinder surface in a vertical line. Piezoresistive pressure transducers (Endevco-series 8510) with a sensor diameter of 3.84 mm were used, see Fig. A2.3.

To obtain the pressure for the whole circumference of the cylinder, the whole cylinder was rotated by a 22.5 degree increments. 16 separate experiments were thus needed to obtain the whole pressure distribution around the cylinder.

In Table A2.3 the estimated maximum error for net pressure at levels of measurement are given (16 experiments). It should be pointed out that these faults are very much smaller than those that are experienced if good correspondence is not obtained betwen the 16 runs. Then the pressure distribution, because of possible different flow modes, may differ significantly at the same phase in the wave.

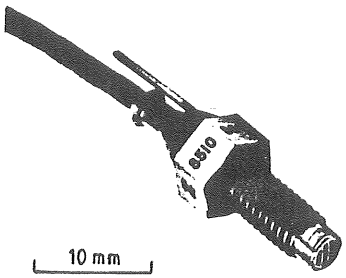

Figure A2.3 Piezoresistive pressure transducer.

Table A2.3 Estimated maximum error for net pressure at levels of measurements of full scale output (FSO) (16 separate experiments). Value in brackets relates to cases when the total error cannot be considered independent and random.

	Noise on output (<10mV) %	Combined linearity and hysteresis %	D/A (±0.5 bit) %	Inaccuracy (±0.1 mm) %	Total %
Net pressure	±0.2	±1.5	±0.01	±0.04	±1.5(±4.9)

The calculation of total force from integrated pressure involves from six to four levels of pressure measurements (wave crest - wave trough). However, the total error will still be of approximately the same order (see Table A2.3), as they are independent and of the same order. Also the comparison between the force obtained from the integrated pressure and the force obtained from the strain gauge cantilever showed good correspondence (maximum deviation < 4.0%).

Calibration of pressure transducers and wave gauges, and possible adjustment of water depth were made for each wave (16 experiments) in the experimental program. Further, the calibration and the 16 separate experiments needed for knowing the pressure distribution were always performed on the same day. The largest change of output signal for a single pressure transducer was measured as 3.51% (decrease) during a 49-hour period.

A2.4 Signal offset

A signal offset occurred when a pressure transducer went from water to air or vice versa. Depending on the wave studied and the water depth, two or three pressure transducers were affected (PRE1, PRE2, PRE3), see Figs. A2.4 a-d. To handle this problem, the measured water level at the cylinder surface (PRO1) was used. With PRO1 it was always possible to define when the relative pressure was zero, i.e. when the pressure transducers were in air. With the use of a small computer program, correct magnitude and distribustion of pressure during the wave period was achieved, see Figs. A2.5 a-c.

A2.5 Transients

The experimental variables were recorded with a Compucorp 625M-II desk top computer. The A/D converter used worked according to the principle of successive approximation, which is characterized by its fast speed. In spite of transient filters in series on the power supply, voltage transients were recorded. No attempts were made to remove the resulted peaks visible for some of the recorded variables. However, the technique of averaging all variables smoothed the peaks substantially.

In conclusion, the influence of transients on reported results were of no mayor importance.

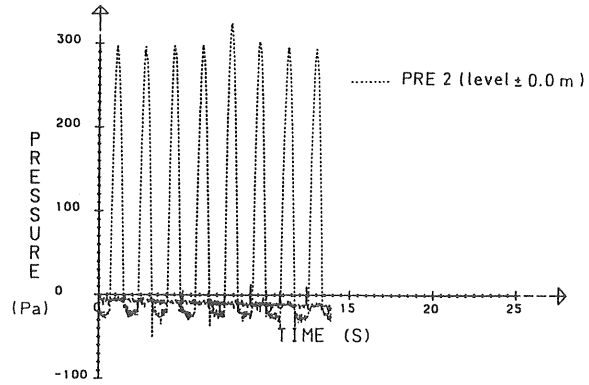

Figure A2.4 a Wave A. Pressure at 135° according to Fig. 3.3.

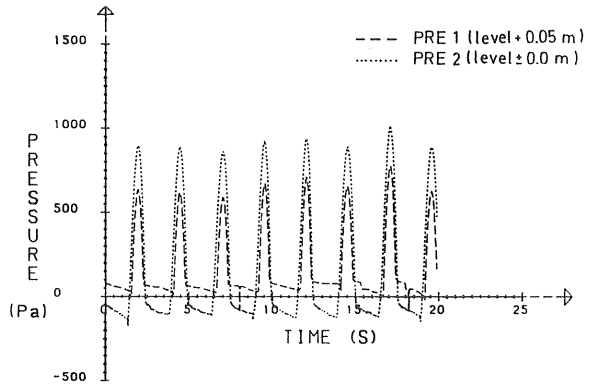

Figure A2.4 b Wave B. Pressure at 22.5° according to Fig. 3.3.

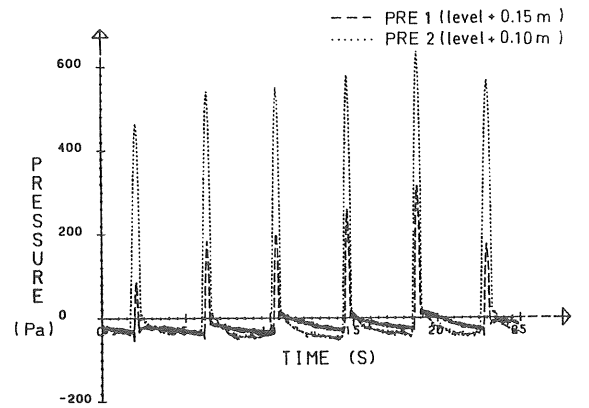

Figure A2.4 c Wave C. Pressure at 0° according to Fig. 3.3.

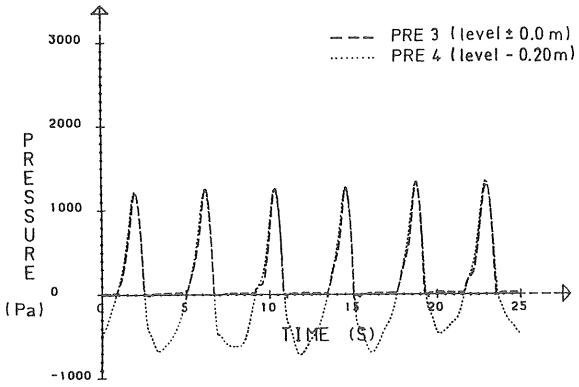

Figure A2.4 d Wave C. Pressure at 0^{o} according to Fig. 3.3.

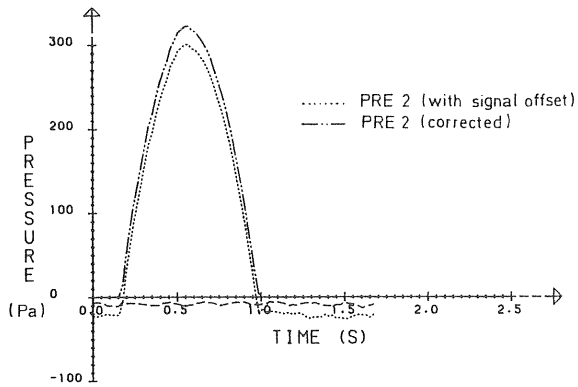

Figure A2.5 a Wave A. Mean pressure at 135^{o} according to Fig. 3.3.

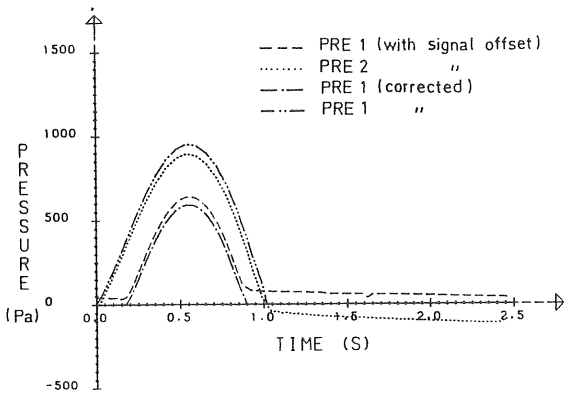

Figure A2.5 b Wave B. Mean pressure at 22.5^{o} according to Fig. 3.3.

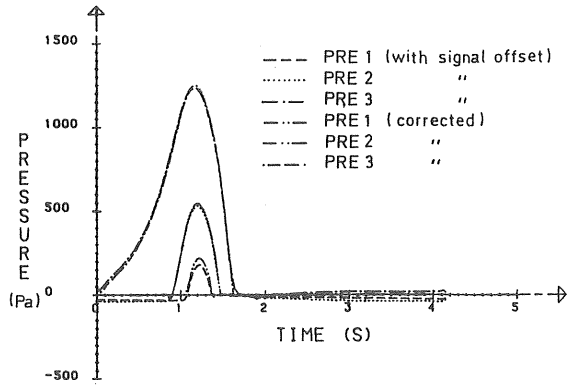

Figure A2.5 c Wave C. Mean pressure at 0^{o} according to Fig. 3.3.

A2.6 Cylinder

The vertical circular cylinder was made of steel and designed so that the resultant force from weight and buoyancy was small and directed downwards. The test cylinder was polished and painted with a glossy paint. With surface roughness set at 0.04 mm it could, thus, be treated as hydrodynamically smooth.

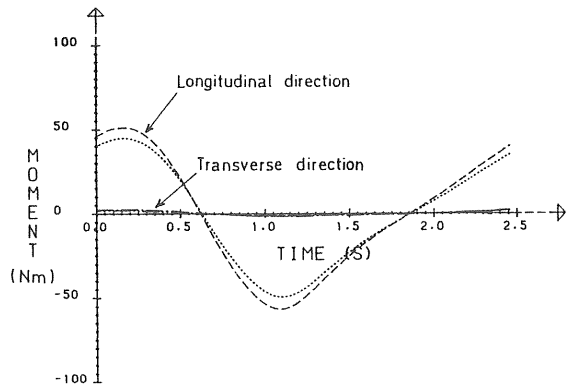

Figure A2.6 Wave B. Moment at a distance of l_1 and l_2 in the longitudinal and transverse direction according to Fig. 6.2. Present phase shift approximately 0.065 s.

A2.7 Gauge cantilever

The cylinder was hung in a cantilever clamped to a rigid heavy frame that was mounted across the top of the wave tank. The cantilever was made of aluminium equipped with strain gauges at two levels in two directions. These strain gauges showed very good characteristics of linearity, sensitivity, noise level and hysteresis of full scale output. However, because of there being different numbers of condensers used in the amplifier units (longitudinal direction), there was a phase shift, see Fig. A2.6. As a consequence the force obtained from the strain gauge cantilever was not used for further processing.

A2.8 Natural frequency

The natural frequency for the combined system, cylinder-gauge cantilever was calculated using the computer program SFVIBAT-II, Division of Solid Mechanics, Chalmers University of Technology. Table A2.4 gives the first six fundamental frequencies of the system. The first mode of natural frequency in the longitudinal direction was calculated to 9.0 Hz, which is approximately 10 to 40 times as great as the wave frequency used. The dynamic amplification could thus be considered negligibly small. In the transverse direction the lowest natural frequency was calculated to be 3.7 Hz which is at least 2.4 times as great as the frequencies of vortex shedding. However, the relatively low natural frequency of the system in the transverse direction did not pose problems during the experimental investigation.

Table A2.4 Bounds of fundamental frequency for combined system cylinder-gauge cantilever given by SFVIBAT-II.

Free harmonic vibration (Euler-Bernoulli theory). Bounds of fundamental frequency.

Mode number	Lower bound (Hz)	Upper bound (Hz)	Type (direction)
1	3.70	3.73	translation z (transverse)
2	9.01	9.07	- " - x (longitudinal)
3	20.72	20.93	rotation y
4	139.24	140.07	translation z
5	321.58	323.24	- " - x
6	344.79	348.10	- " - y

A2.9 Blockage, length to diameter ratio and end effect

Blockage or proximity of a wall, length to diameter ratio and end effects may contribute to the total force acting on the cylinder. Consequently, these possible influences must be investigated.

It is generally observed that the drag coefficient decreases for cylinders with a large length to diameter ratio (l/D). This ratio influences the point of separation, the subsequent formation of vortices and correlation of shedding. Furthermore, the presence of gap(s) near the cylinder end(s) also decreases the value of the drag coefficient, owing to a surplus of high pressure fluid into the wake near the cylinder end(s).

However, these effects appear to be negligible in the subcritical regime, Sarpkaya (1976a). Therefore, end effects were estimated as negligible in the present test. The surplus of high pressure fluid under the cylinder was minimized because of the small gap to diameter ratio ($\ll 0.016$).

Through pressure measurements Sarpkaya (1976a) shows that the blockage effect in harmonic flow is negligible at least for D/W ratios less than 0.18, where W is the width of test section. Sarpkaya also presented an investigation of the effect of wall proximity on the force coefficients. Both the drag and the inertia coefficient are increased by the presence of the wall. The increase on both force coefficients is most evident in the range of e/D values smaller than about 0.5, where e is the distance between the cylinder and the wall. For $e/D > 0.5$ the effect of wall proximity is virtually negligible, Sarpkaya and Isaacson (1981). This was shown by comparing the force coefficients with those obtained for cylinders at larger wall distances. Also, the largest variation of lift coefficient is found in the range of $e/D < 0.5$. Furthermore, the effects of wall proximity on unseparated flow (potential theory) are negligible for e/D of about 1, Sarpkaya and Isaacson (1981). The effects of wall proximity are consequently negligible if the distance between cylinder and wall is about one cylinder diameter.

In Table A2.5 and A2.6 comparisons are made between reported observations and the present test. Potential theory (Eq.(5.3)) and the method of images are used for estimation of wall proximity effects.

In conclusion, the influence of reported effects may be neglected in the present test.

Table A2.5 Wall proximity effects. Increase of free stream velocity for present experimental setup in the case of unseparated flow (potential theory).

Increase of velocity for the present experimental setup

criteria	at wall	at cylinder
Sarpkaya $e/D \cong 1$	1.111 U_s (11.1%)	2.040 U_s (2.0%)
Present test $e/D = 2.83$	1.045 U_s (4.5%)	2.008 U_s (0.4%)

Table A2.6 Comparison of present test with criteria of blockage and wall proximity effects.

Blockage and wall proximity effects

	Sarpkaya	Present test
Blockage	Negligible if D/W (0.18	0.15
Wall proximity	Negligible if e/D) 0.5	2.83

A2.10 Convective acceleration

In wave force calculations u is taken as the horizontal component of the water particle velocity. The acceleration is assumed to be given exclusively by the local component, $\partial u/\partial t$, see Eq. (2.10). However, the total acceleration is given by the sum of local and convective components.

$$\frac{du}{dt} = \frac{\partial u}{\partial t} + u\frac{\partial u}{\partial x} + v\frac{\partial u}{\partial y} \qquad \ldots (A2.1)$$

Using linear theory

$$u = -\frac{\partial \phi}{\partial x}, \quad \phi = \frac{ag}{\omega}\frac{\cosh k(y+d)}{\cosh kd}\cos(kx - \omega t)$$

convective acceleration is given by

$$u\frac{\partial u}{\partial x} = \left(\frac{agk}{\omega}\frac{\cosh k(y+d)}{\cosh kd}\right)^2 \cdot k \sin\omega t \cos\omega t \qquad \ldots (A2.2)$$

$$v\frac{\partial u}{\partial y} = -\left(\frac{agk}{\omega}\frac{\sinh k(y+d)}{\cosh kd}\right)^2 \cdot k \sin\omega t \cos\omega t \qquad \ldots (A2.3)$$

The error introduced by using local instead of total acceleration in wave force calculations may be estimated by studying the ratio of inertia force from the convective to inertia force from local acceleration. The inertia force due to the convective acceleration (F_{Mc}) is obtained by

$$F_{Mc} = \rho\frac{\pi D^2}{4}C_M\int_{-d}^{0}\left(u\frac{\partial u}{\partial x} + v\frac{\partial u}{\partial y}\right)dy = \rho\frac{\pi D^2}{8}C_M a^2 gk\frac{kd}{\sinh 2kd}\sin 2\omega t \qquad \ldots (A2.4)$$

In intermediate to deep water the value of sinh 2kd quickly becomes large. Consequently, the convective acceleration force vanishes.

The ratio of F_{Mc} to F_M is shown in Table A2.7. Eqs. (A2.4) and (2.13) are used.

Isaacson (1979) demonstrated that inertia force calculated in the conventional manner generally overestimates the actual force. He introduced an effective inertia coefficient which considered the contribution of convective acceleration, see Fig. A2.7. The ratio of $C_M/C_M^{\sim}$ given in Fig. A2.7 corresponds well to comparable wave situations in the present test. (Data for present test - see Table 4.1).

In conclusion, the distinction between local and total acceleration may be important for wavy flow, although the use of local acceleration rather than of total acceleration does not affect the practical application of Morison's equation, which, in any case, depends on the experimental coefficients used.

Table A2.7 Ratio of convective acceleration force to local acceleration force for the present test.

wave	H	L	d	$F_{Mc} \times N_r = F_M$	F_{Mc}/F_M
	(m)	(m)	(m)	N_r (times)	%
A	0.082	3.90	0.8	132	0.8
B	0.186	6.54	0.8	42	2.4
C	0.223	10.70	0.7	27	3.8
D	0.038	11.43	0.8	179	0.6
E	0.062	6.51	0.8	125	0.8
F	0.048	8.98	0.8	147	0.7
G	0.198	2.67	0.8	1233	0.1
H	0.190	3.98	0.8	56	1.8
I	0.146	9.15	0.8	53	1.9
J	0.118	11.64	0.8	57	1.7
K	0.274	9.00	0.7	22	4.5
L	0.350	6.52	0.7	19	5.4
M	0.334	12.02	0.7	18	5.7

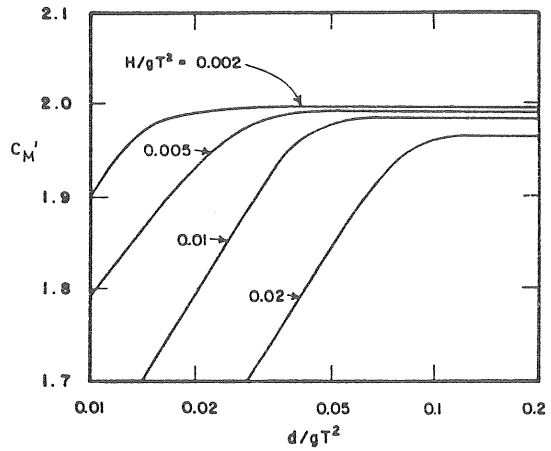

Figure A2.7 Effective inertia coefficient for vertical circular cylinder as function of d/gT^2 and H/gT^2 (for present test given in Table 4.1). Wave theory used - fifth order. (Isaacson, 1979).

APPENDIX 3 EVALUATION APPROACHES OF FORCE COEFFICIENTS

A3.1 Fourier-averaging technique

Assuming a harmonic flow the horizontal velocity variation throughout the cycle is given by

$$u = -u_m \cos \omega t \qquad \ldots (A3.1)$$

where

u_m = maximum velocity

$\omega = \frac{2 \cdot \pi}{T}$

T = wave period

Morison's equation (Eq. (2.7)) may be written providing that C_D and C_M are independent of θ

$$\frac{F}{\rho u_m^2 D} = \frac{\pi^2}{2KC} C_M \sin\theta - \frac{C_D}{2} |\cos\theta|\cos\theta \qquad \ldots (A3.2)$$

where

ρ = density of water

D = diameter of cylinder

$KC = u_m \cdot T/D$

C_M = mass or inertia coefficient

C_D = drag coefficient

$\theta = \frac{2\pi \cdot t}{T}$

Assuming that $F(\theta) = -F(\theta+\pi)$ and that there are only odd harmonics, the force in terms of Fourier series may be written

$$\frac{F}{\rho u_m^2 D} = A_1 \sin\theta + A_3 \sin 3\theta + A_5 \sin 5\theta + \ldots + B_1 \cos\theta + B_3 \cos 3\theta + B_5 \cos 5\theta + \ldots \qquad \ldots (A3.3)$$

The use of only the odd harmonics was justified by Sarpkaya (1981b) for sinusoidally oscillating flow under laboratory conditions. The force on a circular cylinder was concentrated at the fundamental frequency and significant components occurred only at odd harmonics of the fundamental.

By Fourier transform

$$|\cos\theta|\cos\theta = a_o + a_1 \cos\theta + a_2 \cos 2\theta + a_3 \cos 3\theta + \ldots \qquad \ldots (A3.4)$$

where

$a_n = 0$ for even n and

$$a_n = (-1)^{\frac{n+1}{2}} \frac{8}{n(n^2-4)\pi} \quad \text{for n odd}$$

Multiplying and dividing Eq. (A3.4) with B_1 and a_1 gives

$$B_1 \cos\theta = \frac{B_1}{a_1}|\cos\theta|\cos\theta - B_1 \frac{a_3}{a_1} \cos 3\theta - B_1 \frac{a_5}{a_1} \cos 5\theta - \ldots \qquad \ldots (A3.5)$$

Introducing Eq. (A3.5) in Eq. (A3.3) and writing

$$B_1' = \frac{B_1}{a_1}$$

$$B_3^{\sim} = B_3 - \frac{a_3}{a_1} B_1 \qquad \ldots (A3.6)$$

$$B_5^{\sim} = B_5 - \frac{a_5}{a_1} B_1$$

gives

$$\frac{F}{\rho u_m^2 D} = A_1 \sin\theta + A_3 \sin 3\theta + A_5 \sin 5\theta + \ldots + B_1^{\sim} |\cos\theta| \cos\theta + B_3^{\sim} \cos 3\theta + B_5^{\sim} \cos 5\theta + \ldots \qquad \ldots (A3.7)$$

A comparison of Eqs. (A3.2) and (A3.7) gives

$$\frac{\pi^2}{2} C_M \frac{D}{u_m \cdot T} \sin\theta = A_1 \sin\theta + A_3 \sin 3\theta + A_5 \sin 5\theta + \ldots \qquad \ldots (A3.8)$$

Studying the first Fourier component with

$$A_1 = \frac{1}{\pi} \int_0^{2\pi} \frac{F \sin\theta}{\rho u_m^2 D} \, d\theta \qquad \ldots (A3.9)$$

gives

$$C_M = \frac{2}{\pi^3} \frac{u_m T}{D} \int_0^{2\pi} \frac{F \sin\theta}{\rho u_m^2 D} \, d\theta \qquad \ldots (A3.10)$$

and

$$-\frac{C_D}{2} |\cos\theta| \cos\theta = B_1^{\sim} |\cos\theta| \cos\theta + B_3^{\sim} \cos 3\theta + B_5^{\sim} \cos 5\theta + \ldots \qquad \ldots (A3.11)$$

Studying the first Fourier component with

$$B_1 = \frac{1}{\pi} \int_0^{2\pi} \frac{F \cos\theta}{\rho u_m^2 D} \, d\theta \qquad \ldots (A3.12)$$

gives

$$C_D = -\frac{3}{4} \int_0^{2\pi} \frac{F \cos\theta}{\rho u_m^2 D} \, d\theta \qquad \ldots (A3.13)$$

A3.2 Method of least squares

Let F_{mi} represent the instantaneous measured force and F_{ci} the instantaneous force calculated using Morison's equation (Eq. 2.7). Then the mean squared error (ε^2) may be written

$$\varepsilon^2 = \frac{1}{N} \sum_{i=1}^{N} (F_{mi} - F_{ci})^2 \qquad \ldots (A3.14)$$

where

N is the total number of data points of the measurement.

The minimization procedure results in two equations in the two unknown. This gives

$$\frac{\partial \varepsilon^2}{\partial C_D} = \frac{2}{N} \sum_{i=1}^{N} (F_{mi} - F_{ci}) \frac{\partial F_{ci}}{\partial C_D} = 0$$

$$\frac{\partial \varepsilon^2}{\partial C_M} = \frac{2}{N} \sum_{i=1}^{N} (F_{mi} - F_{ci}) \frac{\partial F_{ci}}{\partial C_M} = 0 \qquad \ldots (A3.15)$$

Writing the calculated force (F_c) as

$$F_{c_i} = C_D F_{D_i} + C_M F_{M_i}$$

where

$$F_{D_i} = \frac{1}{2} \rho A |u_i| u_i$$

$$F_{M_i} = \rho V \frac{\partial u_i}{\partial t}$$

ρ = density of water

A = characteristic area

u_i = water particle velocity

V = immersed volume

$\frac{\partial u_i}{\partial t}$ = water particle acceleration

taking the derivatives and substituting into Eq. (A3.15) the equations can be written

$$C_D \sum_{i=1}^{N} (F_{Di}^2) + C_M \sum_{i=1}^{N} (F_{Mi} F_{Di}) = \sum_{i=1}^{N} (F_{mi} F_{Di})$$

$$C_D \sum_{i=1}^{N} (F_{Mi} F_{Di}) + C_M \sum_{i=1}^{N} (F_{Mi}^2) = \sum_{i=1}^{N} (F_{mi} F_{Mi}) \qquad \ldots (A3.16)$$

which can be written

$$B C_D + D C_M = E$$

$$D C_D + G C_M = H \qquad \ldots (A3.17)$$

where

B, D, E, G and H are known constants for a given set of data.

Eliminating the unknowns gives

$$C_D = \frac{HD - EG}{D^2 - BG}$$

$$C_M = \frac{ED - HB}{D^2 - BG} \qquad \ldots (A3.18)$$

where

$$B = \sum_{i=1}^{N} (F_{Di}^2) = \frac{\rho^2}{4} A^2 \sum_{i=1}^{N} (u_i^4)$$

$$D = \sum_{i=1}^{N} (F_{Mi} F_{Di}) = \frac{\rho^2}{2} AV \sum_{i=1}^{N} (|u_i| u_i \frac{\partial u_i}{\partial t}$$

$$E = \sum_{i=1}^{N} (F_{mi} F_{Di}) = \frac{\rho}{2} A \sum_{i=1}^{N} (F_{mi} |u_i| u_i)$$

$$G = \sum_{i=1}^{N} (F_{Mi}^2) = \rho^2 V^2 \sum_{i=1}^{N} ((\frac{\partial u_i}{\partial t})^2)$$

$$H = \sum_{i=1}^{N} (F_{mi} F_{Mi}) = \rho V \sum_{i=1}^{N} (F_{mi} \frac{\partial u_i}{\partial t})$$

Knowing the coefficients, the root mean squared error can be found by expanding Eq. (A3.14)

$$\varepsilon = (\frac{1}{N} \sum_{i=1}^{N} (F_{mi}^2) - 2EC_D - 2HC_M + BC_D^2 + 2DC_D C_M + GC_M^2)^{1/2} \quad \ldots (A3.19)$$

A3.3 Concluding remarks

Neither the Fourier-averaging technique nor the method of least squares garantees that the maximum calculated force is equal to the maximum force. The method of least squares can be applied for asymmetrical waves as either measured kinematics or kinematics chosen from some wave theory can be used. The Fourier-averaged force coefficients as given by Keulegan and Carpenter (1958) are restricted to harmonically oscillating flow. However, the Fourier-averaging technique may be improved by considering additional components in the Fourier series as was done by for example Bearman, Chaplin et al. (1985). The authors used the first six Fourier components for representing the force and velocity signals.

Finally, the two methods may yield almost identical results. With the use of harmonic flow Sarpkaya and Isaacson (1981) show that the Fourier analysis and the method of least squares yield identical C_M values and only slightly different C_D values.

CHALMERS TEKNISKA HÖGSKOLA
Institutionen för vattenbyggnad

Report Series A

A:1 Bergdahl, L.: Physics of ice and snow as affects thermal pressure. 1977.

A:2 Bergdahl, L.: Thermal ice pressure in lake ice covers. 1978.

A:3 Häggström, S.: Surface Discharge of Cooling Water. Effects of Distortion in Model Investigations. 1978.

A:4 Sellgren, A.: Slurry Transportation of Ores and Industrial Minerals in a Vertical Pipe by Centrifugal Pumps. 1978.

A:5 Arnell, V.: Description and Validation of the CTH-Urban Runoff Model. 1980.

A:6 Sjöberg, A.: Calculation of Unsteady Flows in Regulated Rivers and Storm Sewer Systems. 1976.

A:7 Svensson, T.: Water Exchange and Mixing in Fjords. Mathematical Models and Field Studies in the Byfjord. 1980.

A:8 Arnell, V.: Rainfall Data for the Design of Sewer Pipe Systems. 1982.

A:9 Lindahl, J. Sjöberg, A.,: Dynamic Analysis of Mooring Cables. 1983.

A:10 Nilsdal, J-A.: Optimeringsmodellen ILSD. Beräkning av topografins inverkan på ett dagvattensystems kapacitet och anläggningskostnad. 1983.

A:11 Lindahl, J.: Implicit numerisk lösning av rörelseekvationerna för en förankringskabel. 1984.

A:12 Lindahl, J.: Modellförsök med en förankringskabel. 1985.

A:13 Lyngfelt, S.: On Urban Runoff Modelling. The Application of Numerical Models Based on the Kinematic Wave Theory. 1985.

A:14 Johansson, M.: Transient Motions of Large Floating Structures. 1986.

A:15 Mårtensson, N. Bergdahl, L.: On the Wave Climate of the Southern Baltic. 1987.

A:16 Moberg, G.: Wave Forces on a Vertical Slender Cylinder. 1988.

CHALMERS TEKNISKA HÖGSKOLA
Institutionen för vattenbyggnad

Report Series B

B:1 Bergdahl, L.: Beräkning av vågkrafter. (Ersatts med 1979:07) 1977.

B:2 Arnell, V.: Studier av amerikansk dagvattenteknik. 1977.

B:3 Sellgren, A.: Hydraulic Hoisting of Crushed Ores. A feasibility study and pilot-plant investigation on coarse iron ore transportation by centrifugal pumps. 1977.

B:4 Ringesten, B.: Energi ur havsströmmar. 1977.

B:5 Sjöberg, A., Asp, T.: Brukar-anvisning för ROUTE-S. En matematisk modell för beräkning av icke-stationära flöden i floder och kanaler vid strömmande tillstånd. 1977.

B:6 Annual Report 1976/77. 1977.

B:7 Bergdahl, L., Wernersson, L.: Calculated and Expected Thermal Ice Pressures in Five Swedish Lakes. 1977.

B:8 Göransson, C-G., Svensson, T.: Drogue Tracking - Measuring Principles and Data Handling. 1977.

B:9 Göransson, C-G.: Mathematical Model of Sewage Discharge into confined, stratified Basins - Especially Fjords. 1977.

B:10 Arnell, V., Lyngfelt, S.: Beräkning av dagvattenavrinning från urbana områden. 1978.

B:11 Arnell, V.: Analysis of Rainfall Data for Use in Design of Storm Sewer Systems. 1978.

B:12 Sjöberg, A.: On Models to be used in Sweden for Detailed Design and Analysis of Storm Drainage Systems. 1978.

B:13 Lyngfelt, S.: An Analysis of Parameters in a Kinematic Wave Model of Overland Flow in Urban Areas. 1978.

B:14 Sjöberg, A., Lundgren, J., Asp, T., Melin, H.: Manual för ILLUDAS (Version S2). Ett datorprogram för dimensionering och analys av dagvattensystem. 1979.

B:15 Annual Report 1978/79. 1979.

B:16 Nilsdal, J-A., Sjöberg, A.: Dimensionerande regn vid höga vattenstånd i Göta älv. 1979.

B:17 Stöllman, L-E.: Närkes Svartå. Hydrologisk inventering. 1979.

B:18 Svensson, T.: Tracer Measurements of Mixing in the Deep Water of a Small, Stratified Sill Fjord. 1979.

B:19 Svensson, T., Degerman, E., Jansson, B.,Westerlund, S.: Energiutvinning ur sjö- och havssediment. En förstudie. R76:1980. 1979.

B:20 Annual Report 1979. 1980.

B:21 Stöllman, L-E.: Närkes Svartå. Inventering av vattentillgång och vattenanvändning. 1980.

B:22 Häggström, S., Sjöberg, A.: Effects of Distortion in Physical Models of Cooling Water Discharge. 1979.

B:23 Sellgren, A.: A Model for Calculating the Pumping Cost of Industrial Slurries. 1981.

B:24 Lindahl, J.: Rörelseekvationen för en kabel. 1981.

B:25 Bergdahl, L., Olsson, G.: Konstruktioner i havet. Vågkrafter-rörelser. En inventering av datorprogram. 1981.

B:26 Annual Report 1980. 1981.

Report Series B

B:27 Nilsdal, J-A.: Teknisk-ekonomisk dimensionering av avloppsledningar. En litteraturstudie om datormodeller. 1981.

B:28 Sjöberg, A.: The Sewer Network Models DAGVL-A and DAGVL-DIFF. 1981.

B:29 Moberg, G.: Anläggningar för oljeutvinning till havs. Konstruktionstyper, dimensioneringskriterier och positioneringssystem. 1981.

B:30 Sjöberg, A., Bergdahl, L.: Förankringar och förankringskrafter. 1981.

B:31 Häggström, S., Melin, H.: Användning av simuleringsmodellen MITSIM vid vattenresursplanering för Svartån. 1982.

B:32 Bydén, S., Nielsen, B.: Närkes Svartå. Vattenöversikt för Laxå kommun. 1982.

B:33 Sjöberg, A.: On the stability of gradually varied flow in sewers. 1982.

B:34 Bydén, S., Nyberg, E.: Närkes Svartå. Undersökning av grundvattenkvalitet i Laxå kommun. 1982.

B:35 Sjöberg, A., Mårtensson, N.: Regnenveloppmetoden. En analys av metodens tillämplighet för dimensionering av ett 2-års perkolationsmagasin. 1982.

B:36 Svensson, T., Sörman, L-O.: Värmeupptagning med bottenförlagda kylslangar i stillastående vatten. Laboratorieförsök. 1982.

B:37 Mattsson, A.: Koltransporter och kolhantering. Lagring i terminaler och hos storförbrukare. (Delrapport). 1983.

B:38 Strandner, H.: Ett datorprogram för sammankoppling av ILLUDAS och DAGVL-DIFF. 1983.

B:39 Svensson, T., Sörman, L-O.: Värmeupptagning med bottenförlagda slangar i rinnande vatten. Laboratorieförsök. 1983.

B:40 Mattsson, A.: Koltransporter och kolhantering. Lagring i terminaler och hos storförbrukare. Kostnader. Delrapport 2. 1983.

B:41 Häggström, S., Melin, H.: Närkes Svartå. Simuleringsmodellen MITSIM för kvantitativ analys i vattenresursplanering. 1983.

B:42 Hård, S.: Seminarium om miljöeffekter vid naturvärmesystem. Dokumentation sammanställd av S. Hård, VIAK AB. BFR-R60:1984. 1983.

B:43 Lindahl, J.: Manual för MODEX-MODIM. Ett datorprogram för simulering av dynamiska förlopp i förankringskablar. 1983.

B:44 Activity Report. 1984.

B:45 Sjöberg, A.: DAGVL-DIFF. Beräkning av icke-stationära flödesförlopp i helt eller delvis fyllda avloppssystem, tunnlar och kanaler. 1984.

B:46 Bergdahl, L., Melin, H.: WAVE FIELD. Manual till ett program för beräkning av ytvattenvågor. 1985.

B:47 Lyngfelt, S.: Manual för dagvattenmodellen CURE. 1985.

B:48 Perrusquía, G., Lyngfelt, S., Sjöberg, A.: Flödeskapacitet hos avloppsledningar delvis fyllda med sediment. En inledande experimentell och teoretisk studie. 1986.

B:49 Lindahl, J., Bergdahl, L.: MODEX-MODIM. User's Manual. 1987.

B:50 Mårtensson, N.: Dynamic Analysis of a Moored Wave Energy Buoy. 1988.